Immunological responses to retinal gene therapy

A thesis submitted for the degree of Doctor of Philosophy

Laurel Clare Chandler BSc (Hons)

Merton College

Supervisors: Dr Kanmin Xue & Professor Robert E. MacLaren

Hilary Term 2021

Acknowledgements

I would like to express my gratitude to my supervisor Kanmin Xue for his mentorship over the past five years. I am immensely grateful for the time he has set aside to discuss my project and for inspiring me to continually develop as a researcher. I would also like to thank my supervisor Robert MacLaren for his leadership and guidance throughout my DPhil. His support and advice have been invaluable as I embark on my future career.

I am grateful for the support and friendship of all the members of the MacLaren research group I have worked with over the past five years. To Alun Barnard for his wisdom and advice in experimental design; to Michelle McClements for her expertise in molecular biology and patience in answering my many questions; to Maria Patrício for her invaluable help when I first joined the lab; to Tina Storm for her motivation and constant support throughout my DPhil; and to Helen Ferry for spending many hours teaching me flow cytometry. Thank you also to Lewis Fry, Imran Yusuf, Cristina Martinez-Fernandez de la Camara, Jasleen Kaur Jolly, Marta Stevanovic, Harry Orlans, Mark Hassall, Ahmed Salman, Shaun Wood, Arantxa Bolinches Amorós, Federica Staurenghi, Elena Piotter, Ariel Kantor, and Joel Quinn who have provided invaluable support and made this experience so enjoyable. In particular, I would like to thank Caroline Peddle, aka the other half of 'Laureline', for her friendship, support, and commitment to lab fun; her camaraderie has kept me going throughout the past five years.

I am incredibly grateful for the generous financial support from Fight for Sight which enabled me to undertake this research and embark on the DPhil programme. Thank you also to the Nuffield Department of Clinical Neuroscience for providing me with financial support which enabled me to present my research at the ARVO annual meeting in Hawaii. I also extend my thanks to Merton College for the opportunity to undertake a DPhil at the University of Oxford and to my college advisor Nicole Zitzmann for her valued support.

I would like to thank the constant support of my friends and family. I am particularly grateful to my parents for always being there for me, and to my brother Thomas who's own hard work during his DPhil has been an inspiration. Thank you to Wilder for his continued patience and belief in me. Finally, I would like to extend particular appreciation to my tutor and mentor Jim Caunt; thank you for encouraging and inspiring me to pursue a career in science, you are greatly missed.

Abstract

Dose-dependent inflammatory responses in adeno-associated virus (AAV)–mediated retinal gene therapy trials have restricted the use of high vector doses and impeded the ability to enhance therapeutic efficacy. Characterising the nature of this response, and devising methods to overcome it, are thus becoming increasingly important in the clinical application of gene therapies. In the experiments herein, I investigated the composition, timing, and magnitude of the cellular immune response to retinal gene therapy in mice using quantitative flow cytometric analysis. I observed a significant increase in retinal leukocytes from 14 days after subretinal injection of an AAV8 vector expressing green fluorescent protein (GFP). These consisted of a constant population of resident microglia and infiltrating peripheral leukocytes including macrophages, natural killer cells, CD4 and CD8 T cells, and natural killer T cells. An identical vector at an equivalent dose encoding a human therapeutic transgene elicited a diminished response compared to paired injections with a GFP vector. However, the proportions of the leukocyte populations remained similar, suggesting a common mechanism of immunity. In addition to the induction of a cell-mediated immune response, innate detection of AAV vectors may directly restrict transgene expression. Preliminary evidence suggested *in vitro* AAV transduction may be limited by the anti-viral nucleic acid sensors Toll-like receptor 9 and cyclic GMP AMP synthase, suggesting possible detection of transgenic AAV genomes. I also showed that the immunomodulatory drug hydroxychloroquine can significantly enhance AAV transduction *in vitro*, *ex vivo*, and *in vivo,* with indirect indication of the partial antagonism of TLR9. The lack of structural change in the retina following subretinal hydroxychloroquine delivery indicates that it could be a safe adjunct for improving retinal gene therapy efficacy.

Table of contents

List of abbreviations

7-AAD	7-Aminoactinomycin D
AAV	Adeno-associated virus
ABCA4	ATP binding cassette subfamily A member 4
AMD	Age-related macular degeneration
APC	Antigen-presenting cell
ART	Automatic real-time
BAF	Blue autofluorescence
BSA	Bovine serum albumin
CAG	CMV enhancer fused to chicken β-actin promoter
CD	Cluster of differentiation
cDNA	Complementary DNA
cGAMP	Cyclic guanosine monophosphate–adenosine monophosphate
cGAS	cGAMP synthase
CMV	Cytomegalovirus
CNS	Central nervous system
cSLO	Confocal scanning laser ophthalmoscope
C_t	Cycle threshold
CXCL	C-X-C motif ligand

DMEM	Dulbecco's modified eagle medium
dsDNA	Double-stranded DNA
dsRNA	Double-stranded RNA
EBSS	Earle’s balanced salt solution
FBS	Fetal bovine serum
Fc	Fragment crystallisable
FDA	Food and drug administration
FIX	Factor IX
FMO	Fluorescence minus one
GAPDH	Glyceraldehyde 3-phosphate dehydrogenase
gc	Genome copies
GFP	Green fluorescent protein
GRK1	G-protein coupled rhodopsin kinase 1
HIV	Human immunodeficiency virus
HRP	Horseradish peroxidase
HSV	Herpes simplex virus
Iba1	Ionized calcium binding adaptor molecule 1
IFN	Interferon
IL	Interleukin
ILC	Innate lymphoid cell

IRF	Interferon regulatory factor
ISG	Interferon-stimulated gene
ITR	Inverted terminal repeat
JAK-STAT	Janus kinase-signal transducer and activator of transcription
LB	Luria's broth
LCA	Leber's congenital amaurosis
LTi	Lymphoid tissue inducer
MDA5	Melanoma differentiation–associated protein 5
MEF	Mouse embryonic fibroblast
MFI	Median fluorescence index
MHC	Major histocompatibility complex
MOI	Multiplicity of infection
NET	Neutrophil extracellular trap
NF-κB	Nuclear factor kappa B
NIR	Near-infrared reflectance
NK(T)	Natural killer (T)
ODN	Oligodeoxynucleotide
ORF	Open reading frame
pA	Polyadenylation
PAMP	Pathogen-associated molecular pattern

PBMC	Peripheral blood mononuclear cell
PBS-(T)	Phosphate-buffered saline–(tween 20)
PCR	Polymerase chain reaction
pDC	Plasmacytoid dendritic cell
PI	cOmplete™ EDTA-free Protease Inhibitor Cocktail
Poly(I:C)	Polyinosinic:polycytidylic acid
PRR	Pattern recognition receptor
qPCR	Quantitative PCR
REP1	Rab-escort protein 1
RIG-I	Retinoic acid–inducible gene I
RIPA	Radioimmunoprecipitation assay
RPE	Retinal pigment epithelium
RPE65	Retinal pigment epithelium–specific 65
RPGR	Retinitis pigmentosa GTPase regulator
RT-PCR	Reverse transcription PCR
SD-OCT	Spectral domain–optical coherence tomography
SDS	Sodium dodecyl sulfate
SDS-PAGE	SDS-polyacrylamide gel electrophoresis
SEM	Standard error of the mean
ssDNA	Single-stranded DNA

ssRNA	Single-stranded RNA
TBS-(T)	Tris-buffered saline–(tween 20)
TCR	T cell receptor
TLR	Toll-like receptor
TNF	Tumour necrosis factor
TRIM	Tripartite motif–containing
VP	Virion protein
WPRE	Woodchuck hepatitis virus post-transcriptional regulatory element
w/v	Weight/volume

List of figures

List of tables

1 General introduction

1.1 Adeno-associated viruses

1.1.1 Structure

Adeno-associated viruses (AAV) are non-enveloped parvoviruses within the genus *Dependoparvovirus* and are composed of an icosahedral protein capsid ~26 nm in diameter with a 4.7 kb single stranded DNA (ssDNA) genome [1]. The wildtype AAV genome encodes two open reading frames (ORFs), *rep* and *cap*, which are flanked by inverted terminal repeat (ITR) sequences at either end (Figure 1.1) [2]. The *rep* ORF encodes four alternatively spliced transcripts (Rep78, Rep68, Rep52, and Rep40), which are vital in encoding proteins for AAV genome replication. The *cap* ORF encodes three alternatively spliced transcripts (virion protein 1 (VP1), VP2, and VP3), which interact to form the icosahedral AAV capsid in a ratio of 1:1:10 of VP1:VP2:VP3. The *cap* ORF also encodes assembly-activating protein (AAP), which is essential for the construction of the viral capsid [3, 4], and the recently discovered membrane-associated accessory protein (MAAP), which may regulate wildtype AAV replication through an unknown mechanism [5]. Each 145 bp ITR sequence includes a 125 bp palindromic sequence that can anneal by complementary base pairing to form a T-shaped hairpin structure [6]. ITR sequences are key in mediating second-strand synthesis of the viral genome, which is an essential step in gene expression. These sequences are also important in mediating enclosure of the AAV genome within the assembled capsid and its integration into the host cell genome [7].

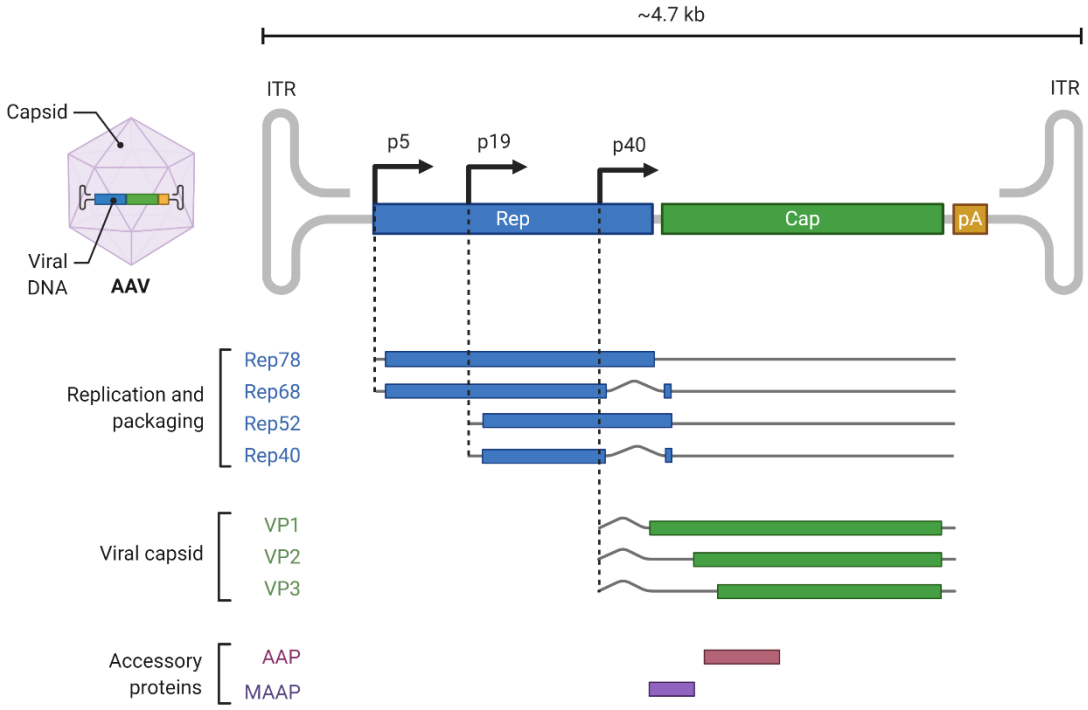

Figure 1.1. Genome of adeno-associated viruses (AAV). The 4.7 kb single stranded DNA (ssDNA) genome of wildtype AAV is enclosed within an icosahedral protein capsid. The genome encodes open reading frames for replication and packaging (*rep*) and the viral capsid (*cap*) with a downstream polyadenylation (pA) sequence; the genome is flanked by hairpin inverted terminal repeat (ITRs) sequences. Each mRNA sequence is displayed below the genome with the three promoters displayed above. Exons are indicated as coloured blocks, introns as grey angulated lines, and untranslated regions as grey horizontal lines. Rep78 and Rep68 are expressed from the promoter p5; Rep52 and Rep40 from p19; and VP1, VP2, VP3, assembly-activating protein (AAP), and membrane-associated accessory protein (MAAP) from p40. Adapted from 'Adeno-Associated Virus Genome', by BioRender.com.

1.1.2 Transduction

AAV transduction is a multi-step pathway that commences with the binding of viral capsid proteins to serotype-specific primary glycan receptors on the target cell surface membrane [8] (Figure 1.2). This interaction is further assisted by a secondary interaction between the capsid and specific proteinaceous receptors. The specificity of these receptor interactions contributes to AAV serotype-specific tropism. The most widely investigated serotype is AAV2, which initially binds to heparan sulfate proteoglycan (HSPG) and can engage various integrins and growth factors, such as $\alpha_v\beta_5$ integrin, human fibroblast growth factor receptor 1, hepatocyte growth factor receptor, and laminin receptor, to mediate internalisation [9-13]. The entry factors AAV receptor (AAVR) and GPR108 have been identified as necessary for infection of several AAV serotypes by facilitating the trafficking of AAV particles from the cell membrane to the *trans*-Golgi network, which further contributes to AAV-specific cellular tropism [14, 15].

Following cell surface receptor binding, AAV particles are internalised by endocytosis. Reports have suggested that this may occur through several different mechanisms including clathrin- and caveolin-mediated endocytosis [16, 17], macropinocytosis [18, 19], and clathrin-independent endocytosis mediated by clathrin-independent carriers (CLICs) [20]. These studies suggest that many routes of AAV entry exist that are likely dependent on the capsid serotype, host cell type, and the presence of specific receptors and co-receptors [21]. Once internalised, AAV particles must escape from endosomal compartments into the cytosol. An important step in endosomal escape is the exposure of the hidden phospholipase A2 domain in the N-terminus of the viral capsid protein

VP1, which is partially triggered by acidification of the endosome [22, 23]. This process is activated by the gradual transition of endosomes from early to late stage and is partially reliant on vacuolar H^+-ATPases that pump protons into the vesicular lumen [24]. The phospholipase A2 domain consequently induces the breakdown of lipids in the endosomal membrane into fatty acids and lysophospholipids to enable virion escape [25-27].

Following their escape into the cytosol, AAV particles accumulate around the perinuclear space and traverse through nuclear pore complexes directly into the nucleus [28, 29]. Their transport is facilitated by nuclear localisation sequences present in the four basic regions (BR1-4) of the VP1/2 region of the viral capsid, which are exposed during endosomal sorting [25, 30]. Once inside the nucleus, the AAV genome is released from the viral capsid to enable conversion of the ssDNA genome into a double-stranded DNA (dsDNA) sequence, which is a key limiting step in AAV transduction. This has been suggested to occur through either second strand synthesis or the annealing of complementary plus and minus strands of the AAV genomes [31, 32]. Packaging of the AAV genome into capsids occurs from the 3' end of the plus and minus strand of the dsDNA sequence, resulting in a 50:50 population of AAV particles that contain either version of the genome [33, 34]. In the absence of a helper virus, such as adenovirus or herpes virus, wildtype AAV is replication defective and will establish latency by preferentially integrating into a specific site in chromosome 19 of the host cell genome [35, 36]. However, in the presence of a helper virus, AAV genomes can replicate to form new virions, which emerge from the host cell by helper virus-mediated cell lysis.

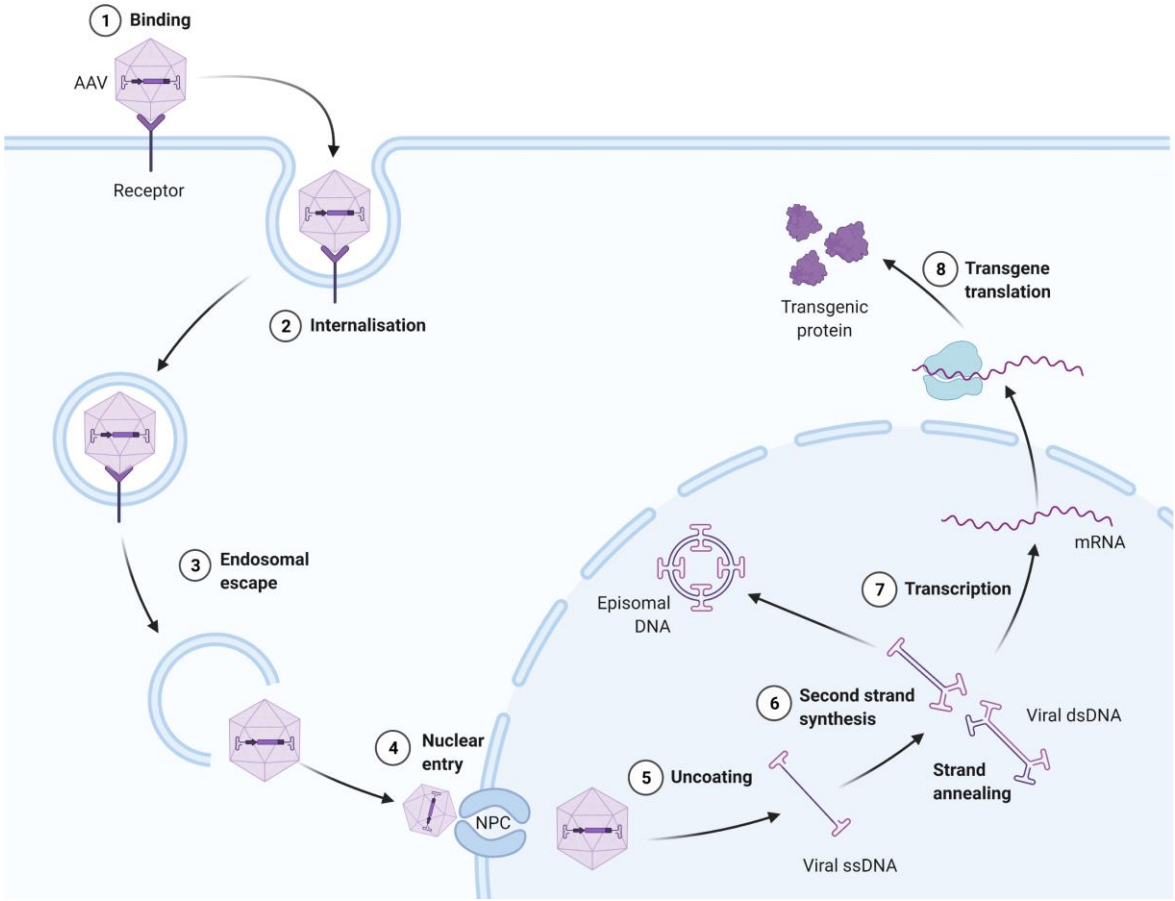

Figure 1.2. Recombinant AAV transduction pathway. Transduction of recombinant AAV vectors requires several successful steps for expression of the transgenic protein. (1) The transduction pathway is initiated by interactions between the AAV capsid and specific cell surface primary glycan and secondary proteinaceous receptors. (2) Successful receptor binding enables AAV internalisation through various endocytic pathways. (3) AAV vectors are exposed to the acidic pH of endosomal compartments to promote their escape into the cytosol. (4) AAV particles accumulate around the perinuclear region prior to entry into the nucleus through nuclear pore complexes (NPCs). (5) Once in the nucleus, AAV vectors are uncoated to release the ssDNA genomes which undergo (6) either second strand synthesis or strand annealing to create a double stranded DNA (dsDNA) intermediate product. dsDNA products can circularise and concatenate to form episomal DNA structures. (7) Transcription and (8)

translation are mediated by the host machinery for expression of transgenic proteins. Adapted from 'AAV Vector Infection', by BioRender.com.

1.1.3 Use in gene therapy

In order to manufacture a recombinant AAV vector for gene therapy, the *rep* and *cap* genes are removed from the AAV genome and replaced by a transgenic DNA sequence [1]. All traces of the viral DNA are removed from the AAV genome except ITR sequences, which are key for AAV replication and packaging during vector production. The removal of viral DNA helps to minimise the immunogenicity and cytotoxicity of recombinant AAV vectors for their use in gene therapy. The transgenic genome can be easily manipulated using molecular techniques, although must remain within the restrictions of the 4.7 kb packaging limit. In the absence of the *rep* and *cap* genes, AAV is unable to replicate, even in the presence of a helper virus, and thus loses the ability to integrate into the host genome [36]. Following second strand synthesis, the dsDNA recombinant AAV vector genome circularises and concatenates to form episomal DNA constructs that autonomously persist in host cell nuclei (Figure 1.2) [37, 38]. This enables long-term persistence and transgene expression, which is particularly important in the treatment of post-mitotic cells. The rate-limiting second strand synthesis step can be overcome with the use of a self-complementary AAV vector, where both strands are packaged into a single genome that can refold upon uncoating to produce a dsDNA construct [39].

A typical recombinant AAV transgenic genome includes a promoter, transgene, and transcription termination signal. Many therapeutic AAV vectors include strong ubiquitous promoters that will enable a high level of transgene expression in

transduced cells, such as a cytomegalovirus (CMV) or a hybrid CMV enhancer fused to chicken β-actin promoter (CAG) [40]. However, increased specificity and reduced off-target expression can be achieved with the use of cell-specific promoters. Increased transgene expression can be attained with the use of additional *cis*-regulatory elements such as the woodchuck hepatitis post-transcriptional regulatory element (WPRE) [41, 42]. The choice of AAV capsid serotype allows for a degree of increased tissue tropism. The majority of AAV gene therapy trials in clinical development target diseases of the central nervous system (CNS) (including the brain and eye), liver, and striated muscle, in part due to the natural tropism of wildtype AAV vectors [1]. Many gene therapies currently in development treat loss-of-function mutations in monogenic autosomal recessive or X-linked diseases with gene supplementation. Following the success in treating these diseases, treatments have been extended to gene editing via the incorporation of CRISPR/Cas (clustered regularly interspaced short palindromic repeats/CRISPR associated protein) components, thus greatly increasing the potential disease targets of gene therapies [43].

1.2 Anti-viral immune responses

1.2.1 Innate immunity

Innate immunity is the first line of defence against microorganisms such as viruses. Initial detection is mediated by a series of pattern recognition receptors (PRRs) that survey the intracellular and extracellular environment for conserved pathogen-associated molecular patterns (PAMPs), such as viral DNA, RNA, and surface glycoproteins that are indicative of infection [44]. PRRs are typically expressed by leukocytes, however are also present or induced in many other cell types. Detection of

PAMPs by host cells leads to the rapid expression of pro-inflammatory cytokines and interferons, which are critical in initiating innate and adaptive immune responses [45]. The primary family of membrane bound PRRs are toll-like receptors (TLRs) which are localised to endosomal and cell surface membranes. Within this family TLR3, TLR7, TLR8, and TLR9 are nucleic acid sensors that are exclusively found within endosomes so to minimise exposure to self-DNA or -RNA [46]. TLR3 detects double-stranded RNA (dsRNA) [47], TLR7 and TLR8 recognise single-stranded RNA (ssRNA) [48], and TLR9 is activated by DNA containing unmethylated CpGs which are abundant in microbial but rare in vertebrate genomes (i.e. 60-90% of mammalian CpGs are methylated) [49, 50] (Figure 1.3). Conversely, TLR2, TLR4, TLR5, and TLR6 are located on the cell surface membrane and detect microbial lipids, lipoproteins, and proteins [51], however only TLR2 and TLR4 are involved in recognition of viral proteins [52]. Conversely, non-membrane bound PRRs are typically located in the cytosol and detect DNA or RNA nucleic acids. A major family of RNA-sensing PRRs are the retinoic acid–inducible gene-I (RIG-I)–like receptors, which detect viral RNA [53]. RIG-I detects 5'-triphosphorylated RNA (a common feature in viral genomes) [54, 55], melanoma differentiation–associated protein 5 (MDA5) is activated by long dsRNA (>2 kb) [56], and laboratory of genetics and physiology 2 (LGP2) is a regulator of RIG-I and MDA5 [57]. Cyclic guanosine monophosphate–adenosine monophosphate (cGAMP) synthase (cGAS) [58, 59] is considered the key cytosolic DNA sensor [60] and can be activated by dsDNA and the stem-loop structures of viral ssDNA [61, 62]. Activation of cGAS induces production of the secondary signalling dinucleotide cGAMP from GTP and ATP [59, 63], which in turn activates the endoplasmic reticulum–bound stimulator of interferon genes (STING) and is small enough the traverse the cell membrane [64, 65].

Many of these PRR-mediated immune pathways converge on a series of transcription factors to induce pro-inflammatory cytokine and interferon expression. Typically, the transcription factor nuclear factor kappa B (NF-κB) mediates upregulation of pro-inflammatory cytokines, while interferon regulatory factors (IRF) induce expression of type I interferons [51]. All members of the TLR family induce NF-kB–mediated pro-inflammatory cytokine expression and many activate members of the IRF family to induce type I interferon expression [66]; cGAS induces activation of NF-kB and IRF3 [67]; and RIG-I-like receptors activate NF-kB, IRF3, and IRF7 [53] (Figure 1.3).

Interferon-mediated responses are coordinated by signalling via the Janus kinase–signal transducer and activator of transcription (JAK-STAT) pathway to induce expression of hundreds of interferon-stimulated genes (ISGs) [68]. In response to viral infection, ISGs function to inhibit all stages of their life cycle including viral entry, translation, replication, and release. Pro-inflammatory cytokines, such as tumour necrosis factor (TNF)-α, interleukin (IL)-1β, and interferon (IFN)-γ, are key in driving inflammatory processes through increasing vascular permeability and stimulating leukocyte proliferation and differentiation [69, 70]. A subset of cytokines, termed chemokines, are involved in mediating the chemotaxis of leukocytes to the site of infection [71]. The coordinated efforts of these various cytokines result in a regulated cell-mediated inflammatory response to viral infection.

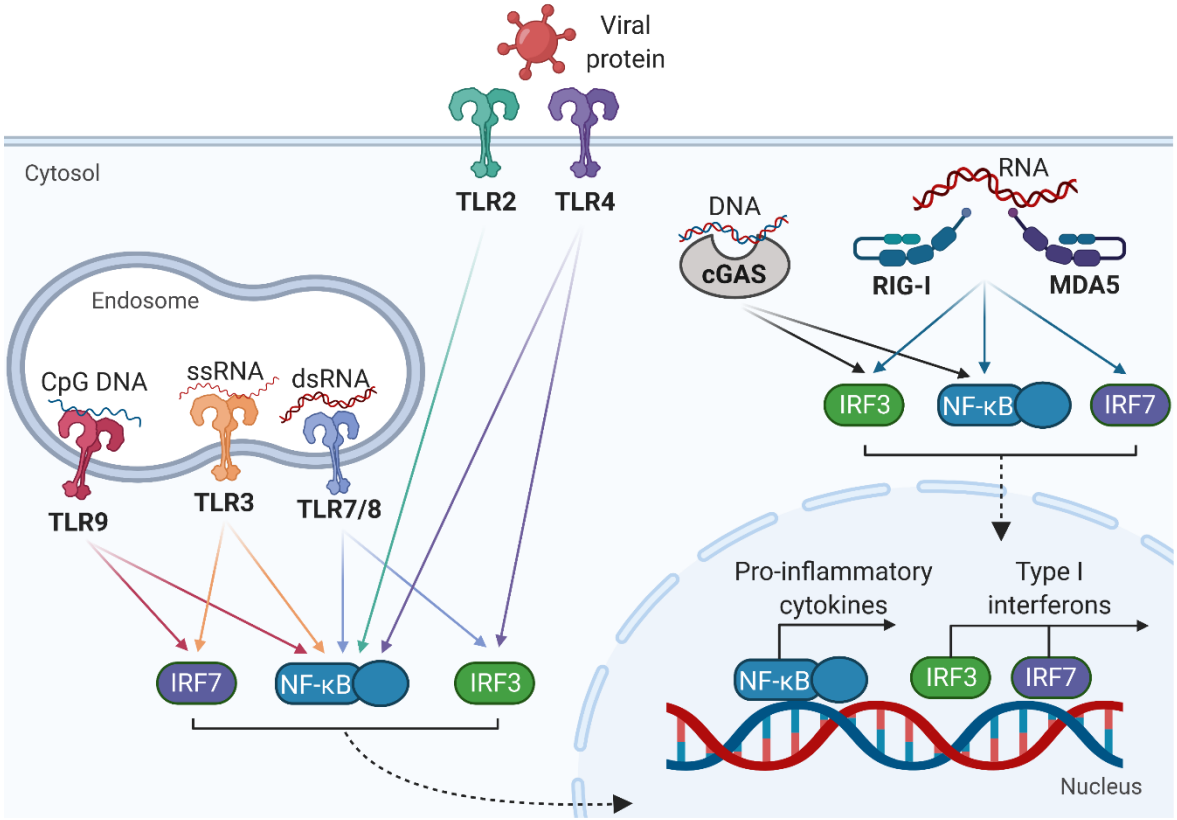

Figure 1.3. Pattern recognition receptor–mediated innate immune pathways to viral infections. Toll-like receptor 9 (TLR9), TLR3, TLR7, and TLR8 are located within endosomes and function to detect viral DNA containing CpG motifs, single-stranded RNA (ssRNA), and dsDNA, respectively. TLR9 and TLR3 induce the transcription factors nuclear factor kappa B (NF-κB) and interferon regulatory factor 7 (IRF7), while TLR7 and TLR8 activate NF-κB and IRF3. TLR2 and TLR4 are located on the cell surface membrane and are activated by viral proteins. TLR2 activates NF-κB and TLR4 induces activation of both NF-κB and IRF3. Cylic GMP AMP synthase (cGAS) is located in the cytosol and detects viral DNA, which in turn activates IRF3 and NF-κB. Retinoic acid-inducible gene-I (RIG-I) and melanoma differentiation–associated protein 5 (MDA5) are located in the cytosol and are activated by viral RNA to induce activation of IRF3, IRF7, and NF-κB. The IRF and NF-κB transcription factors induce type I interferon and pro-inflammatory cytokine expression, respectively, which mediate anti-viral immune responses.

1.2.2 Cellular immunity

All leukocytes can be broadly divided into two main developmental lineages, either deriving from a common myeloid or lymphoid progenitor [72]. Cells of a myeloid lineage are typically limited to macrophages, granulocytes (neutrophils, basophils, eosinophils, and mast cells), erythrocytes, and megakaryocytes, while those of a lymphoid lineage include T cells, B cells, and natural killer (NK) cells. Dendritic cells can be grouped into either lineage as subsets can arise from both myeloid and lymphoid progenitor cells [73]. Leukocytes are further characterised by their role in mediating immunological responses; cells involved in the innate immune response include macrophages, granulocytes, NK cells, and dendritic cells, while T and B cells are key in mediating adaptive immunity.

1.2.2.1 Innate leukocytes

Cytokine production at the site of viral infection coordinates an innate immune response by recruiting neutrophils, monocytes/macrophages, dendritic cells, and NK cells [74]. These innate leukocytes play an important role in the detection and clearance of viral infection and initiate adaptive immunity through pro-inflammatory cytokine release and antigen presentation. One of the earliest leukocytes to respond to a viral infection are neutrophils. Like many other leukocytes, neutrophils express high levels of PRRs and can thus respond directly to viral infection by inducing expression of various cytokines, toxic proteins, and granular enzymes [75]. Neutrophils are also phagocytic and so can engulf infected cells, thus exposing viral PAMPs to intracellular PRRs [76, 77]. An activity unique to neutrophils is the production of neutrophil extracellular traps (NETs), which are networks of extracellular neutrophil genomic

DNA and various antimicrobial proteins [78]. NETs function to bind, disarm, and destroy microorganisms in the extracellular space and, although have been primarily investigated in the context of bacterial infections, NETs have been associated with anti-viral responses [79, 80].

Macrophages also play an important role in the innate immune response to viral infections through PRR-mediated pro-inflammatory cytokine expression and the phagocytosis of microorganisms and cellular debris [81, 82]. Macrophages are also professional antigen-presenting cells (APCs) and can thus present viral antigens, derived either from phagocytosis or direct infection, via major histocompatibility complex (MHC) class II molecules to activate cluster of differentiation 4 (CD4) T cells [83]. Macrophages are typically derived from circulating monocytes in response to an inflammatory stimulus. Upon entry into an infected tissue, the inflammatory microenvironment drives monocyte differentiation into two subtypes of macrophage; pro-inflammatory M1 macrophages or pro-resolving M2 macrophages [84]. M1 macrophages dominant the early stages of an infection by expressing pro-inflammatory cytokines, while M2 macrophages promote return to homeostasis with the expression of anti-inflammatory cytokines. A subset of macrophages, such as microglia in the CNS and Kupffer cells in the liver, are specialised tissue-resident immune cells, which originate during embryonic development and function to maintain active immune surveillance in their resident environment [85].

Another professional APC with an active role in viral infection is the dendritic cell. Like macrophages, dendritic cells detect viral infections through PRRs to induce expression of significant quantities of type I interferons and pro-inflammatory cytokines to

mediate T cell responses [86, 87]. Dendritic cells can be classified as either conventional dendritic cells (cDCs) or plasmacytoid dendritic cells (pDCs). cDCs are the most abundant type of dendritic cell; they are a sentinel cell in surveillance of viral infection and antigen presentation, and primarily populate most lymphoid and non-lymphoid tissues [88]. pDCs are specialised in TLR7- and TLR9-mediated expression of type I interferons in response to viral infections and are mainly located in the peripheral blood and lymphoid tissues [89].

NK cells play a key role in fighting viral infections and can be activated by direct recognition of viral derived products, viral peptide–loaded MHC molecules, and stress-induced ligands, or indirectly by the production of cytokines from infected cells, macrophages, or dendritic cells [90]. Following activation and recruitment, NK cells can kill infected cells by releasing cytotoxic granules such as perforin and granzyme, which permeabilise and apoptose cells, respectively, or by expressing ligands that trigger apoptotic pathways in infected cells [91]. NK cells are considered an innate lymphoid cell (ILC), a class of innate leukocytes derived from a common lymphoid progenitor that lack T cell receptors (TCR). ILCs can be divided into three main groups: group 1 includes NK cells and ILC1s, group 2 includes ILC2s, and group 3 is comprised of ILC3s and lymphoid tissue-inducer (LTi) cells [92]; these classifications are defined based on their ability to produce type 1, 2, or 3 cell-mediated effector immunity, respectively, as discussed in more detail in section 1.2.2.2 [93]. With the exception of NK cells, ILCs are tissue-resident under homeostatic conditions [94]. Group 1 ILCs are typically associated with their involvement in microbial-mediated immune responses. ILC1 cells are the non-cytotoxic equivalent of NK cells which perform a helper function

by expressing inflammatory cytokines, in particular IFN-γ, and, as a tissue-resident cell, are critical in the early stages of viral infection [95].

1.2.2.2 Adaptive leukocytes

Adaptive immunity is mediated by T and B cells, which undertake roles in cell-mediated and antibody responses, respectively. There are two major subtypes of T cells: CD8 (cytotoxic) T cells and CD4 (helper) T cells. CD8 T cells are so named due to their expression of the TCR co-receptor CD8 and can kill infected cells through cytotoxin production and expression of apoptotic ligands to induce apoptosis in infected cells, in a similar mechanism to NK cells [96]. CD4 T cells, however, express the TCR co-receptor CD4 and mediate control of adaptive immune responses through the expression of key cytokines. Activation of T cell–mediated adaptive immune responses are induced by antigen presentation via MHC class I and II molecules, which induce activation of CD8 and CD4 T cells through a direct interaction with their respective TCRs. The TCR is comprised of a highly variable α-chain and β-chain heterodimer that is complexed with multiple CD3 subunits, including CD3γ, CD3δ, CD3ε, and a CD3ζ homodimer [97]. The interaction of a TCR with an MHC molecule recruits the CD8 or CD4 co-receptors, which can bind to conserved regions in the MHC. MHC class I molecules are expressed on all nucleated cells and classically process intracellular antigens by proteasomal degradation for detection by CD8 T cells [98]. The processing of extracellular material for antigen presentation is undertaken by professional APCs (macrophages, dendritic cells, and B cells), which typically utilise the lysosomal pathway to display short peptides on MHC class II molecules for detection by CD4 T cells [99]. However, cross-presentation pathways enable the

display of extracellular antigens on MHC class I molecules, therefore enabling non-APC cells to activate CD8 T cell responses [100]. During cross-presentation, viral antigens are either processed through the vacuolar pathway, where degradation typically occurs in the lysosome, or by the endosome-to-cytosol pathway, where antigens must escape the endosome to be degraded by the cytosolic proteasome; the latter is thought to be a significant pathway for processing of endocytosed viruses such as AAV.

Natural killer T (NKT) cells are a unique subset of leukocytes that occupy the intersection between adaptive and innate immunity. NKT cells perform a range of functions including expression of cytokines and chemokines, cytotoxic activities, cross-talk to other leukocytes, and activation of B cell immunity [101, 102]. These cells express an invariant Vα14–Jα18 TCR which recognises lipids presented on the antigen-presentation molecule CD1d, thus differing from conventional T cells which express diverse TCR complexes [103]. Due to their limited TCR diversity these cells are often termed invariant NKT cells and can typically be found together with conventional T cells throughout the body. In addition to direct activation by antigen-presentation, NKT cells can also be indirectly activated by microbial-mediated immune responses, such as pro-inflammatory cytokine expression following TLR activation [103]. This may explain how viruses, which do not synthesise lipids, can induce NKT cell activation.

Together, innate and adaptive cellular immunity can be categorised into three classes: a type 1, 2, or 3 response [93]. Type 1 immune responses are typically directed against intracellular microorganisms, such as viruses, and include IFN-γ–producing helper (CD4 T_H1 cells and ILC1) and cytotoxic cells (CD8 T_C1 cells and NK cells).

Subpopulations of both CD4 and CD8 T cells are classified by the cytokines they produce, with T_H1 and T_C1 being defined by the production of IFN-γ and TNF-β [93, 104, 105]. In contrast, a type 2 response is typically directed against helminths and venom, while type 3 immunity responds to extracellular bacteria and fungi.

1.2.3 Humoral immunity

Humoral immunity is the extracellular branch of the adaptive immune system which is mediated by the production of specific antibodies by B cells. Following the detection of an antigen by a naïve B cell via its B cell receptor, the antigen is internalised, processed, and displayed on MHC class II molecules for presentation to specialised CD4 T cells (follicular T cells) [106]. This T-cell dependent activation induces B cell proliferation and differentiation through the engagement of the CD40 ligand on T cells with their cognate receptor on B cells. Together with the secretion of cytokines including IFN-γ, IL-4, and IL-21, this interaction induces formation of germinal centres where B cells undergo immunoglobulin isotype switching, somatic hypermutation, and affinity maturation of immunoglobulins, to generate long-lived memory B cells and antibody-secreting plasma cells [107]. In some cases, B cells can be activated in a T cell–independent manner by microbial components, such as unmethylated CpG sequences common in viral genomes [108, 109]. Antibodies, in turn, function to restrict viral infections by several mechanisms, including directly binding to microorganisms to neutralise their infectivity, promoting phagocytosis in leukocytes that can recognise the constant fragment crystallisable (Fc) region of an antibody, promotion of antibody-dependent cellular cytotoxicity by engagement of Fc regions with specific receptors,

and activation of the complement system to promote phagocytosis and lysis of microorganisms [110].

Antibody-bound non-enveloped viruses are detected by the intracellular factor tripartite motif-containing 21 (TRIM21) following infectious entry into cells. In contrast to cell surface Fc receptors, TRIM21 is expressed in all cells and thus occupies a unique position between innate and adaptive immunity [111]. TRIM21 induces rapid neutralisation of viruses by promoting both proteasome-mediated degradation and activation of innate immune pathways to upregulate expression of pro-inflammatory cytokines, interferons, and chemokines [112, 113]. TRIM21-mediated degradation of virions and release of viral genomes can, in turn, enhance RIG-I and cGAS sensing of cytosolic nucleic acids [114].

1.3 The retina

1.3.1 Anatomy

The mammalian retina is comprised of several layers of specialised cells that undertake the detection and initial processing of light stimuli. From the inner to the outer retina, this laminated structure is comprised of the nerve fibre layer, ganglion cell layer, inner plexiform layer, inner nuclear layer, outer plexiform layer, outer nuclear layer, and the inner and outer photoreceptor segments (Figure 1.4). External to this lies the retinal pigment epithelium (RPE) which arises from Bruch's membrane, an elastin- and collagen-rich extracellular matrix that separates the RPE from the choroid [115]. Photoreceptors are the primary light sensing cells in the neural retina and span from their synaptic connections with bipolar cells in the outer plexiform layer

to the RPE. There are two types of photoreceptors, rods, which are the most abundant cell type in the retina and primarily function in dim light to enable night vision, and cones, which function in bright lights and are responsible for colour and high acuity vision [116]. Cones can be further categorised into three subtypes by the wavelength of light they absorb. In humans, the fovea in the central retina is the area of maximal cone density, which has the highest visual acuity. Although the fovea is unique to primates, other mammals, such as mice, have cone-enriched regions [117]. During the process of light detection, or phototransduction, photons travel through the cornea and lens to photoreceptor outer segments; this, in turn, initiates a signal transduction cascade leading to their hyperpolarisation [118]. These changes are detected by bipolar cells, which relay the signal on to ganglion cells, with lateral processing mediated by horizontal and amacrine cells [119]. Ganglion cell axons exit the eye through the optic nerve, which propagates the signal through neurons via the thalamus to the visual cortex.

In addition to the neuronal cells of the retina, there are several types of retinal glial cells (Müller glia, astrocytes, and microglia). Müller glia are the largest cell in the retina and span the entire retinal thickness, which provides a structural role and supports the function and metabolism of retinal neurons, such as through neurotransmitter recycling, ion and water homeostasis, and regulating retinal blood flow [120]. Retinal astrocytes are confined to the nerve fibre layer. They are believed to have migrated from the CNS to the retina via the optic nerve during embryonic development and contribute to the inner blood-retina barrier [121]. Microglia are the resident retinal immune cell and maintain homeostasis in the retina by immune surveillance, phagocytosis of cellular debris, maintaining synaptic structure and function,

neurogenesis, and neural plasticity [122]. Microglia are normally distributed throughout the inner retina, within the ganglion cell layer, inner plexiform layer, inner nuclear layer, and the outer plexiform layer [123].

The RPE is a monolayer of hexagonal pigmented cells firmly attached to the base of the retina and the underlying vascular choroid. Beneath Bruch's membrane and within the choroid is a layer of capillaries termed the choriocapillaris, which is responsible for supplying and removing metabolites from the outer retina [124]. The RPE has several important functions including absorbing scattered light; transport of ions, water, and metabolites; delivery of nutrients to photoreceptors; phagocytosis of shed outer segments; maintenance of photoreceptor excitability; and formation of the outer blood-retina barrier together with endothelial cells of the choriocapillaris [125].

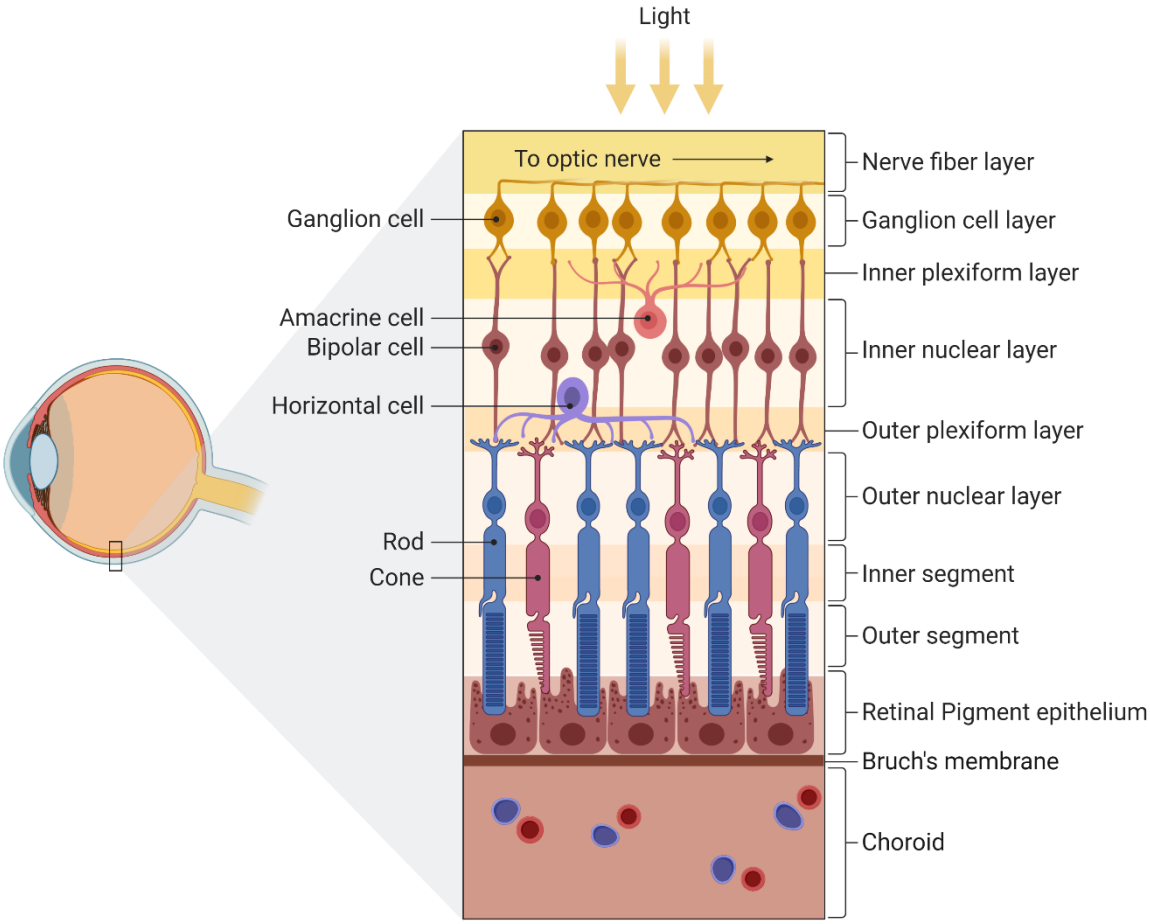

Figure 1.4. Structure of the mammalian retina. Schematic representation of the retinal neural cells that constitute to the laminated structure of the retina. Adapted from 'Structure of the Retina', by BioRender.com.

1.3.2 Immunology

In order to prevent deleterious inflammatory responses from damaging resident non-regenerating and post-mitotic cells, the retina is maintained within an immune privileged environment. The concept of retinal immune privilege has been attributed to several mechanisms including the dual physical barriers of tight junctions between RPE cells (outer blood-retina barrier) and retinal capillary endothelial cells (inner

blood-retina barrier) [126]. Tight junctions are maintained by various transmembrane proteins, including claudins, occludins, and junctional adhesion molecules (JAMs), which are in turn anchored via zonula occluden proteins to the actin cytoskeleton; these barriers are further enforced by basal adheren junctions [127]. These junctions prevent movement of cells and large molecules into and out of the eye, and enable the maintenance of an immunosuppressive environment to subdue inflammation. For instance, retinal neurons have been shown to express CD200 which suppresses microglia-mediated inflammation [128] and RPE cells can express neuropeptides that stimulate immunosuppressive activity in microglia and macrophages [126, 129].

As the retina is excluded from the peripheral immune system, immune surveillance is undertaken by resident microglia cells. Under normal homeostatic conditions, microglia maintain a ramified morphology with multiple projecting cellular processes to enable constant surveillance of the retinal environment [130]. However, upon activation, microglia can retract their processes, adopt an amoeboid morphology, and migrate to the outer retina and subretinal space [122, 131]. In the CNS, microglia express many PRRs that enable intracellular innate immune responses to viral pathogens [132, 133]; several have also been identified in retinal microglia, which are likely to exert similar PRR-mediated responses [134, 135]. Upon activation, microglia induce expression of pro-inflammatory cytokines and chemokines, and, under certain conditions such as viral infection or glaucoma, have been shown to upregulate MHC class II molecules [122, 130, 131, 136].

Although microglia are the primary immune cell of the retina, a small population of perivascular macrophages reside in close proximity with the retinal vasculature [137,

138]. During experimentally-induced inflammation these cells have been shown to upregulate MHC class II molecules and migrate to the sites of injury or damage in the blood-retina barrier, where they phagocytose dead or dying cells [139, 140]. Retinal glial cells can also respond to damage and degeneration in the retina by undergoing reactive gliosis. Although initially induced as a protective response, under sustained stress, chronic gliosis can induce pathological effects including upregulation of pro-inflammatory cytokines, antigen presentation, and breakdown of the blood-retina barrier [141].

Although the blood-retina barrier functions to protect the retina from neuroinflammation, sustained activation of innate immune pathways can induce leukocyte recruitment and infiltration into this immune privileged environment. Expression of pro-inflammatory cytokines, such as IL-1β and TNF-α, can induce expression of adhesion molecules on the luminal surface of the retinal epithelium to enable leukocyte tethering and rolling [142-145]. Engagement of chemokines with G-protein coupled receptors on the surface of leukocytes can induce their activation, which mediates firm adhesion via integrin molecules [127, 146, 147]. Secretion of additional cytokines enables downregulation of tight junction proteins and leukocyte extravasation, which ultimately leads to the breakdown of the blood-retina barrier [127, 148, 149].

1.3.3 Retinal gene therapy

AAV-mediated gene therapies have demonstrated significant potential in the treatment of retinal degenerations, with much of the pioneering work for gene therapy being performed in the eye. The eye is a confined and compartmentalised organ with

a relative immune privileged environment that enables direct delivery of AAV at relatively low concentrations. Voretigene neparvovec, an AAV2 gene therapy encoding retinal pigment epithelium–specific 65 (RPE65) protein for treatment of Leber's congenital amaurosis (LCA) [150], was the first *in vivo* gene replacement therapy to gain US Food and Drug Administration (FDA) approval and has paved the way for other retinal gene therapies. Success has been observed in the treatment of several other retinal dystrophies, such as choroideremia, X-linked retinitis pigmentosa, and Leber's hereditary optic neuropathy [151-153], which have primarily utilised AAV2 and AAV8 capsid serotype vectors due to their ocular tropism [1].

The two primary routes of AAV delivery in retinal gene therapy are intravitreal and subretinal injections. Intravitreal injections are achieved by direct delivery of AAV into the vitreous humour, which enables transduction of anterior segment structures and the inner retina, including retinal ganglion cells and Müller glia [154]. Subretinal injections are technically more challenging and generally require a pars plana vitrectomy in large animals to remove the vitreous fluid; the AAV vector is subsequently delivered through the retina to the subretinal space via a self-sealing retinotomy [155]. Subretinal AAV injections are generally more efficacious for gene therapies targeting cells of the outer retina such as photoreceptors and the RPE [154].

1.4 Immune responses to retinal gene therapy

1.4.1 Immune responses to AAV

AAV vectors are considered minimally immunogenic compared to other major viral vectors such as lentiviruses and adenoviruses [156]. However, several key features of

AAV vectors have the potential to elicit an innate or adaptive immune response, including the capsid, genome, and recombinant transgene. Although retinal inflammation following subretinal and intravitreal AAV vector-mediated gene therapies has been observed, the mechanisms of the immune response are poorly understood. As the immune and inflammatory responses to AAV in the retina could ultimately lead to reduced transgene expression and diminished durability of gene therapy, a better understanding of these immune responses could lead to improved clinical outcomes.

1.4.1.1 Immunity to the capsid

During early stages of transduction, immunological responses to the AAV vector are mediated through detection of epitopes in the proteinaceous capsid shell. One study demonstrated AAV2 and AAV8 capsids to induce TLR2-mediated pro-inflammatory cytokine expression in non-parenchymal liver cells and liver sinusoidal endothelial cells *in vitro*, demonstrating a role of the innate immune system in the detection of viral capsids [157]. Furthermore, structural modifications of AAV capsid proteins appear to drive differential immune responses. For instance, intramuscular injection of macaques with an AAV2 or AAVrh32.33 vector induced a significant capsid-specific T cell response that was not observed with an AAV8 serotype vector [158, 159]. The source of this response was mapped to the VP3 capsid region, suggesting an effect of capsid structure on AAV-mediated immunity.

Since humans are a natural host of AAV, capsid proteins can provide a potential for induction of adaptive immune responses. Concerns for T cell responses to the AAV capsid were first raised in clinical trials for haemophilia B patients following hepatic

delivery of an AAV2 vector encoding the coagulation factor IX (FIX); patients initially demonstrated significant transgene expression, however this gradually decreased to baseline over an eight-week period [160]. Subsequent studies have revealed that a proportion of healthy human donors contained capsid-specific memory CD8 T cells, which may be responsible for this response [161]. In splenocytes approximately 60% of human subjects had an IFN-γ response following stimulation with an AAV capsid peptide library, suggestive of capsid-specific T cell populations [162]. Specific AAV capsid epitopes were shown to be immunogenic and induce CD8 T cell responses, some of which were conserved across multiple serotypes [162]. Nonetheless, not all gene therapy studies have detected AAV capsid-mediated T cell responses [163, 164], thus the effect of pre-existing adaptive immunity currently remains unclear. The presence of CD8 T cells following AAV gene therapy suggests antigen presentation of AAV peptides on MHC class I molecules, likely through cross-presentation pathways that allow for presentation of extracellular antigens [100]. An *in vitro* study demonstrated that AAV antigen presentation was markedly reduced in a hepatocellular carcinoma cell line (HepG2) stably expressing the MHC class I molecule H-2Kb following inhibition of endosomal and proteasomal pathways [165]. The authors suggested that AAV particles rely on the endosomal pathway for internalisation but, upon release into the cytosol, are degraded by the proteasome enabling presentation on MHC class I molecules. Since AAV particles traverse the endosomal pathway, it is possible that antigen presentation could also be achieved with MHC class II molecules to activate CD4 T cells. However, given that the transduction efficiency of AAV in APCs remains unclear, this process has not yet been defined.

In addition to pre-existing cellular adaptive immunity in the population, 40-70% of sampled individuals had pre-existing neutralising antibodies to AAV capsid proteins [166]. The prevalence of humoral immunity in patients poses a potential limitation to gene therapy, where antibodies may bind to AAV particles and reduce transduction efficacy. In the haemophilia B trial, the level of pre-existing neutralising antibodies correlated with the level of transduction [160]. In rhesus macaques, even the presence of low antibody concentrations neutralised the AAV8.FIX vector and consequently reduced transduction efficiency; in animals with undetectable levels of pre-existing antibodies, significant transduction was achieved [167]. Although the effect of circulating antibodies theoretically poses a much greater risk for systemic AAV delivery, antibodies have also been detected in the eye following intravitreal injections [168]. The authors found that the presence of neutralising antibodies prior to injection correlated with weak, decaying, or no transgene expression following intravitreal AAV injections of macaques. Nonetheless, it remains to be seen whether there is a significant impact of pre-existing antibodies on the therapeutic outcome of all gene therapies, as the response will likely be influenced by serotype, dose, and route of administration.

1.4.1.2 Immunity to the genome

Although the removal of the *rep* and *cap* ORFs from the viral genome mitigate the immunogenicity of recombinant AAV vectors, the ITR sequences must be retained, which provide evidence of its viral origin. Furthermore, the presence of DNA within endosomal and cytosolic compartments is, in itself, indicative of a viral infection and can active PRR-mediated responses. For instance, intramuscular injection of

recombinant AAV in wildtype mice elicited TLR9-mediated activation of pDCs and induced a type I interferon response independent of AAV serotype [169]. The TLR9 pathway was critical for activation of a CD8 T cell response against the AAV capsid and transgene, suggesting that this innate pathway is important in mediating adaptive immune responses. The immunogenic serotype AAVrh32.33 has also been shown to elicit a TLR9-mediated CD8 T cell response *in vivo*, which was significantly diminished upon depletion of CpG sequences (the ligands for TLR9 receptors) in the viral genome [170]. These CpG sequences were found throughout the transgenic genome, with 308 in the *lacZ* transgene and 16 in the ITRs; it therefore remains to be seen if a vector with a mammalian transgene with minimal CpG sequences will elicit a comparable response. While AAVs containing self-complementary genomes can provide higher levels of transgene expression *in vitro*, they are associated with greater pro-inflammatory innate immune responses *in vivo* as the double-stranded AAV genome can activate TLR9 more strongly than ssDNA vectors [171]. In immortalised cell lines, primary human hepatocytes, and the hepatocytes of systemically AAV-injected chimeric mice, a dose-dependent upregulation of MDA5 was observed following transduction with a self-complementary AAV vector [172]. Knockdown of MDA5 prevented initiation of this response and increased AAV transduction, suggesting a possible immune response to dsRNA transcribed from the AAV genome. It was hypothesised that reverse mRNA transcripts, generated from inherent promoter activity of the AAV 3'ITR, could anneal to the transgene mRNA to generate immunogenic dsRNA transcriptional intermediates [172]. Together, these studies reveal the ability for AAV, like other viruses, to activate PRRs and elicit both

intracellular and cellular immune responses that can determine the efficacy of gene therapy.

As with capsid proteins, the AAV transgene protein has the potential to elicit adaptive immune responses. Of particular relevance is T cell–mediated immunity to antigen presentation by transduced cells, which may be of increased significance in patients with null mutations where the therapeutic protein has not been previously expressed. As seen with the studies discussed above, TLR9-mediated responses are sufficient to induce a CD8 T cell reaction, suggesting a transgene specific response [169, 170]. AAV-mediated gene therapies targeting the muscle have demonstrated a significantly greater T cell response compared to those targeting other organs [173]. The intramuscular treatment of patients with Duchenne's muscular dystrophy induced significant CD4 and CD8 T cell responses to the transgene dystrophin, which correlated with a loss of long-term transgene expression [174]. Nonetheless, transgene specific T cell responses have been observed in other trials and their presence in retinal gene therapy will be discussed below.

1.4.2 Immune responses in retinal gene therapy

Despite assumptions of immune privilege in the retina, the presence of resident APCs and expression of PRRs make the retina susceptible to AAV-induced immune responses. Key PRRs (TLR9, cGAS, and RIG-I) and downstream pro-inflammatory cytokines and chemokines (IFN-γ, TNF-α, IL-1β, and C-X-C motif ligand 10 (CXCL10)) are upregulated in the retina following AAV gene therapy in wildtype mice and non-human primates, suggesting the activation of intracellular innate immune pathways [175-177]. Several *in vivo* studies have also demonstrated increased

immunohistochemical staining for the microglia activation marker ionized calcium binding adaptor molecule 1 (Iba1) and have observed corresponding morphological changes of microglia following subretinal injection of AAV, suggesting activation of this resident immune cell [176, 177]. Given the implications of pro-inflammatory cytokine and chemokine expression in the eye, these responses have the potential to recruit peripheral leukocytes to the retina. Indeed, following subretinal injection of AAV8 in cynomolgus macaques, co-staining of MHC class I and the macrophage marker F4/80 was detected, suggesting active antigen presentation in macrophage cells [176]. Furthermore, immunohistochemical staining of CD8, CD20, and MHC class II were detected, suggesting the presence of CD8 T cells, B cells, and active antigen presentation in APC cells, respectively [176]. Similar inflammatory responses have been detected in intravitreally injected rats and dogs with retinal staining of macrophages, neutrophils, B cells, CD4 T cells, and CD8 T cells [178, 179]. Together these studies suggest AAV-mediated induction of intracellular and cellular immune responses in the retina.

Signs of retinal inflammation have been identified in gene therapy trials in large animal models following subretinal AAV injections. Several cynomolgus macaques injected with AAV2 and AAV8 serotype vectors demonstrated a dose-dependent increase in capsid-specific neutralising antibodies, despite none present at baseline [180]. A systemic T cell response to the green fluorescent protein (*GFP*) transgene was detected in two of the 14 animals that received high vector doses ($1x10^{11}$ genome copies (gc)/eye), which correlated with the appearance of retinal infiltrates and toxicity [180]. Subretinal injection of cynomolgus macaques with an AAV2tYF vector (with three capsid tyrosine to phenylalanine mutations) expressing the gene *CNGB3* led to

inflammatory responses in the anterior and posterior segments at both $1.2x10^{11}$ and $1.2x10^{12}$ gc/eye, with one animal developing severe inflammatory endophthalmitis; all animals had an increase in neutralising antibodies to the AAV2tYF capsid [181]. Cynomolgus macaques injected with the AAV7m8 demonstrated high expression of the glial activation marker glial fibrillary acidic protein (GFAP) at the highest vector dose ($1x10^{12}$ gc/eye) [182]. Severe retinal inflammation was detected with signs of lymphocytic retinal infiltrates, perivascular inflammation, loss of RPE, and chronic choroidal inflammation [182]. The presence of a dose dependent inflammatory response to AAV2-mediated retinal gene therapy was first observed in humans in a phase 1/2 clinical trial treating *RPE65*-associated LCA where five of the eight high dose patients ($1x10^{12}$ gc/eye) had signs of intraocular inflammation such as anterior uveitis, mild vitritis, and optic disc swelling [183]. In a phase 1/2 clinical trial of AAV2-mediated gene therapy for choroideremia, one of 14 high dose patients ($1x10^{11}$ gc/eye) developed intraocular inflammation in the form of vitritis, retinitis, and choroiditis, which was associated with reduced visual function [151]. Similarly, in a phase 1/2 trial of AAV8-mediated gene therapy for retinitis pigmentosa GTPase regulator (*RPGR*)-associated X-linked retinitis pigmentosa, seven out of nine high dose patients ($0.6\text{-}4x10^{11}$ gc/eye) developed steroid-responsive subretinal inflammation associated with transient changes in retinal sensitivity [152]. Typically, inflammatory responses have been controlled in retinal gene therapy trials using a course of systemic immunosuppression, however, persistent immune responses against the AAV transgene may diminish the long-term durability of the treatment.

Retinal gene therapy trials in animal models and humans demonstrate a significant correlation between vector dosage and the level of AAV-induced retinal inflammation

[184]. However, it is currently unclear whether this intraocular inflammation is directed at the viral capsid, therapeutic cassette, or the transgene product itself. Some studies have implicated the promoter as a potential determinant of inflammation. Vectors expressed in the RPE have been proposed to be associated with a greater risk of retinal toxicity irrespective on the nature of the transgene, with the authors suggesting RPE sensitivity to AAV vectors [177]. Others, have implicated unregulated transgene overexpression driven by ubiquitous promoters as a potential source of retinal toxicity [185]. The route of retinal gene therapy delivery has been strongly implicated in AAV-mediated immune responses. Intravitreal delivery of AAV results in persistent systemic distribution of AAV particles in the blood and lymphatic tissue, suggesting an ability for the vector to leave the eye, likely along aqueous drainage through Schlemm's canal and into systemic circulation [186]. However, following subretinal injections, very little AAV was detected outside of the retina. It seems likely that systemic dissemination of AAV following intravitreal delivery will increase the risk of adaptive immune responses. This is supported by findings that intravitreal AAV injections induce capsid-specific neutralising antibody responses in the serum and intraocular fluid [187, 188]. Neutralising antibody responses can limit transgene expression following intravitreal AAV delivery, suggesting that these responses may be a limiting factor in the therapeutic outcome of intravitreal gene therapy following re-administration to the second eye [168]. Conversely, provided that the AAV vector is delivered via the subretinal route, the presence of pre-existing neutralising antibodies to AAV does not appear to correlate with a higher risk of retinal inflammation or reduced therapeutic efficacy, thus allowing for subsequent AAV gene therapy of the fellow eye [187-189].

1.5 Thesis overview

AAV has emerged as the vector of choice for gene therapies due to its low immunogenicity, good safety profile, and versatility [156]. However, an increasing number of studies have revealed that inherent features of a recombinant AAV vector, including the capsid protein and viral genome, are responsible for activating targeted innate and adaptive immune responses, implicating AAV as a viral immunogen [157, 169-172]. In the context of gene therapy, immune reactions to AAV vectors can greatly differ due to presence of clinical variables such as dose, route of administration, and the presence or absence of pre-existing adaptive immunity to AAV [156]. Due to the compartmentalised and immune privileged nature of the subretinal space, retinal gene therapies have demonstrated significant success in the treatment of retinal dystrophies [150-152, 190]. Despite assumptions of immune privilege, dose-dependent inflammation has been observed in several retinal gene therapy trials [184]. Our current understanding of the cellular immune response to AAV-mediated retinal gene therapy is primarily based upon clinical observations in patients and qualitative data from animal models. Together, these data suggest that peripheral leukocytes can infiltrate the retina and may be a significant feature of intraocular inflammation to retinal gene therapy. Given that it is generally the method of choice for retinal gene therapies targeting photoreceptors and the RPE, this thesis will focus on immune responses to subretinal delivery of AAV during retinal gene therapy.

This thesis will investigate the mechanism of the cellular immune response to retinal gene therapy by characterising and quantifying the infiltrating leukocyte populations. The recruitment of leukocytes to the eye would suggest a resident inflammatory signal,

such as pro-inflammatory cytokines and chemokines, which may enable the chemotaxis and infiltration of circulating leukocytes [127, 175-177] and may explain observations of a transient breakdown of the blood-retina barrier [184]. Since many retinal cell types express PRRs, a resident innate immune reaction to AAV is possible [175, 191, 192]. Unlike innate immunity to bacteria, anti-viral responses are typically directed against intracellular ligands, such as viral nucleic acids [193]. It is therefore possible that the transgenic genome is the predominant source of AAV-mediated immunity. This thesis will investigate the role of the innate anti-viral nucleic acid sensors TLR9 and cGAS in restricting the rate of AAV transduction. Moreover, characterising the exact nature of the immune responses to AAV and devising methods for overcoming these counterproductive responses have become of great interest as gene therapies go from proof of concept to clinical application. This thesis will therefore also investigate the adjunctive use of the immunomodulatory drugs that inhibit innate immune responses in an attempt to enhance the efficacy of retinal gene therapy.

Overall, this thesis aims to:

1. Characterise and quantify the cellular immune response to subretinal AAV retinal gene therapy in mice with the use of quantitative multicolour flow cytometric analysis to identify the presence of key leukocyte populations (Chapter 3).

2. Assess the effect of the *GFP* transgene on the cellular immune response to *in vivo* retinal gene therapy by comparing the leukocyte population with a human therapeutic transgene (Chapter 3).

3. Investigate the effect of the key anti-viral nucleic acid sensors TLR9 and cGAS on AAV transgene expression *in vitro* (Chapter 4).

4. Assess the effect of the immunomodulatory anti-malarial drugs hydroxychloroquine and chloroquine on the efficacy of AAV transduction *in vitro*, *ex vivo*, and *in vivo*, in cell types relevant for retinal gene therapy (Chapters 4 & 5).

5. Assess the effect of the corticosteroid and immunosuppressant dexamethasone on the efficacy of AAV transduction *in vitro* (Chapter 4).

6. Investigate the mechanism of action of hydroxychloroquine-mediated enhancement of AAV transduction (Chapter 6).

2 General materials & methods

2.1 Molecular biology

2.1.1 Restriction digestion

Restriction digestion reactions were undertaken in a 50 µL total volume with 1 µg of DNA, 1 µL of enzyme (20 units), and 5 µL of 10X CutSmart Buffer (New England BioLabs). Control reactions with a single enzyme, no enzyme, or no DNA were run in parallel. Reactions were incubated at the optimal temperature and duration for enzyme activity as recommended by the manufacturer.

2.1.2 Polymerase chain reaction & gel electrophoresis

Custom oligonucleotide primer pairs were designed *in silico* using the Geneious Prime software 2020.2.2. Polymerase chain reaction (PCR) was performed in a total volume of 20 µL with 80 ng of complementary DNA (cDNA) template, 1X KOD Hot Start Master Mix (Sigma-Aldrich), and forward and reverse primers (each at a final concentration of 0.5 µM). PCR conditions consisted of an initial polymerase activation and DNA denaturation step at 95°C for two minutes, followed by 40 cycles of the following conditions: 95°C for 20 seconds to denature, 50°C for 10 seconds for annealing, and 70°C for 10 seconds for extension.

Gel electrophoresis of DNA samples was performed using a 1% agarose gel with an UltraRanger 1 kb DNA ladder (Norgen) for DNA sequences >1 kb in length and a 2% agarose gel with a PCRRanger 100bp DNA ladder (Norgen) for DNA sequences <1 kb in length. Agarose gels were prepared in Tris/acetate/EDTA buffer with 0.5 µg/mL

ethidium bromide. Gels were submerged into an electrophoresis tank containing Tris/acetate/ETDA buffer and DNA samples were pre-stained with a 6X gel loading dye (New England BioLabs) prior to loading into the gel; electrophoresis was performed at 100 V. Following electrophoresis, gels were visualised and photographed using a UV transilluminator (U:Genious, Syngene). Where the DNA was required for downstream applications, the bands were excised with a scalpel under direct visualisation with a blue light. The gel fragments were weighed and the DNA product was extracted using the QIAquick gel extraction kit (QIAGEN) according to manufacturer's instructions. DNA was eluted in 30 µL of nuclease-free water.

2.1.3 RNA extraction & reverse transcription

All surfaces and pipettes were treated with RNaseZap wipes (Invitrogen) prior to RNA extraction to remove environmental RNases. Total RNA was extracted from cell pellets using the RNeasy Mini Kit (QIAGEN) including an additional DNA digestion step with the RNase-free DNase Kit (QIAGEN). Cells were lysed and homogenised in Buffer RLT (QIAGEN) freshly supplemented with 1% β-mercaptoethanol. RNA was extracted following the manufacturer's instructions and eluted in 30 µL RNase-free water. RNA concentrations were quantified using a NanoDrop One Microvolume UV-Vis Spectrophotometer (Thermo Fisher Scientific). Reverse transcription was performed with the Superscript III Kit (Invitrogen) using 1-2 µg RNA and an oligo dT primer (Invitrogen). cDNA products were purified using the QIAquick PCR Purification Kit (QIAGEN).

2.1.4 Quantitative PCR

Quantitative PCR (qPCR) was performed on DNA or cDNA samples to determine gene expression levels using gene-specific primers. qPCR was performed using either the iTaq Universal SYBR Green Supermix (Bio-Rad) or TaqMan assay (Thermo Fisher Scientific). Prior to setting up the reaction, all workspaces and pipettes were disinfected with 10% bleach for 30 minutes to degrade contaminating DNA products. All qPCR assays were prepared on ice using sterile filter pipette tips. Each sample was run in triplicate in opaque Hard-Shell 96-well PCR plates (Bio-Rad). qPCR assays using iTaq were performed in a 10 µL total reaction volume with 5 µL 2X iTaq Universal SYBER Green Supermix (Bio-Rad), 1 µL of both the forward and reverse primer (2 µM), 2 µL of molecular grade water, and 1 µL of the DNA product. TaqMan assays were performed in a 20 µL total reaction volume with 10 µL of 2X TaqMan Fast Universal PCR Master Mix no AmpErase UNG, 1 µL of 20X gene-specific TaqMan assay mix (both Thermo Fisher Scientific), 7 µL molecular grade water, and 2 µL of DNA. The TaqMan assay mix consists of a mixture of gene-specific unlabelled primers, a TaqMan probe with a FAM dye label at the 5' end, and a minor groove binder and nonfluorescence quencher at the 3' end. Controls were run for all qPCR plates with molecular grade water used in place of the DNA template to determine the presence of contaminating DNA sequences. qPCR plates were sealed with a Microseal 'B' PCR plate film (Bio-Rad) and were briefly centrifuged to collect the reaction volume at the bottom of the wells. qPCR reactions were performed using the CFX Connect real-time PCR detection system (Bio-Rad). Before experimental use, the efficiency of the primers and probes was determined using a standard curve prepared with five-fold dilutions of a target DNA

sequence. Primers and probes with 95-105% efficiency were deemed acceptable for experimental use.

The cycle conditions for the iTaq were an initial polymerase activation and DNA denaturation step at 95°C for three minutes, followed by 40 cycles of: 95°C for 10 seconds to denature and 60°C for 30 seconds for annealing and extension. This was followed by a melt curve analysis of 60-95°C with 0.5°C increments (each held for five seconds) to confirm a single distinct peak that indicates the amplified product is a single discrete species. The cycle conditions with the TaqMan assay were an initial step of 95°C for 10 minutes to activate the polymerase, followed by 40 cycles of: 95°C for 15 seconds to denature the DNA and a one minute 60°C annealing and extension step. For gene expression analysis, the gene of interest was normalised to the housekeeping gene *Actb*. The cycle threshold (C_t) was determined based on where the threshold line intersects the reaction curve; this was placed at the beginning of the exponential phase. The three technical repeats were averaged and normalised to the mean of the housekeeper genes (ΔC_t) as per equation 2.1, which were transformed using the function $2^{-\Delta Ct}$ prior to analysis.

$$\Delta C_t = \text{mean } C_t \text{ (gene of interest)} - \text{mean } C_t \text{ (housekeeping gene)} \qquad (2.1)$$

If a treated sample was to be normalised to the control of the group, the difference in ΔC_t between these samples was calculated ($\Delta\Delta C_t$) as per equation 2.2, which was transformed using the function $2^{-\Delta\Delta Ct}$ prior to analysis.

$$\Delta\Delta C_t = \Delta C_t \text{ (treated sample)} - \Delta C_t \text{ (control sample)} \quad (2.2)$$

2.1.5 Protein extraction & quantification

Protein extraction was performed with radioimmunoprecipitation assay (RIPA) lysis buffer supplemented with cOmplete™ EDTA-free Protease Inhibitor Cocktail (PI) (Roche). All retinal samples were homogenised with a hand-held homogeniser and incubated on ice for 30 minutes. Protein samples were centrifuged at 10,000 xg for 20 minutes at 4°C and the supernatant was stored on ice until protein quantification.

The total protein concentration was determined using the Pierce BCA Protein Assay Kit (Thermo Fisher Scientific) as per the manufacturer's instructions. Protein samples were diluted 1:5 with lysis buffer and 10 µL of the diluted protein sample was used for quantification. The colourimetric absorbance of each sample and a standard curve of bovine serum albumin (BSA) (125-2000 µg/mL) was measured at 595 nm using an iMark Microplate Absorbance Reader (Bio-Rad).

2.1.6 Western blot analysis

Protein samples were combined with 6X Laemmli loading buffer to a final 1X concentration and were denatured by heating to 95°C on a hot block. Protein samples and BLUeye prestained protein ladder (Sigma-Aldrich) were loaded onto Criterion TGX precast gels (Bio-Rad) and subject to sodium dodecyl sulphate polyacrylamide gel electrophoresis (SDS-PAGE) in Tris/Glycine/SDS running buffer (National Diagnostics) at 100 V. The separated proteins were transferred onto a polyvinylidene difluoride (PVDF) membranes using the TransBlot Turbo (Bio-Rad) at 2.5 A. The

transfer was performed for seven minutes for proteins 5–150 kDa in size and for 10 minutes for proteins >150 kDa.

The membranes were washed in phosphate buffered saline (PBS) supplemented with 1% Tween-20 (PBS-T) (for analysis with horseradish peroxidase (HRP)-conjugated antibodies) or Tris-buffered saline (TBS) (for fluorophore-conjugated antibodies) for seven minutes. The membranes were blocked with 3% BSA in PBS-T for 45 minutes (for HRP-conjugated antibodies) or 5% donkey serum in TBS supplemented with 1% Tween-20 (TBS-T) for one hour (for fluorophore-conjugated antibodies) at room temperature with gentle agitation. Membranes were incubated in primary antibodies as per Table 2.1 for one hour. Membranes were washed three times for seven minutes each in PBS-T (for HRP-conjugated antibodies) or TBS-T (for fluorophore-conjugated antibodies). Membranes were subsequently incubated in secondary antibodies as per Table 2.1 for 30 minutes. Membranes were washed another three times for seven minutes each with PBS-T or TBS-T and the excess liquid was removed. For membranes with HRP-conjugated secondary antibodies, the protein ladder was marked using a WesternSure pen (LI-COR Inc.) and the membranes were incubated with the Clarity Western enhanced chemiluminescence substrate (Bio-Rad) according to the manufacturer's instructions. Membranes blotted for β-actin were subject to an additional two minute incubation with fresh chemiluminescence substrate to enhance detection. Membranes were imaged using the Odyssey Fc imaging system (LI-COR Inc.) using the chemiluminescence channel. Membranes with fluorophore-conjugated secondary antibodies were protected from light and left to completely dry before imaging with the 700 nm and 800 nm channels.

Table 2.1. Western blot primary and secondary antibody conditions.

Target	Host species	Primary antibody concentration	Primary antibody buffer	Secondary antibody conjugate	Secondary antibody buffer
GFP	Rabbit	1/10,000	3% BSA in PBS-T	HRP	3% BSA in PBS-T
β-actin	Mouse	1/10,000	3% BSA in PBS-T	HRP	3% BSA in PBS-T
ABCA4	Rabbit	1/1,000	1% donkey serum in TBS-T	800CW	TBS-T
α-tubulin	Mouse	1/2,000	1% donkey serum in TBS-T (for ABCA4 blot) TBS-T (for Histone H3 blot)	680RD	TBS-T
Histone H3	Rabbit	1/1,000	TBS-T	800CW	TBS-T

GFP, green fluorescent protein; BSA, bovine serum albumin; PBS-T, phosphate buffered saline–(tween 20); HRP, horse raddish peroxidase; ABCA4, ATP binding cassette subfamily A member 4; TBS-T, Tris buffered saline–(tween 20).

2.2 Plasmid vector cloning

2.2.1 DNA ligation & transformation

DNA ligation reactions were performed in 20 µL reaction volumes with 1 µL of T4 DNA ligase, 2 µL of 10X T4 DNA ligase buffer (both New England BioLabs), and 70 ng of the vector DNA in a 1:3 molar ratio of vector to insert. The following controls were run in parallel: no insert DNA to check for vector re-circularisation, no insert DNA or ligase to determine if the vector was digested, and no vector and insert DNA to check for

contaminating DNA. Ligation reactions were performed at room temperature overnight.

The products of the ligation reaction were transformed into XL-10 Ultracompetent *E. coli* cells (Strategene). 2 µL of 1.43 M β-mercaptoethanol was added to 50 µL of the cells on ice and were stirred every two minutes for 10 minutes with a sterile pipette tip. 5 µL of each of the ligation reactions, including the controls, or the 1/10 diluted pUC18 positive control plasmid (Strategene) were added to the prepared cells. Samples were mixed with a sterile pipette tip and incubated on ice for 30 minutes. The reactions were subsequently heat shocked at 42°C in a water bath for 30 seconds and subsequently incubated on ice for two minutes. Samples were spread with a sterile spreader onto a Luria's broth (LB)-agar plate supplemented with 100 µg/mL ampicillin and the plates were incubated in a 37°C incubator overnight. The number of colonies on each plate was used to estimate the efficiency of the ligation reaction. Colonies from plates transformed with the vector and insert were picked with a sterile pipette and placed into 4 mL of LB media supplemented with 100 µg/mL ampicillin. These starter cultures were incubated for 18 hours in a 37°C shaker at 250 rpm.

2.2.2 Plasmid extraction & amplification

Glycerol stocks were prepared by mixing 500 µL of the starter cultures with 50% glycerol and were frozen at -80°C. The ligated DNA plasmid was extracted from the *E.coli* cells with the endotoxin-free Zyppy plasmid miniprep kit (Zymo Research) according to manufacturer's instructions. DNA was eluted in 30 µL of nuclease-free water.

For vector production, vector plasmids were amplified using a Mega kit (QIAGEN). Glycerol stocks were picked with a sterile pipette tip and placed into 5 mL LB media supplemented with 100 μg/mL ampicillin. The cultures were incubated for eight hours in a 37°C shaker at 250 rpm. Subsequently, the cultures were diluted 1:500 into 0.5 or 2.5 L of LB media with ampicillin depending on whether the plasmid was a high or low copy plasmid, respectively (Table 2.2). These cultures were incubated overnight in a 37°C shaker at 250 rpm. Plasmids were extracted using the Mega kit according to the manufacturer's instructions until the point where plasmids were eluted in 35 mL of Buffer QN (QIAGEN). The eluate was split into two 17.5 mL aliquots and the DNA was precipitated using the PureLink HiPure precipitator module (Thermo Fisher Scientific) according to manufacturer's instructions. The final concentration of plasmid DNA was determined using a NanoDrop Spectrophotometer (Thermo Fisher Scientific).

Table 2.2. Origin of replication and copy number of vector plasmids.

Plasmid	Origin of replication	Low/high copy
CAG.GFP.WPRE	ColE1	High
CAG.nullGFP.WPRE	ColE1	High
pAdDeltaF6	pBluescript	Low
pRep2/Cap8	pBR322	Low

2.3 Cell & tissue culture

2.3.1 Culturing immortalised cell lines

Immortalised cell lines were maintained at 37°C with 5% CO_2 within humidified tissue culture incubators. Immortalised cells were cultured in Dulbecco's Modified Eagle

Medium (DMEM) supplemented with 10% fetal bovine serum (FBS), L-glutamine (2 mM), penicillin (100 U/mL), and streptomycin (100 μg/mL) (complete DMEM) (all Gibco, Thermo Fisher Scientific). Cells were maintained in T-75 flasks (Sarstedt) and passaged twice a week after reaching 80-100% confluence. To passage the cells, the old media was removed from flasks and the cells were washed in warm sterile PBS. TrypLE Express (Gibco, Thermo Fisher Scientific) was added to the cells and the flask was incubated at 37°C for approximately five minutes. Warm complete DMEM media was added to the cells to inactivate the TrypLE and the cells were resuspended by repeat pipetting. An appropriate proportion of the suspension was added to a new T-75 flask and were topped up with fresh complete DMEM media. The remaining cell culture suspension was discarded.

Wildtype and *Cgas*$^{-/-}$ mouse embryonic fibroblasts (MEFs) were provided as a kind gift from Dr Leo James and Dr Sarah Caddy. This knockout cell line was created from *Cgas*$^{-/-}$ mice that have a deletion in the second exon of the *Cgas* gene [194]. For *in vitro* experiments, wildtype and *Cgas*$^{-/-}$ MEFs were seeded at $1.5x10^5$ and $1.8x10^5$ cells per well of a 6-well plate (Sarstedt), respectively.

2.3.2 Harvesting rhesus macaque RPE cells

Primary RPE cells were derived from rhesus macaque (*M. mullata*) eyes collected post-mortem from animals' euthanised for other purposes by the MRC Centre for Macaques, Porton Down, UK. After enucleation, the cornea and lens were removed and incisions were made towards the posterior pole to flatten the eyecup. The retina was removed by blunt dissection and the remaining eyecup was placed in media and stored on ice until processing. To detach the RPE cells, the eye cup was incubated in 3 mL of 2.5%

trypsin (Gibco, Thermo Fisher Scientific) at 37°C for 30 minutes. The trypsin was subsequently neutralised in 5 mL of advanced DMEM supplemented with L-glutamine (2 mM), penicillin (100 U/mL), streptomycin (100 μg/mL), and 10% FBS (all Gibco, Thermo Fisher Scientific). The eye cup was repeatedly washed with the media to detach the RPE cells. Once the media was saturated with cells, the suspension was transferred to a tube and the process was repeated twice more. The cell suspension was centrifuged at 300 xg for five minutes and the pellet was resuspended in advanced DMEM. RPE cells from a single eye were seeded into three wells of a 6-well plate. Cells were maintained at 37°C in a humidified environment maintained with 5% CO_2 and passaged a maximum of two times to prevent loss of the epithelial phenotype.

2.3.3 Culturing human retinal tissue *ex vivo*

Fresh human retinal explants were collected with informed consent during routine retinal detachment surgery where a retinectomy was clinically indicated. The procedure was approved by the UK National Research Ethics Committee (ref: 10/H0505/8). Small retinal fragments approximately 500 μm in diameter were obtained using the 23-gauge cutter of a surgical vitrectomy system (Constellation Vision System, Alcon). Within one hour of tissue collection, individual retinal fragments were transferred using a Pasteur pipette into organotypic culture inserts (Falcon, Corning) within 24-well plates. The retinal explants were cultured in 500 μL (100 μL inside and 400 μL outside the insert) of Neurobasal-A medium supplemented with L-glutamine (0.8 mM), penicillin (100 U/mL), streptomycin (100 μg/mL), 2% B-27 Supplement, and 1% N-2 Supplement (all Thermo Fisher Scientific). Samples were maintained at 34°C in a humidified 5% CO_2 environment.

2.3.4 Cell & tissue treatment

A 0.15 M stock solution was created by weighing hydroxychloroquine sulphate or chloroquine diphosphate (both Acros Organics, Thermo Fisher Scientific) in a fume hood and dissolving in water. The solution was aliquoted and stored at -20°C for up to one month. The 0.15 M stock solution was further diluted to a 1.5 mM working stock solution in DMEM prior to further serial dilutions in DMEM. The media from cells or tissue was removed, and media containing the appropriate concentration of hydroxychloroquine or chloroquine was added. Cells and tissue were incubated in the hydroxychloroquine or chloroquine containing media for one hour prior to AAV transduction.

A 1.9 mM dexamethasone phosphate solution (Dropodex, Rayner) was diluted directly in DMEM media to achieve the appropriate concentrations. For incubation in dexamethasone 24 hours prior to AAV transduction, cells were seeded directly in media containing the appropriate concentration of dexamethasone. For treatment six hours prior to transduction, the media from cells was removed and the dexamethasone-containing media was added.

MEF cells were treated with 754.6 μM of the oligodeoxynucleotide (ODN) sequence CpG-A (5'-GGGGGACGATCGTCGTCGGGGGG-3') (Integrated DNA technologies) 30 minutes prior to transduction. The CpG-A sequences were modified to contain phosphorothioate bonds between each base to protect the DNA from nuclease degradation.

2.3.5 AAV transduction

For immortalised cell lines, cells were counted using either a manual Neubauer Improved haemocytometer (Hawksley) or a TC20 Automated Cell Counter (Bio-Rad) 24 hours after cell seeding. The volume of virus used to achieve a specific multiplicity of infection (MOI) was calculated based on the total number of cells and the titre of the AAV using equation 2.3. The AAV vector was subsequently added directly to the tissue culture well.

$$\text{Volume of virus (mL)} = \frac{\text{MOI x total cell no.}}{\text{AAV titre (genome copies/mL)}} \qquad (2.3)$$

2.3.6 Cell fractionation

Wildtype MEF cells were separated into nuclear, mitochondrial, and cytosolic fractions using the Cell Fractionation Kit (Abcam). Prior to fractionation, the cells were detached with TrypLE Express (Gibco, Thermo Fisher Scientific) and centrifuged at 300 xg for five minutes. The supernatant was discarded and the cells were washed in pre-warmed PBS before centrifugation at 300 xg for five minutes at 4°C. This was step was repeated twice more to ensure all AAV not internalised into cells was removed. Cells were resuspended in 1 mL of 1X Buffer A (Abcam) and a small volume was reserved for cell counting. The cells were centrifuged at 300 xg for five minutes at 4°C, the supernatant was discarded and cells were resuspended to a concentration of $4x10^6$ cells/mL in 1X Buffer A. The remainder of the protocol was followed according to manufacturer's instructions.

2.4 AAV production

AAV vectors were manufactured by co-transfecting HEK293T cells with the following three plasmids:

1. Helper plasmid (pAdΔF6) encoding the adenovirus genes E4, E2a, and VA to mediate AAV replication

2. Rep/Cap plasmid (pRepCap) encoding genes for AAV replication and capsid synthesis

3. Transgene plasmid (pTransgene) encoding the AAV transgenic genome containing a promoter, transgene, and bovine growth hormone pA tail flanked by ITR sequences

2.4.1 HEK293T cell culture

HEK293T cells were seeded into three T-175 flasks (Sarstedt) and cultured in complete DMEM. Once confluent, three T-175 flasks were seeded into two HYPERFlasks (Corning) for each virus manufactured. The HYPERFlasks were carefully topped up with media so to avoid creating bubbles. Each HYPERFlask was gently tapped on the short edge to bring the bubbles to the surface and the bubbles were removed using a pipette. The HYPERFlasks were incubated at 37°C in a humidified environment maintained with 5% CO_2 for 72 hours until confluent.

2.4.2 Transfecting cells

After 72 hours, each HYPERFlask of HEK293T cells was transfected with a total of 500 µg of DNA with the amount of each plasmid depending on its size as described in

Table 2.3. The appropriate amount of each plasmid was supplemented with 150 mM NaCl (prepared in molecular grade water) to a total of 10 mL. In a separate tube, 667 µg polyethylenimine was also supplemented with 150 mM NaCl to 10 mL. The DNA and polyethylenimine were complexed by dropwise addition of the polyethylenimine mixture into the DNA; the complex was subsequently incubated at room temperature for 20 minutes. Transfection media consisting of DMEM supplemented with 2% FBS, L-glutamine (2 mM), penicillin (100 U/mL), and streptomycin (100 µg/mL) was prepared and 50 mL was set aside; the complexed DNA was added to the transfection media. 20 mL of the set aside transfection media was added the now empty complexed DNA tube to collect any residual solution. This was poured into the transfection media containing the complexed DNA. The HYPERFlasks were drained and the full volume of the transfection media containing the complexed DNA was carefully added. The HYPERFlasks were topped up with the remaining transfection media, bubbles were removed per section 2.4.1 and the HYPERFlasks were incubated at 37°C in 5% CO_2 environment for a further 72 hours.

Table 2.3. Calculations to determine the amount of each plasmid required for AAV production.

Plasmid	**Size (kb)**	**Amount per transfection (µg)[1]**
pAdΔF6	15.4	15.4 x R
pRepCap	7.3	7.3 x R
pTransgene	T	T x R
Total	**K**	**500**

[1] Ratio (R) calculated as 500/K.

2.4.3 Harvesting & lysing cells

After 72 hours, 250 mL of media was discarded from the HYPERFlasks before shaking vigorously to mechanically detach the cells. This was confirmed by visualising the cells under a light microscope. The cell suspension from each HYPERFlask was poured into a separate 400 mL centrifugation bottle and were centrifuged at 1,200 xg for 10 minutes at 20°C. The supernatant was carefully removed to leave 20–50 mL of media. The remaining supernatant was used to resuspend the cell pellet and was transferred into a 50 mL tube. The cell suspension was centrifuged again at 1,200 xg for 10 minutes at 20°C. The supernatant was removed and the cell pellet was resuspended in 15 mL lysis buffer (1 M Tris and 150 mM NaCl in water, pH 8.5). 500 µL of lysis buffer supplemented with PI (prepared with one PI tablet in 1 mL lysis buffer) was added to this lysate. The lysates were frozen at -80°C for at least one hour, after which the samples were thawed in a 37°C water bath for 15 minutes. This was repeated twice more and on the final freeze/thaw cycle the lysate was stored at -80°C.

2.4.4 Isolation of AAV particles

The lysates were thawed in a 37°C water bath for 20 minutes. 15 µL of benzonase endonuclease enzyme (Merck Millipore) was added to the thawed lysate to a final concentration of 150 U/mL and were incubated at 37°C for a further 45 minutes with vigorous shaking every 15 minutes. The lysates were centrifuged at 3,700 xg for 20 minutes at room temperature.

Iodixanol gradients were prepared by the layering fractions with different densities as described in Table 2.4. One AAV preparation, with two lysate aliquots, requires three iodixanol gradients. 7.2 mL of the 15% fraction was pipette directly into the base of a

32.4 ml OptiSeal ultracentrifuge tube (Beckman-Coulter Life Sciences) using a 5 mL long-neck Pasteur pipette. 4.8 mL of the 25% fraction was pipette beneath this layer by carefully passing the pipette through the 15% fraction to the bottom of the ultracentrifuge tube. This was repeated first with 4 mL of the 40% fraction and then with 4 mL of the 60% fraction. The supernatant of the lysate was gently layered on top of the iodixanol gradient and was topped up with lysis buffer if necessary (Figure 2.1). The ultracentrifuge tubes were sealed with caps and centrifuged in 70Ti ultracentrifuge rotor (Beckman-Coulter Life Sciences) at 59,000 rpm for 1.5 hours at 20°C in an Optima ultracentrifuge (Beckman-Coulter Life Sciences). The seal was removed from each tube and an 18G needle was passed into the interface between the 60% and 40% fractions with the bevel kept up. As much of the 40% fraction as possible was collected without disturbing the cell debris in the 25% fraction above (approximately 1–1.5 mL). This AAV containing fraction was collected from all gradients and stored at 4°C overnight.

Table 2.4. Preparations for two iodixanol gradients for isolation of AAV particles.

Fraction	Iodixanol (mL)[1]	5M NaCl (mL)[2]	5X PBS-MK (mL)[2]	H_2O (mL)[4]	Phenol Red (µL)[5]
15%	4	3.2	3.2	5.6	-
25%	5	-	2.4	4.6	20
40%	6.7	-	2	1.3	-
60%	10	-	-	-	20

[1] Iodixanol: OptiPrep density gradient medium (Sigma-Aldrich). [2] 5 M NaCl in molecular biology grade water. [3] 5x PBS-MK: PBS with 5 mM $MgCl_2$ and 12.5 mM KCl. [4] Molecular biology grade water. [5] Phenol Red: 0.5% solution (Sigma-Aldrich).

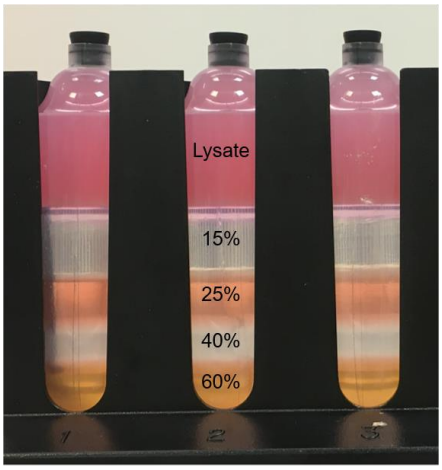

Figure 2.1. Iodixanol gradient for AAV separation prior to centrifugation. HEK293T cell lysates containing AAV particles are layered on top of an iodixanol gradient of 15%, 25%, 40%, and 60% in OptiSeal ultracentrifuge tubes.

2.4.5 Purification & concentration of AAV

The AAV iodixanol fraction was purified and concentrated using an Amicon Ultra 100K filter (Millipore). The Amicon filter was washed with 5 mL of sterile PBS and centrifuged at 3,000 xg for 15 minutes at 20°C; the flow through was discarded. PBS was added to the AAV iodixanol fraction to a total of 15 mL, this was carefully mixed by repeat pipetting. The solution was then applied to the Amicon filter and centrifuged at 3,000 xg at 20°C until the volume was reduced to 500 µL at which point the flow through was discarded. This filter was supplemented with 14 mL of PBS and the solution was mixed by repeat pipetting. The filter was centrifuged again at 3,000 xg until the volume was reduced to 500 µL. This wash was repeated twice more. During the final wash, the Amicon filter was centrifuged until the total volume was reduced to below the 250 µL marker. The AAV concentrate was pipette over the filter 20 times on each side to collect the remaining AAV particles and were separated into 10 µL aliquots

for storage at -80°C. 500 µL PBS was added to the Amicon filter and this was washed over the filter 20 times on each side. The AAV wash was divided into 50 µL aliquots and stored at -80°C.

2.4.6 Titrating AAV & assessing purity

AAV vector genome titres were quantified using qPCR. To remove any contaminating DNA, 1 µL of AAV concentrate or wash was mixed with 1 µL of DNase I, 1 µL of 10X DNase buffer (both New England BioLabs), and 7 µL of molecular biology grade water in a 10µL total reaction. Samples were incubated for 30 minutes in a 37°C water bath and subsequently heated to 95°C on a PCR machine for 10 minutes. The latter step was to terminate the reaction and denature the capsids to release the viral genomes for titration. Samples were stored on ice until titration.

In order to titrate, the AAV samples were diluted 1:10 and 1:100 with water. A five-point 10-fold dilution standard curve was created using the CAG.GFP.WPRE plasmid (1–0.0001 ng). qPCR reactions were performed with 1 µL of the diluted AAV samples using the iTaq method as per section 2.1.4. Primers were directed to the pA tail of the viral genome (forward primer: CCAGCCATCTGTTGTTTGCC; reverse primer: GAAAGGACAGTGGGAGTGGC). Reactions were performed in triplicate as per the reaction conditions detailed in section 2.1.4. The plasmid copy number for the standard curve was calculated based on the size of the plasmid, i.e. 1 ng of the 6,074 bp plasmid equated to $1.53x10^8$ gc. The AAV titres were then interpolated from the standard curve.

The purity of the AAV preparation was determined using SDS-PAGE. 10 µL of concentrated AAV and 24 µL of the AAV wash were stained with 5X protein loading

buffer (National Diagnostics). Samples were heated on a 95°C hot block for 10 minutes and were loaded onto a 10% Criterion™ TGX™ Precast Protein Gel (Bio-Rad) with 10 µL of BLUeye prestained protein ladder (Sigma-Aldrich). Electrophoresis was performed on the protein gel at 100 V for approximately one hour and 45 minutes after which the gel was removed and washed in water with gentle agitation for five minutes. This wash was repeated twice more with fresh water. The protein gel was covered in EZBlue protein stain (Sigma-Aldrich) and incubated at room temperature for one to two hours with gentle agitation until three bands became clearly visible. Three bands should be clearly visible at 87, 72, and 62 kDa, which correspond to the VP1, VP2, and VP3 AAV capsid proteins, respectively. The presence of additional bands would indicate protein contamination in the AAV preparation.

2.5 *In vivo* procedures

2.5.1 Animals

The wildtype mice C57BL/6J were purchased from Charles River, UK and 129S2/SvHsd mice from ENVIGO, UK. Both were housed in the Biomedical Sciences Division, University of Oxford, UK. The *Abca4*$^{-/-}$ mice (129S4/SvJae-*ABCA4*^{tm1Ght}) were provided by Gabriel Travis (David Geffen School of Medicine, University of California, Los Angeles, CA) and bred in the Biomedical Sciences Division, University of Oxford.

Mice were housed in a 12-hour light-dark cycle, with food and water available *ad libitum*. All animal procedures were undertaken in accordance with the Association for Research in Vision and Ophthalmology guidelines for the humane use of laboratory

animals in ophthalmic research, and were approved by local and national ethical and legal authorities.

2.5.2 Anaesthesia & pupil dilation

Mice were anaesthetised by an intraperitoneal injection of ketamine (Vetalar, Boehringer Ingelheim or Narketan, Vetoquinol) at 80 mg per kg of body weight and xylazine (Rompun, Bayer) at 10 mg per kg of body weight. At the end of a procedure, the anaesthetic was reversed by intraperitoneal injection of atipamezole (Antisedan, Zoetis) at 2 mg per kg of body weight. Pupils were dilated whilst the mice were under anaesthesia with sequential drops of phenylephrine hydrochloride 2.5% weight/volume (w/v) and tropicamide 1% w/v (both Minims, Bausch & Lomb); each were allowed to act for 30 seconds.

2.5.3 Subretinal injection

Prior to subretinal injection, mice were anaesthetised and the pupils were dilated as described in section 2.5.2. An additional drop of proxymetacaine hydrochloride 0.5% w/v (Minims, Bausch & Lomb) was applied to the eye for 30 seconds to provide local anaesthesia. A paracentesis was performed by briefly puncturing the mid-peripheral cornea with a 33G needle. This released a small volume of aqueous fluid to lower the intraocular pressure and minimise the risk of trans-scleral reflux during or after subretinal injection. Viscotears Liquid Gel (Alcon) were liberally applied to the corneal surface before placement of a 5 mm glass coverslip over the eye to allow for visualisation of the posterior pole. The animal was positioned on a foam operating mat to be viewed under a foot pedal-controlled Leica microsurgical operating microscope. A NanoFil 10 µL syringe was attached to a 35G NanoFil needle (both World Precision

Instruments) and the injection material was drawn up. The eye was stabilised by grasping the superior rectus muscle with notched forceps and the needle was passed through the sclera and into the subretinal space. Once the bevel was in the subretinal space, the superior rectus muscle was released and the syringe carefully depressed to inject the material into the subretinal space. This injection created a subretinal bleb. The needle was carefully withdrawn and the cover slip was removed. A drop of the antibiotic chloramphenicol 0.5% w/v (Minims, Bausch & Lomb) was applied to the eye followed by Viscotears to prevent corneal dehydration during recovery. All AAV vectors injected were diluted in PBS to achieve the appropriate concentration. All subretinal injections in this thesis were performed by Dr Alun Barnard or Dr Imran Yusuf.

2.5.4 Retinal imaging

Animals were anaesthetised and pupils were dilated as described in section 2.5.2. A drop of hypromellose 0.3% w/v (Blumont Healthcare Ltd.) was applied to the surface of the eye and a polymethyl methacrolate contact lens of specification 3.2 mm diameter, 1.7 mm back optic zone radius, 0.4 mm central thickness, and plano refractive power (Cantor & Nissel Ltd.) was carefully placed onto the eye. Retinal imaging was performed using the Spectralis ophthalmic imaging platform (Heidelberg Engineering) with a 55° lens. The animal was positioned onto a customised platform and aligned to the Spectralis camera. The contact lens was positioned so to allow for optimal imaging. Fundus images were taken using the inbuilt confocal scanning laser ophthalmoscope (cSLO) using the 'High Resolution' (8bits/pixel and 1536 x 1536 pixel resolution) and automatic real-time (ART) mode which averages multiple images into

a single image to increase resolution. Correct alignment was achieved using the near-infrared reflectance (NIR) mode (815 nm wavelength diode laser) and the camera arm was moved to focus on the retina with the image centred on the optic disc. The camera was positioned to align the optic nerve to the centre of the camera field of view, the dioptric focus was adjusted to focus on the plane with the highest infrared reflectance, thought to be the RPE [195]. The sensitivity was adjusted to the maximum brightness without overexposing the image. An image was taken in the NIR mode with an ART of 25 and the normalisation was turned off and kept off for the remainder of imaging to allow for quantification of the images. GFP fluorescence was viewed within this focal plane using the Spectralis blue autofluorescence (BAF) mode with an excitation laser at 486 nm and an emission filter between 498 and 720 nm. BAF images were taken with a range of sensitivities between 60 and 107 with an ART mode of 25.

Spectral domain–optical coherence tomography (SD-OCT) imaging was acquired with the mouse in the same position as for the cSLO imaging on the NIR mode. Using a 55° lens, images were taken with eight equally distributed radial scans centred on the optic nerve at an ART of 25. Total retinal thickness was measured at approximately 3700 µm from the optic disc using the Spectralis software with a calliper to measure from the internal limiting membrane to the RPE basement membrane (the innermost layer of Bruch's membrane) (Figure 2.2) [196].

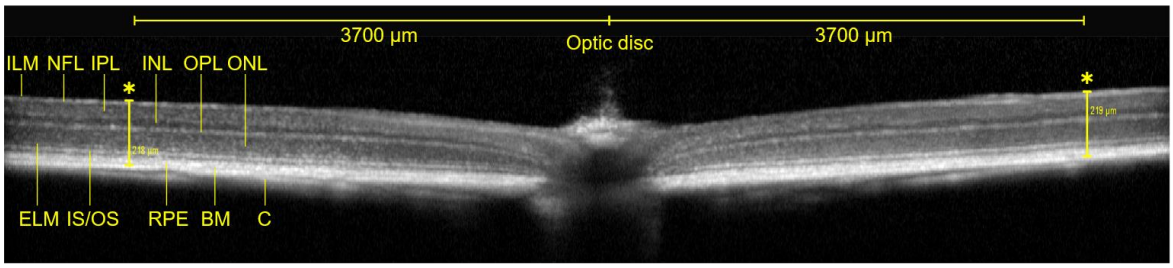

Figure 2.2. Measurement of total retinal thickness of spectral domain optical coherence tomography (SD-OCT) of the mouse retina. A SD-OCT image of a PBS injected mouse eye. Total retinal thickness (indicated with *) is measured from the internal limiting membrane (ILM) to the Bruch's membrane (BM) 3700 µm from the optic disc. NFL: nerve fibre layer; IPL: inner plexiform layer; INL: inner nuclear layer; OPL: outer plexiform layer; ONL: outer nuclear layer; ELM: external limiting membrane; IS/OS: inner segment/outer segment junction; RPE: retinal pigment epithelium; C: choroid.

2.5.5 Tissue collection

Mice were sacrificed by overdose of anaesthetic with 20 mg of pentobarbital (Pentoject, Animalcare) or by cervical dislocation if the mouse was already anaesthetised for a procedure. Death was confirmed using cervical dislocation or decapitation if cervical dislocation was used as the primary method of culling. Eyes were enucleated using curved forceps and dissections were performed in PBS under direct observation with a dissecting microscope. The cornea was punctured with a 30G needle and the cornea was excised with Vannas scissors. The iris was removed, the zonule of Zinn was blunt dissected, and the lens was removed. The optic nerve was cut to its base and retina was carefully separated from the RPE and choroidal tissue.

2.6 Flow cytometry

2.6.1 Processing of MEF cells

MEF cells were detached in TrypLE and resuspended in 1 mL of DMEM media. Cells were centrifuged for five minutes at 600 xg, the supernatant was discarded and cells were washed in 1 mL of PBS to remove residual media. Samples were centrifuged at 600 xg for five minutes and fixed in 500 µL of 4% methanol-free formaldehyde in PBS for 15 min at room temperature. Cells were centrifuged for five minutes at 600 xg and the supernatant was discarded. Cells were washed in 1 mL of 1% BSA in PBS, centrifuged at 600 xg for five minutes and resuspended in 500 µL of 1% BSA in PBS. Samples were stored on ice until assessment. Cells were incubated with the cell viability dye 7-aminoactinomycin D (7-AAD) for five minutes in the dark immediately prior to flow cytometric analysis using a LSRFortessa flow cytometer (BD Biosciences). Wildtype MEFs were stained with 10 µL of 7-AAD and *Cgas*$^{-/-}$ MEFs with 5 µL in a final volume of 500 µL of 1% BSA in PBS.

2.6.2 Flow cytometry of MEF cells

Flow cytometry was performed using the LSRFortessa with a blue laser at the band-pass filter 695 nm/40 mW and 530 nm/30 mW to detect the fluorophores of 7-AAD and GFP, respectively. Events were gated to exclude debris and doublets; a stopping gate of 20,000 events was applied to this gate. Cells expressing GFP were gated for using untransduced controls, and dead (7-AAD^{+}) cells were excluded using a killed cell population control prepared by heating cells to 60°C for 20 minutes. GFP gating was achieved using untransduced cell samples. Analysis was performed using the FlowJo software (v10.7.1; BD Life Sciences).

2.6.3 Retinal dissociation

Dissociation was performed immediately following retinal dissection with the Papain Dissociation System (Worthington Biochemical Corporation). Reagents were prepared according to the manufacturer's instructions and stored at -20°C in individual aliquots. The PBS was carefully removed from the retinae and 250 µL of the papain/DNase solution (20 U/mL papain and 0.005% DNase in Earle's Balanced Salt Solution (EBSS)) was added to each retina. The samples were incubated for 14 minutes in a 37°C water bath and were flicked to dislodge the retinae every two minutes. 500 µL of pre-warmed EBSS was added to each sample to dilute the papain and the samples were centrifuged for five minutes at 300 xg. The supernatant was discarded and the cell pellet was resuspended in a solution of 450 µL EBSS, 50 µL ovomucoid inhibitor (10 mg/mL of ovomucoid and BSA), and 25 µL DNase (2000 U/mL). This suspension was carefully layered over 500 µL of ovomucoid inhibitor without mixing the two solutions. The samples were centrifuged at 70 xg for six minutes. The supernatant was discarded and the cell pellet was resuspended in staining buffer (2% FBS, 2 mM EDTA, and 0.1% sodium azide in PBS).

2.6.4 Antibody staining

Antibody staining of dissociated retinal cells was performed in a 96-well round bottom plate (Corning). Cells were transferred into the 96-well plates and centrifuged at 300 xg for five minutes at 4°C. The supernatant was removed by swiftly inverting the plate over the sink and gently blotting on a paper towel. The pellet was loosened by tapping the side of the plate. To wash the cells, 300 µL of staining buffer was added prior to centrifugation at 300 xg for five minutes at 4°C; the supernatant was removed

as before. TruStain FcX PLUS block (BioLegend) was added at a final concentration of 0.25 μg to the cell suspensions in a total volume of 50 μL to block non-specific binding of antibodies to the leukocyte Fc receptors CD16 and CD32; cells were incubated on ice for 10 minutes. Without removing the Fc block, cells were stained with fluorophore-conjugated antibodies (all Biolegend) in staining buffer at concentrations according to Table 2.5 in a total volume of 100 μL; cells were incubated on ice in the dark for 20 minutes. The cells were washed three times with up to 300 μL of staining buffer as before. The cell pellets were resuspended in staining buffer and cells were stained with 4′,6-diamidino-2-phenylindole (DAPI) at a final concentration of 0.1 μg/mL five minutes prior to flow cytometric analysis.

The appropriate concentration of each antibody was initially optimised in retinal cells for antigens expressed in the normal retina (CD45, CD11b, CD68) or in splenocytes for those not expressed in the retina (CD3, CD4, CD19, CD11c, and NK1.1). For staining of splenocytes, a mouse spleen was dissected from a C57BL/6J mouse and stored in RPMI 1640 media (low HEPES, low bicarbonate, no glutamine; Gibco, Thermo Fisher Scientific) supplemented with 2% FBS, L-glutamine (2 mM), penicillin (100 U/mL), and streptomycin (100 μg/mL). The spleen was cut in half and the cells were gently pushed out of the spleen membrane and through a 70 μm cell strainer using the rubber tip of a syringe plunger. Cells were repeatedly passed through the strainer until a single cell suspension was achieved; cells were subsequently centrifuged at 70 xg for 7 minutes at 4°C. The supernatant was removed and the cells were resuspended in cold RPMI media prior to antibody staining as per section 2.6.4. The appropriate concentration of antibody was selected based on a combination of maximal

segregation between negative and positive populations, and minimal spread of the negative population.

Table 2.5. Flow cytometry antibodies.

Antigen	Clone	Fluorophore	Staining concentration (µg/mL)
CD45	30-F11	Brilliant Violet 711	0.5
CD45	30-F11	PE	0.5
CD11b	M1/70	APC	0.25
CD68	FA-11	PE	0.25
CD3	17A2	Alexa Fluor 700	5
CD4	RM4-5	Brilliant Violet 785	0.5
CD19	6D5	APC/Fire 750	2
NK-1.1	PK136	PE/Cyanine7	1
CD11c	N418	PerCP/Cyanine5.5	1

2.6.5 Flow cytometry of retinal samples

Compensation on the LSRFortessa (BD Biosciences) was performed using single colour controls prepared with CompBeads (BD Biosciences) and GFP BrightComp eBeads (Invitrogen). Events were gated to exclude debris and doublets; a stopping gate of 20,000 events was applied to this gate. Gating was achieved using a fluorescence minus one (FMO) control for the CD68-PE (clone FA-11) and GFP, which included all fluorophores minus one to account for the spread of the negative population.

Spectral unmixing on the Aurora spectral analyser (Cytek Biosciences) was performed using single colour controls prepared with CompBeads (BD Biosciences), UltraComp

eBeads (Invitrogen) (for CD11c clone N418), GFP BrightComp eBeads (Invitrogen), and dead splenocytes which had been heated at 60°C for 20 minutes. A stopping gate of 500,000 events was applied to all events. Gating was achieved using an FMO control for the fluorophores CD45-PE (clone 30-F11), CD11b-APC (clone M1/70), CD3-Alexa Fluor 700 (clone 17A2), CD4-Brilliant Violet 785 (clone RM4-5), NK1.1-PE/Cyanine 7 (clone PK136), CD11c-PerCP/Cyanine 5.5 (clone N418), and GFP. All data analysis was performed using the FlowJo software (v10.7.1; BD Life Sciences).

2.7 Statistical analysis

All statistical analysis was performed and all graphs were created using the Prism software (version 8.4.3; GraphPad Inc.). Data are presented as mean ± standard error of the mean (SEM). Datasets were tested for normality using a Shapiro-Wilk test. Data that were normally distributed were analysed using a parametric test (t test or ANOVA); paired data were handled accordingly. A one-way ANOVA was used for comparing three or more groups with one independent variable, while a two-way ANOVA was used for comparing multiple groups with two variables. For ANOVA tests, multiple comparison's testing was performed with a Dunnett's test for comparing every mean to a control mean or a Sídák's test for selected pairs of means. Data that were skewed were analysed using a non-parametric test; a Mann-Whitney test was used for non-paired data, a Wilcoxon signed-rank test for two paired groups, and a Friedman's test for three paired groups. For a Friedman's test multiple comparisons testing was performed with a Dunn's test. All statistical tests were performed using an alpha level of 0.05 and two-tail *p* values. If multiple comparisons testing has been performed then the *p* value of the respective comparisons test is described in text.

3 Cellular immune response to retinal gene therapy

3.1 Introduction

Despite the low immunogenicity of AAV and relative immune privilege of the eye [126], dose-dependent inflammatory responses in retinal gene therapy clinical trials have impeded the ability to increase vector doses. In the phase 1/2 dose-escalation trials for *RPE65*-associated LCA, choroideremia, and *RPGR*-associated X-linked retinitis pigmentosa, high dose patients have presented various signs of intraocular inflammation, including anterior uveitis, vitritis, and retinitis [151, 152, 183], suggesting the involvement of a cell-mediated immune response. Monitoring of this response has primarily relied on incidental observations of inflammation in patients, therefore little is known about this cellular immune reaction. Characterising the exact nature of this response, and finding a means to prevent it, are thus becoming of increasing interest as gene therapies transition into the clinic.

Attempts to characterise this cellular response *in vivo* have relied on qualitative immunohistochemical staining of leukocyte markers. Subretinal injection of AAV8 in cynomolgus macaques led to positive retinal immunohistochemical staining for MHC class I and II (suggestive of active antigen presentation), CD8 (indicative of infiltrating cytotoxic T cells), and CD20 (suggestive of infiltrating B cells) [176]. One possible source of retinal inflammation following AAV gene therapy may be due to the activation of retinal microglia, which are capable of detecting viral infections, orchestrating local innate immune responses, and recruiting leukocytes to the retina [197]. The involvement of microglia is consistent with reports of increased retinal

immunohistochemical staining for Iba1, a microglia activation marker, following subretinal injection of AAV in macaques and mice [176, 177]. However, immunohistochemical analysis is limited in resolving populations expressing similar marker profiles, for instance between microglia and macrophages, and prevents quantitative analysis of the magnitude and mechanism of this response. Flow cytometry provides a sensitive and quantitative means of investigating the cellular response to AAV retinal gene therapy *in vivo* and enables effective discrimination of leukocyte populations. Flow cytometric analysis using CD45 and CD11b specific antibodies have been used to effectively identify microglial and macrophage populations, which are characterised by $CD11b^{hi}CD45^{lo}$ and $CD11b^{hi}CD45^{hi}$ expression, respectively [138, 198-201].

The mechanism of inflammatory responses to retinal gene therapy remain unclear, in part, due to the majority of investigations focussing on AAV-induced retinal toxicity at high vector doses. For instance, a recent study in wildtype mice demonstrated increased retinal and RPE toxicity with ubiquitous and RPE-specific AAV promoters following subretinal injections at high vector doses ($3x10^9$ gc/eye); in contrast, no response was detected with vectors exclusively targeting photoreceptors [177]. These responses were unaffected by the nature of the transgene, suggesting a potential promoter-induced reaction. A further study in wildtype mice showed retinal toxicity with a null self-complementary vector and, to a greater extent, with a vector encoding retinoschisin, when delivered at very high doses ($1x10^{11}$ gc/eye) [185]. Both vectors were ultimately less toxic than a *GFP*-expressing vector suggesting a role of the transgene in the level of retinal toxicity. However, it remains to be seen whether these

factors are important determinants in the cellular immune response to retinal gene therapy.

In this chapter, I investigate the cellular immune response to subretinal AAV injections in mice using sensitive flow cytometric techniques to define distinct cell populations and quantitatively assess the role of the AAV transgene in retinal inflammation. Although pre-existing immune responses to AAV may influence immune responses to retinal gene therapy [184], analyses were performed in mouse models with no previous exposure to AAV to primarily focus on innate responses to AAV vectors.

3.2 Aims

The aims of this chapter were as follows:

1. To manufacture and test AAV vectors expressing GFP with the serotypes AAV8, AAV8(Y733F), and AAV2.

2. To manufacture and test an AAV8 vector expressing nullGFP.

3. To quantitatively detect resident retinal leukocyte populations using flow cytometry.

4. To assess the effect of AAV subretinal injections on retinal leukocyte populations.

5. To characterise the cellular immune response to AAV subretinal injections.

6. To determine the role of the vector transgene in the cellular immune response to AAV subretinal injections.

3.3 Materials & methods

3.3.1 Vector plasmid cloning

The CAG.GFP.WPRE plasmid was provided as a kind gift from Dr Maria Patrício (Figure 3.1A). The *GFP* transgene was modified using Geneious Prime software to create a nullGFP DNA sequence that does not encode a protein. The double stranded nullGFP DNA sequence was synthesised by Integrated DNA Technologies.

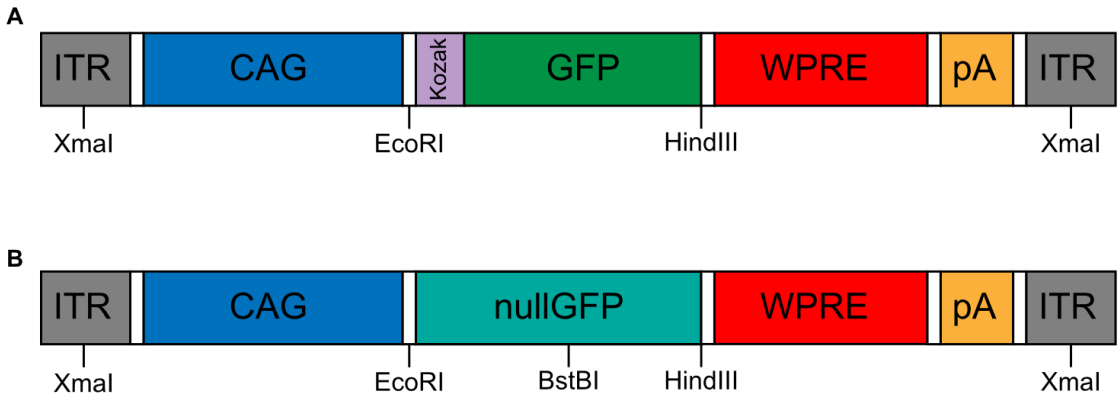

Figure 3.1. AAV genome schematic. (**A**) CAG.GFP.WPRE vector construct with a Kozak consensus sequence for initiation of protein translation. (**B**) CAG.nullGFP.WPRE vector construct. The locations of restriction sites relevant to this study are indicated. CAG, cytomegalovirus enhancer and chicken β-actin hybrid promoter; GFP, green fluorescent protein; nullGFP, GFP sequence modified to not express a protein product; WPRE, woodchuck hepatitis virus post-transcriptional regulatory element.

The CAG.GFP.WPRE and nullGFP DNA insert sequences were digested with the enzymes EcoRI–high fidelity (HF) and HindIII-HF (both New England BioLabs) according to manufacturer's instructions and as per section 2.1.1. Reactions were incubated at 50°C for 20 minutes. The correct size of the digested CAG.GFP.WPRE

plasmid was confirmed by electrophoresis using a 1% agarose gel as described in section 2.1.2. The band corresponding to the digested plasmid was excised and the DNA was extracted using the QIAquick gel extraction kit (QIAGEN) according to manufacturer's instructions. The nullGFP digested DNA was purified using the QIAquick PCR Purification Kit (QIAGEN) and eluted in 50 μL of nuclease-free water.

DNA ligation reactions of the digested CAG.GFP.WPRE plasmid and the nullGFP insert were performed as per section 2.2.1 with 29.3 ng of the nullGFP sequence. The ligated products were transformed into XL-10 Ultracompetent *E. coli* cells (Strategene) as per section 2.2.1. The amplified DNA plasmid was harvested from the *E. coli* cells with the endotoxin-free Zyppy plasmid miniprep kit (Zymo Research) according to section 2.2.2. The isolated CAG.nullGFP.WPRE plasmid was checked for successful ligation by performing a restriction digestion with the BstBI enzyme (New England BioLabs) at 65°C for 15 mins as per section 2.1.1 (Figure 3.1B). Subsequently, the correct DNA sequence was confirmed by Sanger sequencing (Eurofins Genomics). As the ITR regions are difficult to sequence, their presence was confirmed using a restriction digestion to XmaI sites in the ITRs (Figure 3.1A and B) at 37°C for 30 minutes as per section 2.1.1. All plasmids used in the manufacture of AAV were amplified using the Mega kit (QIAGEN) as per section 2.2.1.

3.3.2 AAV production

Four AAV vectors were manufactured for use within this study:

1. AAV8.CAG.GFP.WPRE: a *GFP* transgene with a WPRE enhancer under control by the ubiquitous CAG promoter, which is terminated with a bovine growth

hormone pA sequence. The transgenic sequence was packaged into a wildtype AAV8 serotype capsid.

2. AAV8.CAG.nullGFP.WPRE: a null transgene that doesn't express a protein product due to removal of the Kozak sequence. The transgene contains a WPRE enhancer and is under control by the ubiquitous CAG promoter. The sequence is terminated with a bovine growth hormone pA sequence. The transgenic sequence was packaged into a wildtype AAV8 serotype capsid.

3. AAV2.CAG.GFP.WPRE: as for AAV8.CAG.GFP.WPRE but packaged into a wildtype AAV2 serotype capsid.

4. AAV8(Y733F).CAG.GFP.WPRE: as for AAV8.CAG.GFP.WPRE but packaged into a mutant AAV8 serotype capsid with a one base pair change (Y733F) to minimise proteasomal degradation [202, 203].

AAV8 serotype vectors were manufactured by a triple transfection in HEK293T cells with plasmids encoding pRep2Cap8, pAdΔF6, and pTransgene as described in section 2.4. The AAV2 serotype vector was manufactured using a combined AAV2 Helper and Rep/Cap plasmid (Plasmid Factory). The AAV8(Y733F) vector was manufactured using pRep2Cap8(Y733F) and pAdΔF6. The AAV vectors were manufactured as per section 2.4. Viral genome titres were determined using qPCR and the purity of the capsid proteins was established using SDS-PAGE as per section 2.4.6.

3.3.3 Subretinal injections

Three to five week-old female C57BL/6J mice were subretinally injected with 1.5 µL of either AAV8(Y733F).CAG.GFP.WPRE, AAV8.CAG.GFP.WPRE, AAV8.CAG.nullGFP.WPRE,

or AAV8.CAG.hREP1.WPRE at a total viral dose of $1x10^9$ gc per eye as per section 2.5.3; sham injections of 1.5 μL PBS were performed in paired eyes where appropriate. The AAV8.CAG.hREP1.WPRE vector encoded the h*REP1* (encoding human Rab-escort protein 1) with a WPRE enhancer under control by a ubiquitous CAG promoter; the vector was provided as a kind gift from Dr Cristina Martinez-Fernandez Dela Camara. Injections were delivered in PBS supplemented with 0.001% of the non-ionic surfactant Pluronic F-68 (Thermo Fisher Scientific) to minimise vector loss due to absorbance onto surfaces [204].

3.3.4 Retinal dissociation

Mice were sacrificed by overdose of anaesthetic with 20 mg of pentobarbital (Pentoject, Animalcare), death was confirmed by cervical dislocation. If animals were to be imaged prior to tissue collection, mice were sacrificed by cervical dislocation and death was confirmed by decapitation. cSLO and SD-OCT retinal imaging were performed immediately prior to tissue collection according to section 2.5.4. Retinae were harvested according to section 2.5.5 and were stored in cold PBS on ice until dissociation. Retinal dissociation was performed as per section 2.6.3. Retinal cells from AAV8(Y733F).CAG.GFP.WPRE–injected eyes were resuspended in PBS prior to antibody staining.

3.3.5 Flow cytometry

All retinal cells not undergoing fixation and permeabilisation were processed according to section 2.6.4.

Dissociated retinal cells from AAV8(Y733F).CAG.GFP.WPRE–injected eyes were fixed and permeabilised for intracellular CD68 staining. Cells were stained with the thiol reactive viability dye ViaKrome 405 (Beckman Coulter) at a 1/1000 dilution in 50 µL PBS for 20 mins on ice immediately following retinal dissociation. Cells were incubated with TruStain FcX™ PLUS Fc block (2.5 µg/mL) (BioLegend) in staining buffer on ice for 10 minutes in a total volume of 100 µL, without removing the ViaKrome 405 staining solution. Cells were washed twice with staining buffer prior to cell surface antigen staining; the concentrations used were as per section 2.6.4. Cell surface staining was performed on ice for 20 minutes in a total volume of 100 µL with samples protected from light; cells were subsequently washed three times with staining buffer as per section 2.6.4. Cells were incubated in 100 µL of Fixation/Permeabilization solution (BD Biosciences) on ice for 20 minutes. Cells were washed three times in Perm/Wash Buffer (BD Biosciences) as before. Intracellular antibody staining with CD68-PE (clone FA-11) was performed on ice for 20 minutes in a total volume of 100 µL with samples protected from light. Cells were subsequently washed three times with Perm/Wash Buffer and were resuspended in staining buffer prior to flow cytometric analysis.

Flow cytometry of dissociated retinal cells was performed using the LSRFortessa (BD Biosciences) for AAV8(Y733F).CAG.GFP.WPRE–injected eyes and with the Aurora spectral analyser (Cytek Biosciences) for all other samples as per section 2.6.5. The specificity of the markers used in this thesis are detailed in Table 3.1.

Table 3.1. Distribution of flow cytometry markers on leukocyte populations.

Marker	Leukocyte population
CD45	All leukocytes
CD11b	Monocytes/macrophages, dendritic cells, granulocytes, natural killer cells, subsets of T and B cells
CD68	Monocytes/macrophages, microglia (upregulated in active microglia)
CD3	T cells, natural killer T cells
CD4	CD4 T cells, subsets of natural killer T cells
CD19	B cells
CD11c	Dendritic cells
NK1.1	Natural killer cells, natural killer T cells

3.4 Results

3.4.1 Cloning of the nullGFP plasmid

In order to create the CAG.nullGFP.WPRE plasmid, cloning steps were undertaken to remove the *GFP* sequence from the CAG.GFP.WPRE plasmid and replace it with a nullGFP sequence that does not produce a GFP protein. Initially the nullGFP sequence was designed by editing of the *GFP* sequence; this involved the following steps: reversing the orientation of the *GFP* sequence, swapping the HindIII and EcoRI restriction sites, and replacing the Kozak sequence with a random base pair sequence to prevent protein translation initiation (Figure 3.2). Several studies have implicated the ITR sequences to contain inherent promoter activity that can drive transgene expression [205, 206]. To prevent inadvertent *GFP* expression from the promoter

activity of the 5' ITR, two TAG stop codons were added to the 5'–3' coding sequence (Figure 3.2C).

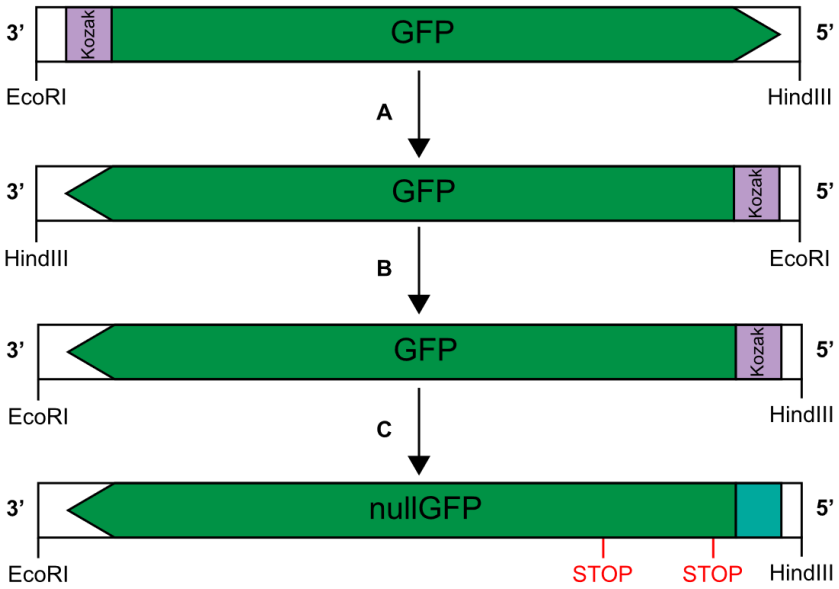

Figure 3.2. Design of nullGFP expressing vector construct. Steps in the creation of a nullGFP DNA sequence that does not express a protein product; sequence editing was performed using the Geneious software. (**A**) Reversal of the *GFP* sequence including the Kozak consensus sequence and regions containing the EcoRI and HindIII restriction sites. (**B**) The EcoRI and HindIII restriction sites were flipped. (**C**) The Kozak sequence was removed and replaced with a random six base pair sequence. The codons encoding the 11th and 22nd amino acid in the 5'–3' direction were altered to create two TAG stop codons (indicated in red).

To excise the *GFP* DNA sequence from the CAG.GFP.WPRE plasmid, the plasmid was incubated with EcoRI and HindIII restriction enzymes; successful digestion of this sequence was confirmed using gel electrophoresis. Two bands were visible corresponding to the plasmid backbone (5537 bp) and excised *GFP* sequence (745 bp) (Figure 3.3A). The synthesised nullGFP sequence has corresponding restriction sites

(Figure 3.2) to enable its ligation into the plasmid backbone. Restriction digestion of the nullGFP DNA sequence could not be confirmed by gel electrophoresis because only 30 bp were removed. The digested plasmid backbone and nullGFP DNA sequence were subsequently ligated to create a CAG.nullGFP.WPRE plasmid (Figure 3.1B). Successful ligation was confirmed by digesting the sequence with a BstBI restriction enzyme, located within the nullGFP transgene, to linearise the plasmid (Figure 3.1B); the linearised plasmid was visualised using gel electrophoresis with a single band at 6,074 bp (Figure 3.3B). The CAG.GFP.WPRE and CAG.nullGFP.WPRE plasmids were digested with an XmaI enzyme to confirm the presence of the ITR sequences (Figure 3.1A and B). The presence of two bands corresponding to the transgene (2,874 bp) and the backbone (3,197 bp) were visualised by gel electrophoresis (Figure 3.3C). Two additional bands were observed in the digested samples which corresponded to the undigested plasmid.

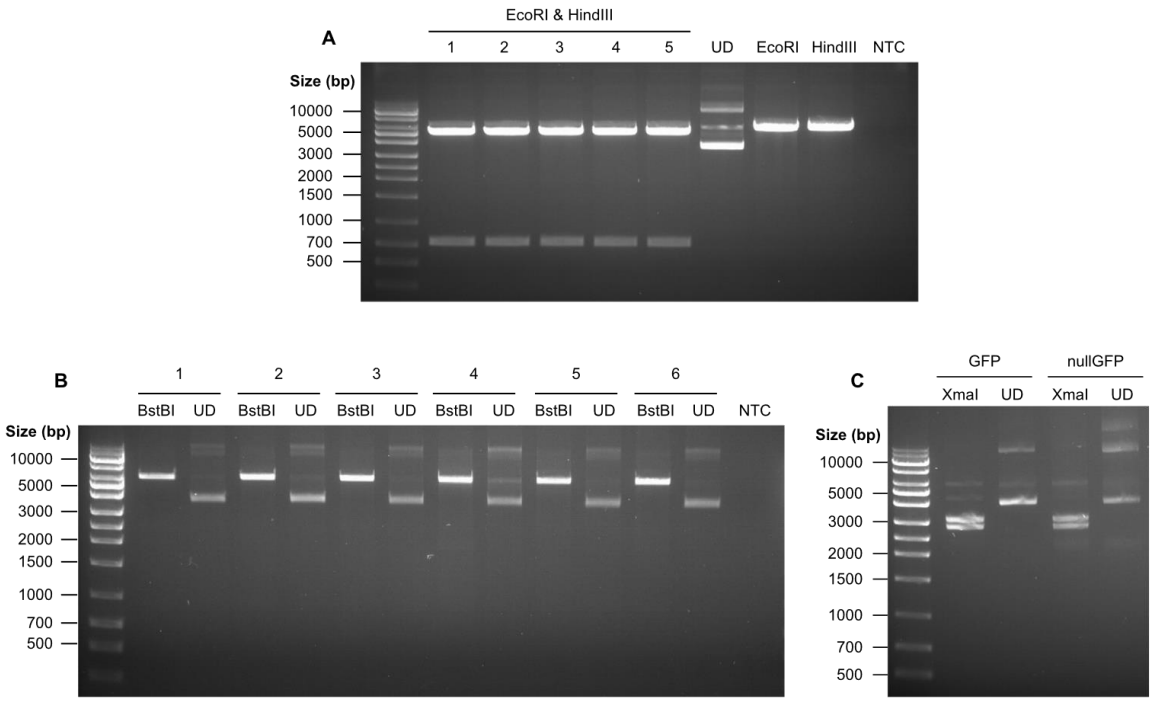

Figure 3.3. Cloning of the CAG.nullGFP.WPRE AAV vector. (**A**) The CAG.GFP.WPRE vector construct was digested with EcoRI and HindIII restriction enzymes to excise the *GFP* transgene, producing a 5,337 and 745 base pair (bp) product; this was repeated with five replicates (1–5). Undigested (UD), single enzyme, and no-template controls (NTC) were run in parallel. (**B**) The presence of the nullGFP transgene in the CAG.nullGFP.WPRE plasmid was confirmed by digesting with the BstBI restriction enzyme to produce a 6,074 bp product (replicates 1–6). (**C**) The presence of the ITR sequences was confirmed by digesting the CAG.GFP.WPRE (GFP) and CAG.nullGFP.WPRE (nullGFP) plasmids with an XmaI restriction enzyme, producing a 2,874 and 3,197 bp product.

3.4.2 Manufacturing of AAV vectors

Four AAV vectors were manufactured for use in this thesis with the capsid serotypes AAV8, AAV2, and AAV8(Y733F). The viral genome titre for the concentrated and wash AAV preparations was determined using qPCR; titres in the order of 10^{12} gc/mL were

achieved for all AAV vectors (Table 3.2). The presence of the three AAV capsid proteins, VP1, VP2, and VP3, and the lack of contaminating proteins was confirmed using SDS-PAGE (Figure 3.4).

Table 3.2. Viral genome titres of AAV vectors.

AAV Vector	AAV concentrate titre (genome copies/mL)	AAV wash titre (genome copies/mL)
AAV8.CAG.GFP.WPRE	$1.27x10^{12}$	$2.58x10^{10}$
AAV8.CAG.nullGFP.WPRE	$1.34x10^{12}$	$3.68x10^{10}$
AAV2.CAG.GFP.WPRE	$1.76x10^{12}$	$1.25x10^{11}$
AAV8(Y733F).CAG.GFP.WPRE	$3.58x10^{12}$	$4.73x10^{10}$

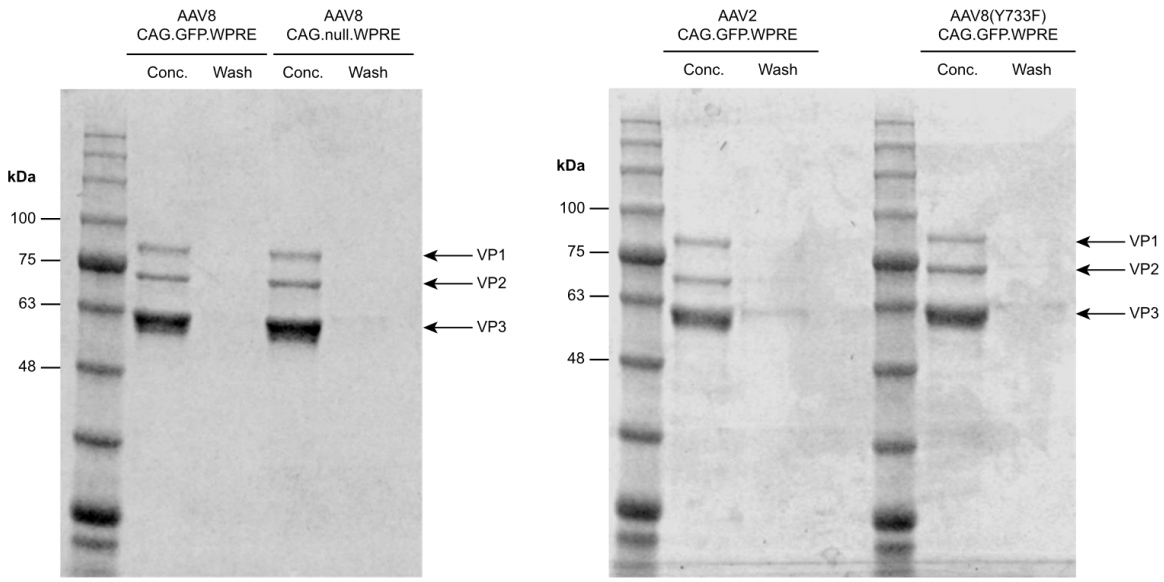

Figure 3.4. SDS PAGE of AAV capsid proteins. EZBlue dye stained SDS-PAGE gels of purified preparations of AAV8.CAG.GFP.WPRE, AAV8.CAG.nullGFP.WPRE, AAV2.CAG.GFP.WPRE, and AAV8(Y733F).CAG.GFP.WPRE; image taken on the Odyssey Imaging System (LI-COR Biosciences). Bands corresponding to VP1 (87 kDa), VP2 (72 kDa), and VP3 (62 kDa) are indicated in the concentrated (conc.) and wash AAV preparations.

All AAV vectors were tested *in vitro* to establish transgene expression. HEK293T cells were transduced with AAV8.CAG.GFP.WPRE, AAV8.CAG.nullGFP.WPRE, and AAV8(Y733F).CAG.GFP.WPRE at an MOI of 20,000 (Figure 3.5A). HEK293 cells were transduced with AAV2.CAG.GFP.WPRE at an MOI of 10,000 (Figure 3.5B). GFP fluorescence was observed in cells transduced with GFP expressing AAV vectors while no fluorescence was seen following transduction with AAV8.CAG.nullGFP.WPRE, thus confirming a lack of GFP expression. No cytotoxicity was observed with any of the vectors at the MOIs tested.

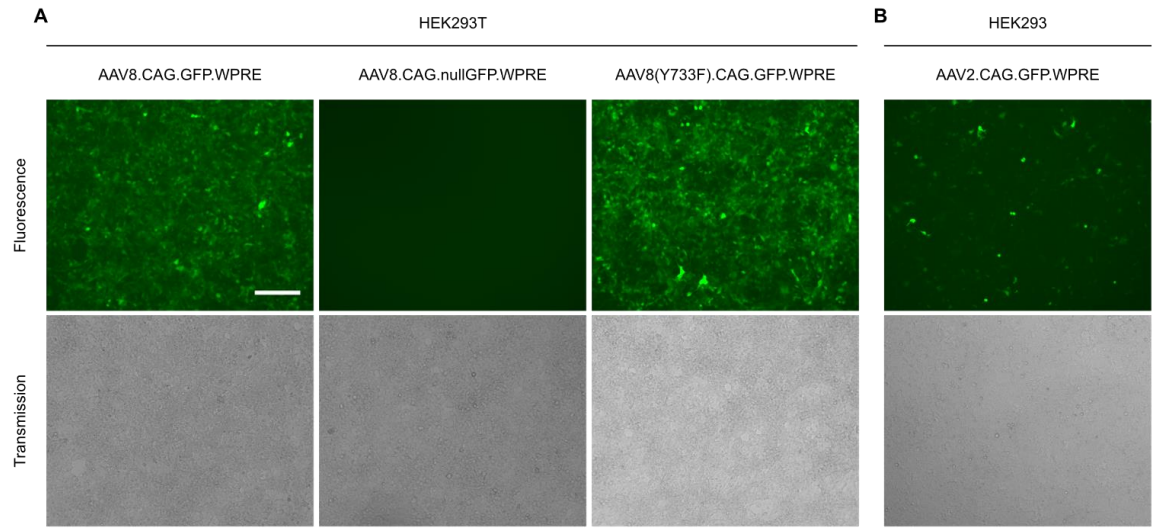

Figure 3.5. Testing AAV vectors *in vitro*. (**A**) Fluorescence and transmission microscopy images of HEK293T cells transduced with AAV8.CAG.GFP.WPRE, AAV8.CAG.nullGFP.WPRE, and AAV8(Y733F).CAG.GFP.WPRE at an MOI of 20,000. (**B**) Fluorescence and transmission microscopy images of HEK293 cells transduced with AAV2.CAG.GFP.WPRE at an MOI of 10,000. Images were acquired three days post-transduction (scale bar: 200 μm).

3.4.3 Detection of retinal leukocytes by flow cytometry

To detect the retinal leukocyte population, whole retinae from five week-old wildtype C57BL/6J mice were dissociated, stained with the pan-leukocyte marker CD45, the myeloid marker CD11b, and the macrophage marker CD68, and were analysed by flow cytometry. Although $CD45^+$ retinal leukocytes constituted a mean 0.4% of all live cells in the normal retina, three leukocyte populations were consistently identified (Figure 3.6). Although both microglia and macrophages are $CD11b^+$, they can be distinguished by their level of CD45 expression; microglia typically express low levels of CD45, while macrophages express relatively higher levels of CD45 [198]. The majority (88.6%) of immune cells found in the normal retina were $CD45^{lo}CD11b^{hi}$ (P1)

and were CD68^{+} (Figure 3.6F), suggesting these to be the resident microglial population, while the 7.0% of cells defined as CD45^{hi}CD11b^{hi} (P2) were likely to be macrophages (Figure 3.7A). In addition to the two CD11b^{+} populations, 2.8% of cells were CD45^{hi}CD11b^{-} (P3). These cells had a relatively low light scatter compared to microglia and macrophage populations, hence were predicted to lymphocytes (Figure 3.7B).

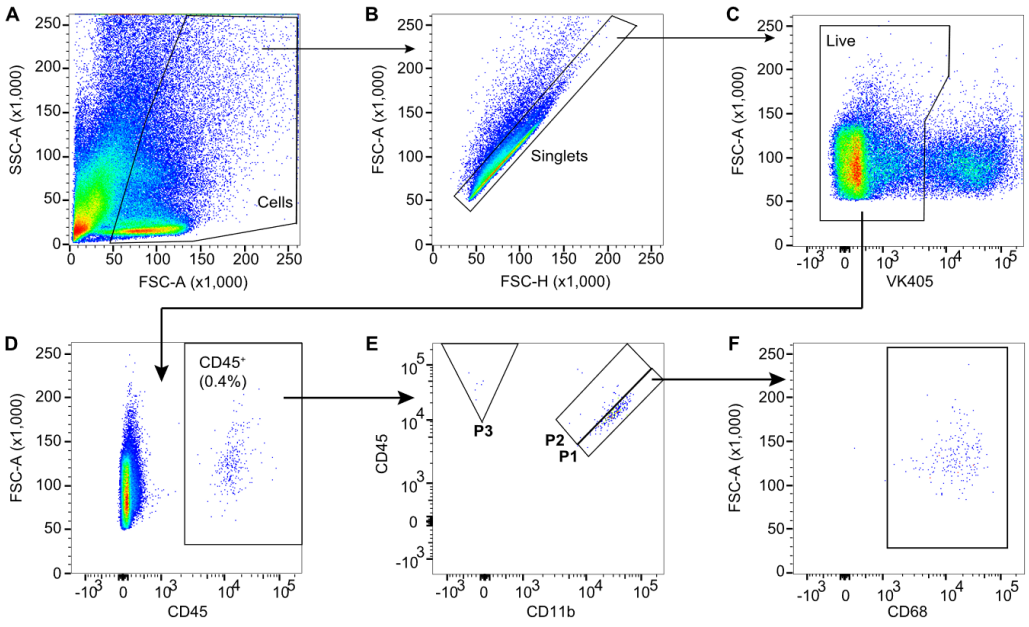

Figure 3.6. Gating strategy for detection of leukocytes in the normal mouse retina. The sequential exclusion of (**A**) debris, (**B**) cell doublets, and (**C**) dead cells in C57BL/6J mice assessed using the BD LSRFortessa. (**D**) CD45^{+} immune cells are gated (mean percentage of CD45^{+} cells in the total retina is indicated) and (**E**) three retinal immune cell populations are identified with differing levels of CD45 and CD11b co-expression; (P1) CD45^{lo}CD11b^{hi}, (P2) CD45^{hi}CD11b^{hi}, and (P3) CD45^{hi}CD11b^{-}. (**F**) All microglia cells were identified as CD68^{+}. SSC-A, side scatter area; FSC-A, forward scatter area; FSC-H, forward scatter height; VK405, ViaKrome 405.

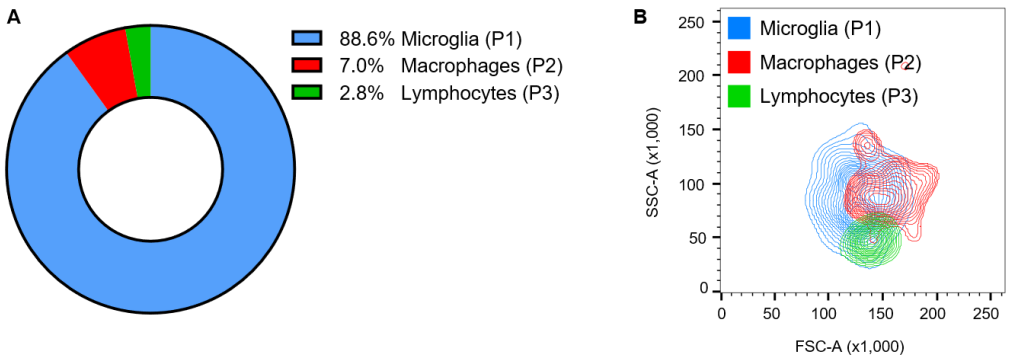

Figure 3.7. Retinal leukocytes in the normal mouse retina. (**A**) The mean proportions of the retinal CD45⁺ leukocyte populations (P1, P2, and P3) in a wildtype C57BL/6J mouse as a fraction of the total CD45⁺ retinal population; assessed using the BD LSRFortessa and representative of n=4. (**B**) Representative FSC-A vs SSC-A plot demonstrating the light scatter profile of these sub-populations.

3.4.4 AAV gene therapy induces a cellular immune response in the retina

In order to assess the effects of AAV gene therapy on the retinal leukocyte population, three week-old wildtype C57BL/6J mice underwent subretinal injections of either PBS or $1x10^9$ gc of AAV8(Y733F).CAG.GFP.WPRE in paired eyes. Retinae were harvested at three, seven, and 14 days post-injection (n=5 for each time-point), and were stained with CD45, CD11b, and CD68 antibodies prior to flow cytometric analysis. The CD68 antibody was used to assess microglia activation, as this marker is upregulated in activated cells [207]. Although no significant difference was seen between paired PBS- and AAV-injected eyes at three and seven days, by 14 days there was a significant increase in the percentage of total CD45⁺ cells in AAV-injected eyes (two-way ANOVA, p=0.0038; n=5) (Figure 3.8A). Based on the co-expression of CD45 and CD11b, the three distinct populations of leukocytes (P1, P2, and P3) could be seen in PBS-injected

eyes. However, in AAV-injected eyes these immune cells spanned a spectrum of CD11b expression levels, with cells appearing outside of these three gates (Figure 3.8B).

There was no significant change in the proportion of the microglia population (P1) at any time-point tested (Figure 3.8C). However, by day 14 post-injection, there was a significant increase in the percentage of macrophages (P2) (two-way ANOVA, p=0.0031; n=5) (Figure 3.8D) and presumed lymphocytes (P3) (p=0.0066; n=5) (Figure 3.8E) in AAV-treated retinae. There was no difference in the mean fluorescence index (MFI) of CD68 in microglia cells between PBS- and AAV-injected mice at any time point tested, despite a general trend to decreased MFI over time (Figure 3.8F).

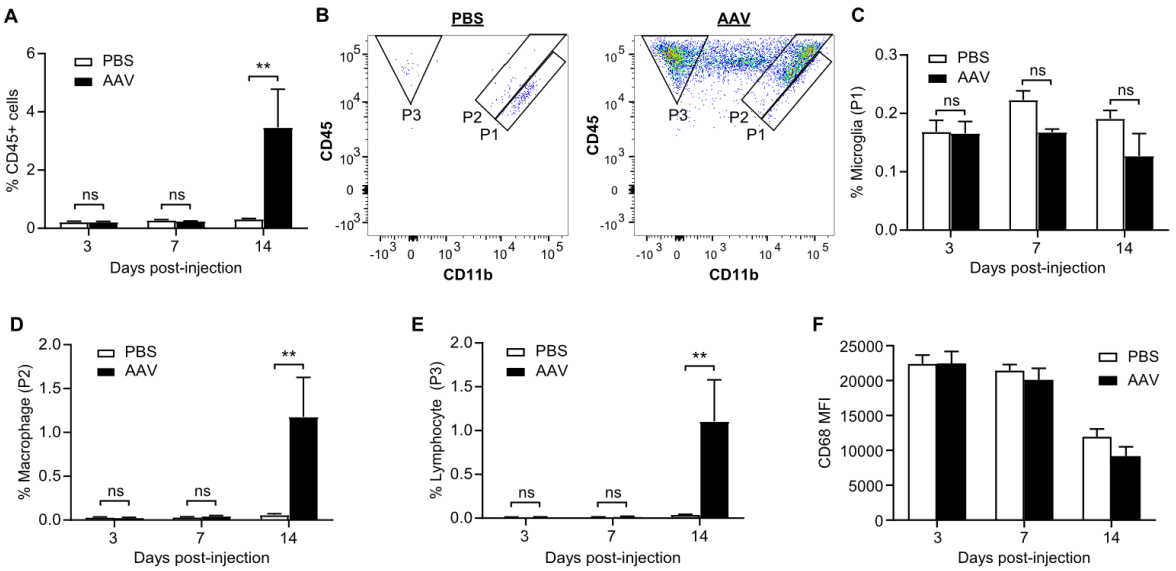

Figure 3.8. Subretinal AAV gene therapy leads to an increase in retinal leukocytes. Wildtype C57BL/6J mice received subretinal injections of PBS or $1x10^9$ gc of AAV8(Y733F).CAG.GFP.WPRE in paired eyes. Retinae were harvested for flow cytometric analysis at 3, 7, and 14 days post-injection and assessed using the BD LSRFortessa cytometer. (**A**) Percentage of $CD45^+$ cells in the retina gated to total live cells showing a significant increase in immune cells in AAV-treated eyes by day 14. (**B**) Based on distinct patterns of CD45 and CD11b expression, paired PBS- and AAV-injected retina from a representative mouse 14 days post-injection show three immune cell populations: P1, P2 and P3, which are likely to represent resident microglia, macrophages and lymphocytes, respectively. Changes in the percentages of (**C**) microglia, (**D**) macrophages, and (**E**) lymphocytes gated to total live cells (two-way repeated measures ANOVA with Šidák's correction for multiple comparisons). (**F**) Mean fluorescence index (MFI) of CD68 expressing microglia (two-way repeated measures ANOVA with Šidák's multiple comparisons test). $^{**}p \leq 0.01$ (± standard error of the mean (SEM), n=5).

In addition, *in vivo* SD-OCT imaging was performed on all mice analysed by flow cytometry. Vitreous opacities were detected in three of the five animals in eyes injected

with AAV, which are suggestive of immune cell infiltration (Figure 3.9). Moreover, the presence of vitreous opacities correlated with the highest proportions of viral transduction (as indicated by the percentage of GFP^+ cells) and immune cell infiltration ($CD45^+$ cells) (Table 3.3).

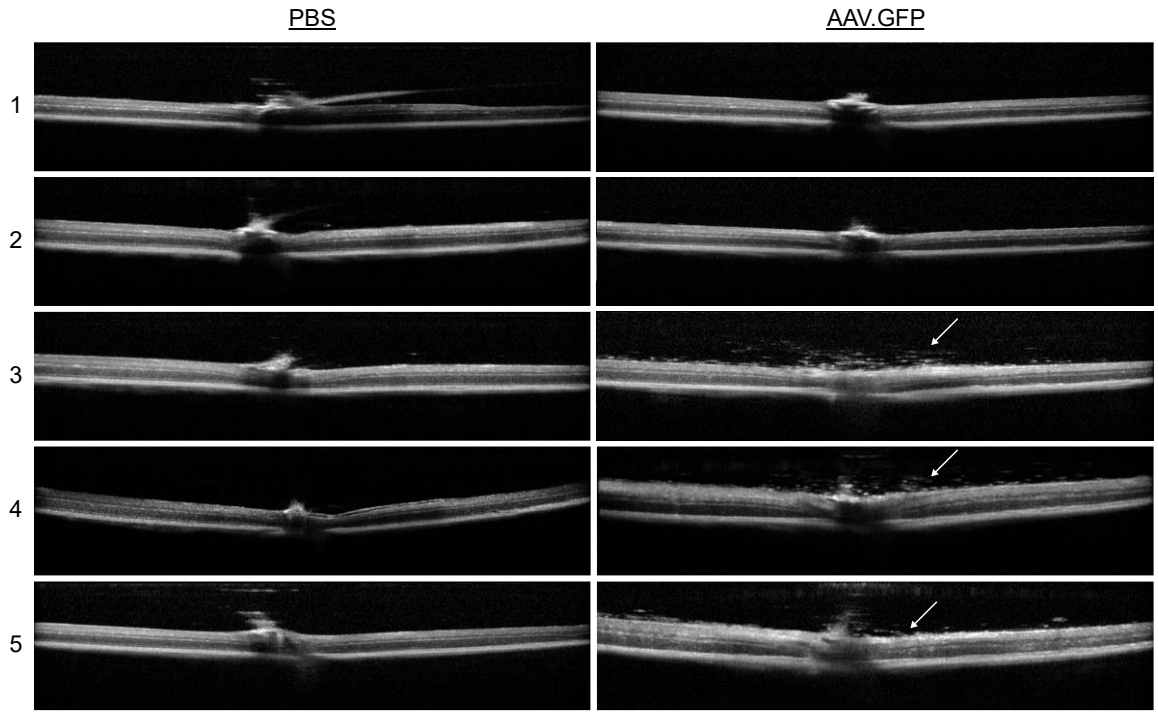

Figure 3.9. Vitreous opacities in SD-OCT images of AAV-injected retinae. Wildtype C57BL/6J mice received subretinal injections of PBS or $1x10^9$ gc of AAV8(Y733F).CAG.GFP.WPRE (AAV.GFP) in paired eyes. SD-OCT images were taken 14 days post-injection in five animals (1-5), which correspond to the data presented in Table 3.3. Arrows indicate vitreous opacities, suggestive of inflammation.

Table 3.3. GFP$^+$ and CD45$^+$ retinal cells and vitreous opacities 14 days following subretinal injections of AAV8(Y733F).CAG.GFP.WPRE.

Replicate	GFP$^+$ cells (%)[1]	CD45$^+$ cells (%)[1]	Vitreous opacities[2]
1	28.0	0.3	Absent
2	56.7	1.4	Absent
3	81.6	2.6	Present
4	81.9	6.3	Present
5	81.9	6.8	Present

[1] GFP$^+$ and CD45$^+$ cells were quantified using the BD LSRFortessa flow cytometer.
[2] Vitreous opacities were identified on SD-OCT images by a masked individual.

GFP fluorescence, a readout for successfully transduced cells, was detected in a mean 3.0% of total retinal cells three days post-transduction, which increased to 41.4% by seven days and 66.0% by 14 days (Figure 3.10A). A positive correlation of the percentage of GFP$^+$ cells to the percentage of CD45$^+$ cells was identified at day 14 post-injection (Spearman's rank test, correlation coefficient=0.9429, p=0.0167) (Figure 3.10B). Furthermore, a percentage of CD45$^+$ were GFP$^+$ at all time points post-injection; at day three a mean 2.4% of CD45$^+$ were GFP$^+$, which increased to 11.8% by day seven and 11.0% by day 14 (Figure 3.10C). Notably, a mean 81.5% of GFP$^+$CD45$^+$ cells on day three, 89.9% on day seven, and 91.6% on day 14 were CD11b^{hi}, suggesting the presence of GFP protein within either microglia or macrophages (Figure 3.10C and D).

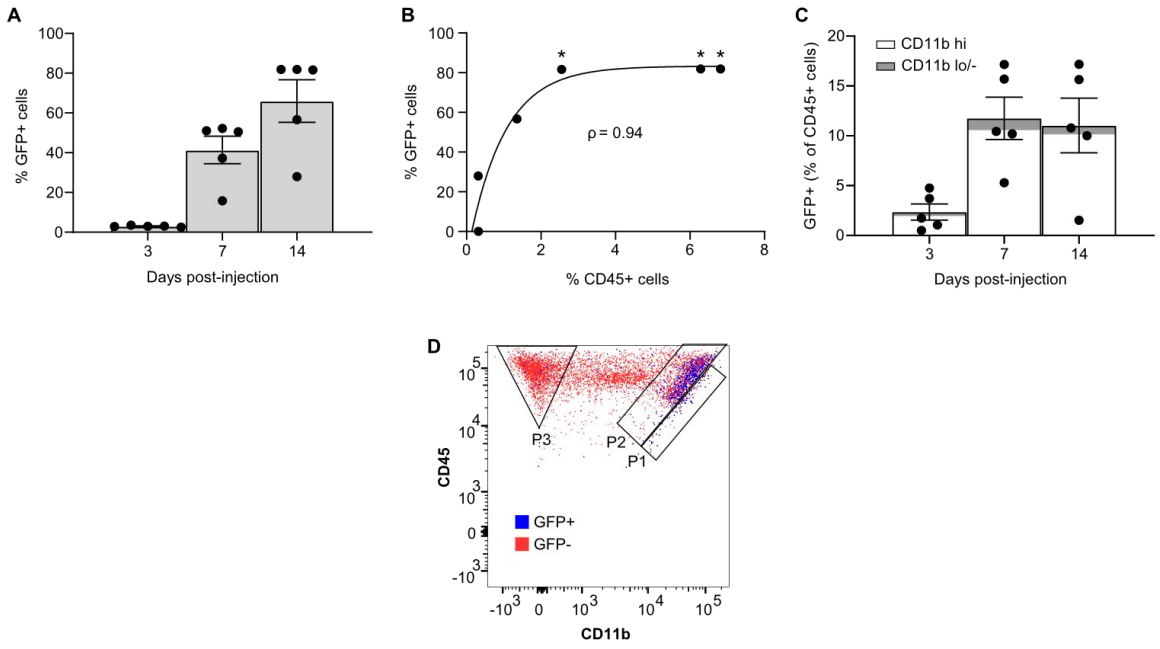

Figure 3.10. GFP expression following subretinal injections of AAV8(Y733F).CAG.GFP.WPRE in mice. Wildtype C57BL/6J mice received a subretinal injection of either AAV8(Y733F).CAG.GFP.WPRE vector or PBS in paired eyes. Retinae were harvested for flow cytometric analysis at 3, 7, or 14 days post-injection and assessed using the BD LSRFortessa cytometer. (**A**) Percentage of GFP^+ cells in the retina gated to total live cells (±SEM, n=5). (**B**) Non-linear fit of the correlation between the percentage of GFP^+ and $CD45^+$ at 14 days post-transduction. Correlation coefficient (ρ) indicated on graph. (*) indicates presence of vitreous opacities on SD-OCT images. (**C**) Percentage of GFP^+ cells within the $CD45^+$ population (±SEM, n=5), the proportion of this population that is $CD11b^{hi}$ compared to $CD11b^{lo/-}$ is indicated. (**D**) Representative CD45 vs CD11b plot of an AAV-injected retina 14 days post-injection with GFP^+ (blue) and GFP^- (red) $CD45^+$ immune cells.

3.4.5 Optimisation of leukocyte detection

In order to further characterise the AAV-induced inflammatory response in the retina, multicolour flow cytometric analysis was performed using a panel of immune cell

markers with the Aurora spectral analyser (Cytek Biosciences). Initially these markers were optimised in mouse splenocytes to identify cells of lymphoid lineage: helper T cells ($CD3^+CD4^+NK1.1^-CD11b^-$), cytotoxic T cells ($CD3^+CD4^-NK1.1^-CD11b^-$), NKT cells ($CD3^+NK1.1^+CD11b^-$), NK cells ($CD3^-CD19^-NK1.1^+CD11b^-$), B cells ($CD3^-CD19^+NK1.1^-CD11b^-$), and natural killer-like B cells ($CD3^-CD19^+NK1.1^+CD11b^-$); and of myeloid lineage: monocytes ($CD11b^{hi}CD11c^-$) and classical dendritic cells ($CD11b^{lo}CD11c^+$) (Figure 3.11).

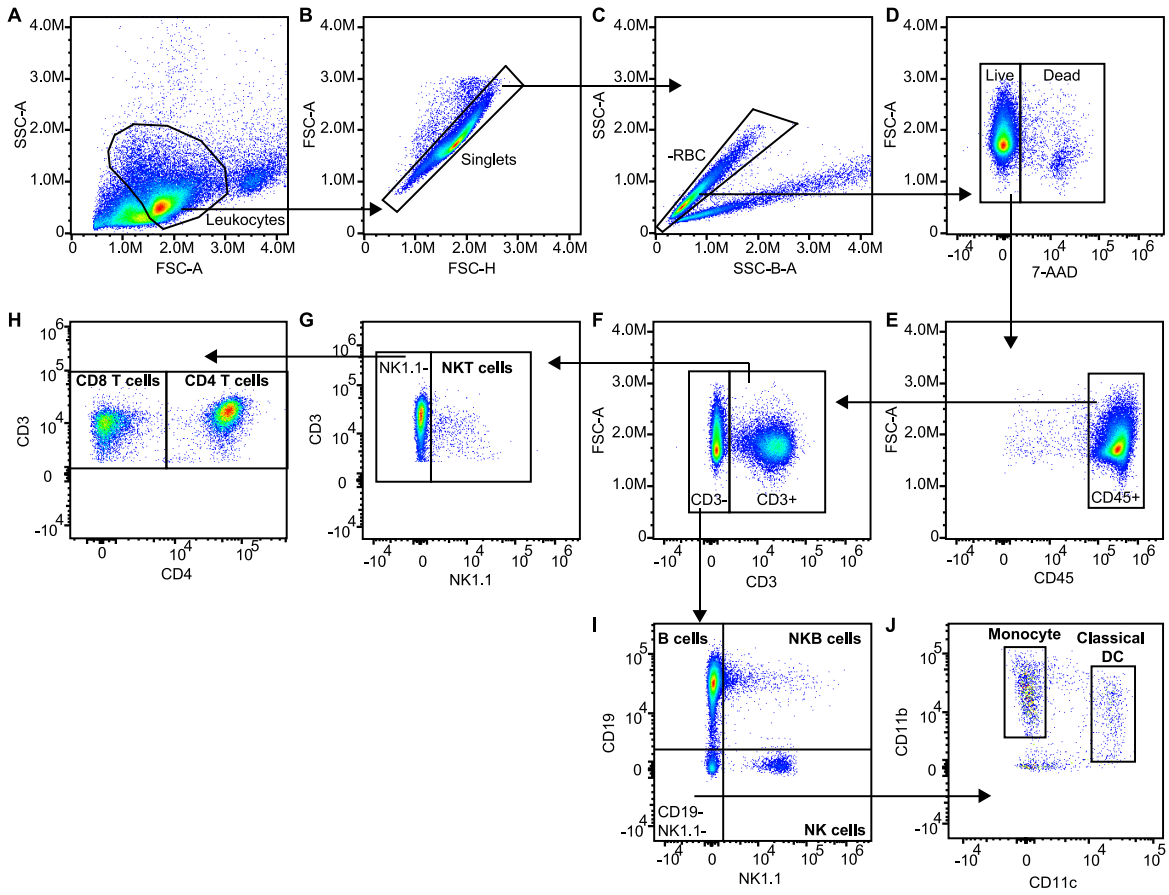

Figure 3.11. Gating strategy of leukocyte populations in mouse splenocytes. The flow cytometry gating strategy of C57BL/6J mouse splenocytes using the Cytek Aurora spectral cytometer. The sequential exclusion of (**A**) debris, (**B**) cell doublets, (**C**) red blood cells, and (**D**) dead cells. (**E**) $CD45^+$ immune cells are selected and (**F**) cells were gated according to CD3 expression. (**G**) $CD3^+NK1.1^+$ cells were identified as natural killer T (NKT) cells and (**H**) $NK1.1^-$ cells were identified as $CD3^+CD4^+NK1.1^-$ (CD4 T cells) and $CD3^+CD4^-NK1.1^-$ (CD8 T cells). (**I**) $CD3^-$ populations were gated as $CD3^-CD19^+NK1.1^-$ (B cells), $CD3^-CD19^+NK1.1^+$ (natural killer-like B (NKB) cells), and $CD3^-CD19^-NK1.1^+$ (natural killer (NK) cells). (**J**) $CD19^-NK1.1^-$ cells were gated as $CD11b^{hi}CD11c^-$ (monocytes) and $CD11b^{lo}CD11c^+$ (classical dendritic cells (DC)).

3.4.6 Characterising the cellular immune response to retinal gene therapy

To characterise the response to AAV, C57BL/6J mice underwent paired injections of either PBS or $1x10^9$ gc of AAV8.CAG.GFP.WPRE, with a wildtype AAV8 capsid serotype. As seen with injections of AAV8(Y733F).CAG.GFP.WPRE (Figure 3.8), there was no difference in the percentage of retinal $CD45^+$ cells at day three post-injection, however by day 14 there was a substantial increase in this population (Figure 3.12A). The difference in the percentage of $CD45^+$ cells between AAV- and PBS-injected eyes reached statistical significance upon multiple comparisons testing at day 28 post-injection (two-way ANOVA, p=0.0088; n=6); at day 28 a mean 1.1% of total retinal cells were detected as $CD45^+$ in PBS-injected samples which rose to 12.0% in AAV-injected samples.

Retinal cells demonstrate a high level of autofluorescence [208, 209], therefore it was necessary to select fluorophores for the flow cytometry panel that minimise spectral overlap with channels containing significant contribution from retinal autofluorescence; this meant utilising many long-emiting fluorophores, which, due to their inherent properties, can result in a greater data spread. A limited antibody panel was thus used against the markers: CD45, CD11b, CD3, CD4, NK1.1, CD19, and CD11c. Using the panel of immune cell markers, a range of different cell populations were identified within the retina following subretinal injections with AAV8.CAG.GFP.WPRE (Figure 3.13). At day 28 post-injection, the majority of immune cells populations were significantly increased compared to paired PBS-injected eyes (Figure 3.12B). These included cells of myeloid lineage (microglia, macrophages, and an unidentified $CD11b^{lo}CD11c^-NK1.1^-CD3^-$ myeloid cell) and cells of lymphoid lineage (NK cells, CD8 T

cells, and CD4 T cells). Although CD11b is typically used as a marker for myeloid cells, low level CD11b expression ($CD11b^{lo}$) was identified in a minority of population of $CD3^+$ lymphocytes (~3% of all leukocytes present by day 28), with subsets both negative and positive for CD4 that were predicted to be subsets of CD8 and CD4 T cells, respectively (P5 and P7) (Figure 3.13L). NK and NKT cell populations were also identified as positive and negative for CD11b; the majority populations for these two cell types were detected as $CD11b^{lo}$ and $CD11b^-$, respectively, and were significantly increased in AAV-injected retinae (Figure 3.12B). Furthermore, two unknown populations were detected: a $CD4^+CD3^-$ population (P9), which was not significantly increased at day 28, and a population that was negative for all immune cell markers except CD45 (P10) that was significantly upregulated compared to PBS-injected eyes (Figure 3.12B and 3.13J). Notably, there were no CD19 or CD11c expressing cell populations detected in either PBS- or AAV-injected eyes, suggesting an absence of B cells and classical dendritic cells. There was no significant change in the microglia population between PBS- and AAV8.CAG.GFP.WPRE-injected eyes, which represent ~1% of the total retinal cells.

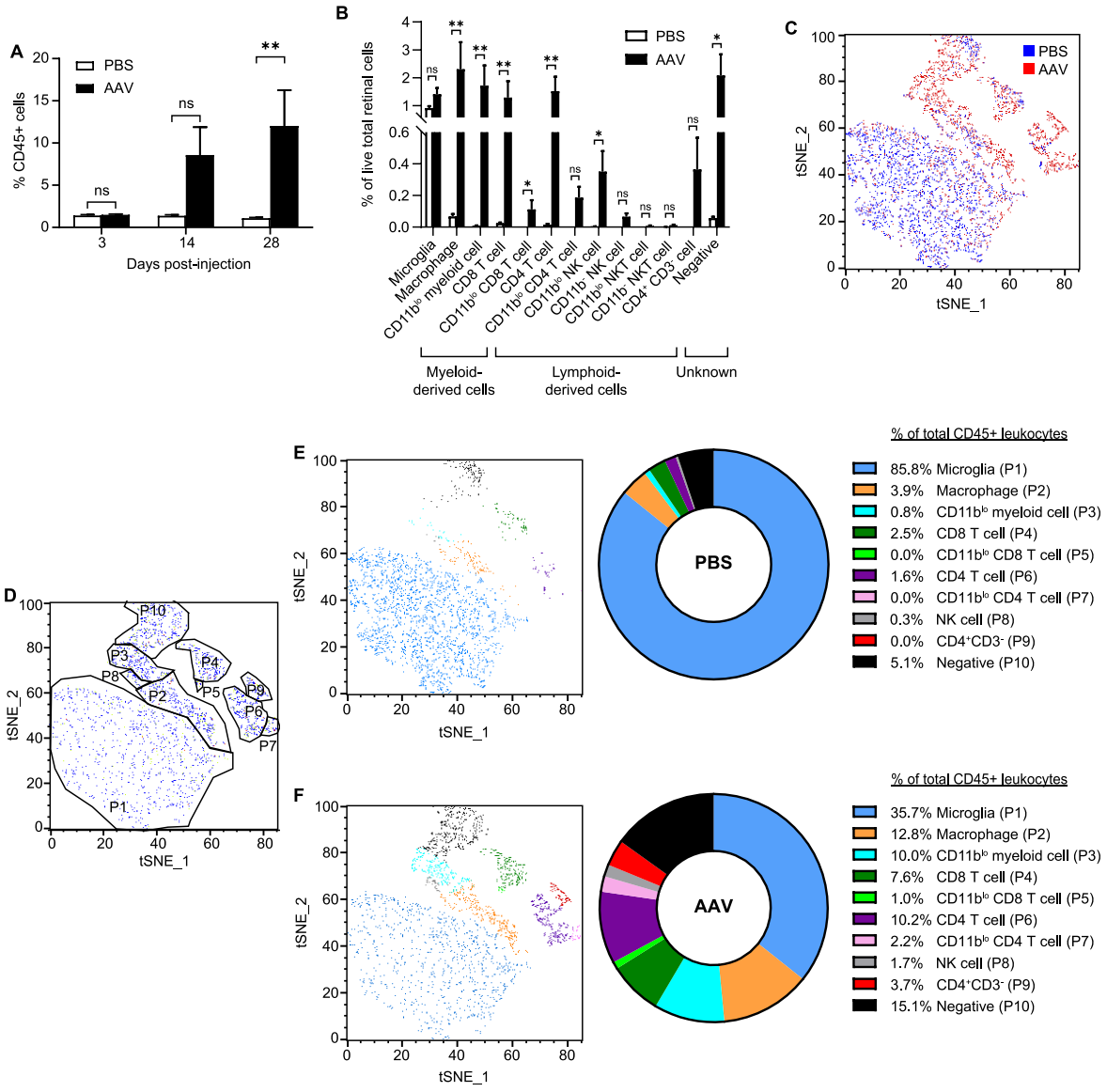

Figure 3.12. Characterisation of the cellular immune response to AAV8.CAG.GFP.WPRE subretinal injections in mice. Wildtype C57BL/6J mice received a subretinal injection of either AAV8.CAG.GFP.WPRE vector or PBS in paired eyes. Retinae were harvested for multicolour flow cytometric analysis using the Cytek Aurora spectral cytometer at 3, 14, or 28 days post-injection. (**A**) Percentage of CD45⁺ cells in the retina gated to total cells (two-way repeated measures ANOVA with Šidák's multiple comparisons test). (**B**) Percentage of immune cell populations gated to total cells at day 28 post injection (each population was assessed with a ratio paired t-test or a Wilcoxon test depending if the populations were parametric or non-

parametric, respectively). *$p \leq 0.05$, **$p \leq 0.01$ (±SEM, n=6). (**C**) Scatter plot of t-distributed stochastic neighbour embedding (t-SNE) dimensional reduction of C57BL/6J mice at day 28 post-injection; cells from either PBS- or AAV-injected eyes are coloured as blue or red, respectively, and were concatenated from n=6 per injection material (2,730 $CD45^+$ events per injection material). (**D**) Gating of different immune cell populations informed by both marker expression and clusters. Scatter plot of t-SNE dimensional reduction of (**E**) PBS- and (**F**) AAV-injected eyes, cell populations are coloured as indicated on the corresponding pie charts demonstrating the percentages of leukocyte populations within the total $CD45^+$ population.

In order to visualise these leukocyte populations, t-distributed stochastic neighbour embedding (t-SNE) dimensional reduction was performed on concatenated samples from both PBS- and AAV-injected eyes of all animals. A scatter plot of this t-SNE analysis indicated the appearance of clusters that were absent in PBS-injected eyes but present in those injected with AAV (Figure 3.12C). Characterisation of these clusters using co-expression of specific markers enabled visualisation of these leukocyte populations (Figure 3.12D). In PBS-injected eyes, t-SNE analysis revealed the majority of immune cells were microglia (Figure 3.12E); the proportions were relatively equivalent to those seen in uninjected retinae (Figure 3.14). In AAV-injected eyes, significant proportions of the total $CD45^+$ leukocytes consisted of cells from both myeloid and lymphoid lineages, rather than primarily consisting of microglia (Figure 3.12F).

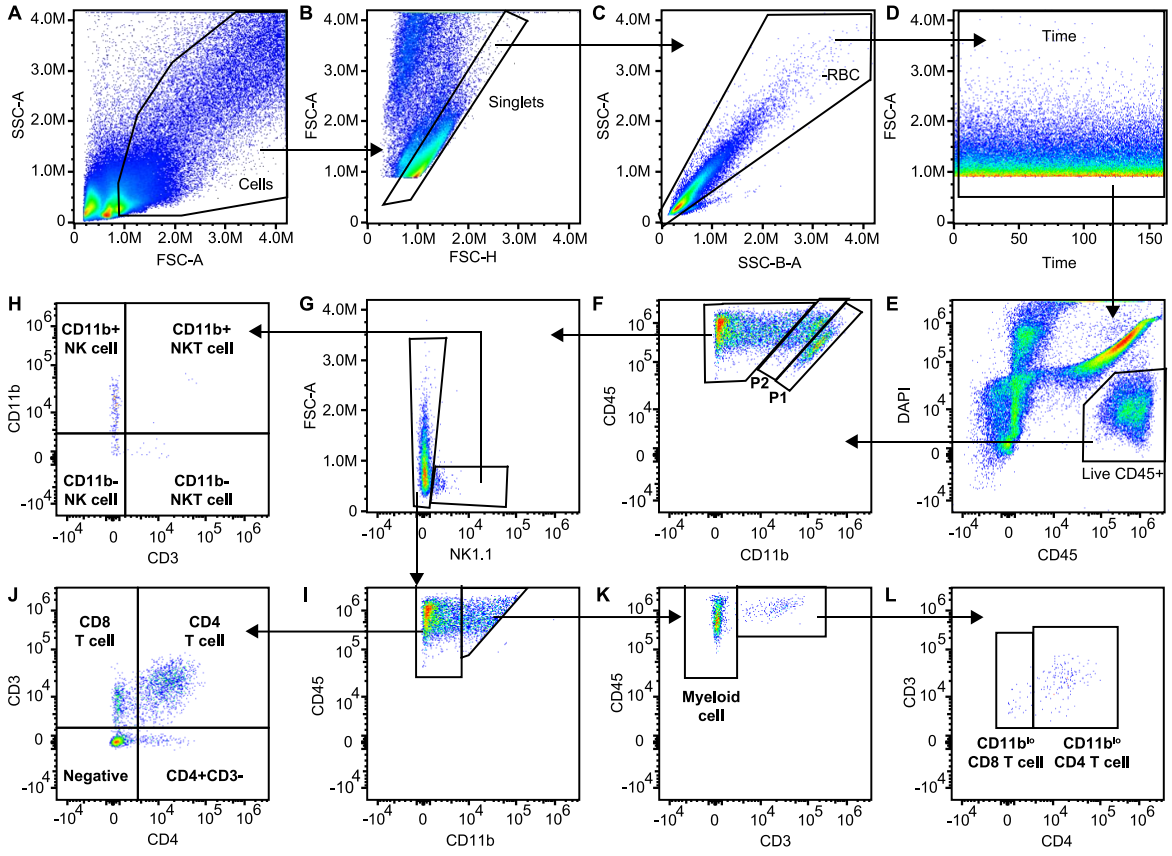

Figure 3.13. Gating strategy in AAV8.CAG.GFP.WPRE-injected mouse retina. The flow cytometry gating strategy of dissociated retinal cells 28 days following injection with an AAV8.CAG.GFP.WPRE vector in C57BL/6J mice assessed using the Cytek Aurora spectral cytometer. The sequential exclusion of (**A**) debris, (**B**) cell doublets, and (**C**) red blood cells. (**D**) Cells that were not acquired in a continuous flow stream were excluded by applying a time gate. (**E**) Live CD45^{+} leukocytes are gated to exclude dead cells and those not of interest in this study. (**F**) Two CD11b^{hi} expressing populations are identified; microglia (P1) and macrophages (P2). (**G**) NK1.1^{+} cells were identified and (**H**) further delineated as CD11b$^{+/-}$ NK and CD11b$^{+/-}$ NKT cells. (**I**) CD11b^{-} NK1.1^{-} cells were (**J**) identified as CD3^{+}CD4^{-} (CD8 T cells), CD3^{+}CD4^{+} (CD4 T cells), CD3^{-} CD4^{+}, and CD3^{-}CD4^{-} (negative). CD11b^{lo}NK1.1**-** cells were identified as (**K**) CD3^{-}

myeloid cells and (**L**) $CD3^+$ cells, with the populations $CD11b^{lo}CD3^+CD4^-$ ($CD11b^{lo}$ CD8 T cells) or $CD11b^{lo}CD3^+CD4^+$ ($CD11b^{lo}$ CD4 T cells).

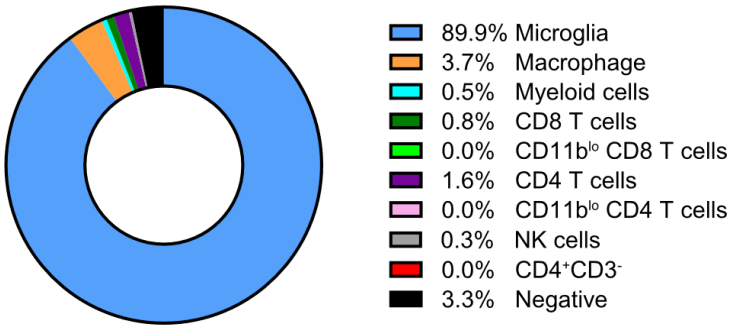

Figure 3.14. Leukocyte populations in an uninjected mouse retina. The mean proportions of each of leukocyte population within an uninjected C57BL/6J mouse retina assessed using the Cytek Aurora spectral cytometer; representative of n=6.

To further evaluate AAV transduction of retinal immune cells in this injected cohort, which could indicate a potential source of retinal inflammation, the level of GFP transgene expression was assessed. GFP fluorescence was detected in a mean 13.7% of total retinal cells at day three, 57.1% at day 14, and 58.3% at day 28 post-injection (Figure 3.15A). Within the $CD45^+$ immune cell population, a mean 1.5% of cells were GFP^+ at day three, 37.2% at day 14, and 46.7% at day 28 post-injection (Figure 3.15B). AAV transduction of retinal immune cells might be expected to primarily target the resident microglia, however, while a mean 44.0% of the GFP^+ leukocytes were microglia, the remaining 56.0% included cells that would not be resident at the time of injection (Figure 3.15B). Nevertheless, the GFP MFI, used as a readout for the level of transgene expression per cell, was significantly greater in microglia (P1) cells than $CD11b^{lo}$ cells (P3; one-way ANOVA, p=0.0192, n=6) and lymphocytes (P4; p=0.0132,

n=6). Similarly, the GFP MFI was significantly greater in macrophages (P2) than in P3 (p=0.0267, n=6) and P4 (p=0.007, n=6) (Figure 3.15C). The majority of microglia were GFP⁺ at days 14 and 28 with means of 68.1% and 78.5%, respectively (Figure 3.15D).

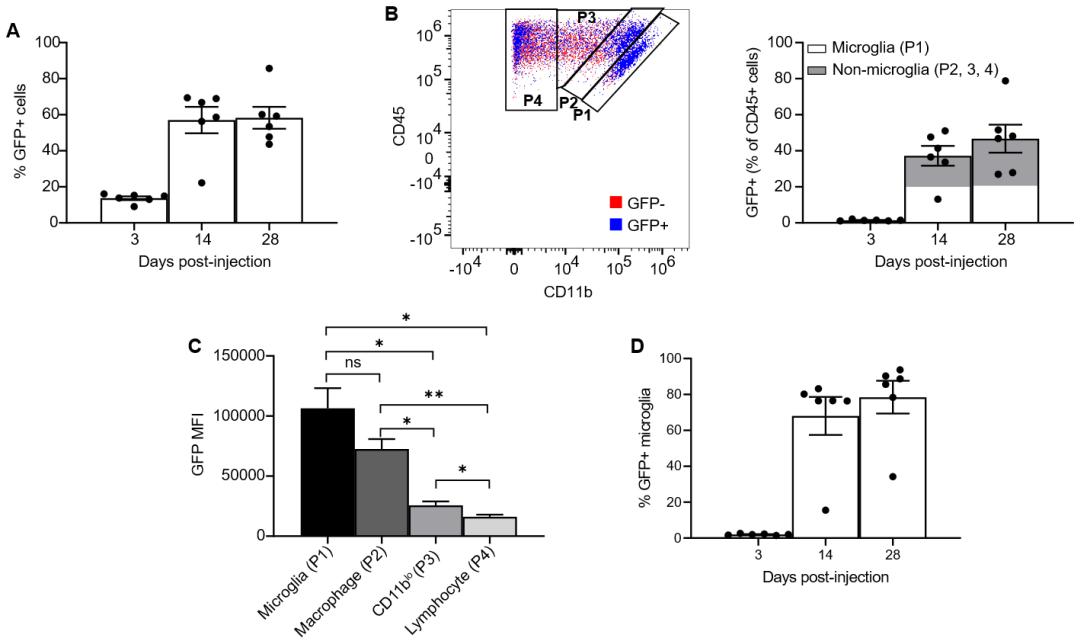

Figure 3.15. Retinal GFP expression following subretinal injections of AAV8.CAG.GFP.WPRE in mice. Wildtype C57BL/6J mice received a subretinal injection of either AAV8.CAG.GFP.WPRE vector or PBS in paired eyes. Retinae were harvested for multicolour flow cytometric analysis at 3, 14, or 28 days post-injection and assessed using the Cytek Aurora spectral cytometer. (**A**) Percentage of GFP⁺ cells in the retina gated to total live cells (±SEM, n=6). (**B**) Representative plot of an AAV-injected retina 28 days post-injection with GFP⁺ (blue) and GFP⁻ (red) CD45⁺ leukocytes, and the percentage of GFP⁺ cells within the CD45⁺ population. The proportion of microglia (P1) versus non-microglia cells (P1, P2 and P3) is indicated. (**C**) GFP MFI of four gated GFP⁺ immune cell populations as indicated (±SEM, n=6) *p ≤0.05, **p ≤0.01 (one-way repeated measures ANOVA with Šidák's multiple comparisons test). (**D**) Percentage of GFP⁺ microglia (P1) gated to total microglia. (±SEM, n=6).

3.4.7 AAV transgene influences the cellular immune response to retinal gene therapy

To assess whether retinal inflammation following AAV gene therapy is dependent on the expression of a transgene protein, subretinal injections of AAV8 vectors that were identical except for the transgene ($1x10^9$ gc of either AAV8.CAG.GFP.WPRE or AAV8.CAG.nullGFP.WPRE) were performed in paired eyes of wildtype C57BL/6J mice. The AAV8.CAG.nullGFP.WPRE vector construct was identical to the AAV8.CAG.GFP.WPRE vector in terms of the DNA sequences present, except that the transgene has been reversed and modified with stop codons to prevent the production of any GFP protein (Figure 3.1 and 3.2). Unexpectedly, the AAV8.CAG.nullGFP.WPRE vector induced significant retinal toxicity with dramatic levels of retinal thinning and loss of the ellipsoid zone on SD-OCT images at day 28 post-injection (Figure 3.16A and B). The nullGFP vector induced a marked cellular immune response in the retina compared with PBS-injected eyes; by 28 days post-injection a mean 91.6% of total live retinal cells were $CD45^+$, in keeping with loss of photoreceptors (two-way ANOVA, day 14: p=0.0002; day 28: p<0.0001; n=6) (Figure 3.16C).

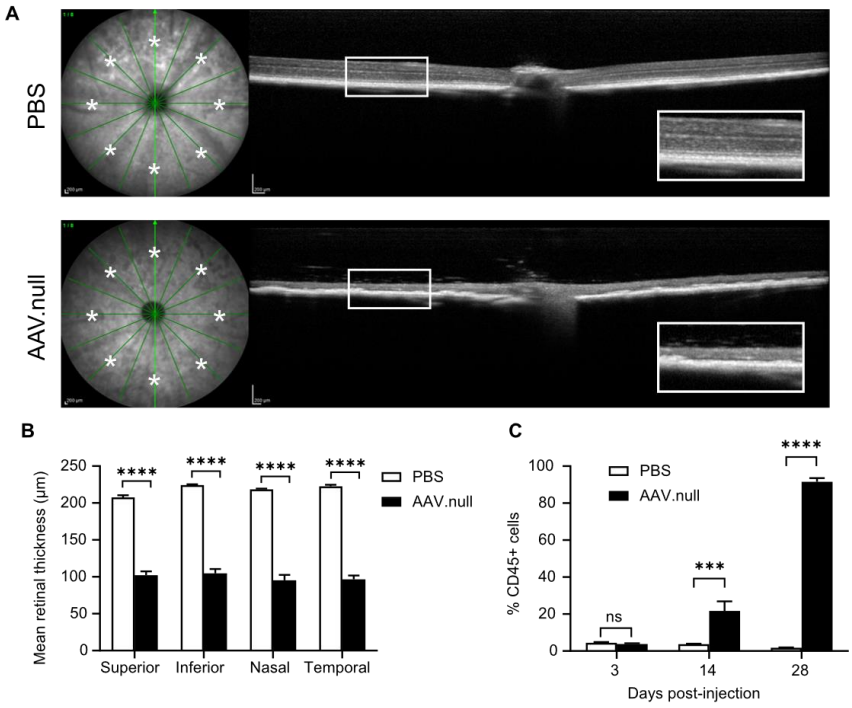

Figure 3.16. AAV8.CAG.nullGFP.WPRE vector induces significant toxicity in the mouse retina. Wildtype C57BL/6J mice received a subretinal injection of either AAV8.CAG.nullGFP.WPRE vector or PBS in paired eyes. (**A**) Representative SD-OCT images from fellow eyes that received either PBS or AAV8.CAG.nullGFP.WPRE at day 28 post-injection. Total retinal thickness was measured at indicated points (*). (**B**) Mean total retinal thickness of points (*) of the superior, inferior, nasal, and temporal regions at 28 days post-injection. (**C**) Percentage of $CD45^+$ cells in the retina gated to total live cells at 3, 14, and 28 days post-injection measured by flow cytometric analysis using the Cytek Aurora spectral cytometer (two-way repeated measures ANOVA with Šidák's multiple comparisons test). ***$p \leq 0.001$, ****$p \leq 0.0001$ (±SEM, n=6).

Due to the toxicity of the AAV8.CAG.nullGFP.WPRE vector, an AAV8.CAG.hREP1.WPRE vector was subsequently used to determine whether retinal inflammation following AAV gene therapy is dependent on the nature of the transgene. The expression of both *GFP* and h*REP1* transgenes were driven by the ubiquitous CAG promoter, enhanced by

WPRE, and packaged into a wildtype AAV8 capsid serotype. REP1 aids addition of a geranylgeranyl group to Rab GTPases, through a process termed prenylation [210]. A similar AAV2 construct has previously been used in retinal gene therapy trials to treat choroideremia, a blinding disease caused by loss-of-function mutations in the *CHM* gene [151, 211]. C57BL/6J mice underwent paired injections of $1x10^9$ gc of either AAV8.CAG.GFP.WPRE or AAV8.CAG.hREP1.WPRE; neither vector induced any retinal thinning (Figure 3.17). Retinae were stained with an antibody panel specific for leukocyte markers and harvested for flow cytometric analysis at 14 days post-injection; CD19 and CD11c antibodies were omitted from these experiments due to lack of staining in Figure 3.12. The results showed a significant difference in the total percentage of $CD45^+$ retinal leukocytes between paired AAV8.CAG.GFP.WPRE (mean 8.3%) and AAV8.CAG.hREP1.WPRE (mean 2.0%) injected eyes at 14 days post-injection (Figure 3.18A). In particular, the AAV8.CAG.GFP.WPRE injected retinae contained substantially greater numbers of the majority of leukocyte populations detected (Figure 3.18B). No difference was seen in the resident microglia population between the GFP and REP1 vector-treated eyes, which remained at ~1% of all retinal cells.

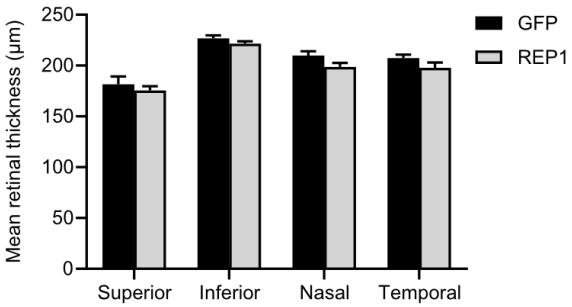

Figure 3.17. Retinal toxicity is not observed with either the *GFP*- or h*REP1*-expressing AAV8 vector. Wildtype C57BL/6J mice received a subretinal injection of $1x10^9$ gc of either AAV8.CAG.GFP.WPRE (GFP) or AAV8.CAG.hREP1.WPRE (REP1) vector in paired eyes. Mean total retinal thickness of the superior, inferior, nasal, and temporal regions at 14 days post-injection analysed using SD-OCT images (±SEM, n=6).

A t-SNE dimensional reduction was performed on the concatenated samples from both AAV8.CAG.GFP.WPRE and AAV8.CAG.hREP1.WPRE injected eyes of all animals. A scatter plot of the t-SNE analysis indicated that all the major infiltrating leukocyte clusters were present in eyes injected with both vectors (Figure 3.18C and D). The $CD45^+$ cells detected in AAV8.CAG.GFP.WPRE-injected eyes consisted of significant proportions of a range of cells of both myeloid and lymphoid lineages (Figure 3.18E). The total $CD45^+$ cells detected in AAV8.CAG.hREP1.WPRE-injected eyes primarily consisted of microglia cells, however, all other immune cell populations were detected (Figure 3.18F). The relative proportions of infiltrating leukocyte populations were generally very similar between the two vectors, although macrophages and NK cells appeared to be more prevalent in the AAV8.CAG.GFP.WPRE-treated retinae (Figure 3.18G).

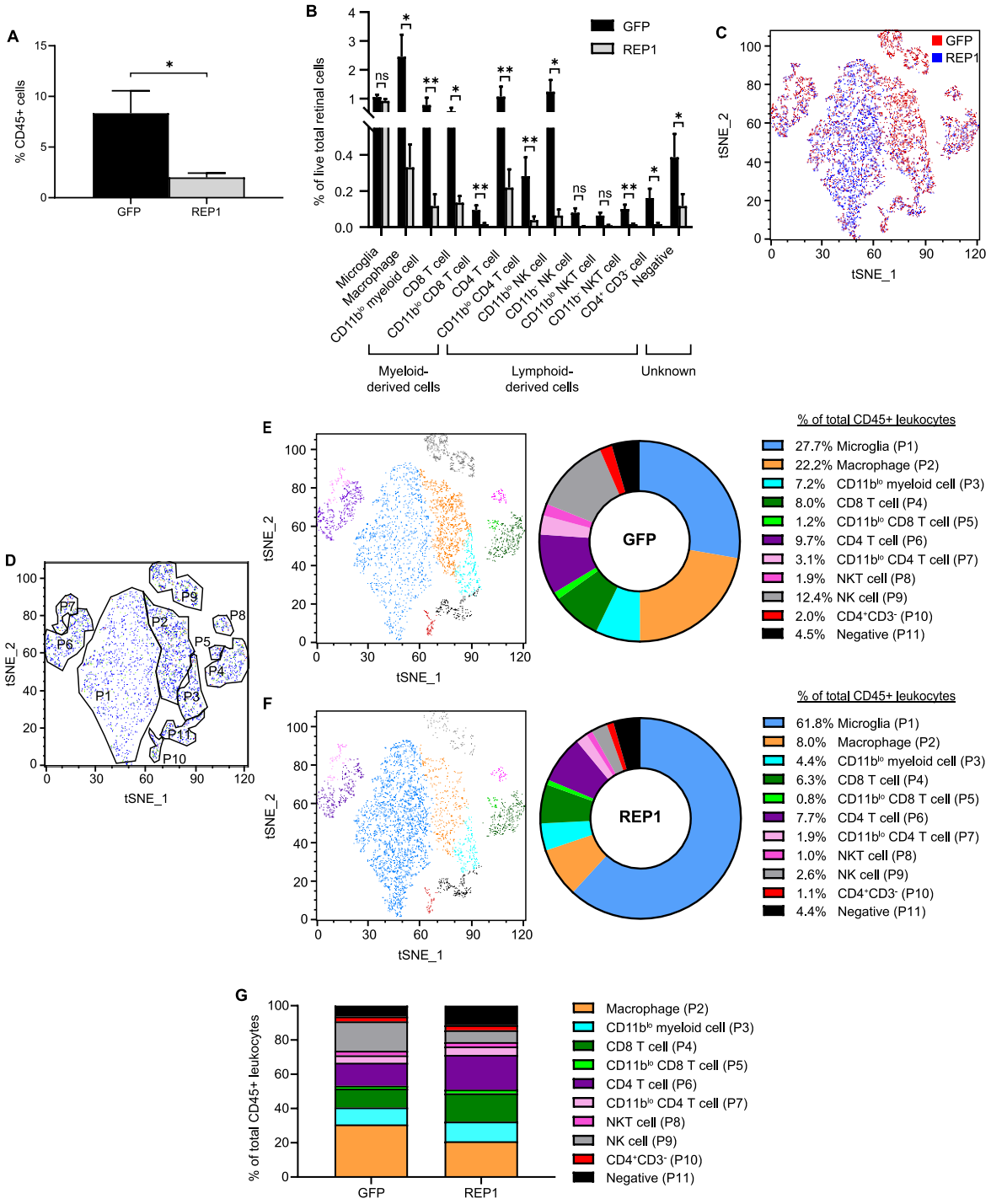

Figure 3.18. Effect of transgene on the cell-mediated immune response to subretinal AAV gene therapy. Wildtype C57BL/6J mice received a subretinal injection of 1x10^9 gc of either AAV8.CAG.GFP.WPRE (GFP) or AAV8.CAG.hREP1.WPRE (REP1) vector in paired eyes. Retinae were harvested for multicolour flow cytometric analysis using the Cytek spectral cytometer at 14 days post-injection. (**A**) Percentage of live CD45$^+$ cells in the retina gated to

total cells (paired t test). (**B**) Percentage of live immune cell populations gated to total cells (each population was assessed with a ratio paired t test or a Wilcoxon test depending if the populations were parametric or non-parametric, respectively). *$p \leq 0.05$, **$p \leq 0.01$. (**C**) Scatter plot of t-SNE dimensional reduction of cells from either eyes injected with GFP or REP1, which are coloured red or blue, respectively. Data is concatenated from n=6 per injection material (9,000 $CD45^+$ events per injection material). (**D**) Gating of different immune cell populations informed by both marker expression and clusters. Scatter plot of t-SNE dimensional reduction of (**E**) GFP vector and (**F**) REP1 vector-injected eyes. Cell populations are coloured as indicated on the legend with the corresponding percentages of leukocyte populations as a fraction of the total retinal $CD45^+$ leukocyte population, which is demonstrated in corresponding pie charts. (**G**) Bar chart of GFP and REP1 vectors indicating the relative proportions of infiltrating leukocyte populations as a percentage of the total retinal $CD45^+$ leukocyte population (as a fraction of 100%). Note that resident microglia have been excluded from the bar charts for clarity as their numbers remain unchanged as seen in panel B. The identity of each population corresponds with those in panel E and F.

The total percentage of $CD45^+$ leukocytes was compared between the cohort of mice that underwent paired injections of PBS vs AAV8.CAG.GFP.WPRE used for Figure 3.12 (cohort 1), and those injected with AAV8.CAG.GFP.WPRE vs AAV8.CAG.hREP1.WPRE in Figure 3.18 (cohort 2). Although the data in these cohorts were collected on separate days, all experimental settings were equivalent. The overall percentage of leukocytes at day 14 was equivalent between the AAV8.CAG.GFP.WPRE injected eyes in the two cohorts, indicating reproducibility of the immune response. There was, however, no significant difference between the PBS and AAV8.CAG.hREP1.WPRE injected eyes in these two cohorts (Figure 3.19).

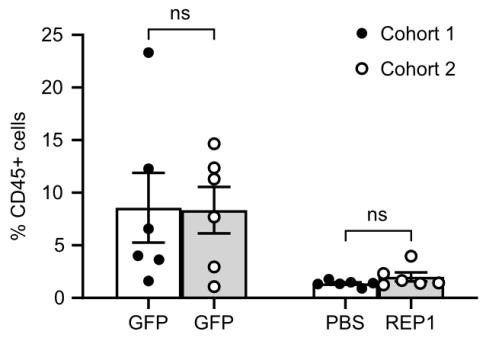

Figure 3.19. The magnitude of the cellular immune response to AAV8.CAG.hREP1.WPRE is comparable to sham injections. Comparison between the percentage of total live CD45^{+} cells from C57BL/6J mice injected with PBS vs AAV8.CAG.GFP.WPRE (GFP) in paired eyes eyes (cohort 1) and mice injected with AAV8.CAG.GFP.WPRE vs AAV8.CAG.hREP1.WPRE (REP1) (cohort 2) (two-way ANOVA with Sidak's multiple comparisons test) (±SEM, n=6). All injections were performed with 1x10^{9} gc/eye and retinae were analysed at 14 days post-injection.

In vivo SD-OCT imaging was performed on all mice analysed by flow cytometry. Very mild vitreous opacities were detected in five of the six animals injected with AAV8.CAG.GFP.WPRE and two animals injected with AAV8.CAG.REP1.WPRE (Figure 3.20). The number of opacities appeared significantly reduced compared to eyes injected with the equivalent mutant capsid vector (AAV8(Y733F).CAG.GFP.WPRE) (Figure 3.9). However, the percentage of CD45^{+} cells correlated with the presence of vitreous opacities on SD-OCT images (Table 3.4).

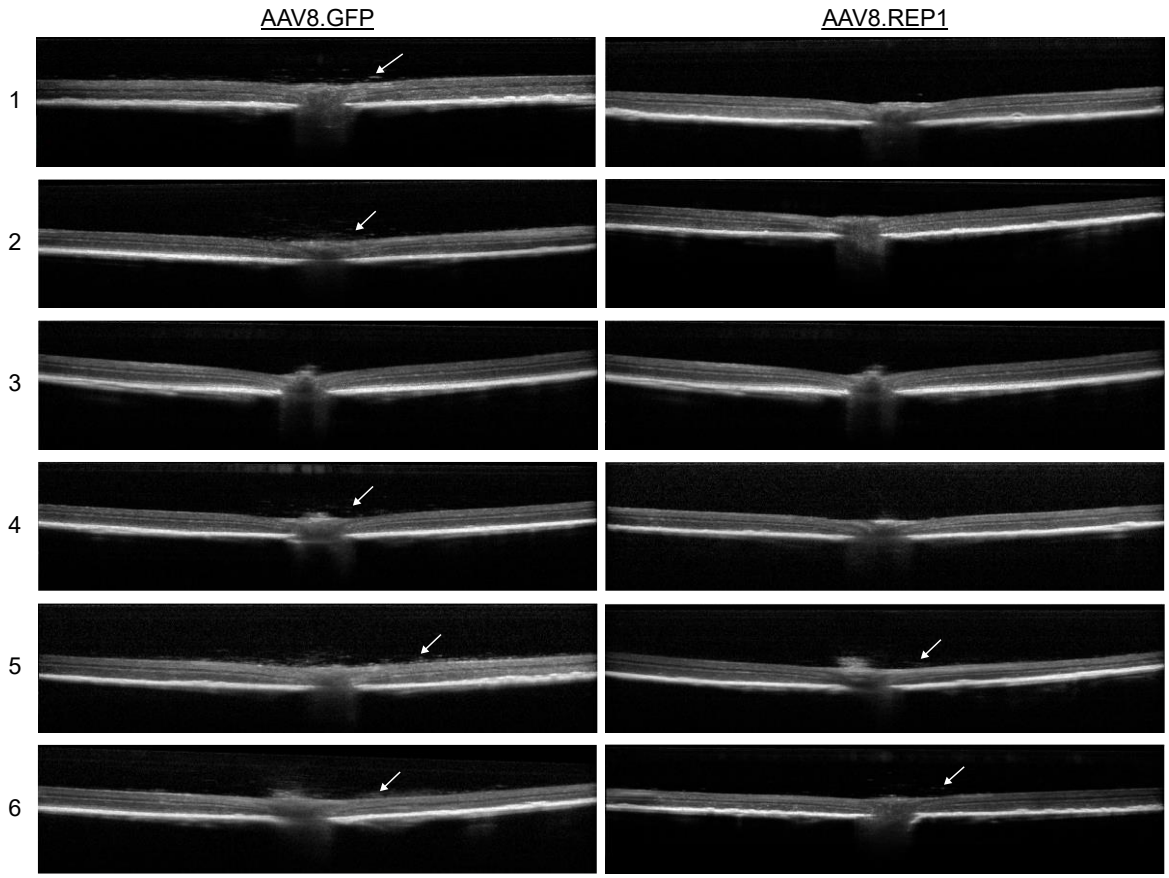

Figure 3.20. Mild vitreous opacities in SD-OCT images of AAV-injected retinae. Wildtype C57BL/6J mice received subretinal injections of $1x10^9$ gc of either AAV8.CAG.GFP.WPRE (AAV8.GFP) or AAV8.CAG.hREP1.WPRE (AAV8.REP1) vector in paired eyes. SD-OCT images were taken 14 days post-injection in six animals (1-6), which correspond to the data presented in Table 3.4. Arrows indicate vitreous opacities, suggestive of inflammation.

Table 3.4. Retinal leukocytes 14 days following subretinal injections with the *GFP*- or h*REP1*-expressing AAV8 vector.

	AAV8.CAG.GFP.WPRE		AAV8.CAG.REP1.WPRE	
Animal	CD45$^+$ cells (%)[1]	Vitreous opacities[2]	CD45$^+$ cells (%)[1]	Vitreous opacities[2]
1	12.4	Present	1.7	Absent
2	7.7	Present	1.2	Absent
3	1.1	Absent	1.4	Absent
4	3.0	Present	1.4	Absent
5	14.7	Present	4.0	Present
6	11.3	Present	2.3	Present

[1] CD45$^+$ cells were quantified using the Cytek Aurora spectral cytometer. [2] Vitreous opacities were identified on SD-OCT images by two independent individuals.

It was noted that there were two NK1.1$^+$ populations, a population with a low scatter that was in line with lymphocytes (P1) and one with a higher scatter that was similar to macrophages detected in this study (P2) (Figure 3.21A). Neither of these populations were present in the NK1.1 FMO (which included all antibodies except NK1.1) (Figure 3.21B), suggesting that the population was as a result of antibody staining. P1 was situated within the CD11b$^-$ and CD11b^{lo} gates, while P2 was situated within the gates for macrophages and microglia (Figure 3.21C). Cells within P1 were confirmed to have a low light scatter, indicative of lymphoid NK cells, while those in P2 had a higher scatter, which may suggest non-specific staining of myeloid cells (Figure 3.21D). One explanation could be due to non-specific binding of the NK1.1 antibody to Fc receptors that are commonly expressed on the surface of macrophages. To investigate this, a 10-fold greater concentration of Fc block was used, which induced a significant reduction in the number of cells within P2, however, did not affect those

within P1 (Figure 3.21E); this supports the NK1.1 expression in P1 as genuine staining. Nonetheless, the spread in the P2 gate did not return to the level of the FMO. It was also noted that the intensity of NK1.1 staining in P1 was significantly lower in cohort 1 (Figure 3.21F) compared to cohort 2 (Figure 3.21A), which may have resulted in a loss of resolution between $NK1.1^+$ and $NK1.1^-$ cells and could explain the greater numbers detected in cohort 2. The NK1.1 MFI was significantly higher in cohort 2 compared to cohort 1 (t test, $p \leq 0.0001$; n=6) and was comparable to the MFI of $NK1.1^+$ cells initially detected in splenocytes (Figure 3.21G). It is therefore likely that NK cells were inadvertently classified as the undefined myeloid and negative populations, while NKT were classified as CD8 T cells, due to the lack of a CD8 antibody in flow cytometry panel.

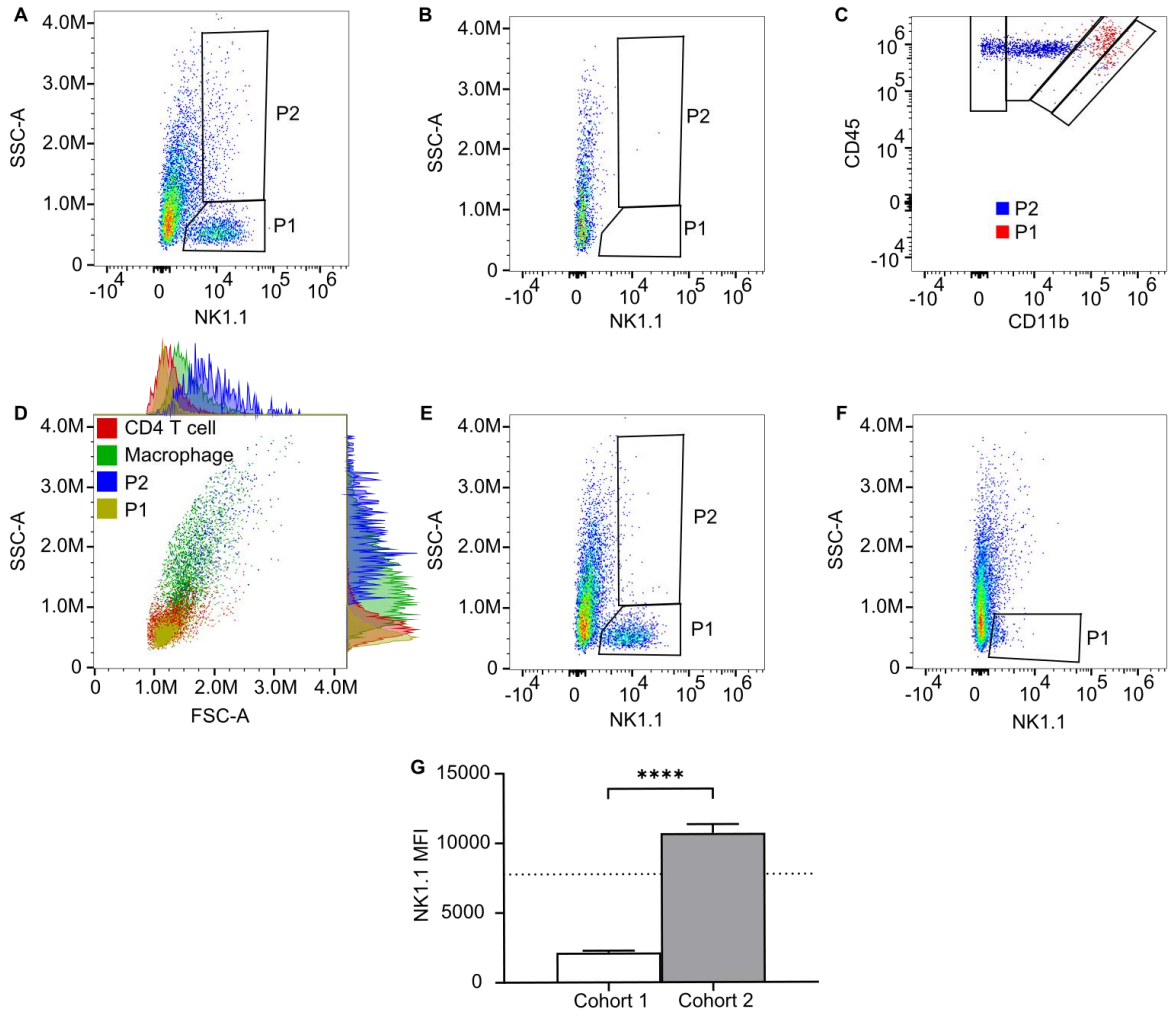

Figure 3.21. NK1.1 staining in AAV8.CAG.GFP.WPRE-injected mouse retinae. Representative plots of C57BL/6J mice subretinally injected with $1x10^9$ gc of AAV8.CAG.GFP.WPRE 14 days post-injection and analysed using the Cytek spectral cytometer. (**A-D**) NK1.1 expression in total live CD45$^+$ cells of a mouse from cohort 2; (**A**) a fully stained representative plot, (**B**) a NK1.1 FMO control, (**C**) overlay of events in gate P1 and P2 from the fully stained sample, (**D**) light scatter profile of P1, P2, macrophages, and CD4 T cells with corresponding histograms, and (**E**) a sample with 10-fold more Fc block. (**F**) Fully stained representative plot of total live CD45$^+$ cells of a mouse in cohort 1. (**G**) NK1.1 MFI of NK1.1$^+$ events in the P1 gate from cohort 1 and 2; dashed line indicates the NK1.1 MFI from fully stained splenocytes. ****$p \leq 0.0001$ (unpaired t test) (±SEM, n=6).

3.4.8 Identification of undefined leukocyte populations

To better characterise the poorly defined leukocyte populations (P3, P5, P7, P10, and P11 in Figure 3.18), their light scatter patterns were compared against known leukocyte populations identified by the antibody panel. Forward and side scatter are related to cell size and internal complexity, respectively. Myeloid cells are typically higher in forward and side scatter than resting lymphocytes, which is reflected in their scatter profiles. The $CD11b^{lo}CD11c^{-}NK1.1^{-}CD3^{-}$ myeloid population (P3 in Figure 3.18) had a scatter profile similar to macrophages, suggesting that it was of myeloid origin (Figure 3.22A). The $CD11b^{lo}$ expressing T cell populations (P5 and P7) were confirmed as lymphocytes by their lower scatter profiles, which were comparable with the $CD11b^{-}$ T cells detected in this study (Figure 3.22B). The $CD3^{-}CD4^{+}$ cell population had a scatter slightly higher than CD4 T cells, however, was significantly less than the macrophages identified in this panel, suggesting that this population was likely derived from a lymphoid lineage and could reflect an active state (Figure 3.22C). The $CD45^{+}$ immune population that was negative for all other markers (P11) had a scatter profile close to that of CD4 T cells, suggesting that it was also of lymphoid lineage (Figure 3.22C).

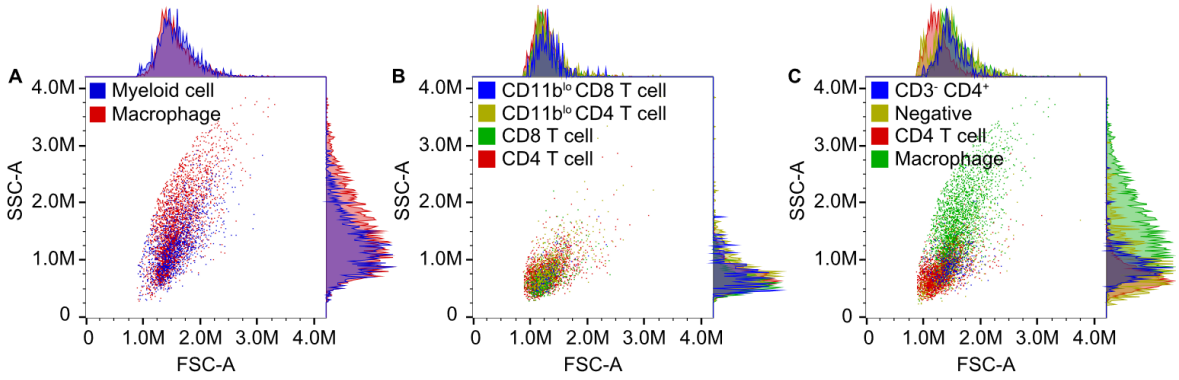

Figure 3.22. Light scatter profiles of unknown leukocyte populations. Representative FSC-A vs SSC-A plots with corresponding histograms of a single C57BL/6J mouse 14 days after receiving a subretinal injection of $1x10^9$ gc of AAV.CAG.GFP.WPRE. Overlay of (**A**) macrophages and unidentified myeloid cells; (**B**) CD4 T cells, CD8 T cells, $CD11b^{lo}$ CD4 T cells, and $CD11b^{lo}$ CD8 T cells; and (**C**) macrophages, CD4 T cells, immune cells negative for all makers, and $CD3^-$ $CD4^+$.

3.5 Discussion

Observations of dose-dependent inflammatory responses to AAV retinal gene therapy have primarily relied on qualitative descriptions of cell-mediated reactions. In this chapter, I apply the use of sensitive multicolour flow cytometric analysis to quantify and characterise the cellular immune response to AAV8 retinal gene therapy over time. The results reveal a significant increase in the number of leukocytes in the retina from 14 days post-injection of an AAV8 serotype vector expressing GFP driven by the ubiquitous CAG promoter. Using a panel of immune cell markers, cells of both myeloid and lymphoid lineage, which are typically absent from the normal retina [212], were identified, suggesting AAV-mediated recruitment and infiltration of leukocytes. Among the myeloid cells detected were resident microglia, macrophages, and an unidentified

$CD11b^{lo}CD11c^{-}NK1.1^{-}CD3^{-}$ myeloid population. The light scatter profile of this population suggests that these cells are of myeloid origin, however, the use of additional markers may aid further identification. Normal retinal tissue contains almost no dendritic cells and only occasional macrophages [213]. The absence of $CD11c^{+}$ cells found in this study suggests that recruitment of classical dendritic cells is unlikely to play a significant role in AAV-induced retinal inflammation. However, enzymatic dissociation of the retina with papain may lead to the unintended destruction of epitopes, therefore, additional experiments with mechanical dissociation could be performed to confirm the absence of CD11c and CD19 staining. The lymphoid cells detected in this study include CD4 T cells, CD8 T cells, NK cells, and NKT cells. Due to the significant background autofluorescence of retinal cells the number of markers available for use in this study was limited, a decision was therefore made to indirectly identify CD8 T cells by the expression profile of $CD4^{-}CD3^{+}$. The use of a CD8 antibody would therefore aid in confirming the presence of CD8 T cells in this immune response. The majority sub-populations of NK and NKT cells were found to be $CD11b^{+}$ and $CD11b^{-}$, respectively, which would be expected on mature NK cells and NKT cell populations [214]. A small subset (~3% of all leukocytes present by day 28) of CD4 and CD8 T cells were also detected with relative low levels of the marker CD11b. Although CD11b is typically used as a myeloid cell marker, the scatter profile of these populations suggested lymphoid origin. While the low CD11b positivity was determined with the use of a FMO control, non-specific CD11b staining of T cell populations cannot be ruled out. Alternatively, CD11b expression in T cells can be used as a marker of T cell activation [215, 216], so it is possible that these immune cells represent an active T cell population. To further investigate the activation status of

these T cells, assessment of the expression of other activation markers (e.g. CD69, CD25 and CD70) and pro-inflammatory cytokines could be performed [217].

The cellular immune response to subretinal AAV injections was detected at days 14 and 28 post-injection suggesting that this response was not resolved within the time frame of this study. The delay in detection of this response and the presence of significant numbers of T cells in the retina is in keeping with an adaptive immune response to AAV retinal gene therapy, where an innate reaction would, in contrast, be expected to be observed soon after subretinal injection. A recent study revealed the presence of significant numbers of neutrophils in the eye one day after intravitreal AAV injections, which had resolved by the subsequent seven day time point [218]. Therefore, it is possible that an early response was missed within the time frame assessed in this chapter. This could potentially be interrogated with the use of regular non-invasive SD-OCT imaging as a readout for retinal inflammation.

Two unknown immune cell populations were detected in this study: a population negative for all markers except CD45 and a $CD11b^{-}CD3^{-}CD4^{+}$ population. Both these leukocyte populations were $CD11b^{-}$ and had lower scatter profiles, suggestive of cells of lymphoid lineage. It is possible that these two populations represent subsets of ILCs. Many of these subsets are negative for the markers typically associated with other immune cell lineages and do not express the CD3 TCR co-receptor that contributes to antigen-specific responses [92]. Group 1 ILCs include NK cells and ILC1 cells, which are typically involved in mediating a type 1 immune response [92]. The presence of NK cells in this AAV-mediated immune response may suggest that the leukocyte population negative for all markers except CD45, which was significantly increased in

AAV-injected eyes, may be ILC1 cells. Tissue-resident ILC1 cells have recently been described in the central nervous system but have not yet been reported in the retina [219]. Alternatively, this $CD45^+$ only population might represent RPE cells which have adhered to the retina during tissue harvesting [220], although this might not explain the significant increase in AAV8.GFP-injected eyes. Furthermore, the $CD11b^-CD3^-CD4^+$ cells were detected in AAV vector-treated but not PBS-treated retinae. These might represent a small subset of ILCs termed LTi cells, which are $CD3^-CD4^+$ and play a role in promoting the survival of T cells that support memory B cells within lymphoid tissue [221]. However, LTi cells typically interact with T cells in lymphoid tissue and are not known to be present in the retina. Alternatively, a subset of $CD3^-CD4^+$ lymphocytes, which are distinct from ILCs and LTi cells, have been detected in the peripheral blood of humans [222]. Although not expressed on the cell surface, CD3 was expressed intracellularly, consequently, the expression of intracellular markers may have been missed in the experiments performed in this chapter. Therefore, further characterisation is needed to validate the hypothesised identities of these unknown leukocyte populations. As the antibody panel size for multicolour flow cytometry is limited and accounting for the autofluorescent spectra in retinal tissue is technically challenging, these methods and results provide the basis for further in-depth exploration of the retinal immune cell identities and activation states by single cell RNA sequencing in the future.

A high proportion of retinal leukocytes, in particular microglia and macrophages, were GFP positive, suggesting successful transduction by the AAV8 vector. Notably, high levels (~80%) of GFP fluorescence was found in the microglia. These cells can function in antigen presentation and produce pro-inflammatory cytokines in response to viral

injection [197], therefore, may be a key source for the recruitment of adaptive immunity. However, it has been previously suggested that microglia are difficult to transduce, with one group detecting no transgene expression following transduction of primary murine microglia *in vitro* with serotypes AAV1-9 [223]. A recent *in vivo* study also demonstrated that, following subretinal AAV delivery, microglia were able to internalise AAV, however, the genomes did not reach the nucleus, which would preclude transgene expression [224]. The use of higher doses of AAV in the experiments in this chapter and the quantification of GFP expression with sensitive flow cytometric analysis may explain some of the differences between these studies, however, further gene expression analysis in these cells would help to confirm AAV transduction of microglia. Interestingly, infiltrating leukocytes not resident at the time of subretinal injection were also sometimes weakly GFP positive. This may be the result of retained viable AAV particles in the retina, which have been detected in dogs and primates up to six years after retinal gene therapy [225]. Alternatively, the low GFP intensity (MFI) observed in lymphocytes compared with microglia and macrophages could suggest non-specific binding of GFP protein from lysed photoreceptor cells. Lymphocytes are also capable of acquiring surface proteins from APCs during antigen receptor signalling through a process termed trogocytosis, which could also contribute to the low level GFP expression in these cells [226, 227]. The reduced MFI in these populations is a likely explanation for the lack of detection of GFP^+ infiltrating leukocytes with the BD LSRFortessa, which has a reduced sensitivity compared to the Cytek Aurora used in subsequent experiments.

Despite detection of a substantial immune cell population in mice injected with an AAV8 vector expressing GFP, a significantly diminished response (approximately 4-

fold less) was observed in paired eyes injected with an equivalent AAV8 vector expressing a hREP1 protein. Although these differences were seen evenly distributed across all infiltrating leukocyte populations, the proportion of resident microglia as a percentage of total retinal cells was similar in the AAV8.CAG.GFP.WPRE and AAV8.CAG.hREP1.WPRE–treated retinae (at ~1% of all retinal cells). There was no significant difference in the percentage of $CD45^+$ cells in AAV8.CAG.hREP1.WPRE–injected eyes in this cohort (cohort 2) compared to PBS–injected eyes in the previous cohort (cohort 1), suggesting that the hREP1 expressing vector does not induce a significant cellular immune response above that induced by surgical trauma. Nonetheless, experiments directly comparing the cellular immune response between paired PBS- and AAV8.CAG.hREP1.WPRE–injected eyes would help further explore this reaction. However, using t-SNE analysis, the relative proportions of the infiltrating leukocyte populations can be seen to be relatively conserved between GFP and hREP1 vector-injected eyes, with the exception of NK cells and macrophages which were overrepresented in the GFP vector-treated eyes. Taken together, these findings suggest that the mechanisms of the cell-mediated immune response to the GFP- and hREP1-expressing vectors were similar albeit the latter was perhaps occurring at a 'subclinical' level. As the capsid and regulatory features of these two vectors were identical, the increased cellular response to the GFP vector may be, at least in part, directed towards the GFP transgene protein. GFP represents a novel antigen in the mouse retina with the potential to trigger a cytotoxic immune response [185]. This corroborates findings in AAV2- and AAV8-injected cynomolgus macaques demonstrating a GFP-specific systemic T cell response in two of the 14 animals that received high vector doses ($1x10^{11}$ gc/eye) [180]. In contrast, while human REP1 is

also an exogenous protein, it may be sufficiently similar to murine REP1 as to be better tolerated. To further explore the effect of a novel antigen on the cellular immune response, AAV8.CAG.GFP.WPRE injections could be performed in a mouse line that expresses retinal GFP, or AAV8.CAG.hREP1.WPRE injections may be undertaken within a REP1 knockout mouse. The other factor to consider is that, while the GFP and hREP1 vectors were both titrated using standardised quantitative PCR and purified to be free of toxic excipients, differences in the level of transduction and protein expression *in vivo* is difficult to control and could potentially affect the scale of any innate immune response; this may be investigated using semi-quantitative western blot analysis. Furthermore, cells overexpressing GFP demonstrate signs of oxidative stress and inflammation, including IFN-α, IFN-γ, and TNF-α–mediated responses [228], which may contribute to the increased immunogenicity of the GFP vector. Ultimately, it remains to be seen whether other therapeutic transgenes and increased vector doses produce a comparable cellular immune response.

Unexpectedly, the nullGFP control vector designed in this chapter induced generalised thinning with complete disruption of photoreceptors throughout the entire retina, suggesting a toxic reaction to the AAV vector. As recent studies have implicated AAV-encoded mRNA to induce innate immune responses through the RNA sensor MDA5 [172], a vector capable of transcription, but not translation, was created to isolate the role of the transgene protein on the AAV-mediated cellular immune response. The null vector used in this study, therefore, contained an open reading frame that would likely produced a full-length non-functional mRNA transcript. The Kozak sequence of the null vector was removed to prevent translation initiation, however, it is possible that low level protein expression may have persisted, or indeed, that the absence of a Kozak

consensus on the mRNA might have activated an immune response. Accumulation of unfolded or misfolded proteins in the endoplasmic reticulum could potentially activate cellular stress mechanisms, termed the unfolded protein response [229]. During conditions of prolonged stress, an apoptotic cascade is activated, leading to photoreceptor death. AAV transduction has been demonstrated to activate the unfolded protein response pathway, suggesting that AAV vectors are processed through these stress pathways [230], which may explain the wide-spread toxicity observed with the null vector. However, no cytotoxicity was observed following *in vitro* transduction of HEK293T cells with the nullGFP vector at the MOI tested. This may suggest that either the *in vitro* dose was insufficient to induce a toxic response or that the retina is more sensitive to vector-mediated toxicity. Furthermore, although all AAV preparations were confirmed to have minimal protein contaminants by SDS-PAGE, the presence of potentially inflammatory by-products cannot be completely ruled out. To further investigate the role of the AAV transgene in cellular immune responses to retinal gene therapy, a vector could be designed which includes a premature stop codon in the transgene sequence to trigger non-sense mediated decay of the mRNA transcript and prevent aberrant protein production.

In this chapter, the preliminary investigations into the cellular immune response were performed using a tyrosine mutant capsid AAV8(Y733F) vector due to the availability of this vector at the time of experimental set up. To avoid extraneous effects that may arise from this mutant capsid and confound investigation of the cell-mediated immune response to retinal gene therapy, all subsequent experiments were performed with a wildtype AAV8 capsid serotype. However, the level of vitreous opacities detected using SD-OCT imaging appeared to be significantly greater in mice injected with the mutant

capsid vector (AAV8(Y733F).CAG.GFP.WPRE) compared to the experimental cohort injected with the wildtype vector (AAV8.CAG.GFP.WPRE), suggesting a stronger inflammatory response. Nonetheless, the comparable level and time frame of the cellular responses seen with the mutant and wildtype AAV8 vectors suggests that the mutation is unlikely to be a strong source of the inflammatory response. In preliminary experiments with the AAV8(Y733F).CAG.GFP.WPRE vector, a CD68 antibody was utilised to assess microglial activation. CD68 can be upregulated upon microglial activation in the CNS [207], which may be detected by an increase in CD68 MFI. However, no significant difference was observed between the CD68 MFI of PBS- or AAV-injected eyes suggesting that microglia did not upregulate CD68 during this response. Nonetheless, the level of CD68 expression detected in resting microglia in the normal mouse retina was higher than expected, with other studies detecting minimal expression by immunohistochemistry [231]. It thus cannot be ruled out that the process of permeabilisation and fixation involved in staining this intracellular antigen may have led to spurious results. To assess the activation status of microglia more specifically and sensitively, single cell RNA sequencing could be performed on this leukocyte sub-population in the future.

In the preliminary experiments performed with the BD LSRFortessa, populations spanning a range of CD11b expression levels were detected in AAV-injected retinae outside of the three established gates (P1, P2, and P3) and a defined $CD11b^{lo}$ population was visible. Thus, this gating strategy is limited in the assessment of retinal leukocyte populations in response to subretinal AAV injections. Nonetheless, equivalent populations were observed with the Cytek Aurora spectral cytometer confirming the pattern of expression. With the use of additional markers, the $CD11b^{lo}$

population was identified as NK cells and a unidentified myeloid population. Furthermore, AAV-injected eyes analysed using the BD LSRFortessa demonstrated a trend for a reduced number of microglia at days seven and 14 post-injection that was not observed with the Cytek Aurora. This may partially stem from incorrectly compensated samples in the BD LSRFortessa, which may be affected by the high level of expression of the CD45 antibody on the retinal cells and the relative brightness of stained compensation beads. Alternatively, although the co-expression of CD45 and CD11b has effectively been used to distinguish microglia and macrophages [138, 198-201], microglia can increase CD45 expression following activation which may limit the resolution between these two populations [232, 233]. To further identify retinal microglia, additional antibodies could be utilised such as the recently identified microglia-specific marker transmembrane protein 119 (TMEM119) or the co-expression of CD45, CD11c, F4/80, and I-A/I-E [201, 234]. Alternatively, the use of fate-mapping to selectively label microglia could help identify these populations to more specifically analyse their response to AAV retinal gene therapy [201, 233].

A substantial increase in the intensity of NK1.1 staining was observed in AAV8.CAG.GFP.WPRE–injected retinae analysed in cohort 2 compared to those assessed in cohort 1. The NK1.1 conjugate PE/Cyanine 7 is a tandem fluorophore consisting of the covalent attachment of two dyes that can be subject to breakdown as a result of light exposure and poor storage conditions. In fact, PE/Cyanine7 has one of the highest degradation rates of PE-conjugated antibodies [235]. Due to the repeated use of this antibody, it is likely that it may have undergone tandem-dye degradation due to inadvertent light exposure. Although the voltage settings of all detectors used at day 14 in both cohorts were equivalent and antibodies used were from the same lot,

a new antibody aliquot was used for cohort 2 that would have no previous light exposure. The antibody aliquot used for cohort 1 was initially tested in splenocytes and demonstrated high levels of fluorophore intensity similar to those observed in cohort 2. This supports the sequential loss of antibody activity through tandem-dye degradation. The antibody panel for cohort 1 also included the antibodies CD19-APC/Fire750 and CD11c-PerCP/Cyanine5.5, which were removed from the panel in cohort 2 due to a lack of positive staining. Although there is a possibility of these antibodies increasing spread into the PE/Cyanine7 channel, these three antibodies demonstrate relatively low levels of similarity, ranging from 0.13–0.27 when assessed using the Cytek Full Spectrum Viewer (similarity can range from 0–1, with 1 indicating very similar spectra) [236]. These antibodies were also tested together in splenocytes where each presented good resolution between negative and positive populations. Another possibility for low intensity of NK1.1 staining may be due to reduced expression of the target protein on the cells of interest. Although mice were injected with the same material and dose, and were measured at the same time points, there may be inherent differences in the level of NK1.1 expression. However, as this was consistently seen across all six mice in each cohort, it is unlikely to be due to mouse variability but technical differences in each cohort.

Non-specific staining of macrophages and microglia was also observed in the NK1.1 detector channel, which was substantially reduced in the presence of an increased concentration of Fc block, suggesting non-specific NK1.1 antibody binding to Fc receptors found on many myeloid cells. Nonetheless, even with a 10-fold increase in the concentration of Fc block, the spread in the macrophage population did not return to the level of the NK1.1 FMO. One explanation may be that tandem dyes such as the

NK1.1 conjugate PE/Cyanine7 can non-specifically bind to monocytes and macrophages despite use of a Fc block [237]. True-Stain Monocyte Blocker (BioLegend) [238] and phosphorothioate-modified ODN sequences are able to block this additional source of non-specific staining and could be tested in subsequent experiments [237]. Overall, the limitations observed with the NK1.1 antibody support the use for a different fluorophore conjugate in future experiments.

FMO controls were included for each injection material at every time point to enable accurate gating of positively stained populations. To account for the spread of all replicates, a small volume was taken from each sample and pooled to create the FMO controls. Due to the variable levels of antibody staining between replicates, these populations may shift, which could lead to inaccuracies in gating. To accurately represent the spread in each individual sample, FMO controls should be created for each retina, however, due to the limited number of cells, this was unachievable in these experiments. Although FMO controls are able to account for background induced by spill over between fluorophores, they are unable to control for the non-specific staining of negative populations, as seen with the NK1.1 antibody above [239]. Background staining can be explored using an isotype control, an antibody raised against an antigen not present in the sample that matches the fluorophore conjugate, Ig subclass, and host species of the test antibody. However, the use of isotype controls remains controversial as variables in the design of these antibodies can lead to significant differences in background staining. Furthermore, the use of isoclonic controls that consist of a mixture of a fluorophore conjugated antibody and excess quantities of the same, unlabelled antibody can be used as an indicator of free fluorochrome binding [240]. Together these controls can provide a quality assurance

step in the creation of an antibody panel. Internal negative controls can also provide an effective means of isolating positive populations, however, require a negative population of the same cell type which is difficult to attain for these retinal samples. Populations of interest can be further defined using sequential Boolean gating with additional markers to distinguish positively stained cells that are poorly segregated from the negative population [240]. The use of cytometry time of flight (CyTOF), a variation on flow cytometry whereby antibodies are labelled with heavy metal ions rather than fluorophores, could enable the use of a larger antibody panel while overcoming the limitation of significant autofluorescence in the retina.

3.6 Conclusion

In this chapter, I conducted quantitative analysis of the cellular immune response to AAV vector-mediated retinal gene therapy in mice using multicolour flow cytometry. This provides significant benefits over current qualitative techniques, enabling assessment of the timing and magnitude of cellular immunity *in vivo,* whilst providing a comprehensive visualisation of all leukocyte populations. A significant number of infiltrating leukocytes were detected in retinae from 14 days following subretinal injection of an AAV8 vector expressing a *GFP* transgene under control by a ubiquitous CAG promoter. The cellular immune response comprised resident microglia and infiltrating leukocytes including macrophages, NK cells, CD4 and CD8 T cells, and NKT cells, indicative of a type 1 dominated effector immune response. In particular, microglia and macrophages appear to be significantly transduced by the AAV8 vector, although further analysis will help to validate this finding. Compared with AAV8.CAG.GFP.WPRE, a significantly lower level of cellular immune response was

detected in eyes injected with an AAV8.CAG.REP1.WPRE vector expressing a human retinal protein. This indicates that the level of cellular immune response in the retina is potentially dependent on the nature of the viral transgene.

4 Intracellular innate immune responses to AAV and the effect of immunomodulatory drugs on *in vitro* transduction

4.1 Introduction

AAV is widely considered the vector of choice for gene therapies, in part, due to its low immunogenicity compared with other viral vectors, such as lentiviruses and adenoviruses [156]. However, an increasing number of studies have revealed that intracellular innate immune pathways can elicit AAV-specific immune responses, suggesting the presence of inherent immunogenic features in AAV vectors [241]. PRRs play an essential role in the initiation of innate immune responses through the detection of specific microbial molecules, which induce downstream host immune reactions. Among these receptors are TLR9, an endosomal PRR capable of detecting unmethylated CpG motifs in DNA sequences in viral genomes [49, 50]. Previous studies have demonstrated TLR9 can sense AAV genomes, eliciting a cellular immune response that is significantly diminished upon depletion of CpG sequences [169-171]. Furthermore, TLR2, which is located at the cell surface and detects a range of microbial PAMPs, such as viral proteins [52], can induce an innate immune response to AAV capsids [157]. A recent study also demonstrated MDA5, which is activated by long viral dsRNA, can induce an immune response to AAV genomes at later time points following transduction [172]. It was hypothesised that reverse mRNA transcripts, generated from inherent promoter activity of the AAV 3'ITR, could anneal to the transgene mRNA to generate immunogenic dsRNA transcriptional intermediates [172]. Although there

have been no studies to date investigating the role of the anti-viral cytosolic DNA sensor cGAS in AAV-mediated immune responses [58, 59], *in vivo* studies have demonstrated a range of innate immune responses to AAV, including the upregulation of TLR9- and cGAS-specific pathways following subretinal AAV injections, suggesting the activation of innate immunity in the retina [175-177]. Activation of TLR9, MDA5, and cGAS induces NF-κB- and IRF-mediated upregulation of pro-inflammatory cytokines and type I interferons, respectively [53, 66, 67], with TLR2 signalling solely through NF-κB [66]. In addition to the potential implication of pro-inflammatory cytokines in mediating a cellular response, as characterised in Chapter 3, intracellular innate immune responses can create restrictive environments that may limit transgene expression. For instance, a type I interferon response following TLR9 or cGAS activation can inhibit transcription and translation within infected and neighbouring cells by upregulating numerous ISGs via the JAK-STAT pathway [68]. Examples include, TRIM5α that can bind to viral capsid proteins to promote viral disassembly and restrict infection [68]; ISG15 which is a ubiquitin-like protein that can covalently bind to viral proteins to disrupt replication [242]; and IL-15 that helps to eliminate infected cells by inducing the proliferation and maintenance of NK cells and $CD8^+$ T cells [243, 244]. A means of suppressing these immune pathways may be key in preventing damaging inflammatory responses in the retina and ultimately enhancing the level of transgene expression to improve the therapeutic outcome of retinal gene therapy.

Hydroxychloroquine and chloroquine are immunomodulatory agents used in the treatment of autoimmune diseases such as systemic lupus erythematosus and rheumatoid arthritis [245]. A hallmark of autoimmune diseases is the accumulation of

DNA- or RNA-containing complexes due to a build-up of apoptotic bodies, which can, in turn, activate TLR9, TLR7, and cGAS [246-249]. Investigation into the mechanism of hydroxychloroquine and chloroquine in the treatment of these diseases, has since revealed the inhibition of TLR9 and cGAS [250-252]. Initial *in vitro* studies demonstrated that chloroquine could suppress the stimulatory activity of CpG-ODNs, thereby inhibiting cytokine release [253, 254]. Subsequent experiments demonstrated the dose-dependent inhibition of CpG-ODN binding to TLR9 by chloroquine in HEK293 cells [255]. Additional studies have since confirmed the inhibition of TLR9 by these drugs, proposing a mechanism of action whereby hydroxychloroquine and chloroquine bind to CpG-containing nucleic acids and induce conformational changes that prevent TLR9 activation [251, 256]. Furthermore, chloroquine led to the dose-dependent inhibition of ssRNA-mediated TLR8 activation and polyinosinic: polycytidylic acid (poly(I:C)) (synthetic analogue of dsRNA)–mediated TLR3 activation in HEK293 cells [251]. In human monocyte-derived dendritic cells and peripheral blood mononuclear cells (PBMCs), chloroquine inhibited poly(I:C)-induced TLR3 responses [257]. Chloroquine has also been shown to inhibit TLR7-mediated responses to small nuclear ssRNA in human PBMCs, resulting in the downregulation of IFN-α expression [258]. An *in silico* screen of drug libraries to find cGAS antagonists identified several antimalarial drugs as putative inhibitors and further computational analysis predicted an interaction between hydroxychloroquine and the DNA binding site of cGAS [250]. Following dsDNA transfection of a human monocytic cell line (THP1), hydroxychloroquine treatment decreased expression of IFN-β, a downstream cytokine of cGAS activation, in a dose-dependent manner [250]. By preventing the activation of these PRRs, hydroxychloroquine and chloroquine may be able to dampen

an overactive innate immune response to self-nucleic acids. The same mechanism may also enable the reduction of the immune response to viral nucleic acid antigens, as demonstrated by the inhibition of TLR9-mediated responses to the DNA viruses herpes simplex virus (HSV)-2 [259] and Epstein-Barr virus [260, 261], and TLR7-mediated responses RNA viruses such as hepatitis C [262, 263], influenza [264], and vesicular somatic virus [265].

Typically, inflammatory responses have been controlled in retinal gene therapy trials using a course of systemic immunosuppression (e.g. oral corticosteroids). Corticosteroids, including the glucocorticoids dexamethasone and prednisolone, provide an additional means of controlling AAV-mediated inflammation and have been widely used in retinal gene therapy trials to control inflammatory responses [150-152]. Glucocorticoid activity exists at the apex of an extensive signalling pathway that blocks several downstream inflammatory responses. For instance, by inducing expression of the anti-inflammatory molecule mitogen-activated protein kinase (MAPK) phosphatase 1, preventing transcriptional activity of NF-κB that regulates downstream transcription of a vast range of cytokines, and blocking c-Jun–mediated transcription of pro-inflammatory cytokines [266]. Of interest in this study is the inhibitory activity of glucocorticoids on NF-κB–mediated expression of pro-inflammatory cytokines, which is a downstream regulatory factor of the anti-viral nucleic acid sensors TLR9 and cGAS [66, 67]. Indeed, dexamethasone treatment of macrophages blocked expression of TLR9-responsive genes following stimulation with CpG-containing sequences [267]. The ligand-bound glucocorticoid receptor is thought to directly interact with subunits of NF-κB and the NF-κB response elements to mediate its repression of pro-inflammatory genes [268, 269].

In this chapter, I investigate the effect of the PRRs TLR9 and cGAS on AAV transgene expression to further explore the restrictive role of intracellular innate immune responses in AAV transduction. I also explore the ability of the immunomodulatory drug hydroxychloroquine, an inhibitor of these PRRs, and the corticosteroid dexamethasone, an inhibitor of downstream immune pathways, to enhance AAV transgene expression *in vitro*.

4.2 Aims

The aims of this chapter are as follows:

1. To assess the effect of TLR9 and cGAS on AAV transduction *in vitro*.
2. To assess the effect of hydroxychloroquine and chloroquine on AAV transduction *in vitro.*
3. To investigate the effect of hydroxychloroquine on AAV transduction in primary non-human primate RPE cells.
4. To test the effect of dexamethasone on AAV transduction *in vitro.*

4.3 Materials & methods

4.3.1 Cell treatment & transduction

MEF cells were seeded 24 hours prior to treatment as per section 2.3.1 and transduced with an AAV2.CAG.GFP.WPRE vector at a MOI of 1,000 as described in section 2.3.5. For TLR9-activating experiments, wildtype MEFs were treated with either 0 or 754.6 μM CpG-A as per section 2.3.4. For testing of hydroxychloroquine and

chloroquine, wildtype MEFs were treated with ≤50 μM hydroxychloroquine and ≤12 μM chloroquine as per section 2.3.4. For testing of dexamethasone, wildtype MEFs were treated with ≤0.40 mM dexamethasone as per section 2.3.4; cells in these experiments were transduced with a MOI of 1,000 or 10,000 as indicated.

Prior to harvesting, the growth media was removed from MEFs and replaced with pre-warmed PBS to reduce background autofluorescence before imaging with the EVOS Cell Imaging System (Thermo Fisher Scientific). Cells were processed for flow cytometry three days post-transduction as described in section 2.6.1 and flow cytometry was performed as per section 2.6.2.

RPE cells were harvested from rhesus macaque eyes and cultured according to section 2.3.2. The cells were treated with a final concentration of either 0, 3.13, or 18.75 μM hydroxychloroquine in complete Neurobasal A media for one hour prior to transduction with an AAV2.CAG.GFP.WPRE vector at $5x10^7$ gc per well as described in section 2.3.4. Three days post-transduction, images were taken with a RetiGA-200R digital camera (QImaging) attached to a light microscope (Leica Microsystems) prior to harvesting the cells. Briefly, cells were harvested by washing with cold PBS before being detached in TrypLE Express (Gibco, Thermo Fisher Scientific). Cells were resuspended in complete Neurobasal A media, centrifuged at 300 xg for five minutes at room temperature, and the pellets were washed once in cold PBS. The supernatant was removed and the pellets were snap frozen on dry ice before storing at -80°C.

4.3.2 RNA extraction & reverse transcription

MEF cells pellets were homogenised in 350 µL of RLT buffer (QIAGEN) using a hand-held homogeniser with RNase free pestles; total RNA was extracted and reverse transcribed as per section 2.1.3.

Frozen rhesus macaque primary RPE cell pellets were lysed in 75 µL of buffer RLT and homogenised by vortexing for 20 seconds. Samples were centrifuged at 17,000 xg for three minutes to collect the non-lysed pigmented material. The supernatant was used for downstream RNA extraction as per section 2.1.3. The first flow through from the RNeasy Kit (QIAGEN) was kept on ice for subsequent protein extraction.

4.3.3 PCR & gel electrophoresis

80 ng of reverse transcribed cDNA from wildtype and *Cgas*$^{-/-}$ MEFs was subject to PCR (RT-PCR) with 10 µM of either *Cgas* (forward primer: TGGCAGCTACTATGAAC; reverse primer: ACAGCATCTTGGTAGC) or *Actb* (forward primer: AGCCATGTACGTAGCCA; reverse primer: GAAGCTGTAGCCACGCT) specific primers according to section 2.1.2. The *Cgas* primers span the first and second exon boundary of the corresponding mRNA sequence to produce a 200 bp PCR product, while the *Actb* primers are situated within the fourth exon and produce a 211 bp PCR product. Gel electrophoresis was performed on a 2% agarose gel as per section 2.1.2.

4.3.4 qPCR

qPCR of reverse transcribed cDNA samples from rhesus macaque RPE cells was performed as per section 2.1.4 using TaqMan probes (Thermo Fisher Scientific)

directed to *GFP* (assay ID: Mr03989638_mr) and rhesus macaque specific *Actb* (assay ID: Rh03043379_gH). *GFP* mRNA expression was normalised to *Actb* expression.

4.3.5 Protein extraction & western blot analysis

The flow through collected during RNA extraction of rhesus macaque RPE cells was mixed with four volumes of ice-cold acetone and incubated on ice for 30 minutes. Samples were centrifuged at room temperature for 30 minutes at 17,000 xg, the supernatant was removed, and the pellet washed in 100 µL of ice-cold 100% ethanol. The ethanol was removed and the pellets were air-dried on ice for five minutes. 50 µL of 1% SDS was added to each sample and the pellet was resuspended by repeat pipetting. The samples were incubated at 95°C on a hot block for three minutes followed by repeat pipetting; this was repeated twice more. The samples were centrifuged at room temperature for three minutes at 17,000 xg and the supernatant was transferred to a new tube to be stored at -20°C.

Protein samples from two biological replicates of RPE cells were thawed and quantified as per section 2.1.5. The Pierce BCA Protein Assay Kit (Thermo Fisher Scientific) was only sensitive enough to detect protein from one replicate. For this replicate, 17 ng of total protein was subject to SDS-PAGE. For the second replicate where the protein concentration couldn't be determined, the maximum volume of protein lysate was subject to SDS-PAGE. Western blot analysis was performed as per section 2.1.6. Membranes were stained with primary antibodies to GFP and β-actin, followed by staining with HRP-conjugated secondary antibodies (Table 2.1). GFP protein expression was normalised to β-actin expression.

4.4 Results

4.4.1 TLR9 agonist reduces AAV transduction *in vitro*

The role of TLR9 in AAV transduction was explored with the use of the agonistic TLR9 ODN CpG-A [169], which contains unmethylated CpG sequences known to stimulate TLR9 activity [49]. Initially, cells were treated with and without CpG-A for 30 minutes prior to AAV2.CAG.GFP.WPRE transduction and GFP fluorescence was quantified using flow cytometry three days post-transduction. Using flow cytometric analysis, a gating strategy was applied to exclude debris, doublets, and dead cells (Figure 4.1A–C), and to detect GFP^+ cells (Figure 4.1D and E). CpG-A treatment significantly reduced the mean number of GFP-fluorescing cells by 2.7-fold relative to untreated cells (paired t-test, p=0.0001; n=7) (Figure 4.2A and B) and the MFI of GFP^+ cells by a mean 1.1-fold (paired t-test, p=0.0007; n=7) (Figure 4.2C). While an increase in the percentage of GFP^+ cells provides a readout for level of successful transduction, the MFI indicates the level of GFP fluorescence per successfully transduced cell.

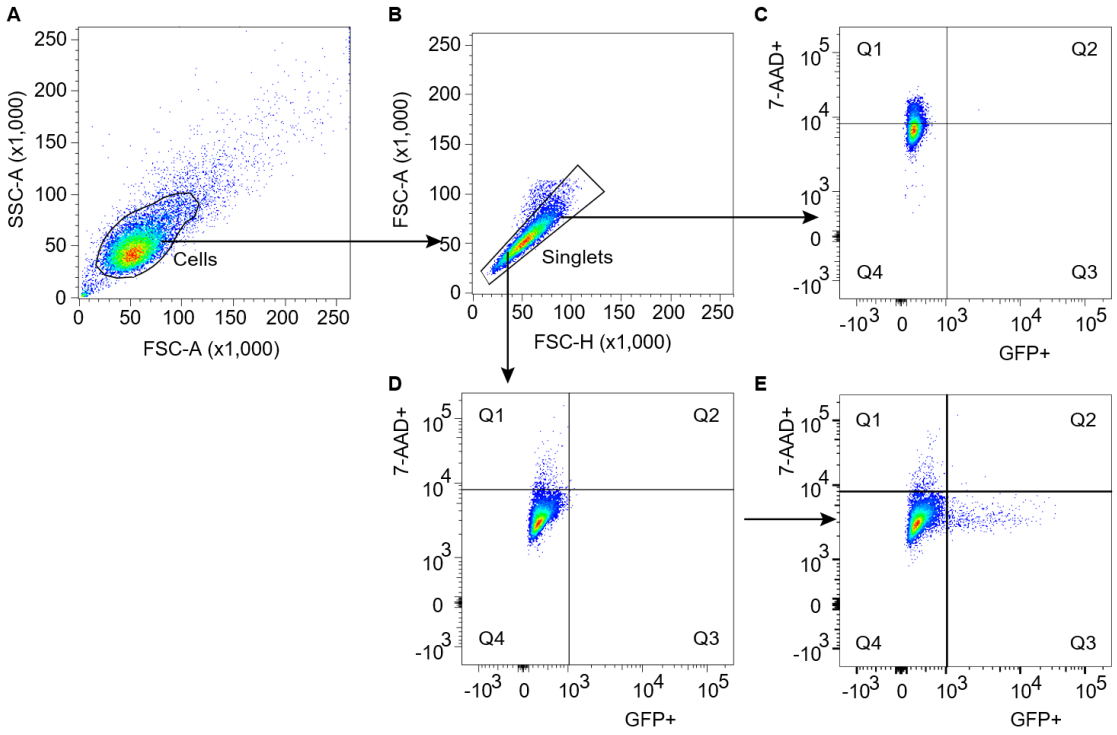

Figure 4.1. Flow cytometry gating strategy for wildtype mouse embryonic fibroblasts (MEFs). The exclusion of (**A**) debris and (**B**) cell doublets in wildtype MEFs using a flow cytometry gating strategy. (**C**) Increased 7-aminoactinomycin D (7-AAD) staining was observed in the positive control, which had been killed by heating at 60°C. The killed cell sample was used to exclude dead (7-AAD$^+$) cells in a (**D**) live cell sample. The live cell sample also served as a fluorescence minus one control for GFP expression in (**E**) MEFs transduced with AAV2.CAG.GFP.WPRE. Four populations were identified: GFP$^-$7-AAD$^+$ (Q1), GFP$^+$7-AAD$^+$ (Q2), GFP$^+$7-AAD$^-$ (Q3), and GFP$^-$7-AAD$^-$ (Q4). Q3 was used for quantification of live GFP$^+$ cells.

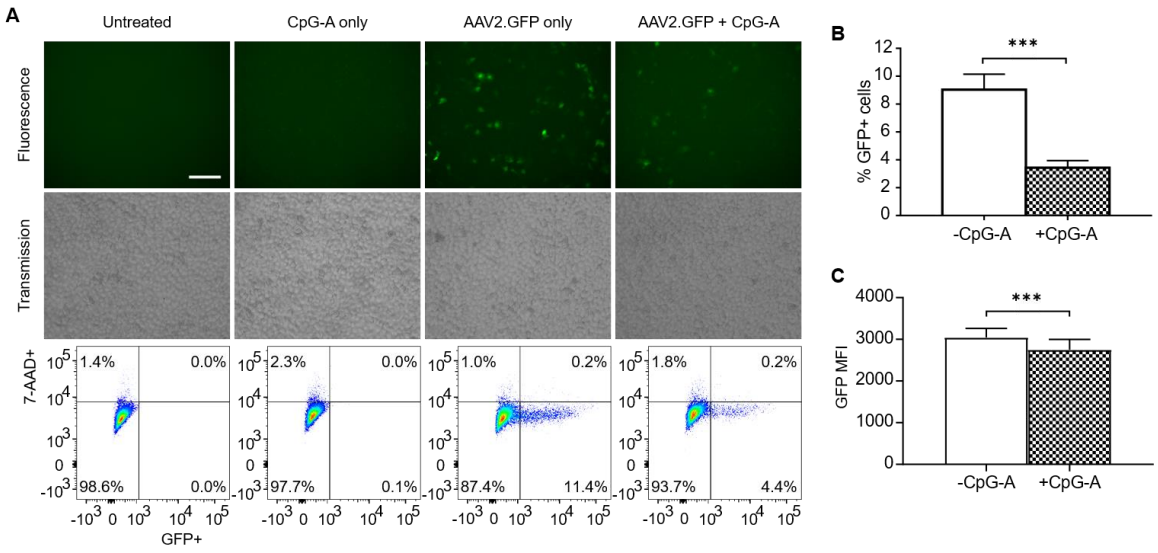

Figure 4.2. The agonistic TLR9 oligodeoxynucleotide CpG-A decreases AAV transduction in wildtype MEFs. Wildtype MEFs were treated with or without CpG-A (754.6 µM) 30 min prior to transduction with AAV2.CAG.GFP.WPRE at an MOI of 1,000. GFP fluorescence and cell viability (7-AAD staining) were assessed on day three post-transduction by flow cytometry. (**A**) Representative fluorescence and transmission images and flow cytometry plots (scale bar: 200 µm). (**B**) The mean proportion of GFP^+ cells expressed as a percentage of the total number of live ($7\text{-}AAD^-$) cells. (**C**) The mean MFI of live GFP^+ cells. ***$p \leq 0.001$ (paired t test) (±SEM, n=7).

4.4.2 Absence of cGAS increases AAV transduction *in vitro*

In order to investigate the effect of cGAS on AAV transduction, rates of transduction were compared between wildtype and *Cgas*$^{-/-}$ MEFs by flow cytometric analysis. *Cgas* mRNA expression was confirmed as present in wildtype MEFs and absent in *Cgas*$^{-/-}$ cells by visualising the 200 bp RT-PCR product using gel electrophoresis (Figure 4.3A). Wildtype and *Cgas*$^{-/-}$ MEFs were subsequently transduced with an AAV2.CAG.GFP.WPRE vector and GFP fluorescence was quantified using flow

cytometry three days post-transduction. *Cgas*$^{-/-}$ MEFs transduced with a 6.4-fold greater efficacy than wildtype MEFs at the same MOI (paired t test, p=0.0008; n=6) (Figure 4.3B and C). The MFI of GFP^{+} cells was significantly greater in *Cgas*$^{-/-}$ compared to wildtype MEFs (mean 2.8-fold increase) (Mann-Whitney test, p=0.0087; n=6) (Figure 4.3D). Differences in the rate of growth and morphology of wildtype and *Cgas*$^{-/-}$ MEFs were noted during these experiments.

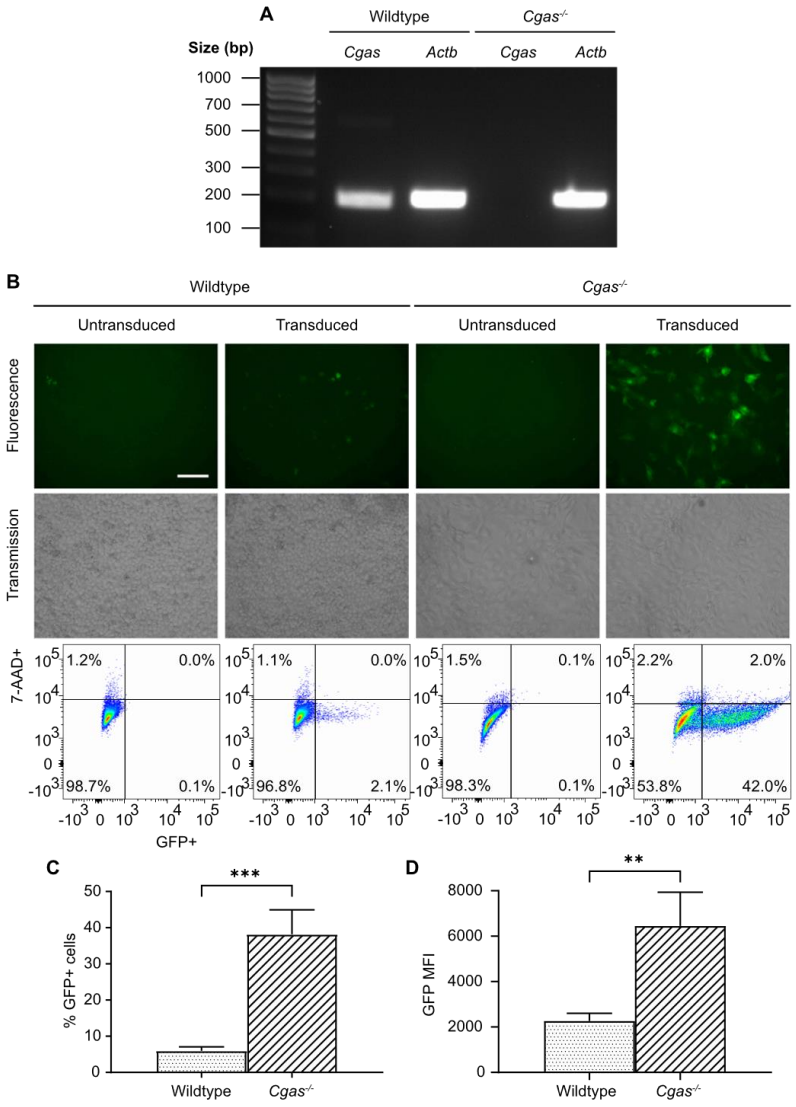

Figure 4.3. AAV transduction is significantly enhanced in *Cgas*$^{-/-}$ MEFs. (**A**) Agarose gel of RT-PCR amplified *Cgas* in wildtype and *Cgas*$^{-/-}$ MEFs, with *Actb* expression used as a positive control. (**B**) MEFs were transduced with AAV2.CAG.GFP.WPRE at an MOI of 1,000. Representative microscopy images and flow cytometry plots, gated for GFP and the cell viability marker 7-AAD, acquired three days post-transduction (scale bar: 200 μm). (**C**) Mean proportion of GFP^{+} cells expressed as a percentage of the total number of live (7-AAD^{-}) cells (±SEM, n=6). ***p ≤0.001 (unpaired t test). (**D**) Mean MFI of live GFP^{+} cells (±SEM, n=6). **p ≤0.01 (Mann-Whitney test).

4.4.3 Hydroxychloroquine enhances AAV transduction *in vitro*

In order to further explore the role of cGAS and TLR9 in AAV transduction, I examined the effect of the immunomodulatory anti-malarial drug hydroxychloroquine, which has been shown to inhibit both TLR9 and cGAS [250-252]. Initially, wildtype MEF cells were treated with 25 μM hydroxychloroquine at various time points prior to AAV transduction. This concentration was selected based on an *in vitro* study demonstrating a half maximal inhibitory concentration (IC50) of 25 μM in the human monocytic cell line THP1 [250]. Areas of no cell growth were observed in cells treated at 24 and seven hours prior to transduction, while those treated at one hour and five minutes grew normally (Figure 4.4). Based on these preliminary findings, cells were treated with hydroxychloroquine one hour prior to transduction in all subsequent experiments.

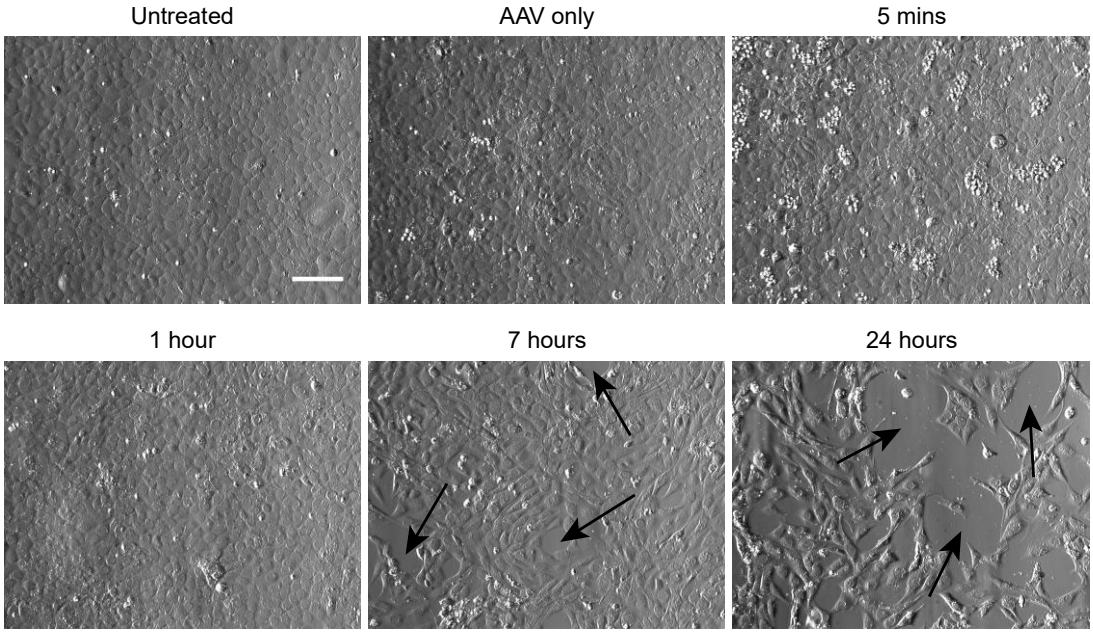

Figure 4.4. Optimisation of hydroxychloroquine incubation time. Wildtype MEFs were treated with 25 μM hydroxychloroquine at 5 minutes or 1, 7, or 24 hours prior to AAV2.CAG.GFP.WPRE transduction. Cells were transduced with AAV 24 hours after cell seeding and light microscopy images were taken three days post-transduction (scale bar: 200 μm). Arrows indicate areas of cell death.

To assess the cytotoxicity of hydroxychloroquine, wildtype MEFs were treated with increasing concentrations up to 50 μM hydroxychloroquine prior to transduction with AAV2.CAG.GFP.WPRE; GFP fluorescence and cell viability were analysed three days post-transduction by flow cytometry (Figure 4.5A and B). Hydroxychloroquine treatment increased the percentage of GFP^+ cells in a dose-dependent manner up to 18.75 μM; however, concentrations greater than 18.75 μM were cytotoxic, as evidenced by an increase in 7-AAD staining, which coincided with a decrease in GFP positivity (Figure 4.5C). Cytotoxicity was also observed in light microscopy images,

with large patches of no cell growth (Figure 4.5A). Subsequent testing of hydroxychloroquine was limited to ≤18.75 μM for all future experiments.

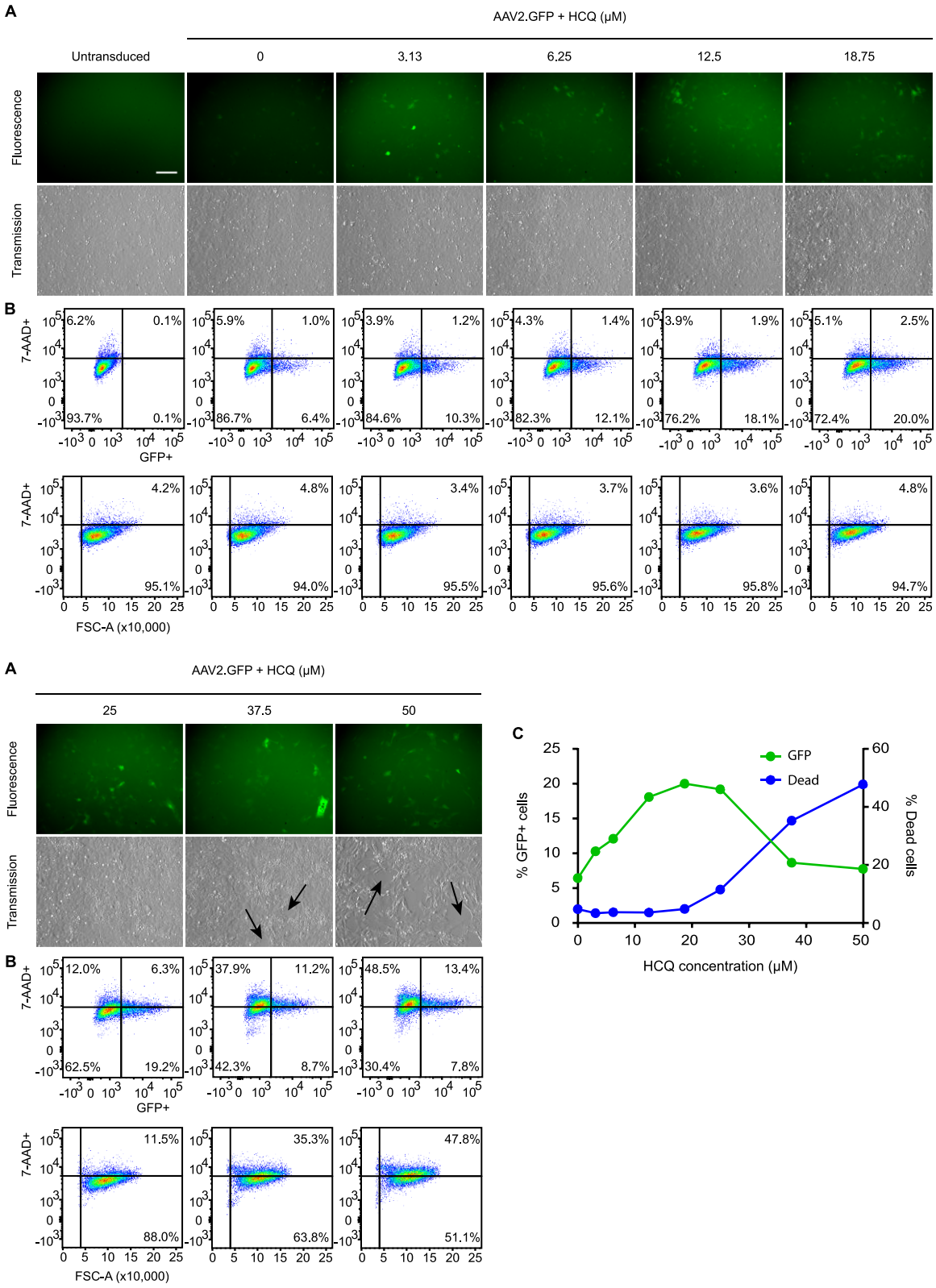

Figure 4.5. Toxicity and dose-response of hydroxychloroquine treatment of wildtype MEFs. MEFs were pre-treated with ≤50 μM hydroxychloroquine one hour prior to

transduction with AAV2.CAG.GFP.WPRE at a MOI of 1,000. (**A**) Representative microscopy images acquired three days post-transduction (scale bar: 200 μm). Arrows indicate areas of cell death. (**B**) Flow cytometry plots used for quantification of live GFP^+ cells (GFP vs 7-AAD) and cell viability (7-AAD vs FSC-A) three days post-transduction. (**C**) Dose-response curve of hydroxychloroquine concentration plotted against either GFP^+ or dead ($7\text{-}AAD^+$) cells gated to total cells demonstrating the level of transduction or toxicity, respectively (n=1).

The mean proportion of GFP positive cells increased from 6% with no hydroxychloroquine, to 9% with 3.13 μM and 19% with 18.75 μM hydroxychloroquine (Friedman test, p=0.0001; n=6) (Figure 4.6A and B). A mean 3.1-fold increase in GFP fluorescence was observed in cells treated with 18.75 μM hydroxychloroquine. There was no significant difference in the MFI of GFP^+ cells between hydroxychloroquine treated and untreated cells (Figure 4.6C).

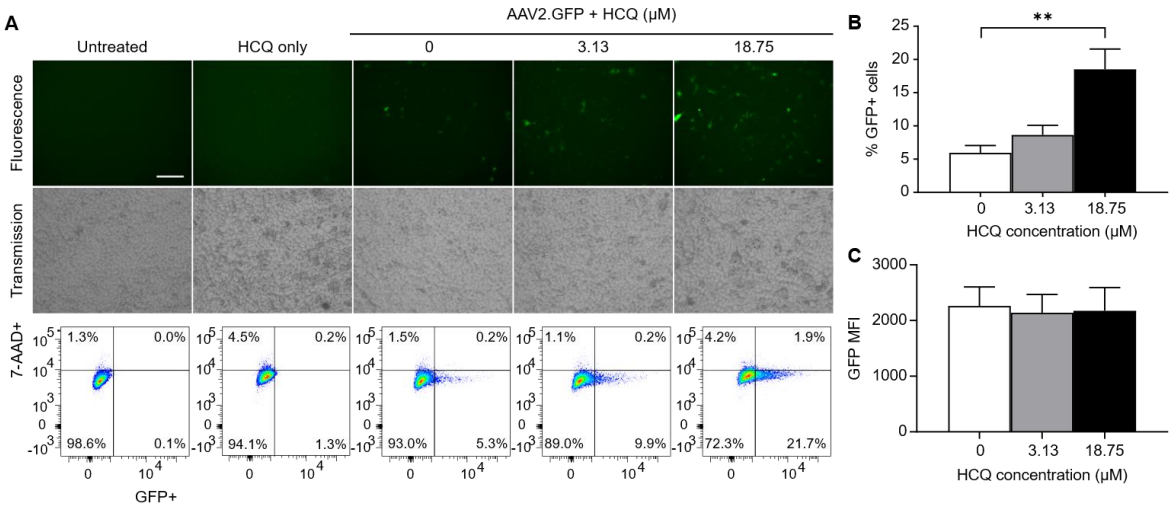

Figure 4.6. Hydroxychloroquine increases AAV transduction in wildtype MEFs. Wildtype MEFs were pre-treated with 0, 3.13, or 18.75 μM hydroxychloroquine for one hour prior to transduction with AAV2.CAG.GFP.WPRE at an MOI of 1,000. (**A**) Representative fluorescence microscopy images of MEFs treated with hydroxychloroquine acquired at three days post-transduction (scale bar: 200 μm), alongside flow cytometry analyses gated for GFP fluorescence and the cell viability marker 7-AAD. (**B**) Mean proportion of GFP^+ cells expressed as a percentage of the total number of live ($7\text{-}AAD^-$) cells (± SEM n=6). $^{**}p \leq 0.01$ (Friedman test with Dunn's multiple comparison test). (**C**) Mean MFI of live GFP^+ cells (±SEM, n=6).

4.4.4 Chloroquine enhances AAV transduction *in vitro*

To determine if the enhancement of AAV transduction by hydroxychloroquine might be due to a drug class effect, the structurally similar anti-malarial compound chloroquine was also tested. Pre-incubation of MEFs with chloroquine prior to transduction with AAV2.CAG.GFP.WPRE improved GFP fluorescence in a dose-dependent manner from 2.5% with no chloroquine to 6.4% with 12 μM chloroquine; there was no detectable cytotoxicity with the doses tested (Figure 4.7A and B). Since long-term oral intake of hydroxychloroquine (for treating autoimmune diseases) is

known to be associated with lower rate of retinal toxicity than chloroquine [270], hydroxychloroquine was selected for all further experiments.

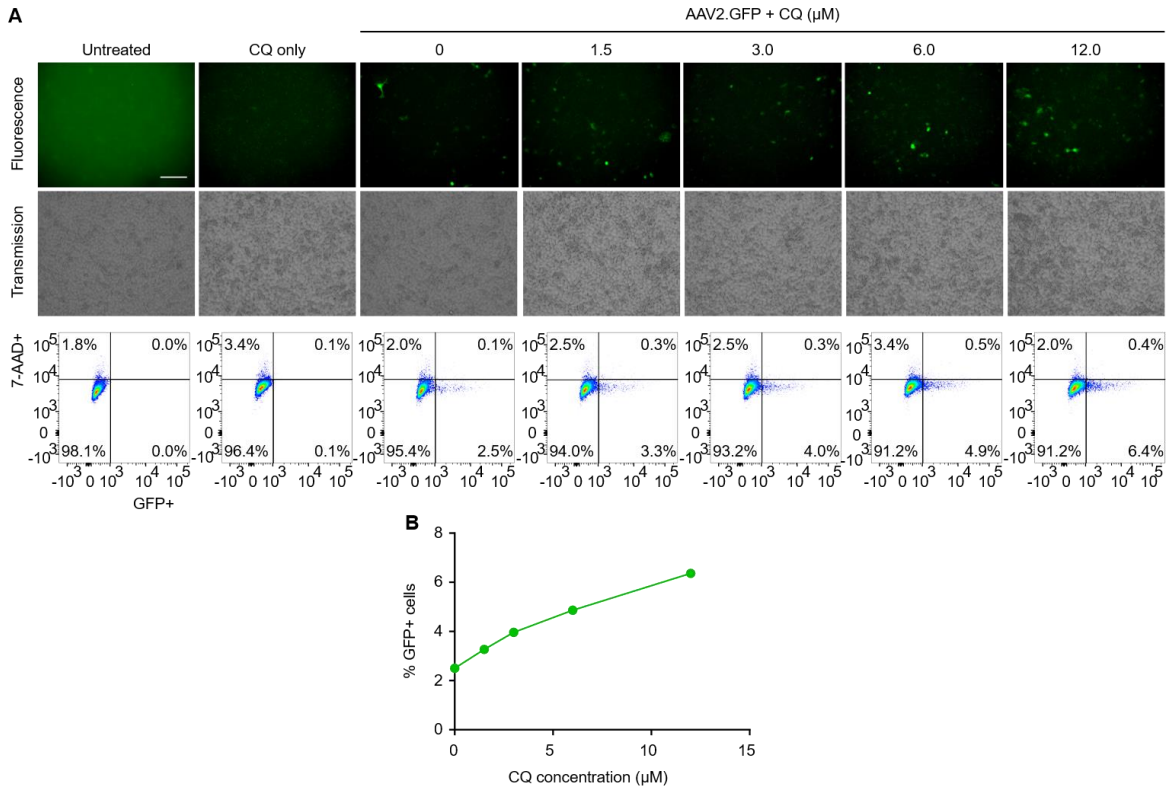

Figure 4.7. Chloroquine increases AAV transduction in wildtype MEFs. Wildtype MEFs were pre-treated with ≤12 μM chloroquine one hour prior to transduction with AAV2.CAG.GFP.WPRE at an MOI of 1,000. (**A**) Representative microscopy images and flow cytometry plots, gated for GFP and 7-AAD, acquired three days post-transduction (scale bar: 200 μm). (**B**) Proportion of GFP^+ cells expressed as a percentage of the total number of live ($7\text{-}AAD^-$) cells (n=1). Figure published in [175].

4.4.5 Hydroxychloroquine enhances AAV transduction in primary RPE cells

I subsequently tested the efficacy of hydroxychloroquine in rhesus macaque primary RPE cells to explore its potential in a cell type relevant to retinal gene therapy. The RPE

cells were treated with 0, 3.13, or 18.75 μM hydroxychloroquine prior to transduction with $2x10^9$ gc of AAV2.CAG.GFP.WPRE. At three days post-transduction, GFP mRNA expression was visualised by fluorescence microscopy and quantified by qPCR and western blot analysis. A visible increase in GFP fluorescence could be seen in RPE cells treated with hydroxychloroquine compared with AAV vector alone (Figure 4.8A), which correlated with a mean 3-fold increase in GFP mRNA expression in cells treated with 18.75 μM hydroxychloroquine (one-way ANOVA, p=0.0253; n=3 eyes) (Figure 4.8B). A similar magnitude of increase in GFP protein expression associated with hydroxychloroquine was detected by western blot; however, this did not reach statistical significance due to limited tissue availability (n=2) (Figure 4.8C and D).

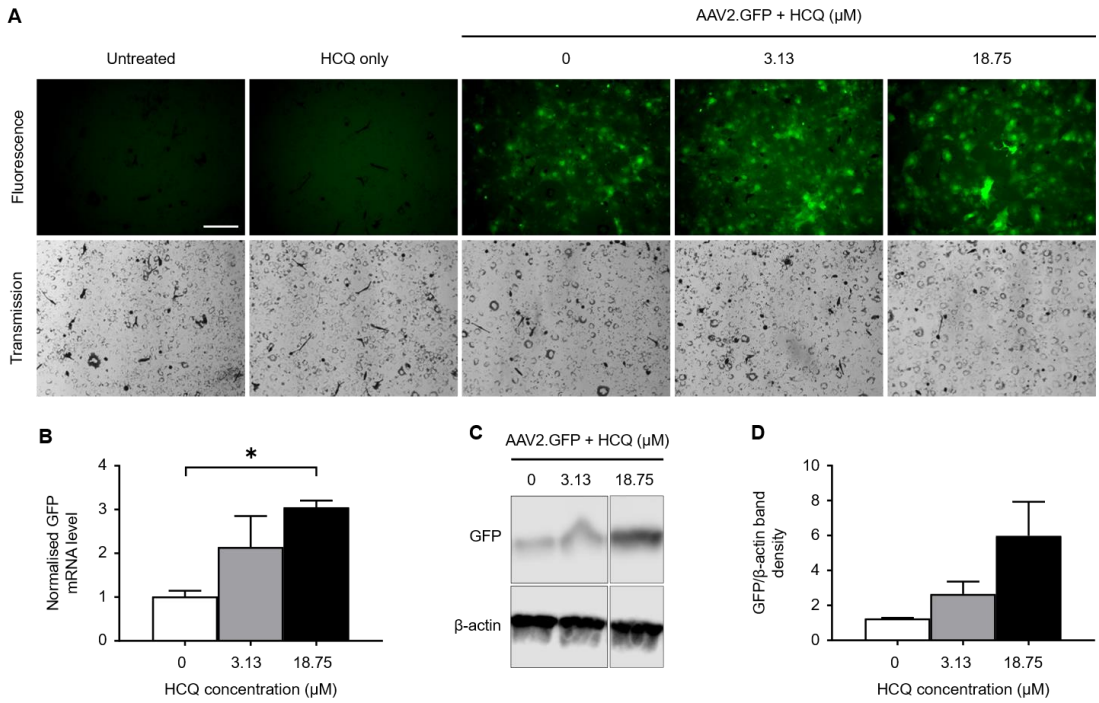

Figure 4.8. Hydroxychloroquine increases AAV transduction in primary RPE cells. Rhesus macaque primary RPE cells were pre-treated with 0, 3.13, or 18.75 μM hydroxychloroquine one hour prior to transduction with $2x10^9$ gc of AAV2.CAG.GFP.WPRE. (**A**) Representative microscopy images acquired three days post-transduction (scale bar: 200 μm). (**B**) *GFP* mRNA levels were quantified using quantitative PCR (qPCR) and expressed as mean fold change relative to AAV only treated cells (±SEM, n=3). **p* ≤0.05 (one-way ANOVA with Dunnett's multiple comparison test). (**C**) Representative western blot analysis of GFP protein expression. β-actin was used as loading control. (**D**) Quantification of western blot GFP band density normalised to β-actin (±SEM, n=2). Figure published in [175].

4.4.6 Dexamethasone has no effect on AAV transduction *in vitro*

Given the efficacy of the immunomodulatory drugs hydroxychloroquine and chloroquine in the enhancement of AAV transduction, I next tested the effect of the glucocorticoid dexamethasone. Glucocorticoids can inhibit NF-κB activity, which is

downstream of both TLR9- and cGAS-induced immune pathways [267-269]. To optimise the incubation time, wildtype MEFs were treated with 0.20 mM dexamethasone up to 24 hours prior to transduction. Although there was some evidence of cytotoxicity on light microscopy images (Figure 4.9A), this did not correlate to an increase in 7-AAD staining detected by flow cytometry (Figure 4.9B). The patches of no cell growth may therefore be a consequence of inadvertent mechanical detachment by replacement of the media with PBS prior to imaging. An increased incubation time with dexamethasone correlated with a higher percentage of GFP positivity without any significant effect on cell viability (Figure 4.9C). Although a slight enhanced percentage of dead cells was observed with cells incubated with dexamethasone for 24 hours prior to transduction, this was within the expected variability of cell viability. Therefore, a 24-hour incubation period was selected for all additional experiments.

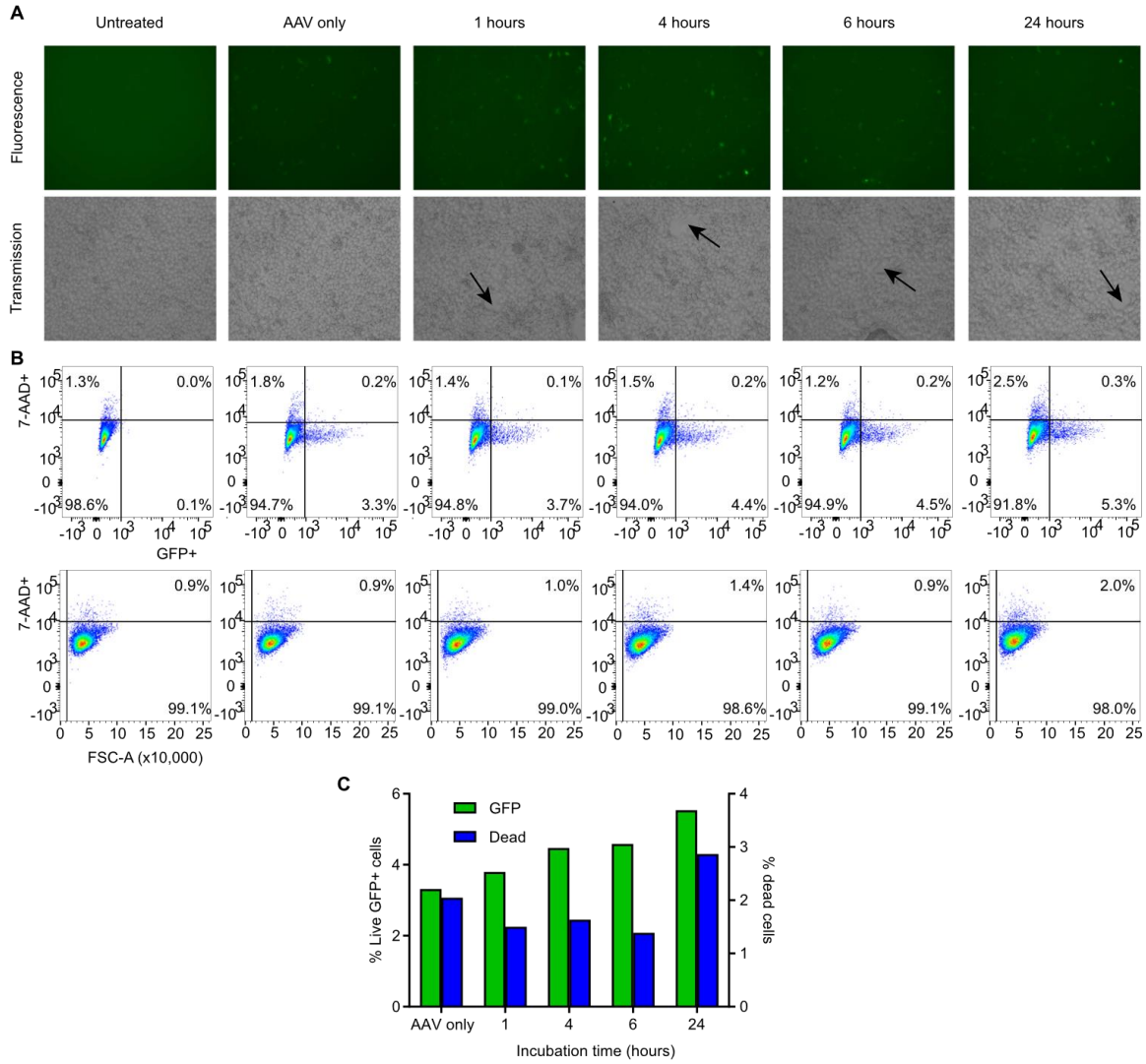

Figure 4.9. Optimisation of dexamethasone incubation time. Wildtype MEFs were pre-treated with 0.20 mM dexamethasone either 1, 4, 6, or 24 hours prior to transduction. Cells were transduced with AAV2.CAG.GFP.WPRE at a MOI of 1,000 24 hours after seeding. (**A**) Representative microscopy images (scale bar: 200 µm). Arrows indicate areas of no cell growth. (**B**) Flow cytometry plots used for quantification of live GFP⁺ cells (GFP vs 7-AAD) and cell viability (7-AAD vs FSC-A). (**C**) Percentage of GFP⁺ and dead (7-AAD⁺) cells gated to total cells for samples either not treated with dexamethasone (AAV only) or incubated with dexamethasone at various times prior to AAV transduction (n=1).

As very few wildtype MEFs were GFP^+ when using a MOI of 1,000, a MOI of 10,000 was used in subsequent experiments with dexamethasone. To assess the cytotoxicity of dexamethasone, wildtype MEFs were treated with increasing concentrations up to 0.40 mM dexamethasone prior to transduction with AAV2.CAG.GFP.WPRE; GFP fluorescence and cell viability were analysed three days post-transduction by flow cytometry (Figure 4.10A and B). Treatment with 0.40 mM dexamethasone led to a significant increase in 7-AAD staining, suggesting that this concentration was cytotoxic (Figure 4.10C). However, cytotoxicity was not observed in the light microscopy images (Figure 4.10A). Upon further testing with the safe dexamethasone concentrations (0.02, 0.10, or 0.20 mM), no significant difference in the mean percentage of GFP^+ cells was observed compared to untreated cells (Figure 4.10D), nor was there any difference in the GFP MFI (Figure 4.10E). Overall, these data suggest that dexamethasone had no effect on AAV transduction *in vitro*.

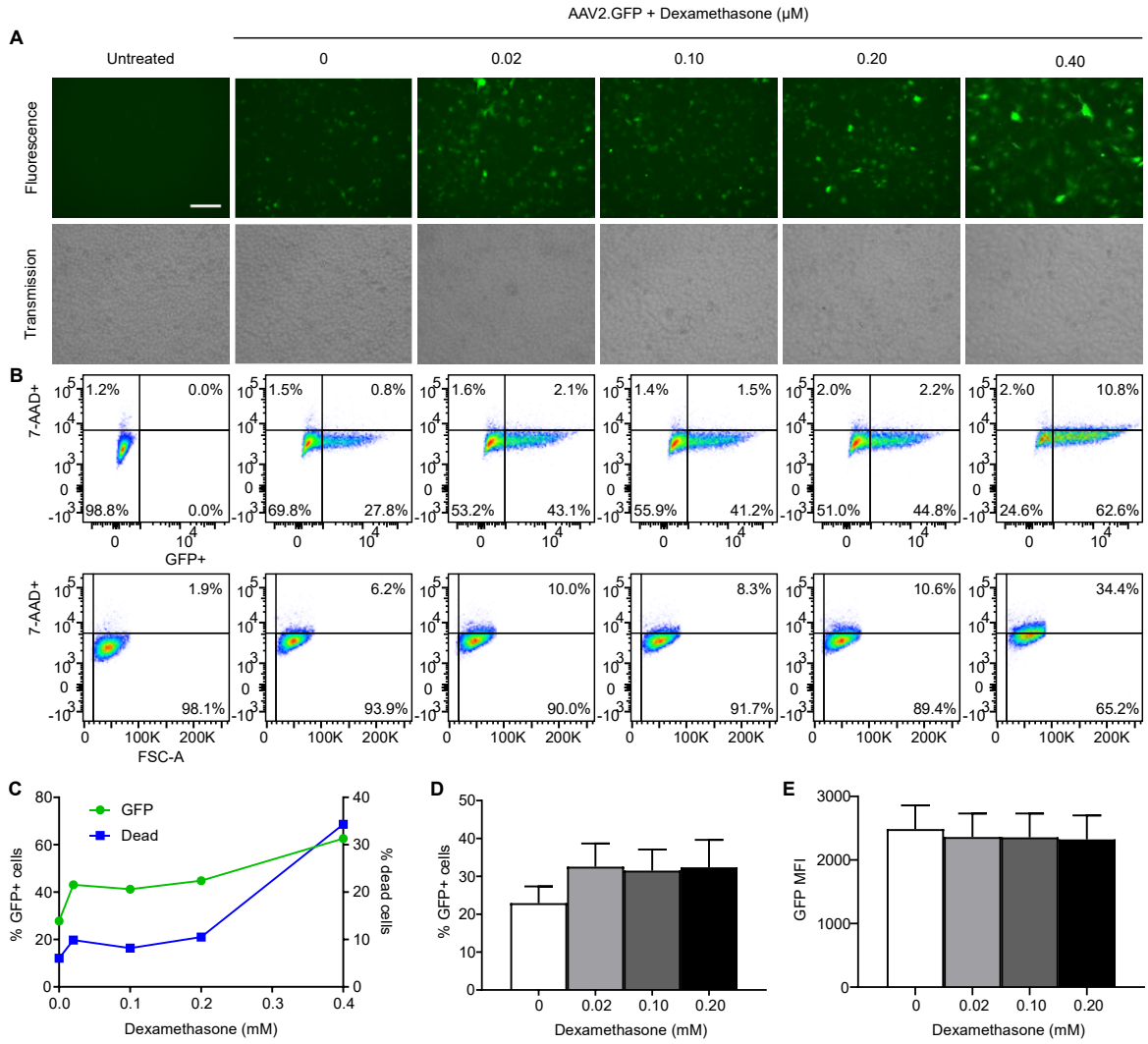

Figure 4.10. Dexamethasone treatment has no effect on AAV transduction in wildtype MEFs. Wildtype MEFs were pre-treated with 0, 0.02, 0.10, 0.20, or 0.40 mM dexamethasone for 24 hours prior to transduction with AAV2.CAG.GFP.WPRE at a MOI of 10,000. (**A**) Representative microscopy images (scale bar: 200 μm) and (**B**) flow cytometry plots used for quantification of live GFP$^+$ cells (GFP vs 7-AAD) and cell viability (7-AAD vs FSC-A) at three days post-transduction. (**C**) Dose-response curve of dexamethasone concentration plotted against either GFP$^+$ or dead (7-AAD$^+$) cells gated to total cells (n=1). (**D**) Mean proportion of GFP$^+$ cells expressed as a percentage of the total number of live (7-AAD$^-$) cells and (**E**) the mean MFI of live GFP$^+$ cells (±SEM, n=3).

4.5 Discussion

In this chapter I investigated the immunogenicity of AAV vector genomes by assessing the effect of the anti-viral DNA sensors TLR9 and cGAS on *in vitro* AAV transduction. The treatment of wildtype MEFs with a TLR9 agonist (CpG-A) induced a 2.7-fold reduction in AAV transgene expression, suggesting that stimulation of TLR9 can inhibit AAV transduction. Although there was a statistically significant reduction in GFP MFI following CpG-A treatment, the 1.1-fold decrease may suggest that TLR9 activation has a minimal effect on the level of cellular transgene expression. The potential restrictive role of TLR9 in AAV transduction supports previous studies that demonstrate AAV to induce a TLR9-mediated immune response, which is diminished upon depletion of CpG sequences in the viral genome [169, 170]. Furthermore, the percentage of GFP^+ cells and mean MFI was significantly greater in *Cgas*$^{-/-}$ compared to wildtype cells following *in vitro* AAV transduction. At a given MOI, enhancement to both the percentage of GFP^+ events and MFI could reveal increased viral infectivity [271], which may have been suppressed by AAV-induced activation of intracellular innate immune pathways. Due to differences in the mode of inhibition, it is difficult to make direct comparisons between the experiments investigating TLR9 and cGAS. To further explore and compare the restrictive role of these PRRs in AAV transduction, siRNA knockdown of factors within the TLR9 and cGAS pathway could establish their relative influence. This may also overcome the differences in morphology and growth rates observed between wildtype and *Cgas*$^{-/-}$ MEFs, which may have led to discrepancies in the rates of transduction. Activation of cGAS induces synthesis of the secondary signalling messenger cGAMP, which induces upregulation of type I interferon expression [63, 65]; cGAMP production can be detected by thin layer chromatography and could also

be used as a readout for AAV-mediated cGAS activation. Nonetheless, this is the first evidence of a role of cGAS in the restriction of AAV transduction. Overall, these findings support an increasing number of studies that implicate AAV as a viral immunogen that can activate intracellular innate immune responses through anti-viral nucleic acid sensors [184].

Hydroxychloroquine, an approved immunomodulatory drug that can inhibit the innate immune factors TLR9 [251, 255] and cGAS [250], was identified as a means of enhancing AAV transduction. Pre-treatment of wildtype MEFs with hydroxychloroquine demonstrated a dose-dependent increase in AAV transgene expression, which, at 18.75 μM, was both efficacious and non-cytotoxic. Despite an increase in the overall proportion of transduced cells, there was no significant difference in GFP MFI, suggesting that hydroxychloroquine treatment did not enhance the level of GFP expression in a given transduced cell. This suggests that hydroxychloroquine may function by enhancing successful viral transduction rather than transgene expression. The enhancement of AAV transduction was also observed with the structurally similar drug chloroquine. Both hydroxychloroquine and chloroquine exert similar immunomodulatory effects [245], supporting a common mechanism of action. The role of TLR9 and cGAS in the hydroxychloroquine-mediated enhancement of AAV transduction will be further explored in Chapter 6.

Flow cytometric analysis of MEF viability was determined using the fluorescent dye 7-AAD, which is typically excluded from live but permeant to dead cells. Once in the nucleus, 7-AAD can intercalate with double stranded DNA to undergo a spectral shift which allows for flow cytometric detection and assessment of cell viability [272]. In

the experiments in this chapter, wildtype MEFs were fixed with formaldehyde prior to 7-AAD staining to preserve cell integrity and limit autolysis of cells through the cross-linking of proteins via free amine groups. Fixation can result in disruption of membrane integrity which may result in inadvertent staining of the live cell population and a slight overestimation of the percentage of dead cells [273]. Although increased 7-AAD staining was observed in the control killed cell sample, which suggests that discrimination could still be achieved using fixed cells, these cells lacked the classical appearance of dead cell population where a distinct 7-AAD$^+$ population would be expected. Nonetheless, the increased 7-AAD staining of cells treated with hydroxychloroquine concentrations ≥25 μM correlated with areas of death observed using microscopy prior to flow cytometric analysis.

Enhanced AAV transgene expression was also achieved in non-human primate primary RPE cells, which provide a significant benefit over highly divergent immortalised cell lines and demonstrate a relevance to retinal gene therapy. To maintain the classical RPE phenotype, cells were passaged a minimal number of times, however, progressive depigmentation and morphological changes, consistent with the epithelium to mesenchymal transition, were evident [274]. *In vivo* testing would confirm the effectivity of hydroxychloroquine in RPE cells that maintain a typical epithelial phenotype.

Given the restrictive role of TLR9 and cGAS on AAV transduction, the glucocorticoid dexamethasone was investigated as a means of blocking downstream NF-κB activity and enhancing AAV transduction. However, no significant difference in AAV transgene expression or GFP MFI was observed following dexamethasone treatment *in vitro*,

suggesting that adjunctive treatment with this glucocorticoid has no detectable effect on AAV transduction. This may suggest that either NF-κB activity is not a key limiting factor in AAV transduction, or that adjunctive treatment of dexamethasone in these conditions had no effect on these pathways; to further investigate this, quantification of key cytokines could be performed. Previous experiments assessing the inhibitory effect of dexamethasone on TLR9-mediated gene expression used a concentration of 1 μM, 20-fold less than the lowest dose used in this chapter [267]. Therefore, additional experiments could be performed using these lower concentrations, which may exhibit a different mechanism of action. Given the effect of systemic glucocorticoid treatment on inflammation during retinal gene therapy [150-152], dexamethasone may present a greater efficacy in the direct suppression of the cellular immune response characterised in Chapter 3, rather than by directly enhancing AAV transduction. Overall, these findings support the efficacy and specificity of hydroxychloroquine in enhancing AAV transduction *in vitro*.

4.6 Conclusion

In summary, AAV transduction is limited by the intracellular innate immune factors TLR9 and cGAS. This is the first evidence of the role of the cytosolic nucleic acid sensor cGAS in AAV transduction and supports previous findings that AAV can induce TLR9-mediated responses; together these data suggest the presence of intracellular innate immunity to vector genomes. Pre-treatment with hydroxychloroquine, an inhibitor of TLR9 and cGAS, led to a dose-dependent increase in AAV transduction of wildtype MEFs and primary non-human primate RPE cells. In contrast, the immunosuppressant dexamethasone had no effect on AAV transduction *in vitro*. Hydroxychloroquine may

thus present an opportunity to enhance AAV transduction efficacy by evading AAV-mediated immunity.

5 Effect of hydroxychloroquine on retinal gene therapy *ex vivo* and *in vivo*

5.1 Introduction

Gene therapies based on AAV vector-mediated gene transfer are at advanced stages of clinical development to treat a broad range of monogenic disorders and have shown significant potential in the treatment of retinal dystrophies [151, 152, 190, 275-278]. The clinical efficacy of AAV-mediated gene therapy is strongly dependent on the proportion of target cells transduced, particularly when trying to halt disease progression in post-mitotic tissues such as the RPE and photoreceptors. Despite the success of voretigene neparvovec in the treatment of *RPE65*-associated LCA, variability in visual acuity improvements have been observed across other trials and the long-term efficacy in these patients remains unclear. Even across the various gene therapy trials for *RPE65*-associated LCA, the long-term data from several trials demonstrated advancing retinal degeneration despite initial improvements in visual acuity [183, 279, 280]. Although there are several differences between these trials, this effect has, in part, been suggested to be due to insufficient levels of retinal transduction and transgene expression [183, 280]. While transduction can be increased to some extent by vector dosage, host inflammatory and immune responses to AAV are limiting at high vector doses and may compromise the persistence of transgene expression and the therapeutic efficacy [156, 176, 180, 241, 281, 282]. Therefore, one of the major challenges of gene therapy for retinal diseases will be how to achieve sufficient levels of gene replacement at a safe vector dose.

As demonstrated in Chapter 4, hydroxychloroquine can increase AAV transduction *in vitro*, which presents an opportunity to maximise the therapeutic effect of retinal gene therapy at a given vector dose. This could have significant implications on inefficient gene therapies that require high AAV doses to achieve a therapeutic effect. Stargardt disease, caused by mutations in the gene ATP binding cassette subfamily A member 4 (*ABCA4*), is the most prevalent monogenic inherited retinal dystrophy [283]. The monogenic nature of the disease and autosomal recessive method of inheritance would suggest Stargardt disease to be a feasible therapeutic target for retinal gene therapy, however, the large size of the *ABCA4* gene exceeds the 4.7 kb packaging capacity of a single AAV vector. One approach to overcome this, is the use of a dual vector system where the *ABCA4* transgene is split between two different vectors [284]. Within these vectors is an overlap region which, following homologous recombination, creates a single DNA sequence that can encode the full length *ABCA4* transcript. However, high AAV doses are necessary to overcome this limiting recombination step and achieve a therapeutic effect [284]. Given the dose-dependent inflammation observed in clinical trials with single AAV vectors, it is possible that the high doses needed for sufficient transgene expression in this dual *ABCA4* system would induce inflammatory effects. Thus, enhancement of transgene expression in these systems could have significant implications for the possibility of using lower and safer vector doses.

Chronic systemic intake of hydroxychloroquine has been associated with an increased risk of retinopathy. Daily dose and duration of treatment are major risk factors for hydroxychloroquine-associated retinal toxicity, with 7.5% of patients experiencing retinopathy when taking the drug for more than five years, which increases to 20–50% after 20 years of therapy [285]. Nevertheless, retinopathy is unlikely in the first 5 years

of therapy unless concomitant risk factors are present [285]. Although the mechanism for hydroxychloroquine-associated retinopathy is unclear, its occurrence implies that hydroxychloroquine could accumulate in the retina following systemic delivery. Indeed, hydroxychloroquine has a high affinity for melanin and has consequently been detected in pigmented ocular tissues such as the RPE, choroid, and ciliary body [286, 287]. The use of SD-OCT retinal imaging has enabled detection of pre-symptomatic toxicity and provides a means of monitoring this response [288].

In this chapter, I investigate the effect of hydroxychloroquine on AAV transduction *ex vivo* in human retinal tissue and *in vivo* in mice when administered systemically or locally. The efficacy of hydroxychloroquine was assessed on two single AAV vectors and a dual AAV vector system expressing *ABCA4*, with SD-OCT employed to monitor potential signs of retinal toxicity.

5.2 Aims

The aims of this chapter were as follows:

1. To investigate the effect of hydroxychloroquine on AAV transduction in *ex vivo* human retinal tissue.

2. To assess the effect of orally delivered hydroxychloroquine on AAV transgene expression following subretinal injection of AAV2.CAG.GFP.WPRE *in vivo.*

3. To assess the safety of subretinal injections of hydroxychloroquine *in vivo.*

4. To investigate the effect of subretinal delivery of hydroxychloroquine on AAV2.CAG.GFP.WPRE transgene expression *in vivo.*

5. To investigate the effect of subretinal delivery of hydroxychloroquine on AAV8(Y733F).GRK1.GFP transgene expression *in vivo.*

6. To investigate the effect of subretinal delivery of hydroxychloroquine on AAV8(Y733F).GRK1.ABCA4.WPRE dual vector transgene expression *in vivo.*

5.3 Materials & methods

5.3.1 *Ex vivo* human retinal tissue treatment

Human retinal explants from two patients were cultured as per section 2.3.3, with three replicates per condition. The retinal tissue was treated with 0 or 3.13 μM hydroxychloroquine one hour prior to transduction with AAV2.CAG.GFP.WPRE at a dose of $1x10^9$ gc/well. The media and hydroxychloroquine were replaced from below the insert every two days, at which point the retinal explants were imaged using fluorescence microscopy. To measure the mean grey value of the retinal explants, the area of unfolded retina was traced on transmission light images taken with a RetiGA-200R digital camera (QImaging) attached to a light microscope (Leica Microsystems) using the programme ImageJ (Version 1.51j8, NIH) (Figure 5.1A). This area was superimposed onto the fluorescence image and the mean grey value was measured (Figure 5.1B). To account for background autofluorescence of the well, the mean grey value of a 2.54 mm band around the retinal tissue was subtracted from the total grey value of the explant (Figure 5.1C). The normalised grey value was calculated by subtracting the mean grey value of untransduced retinal tissue (treated with the same hydroxychloroquine concentration) to account for any background autofluoresence of the tissue and drug.

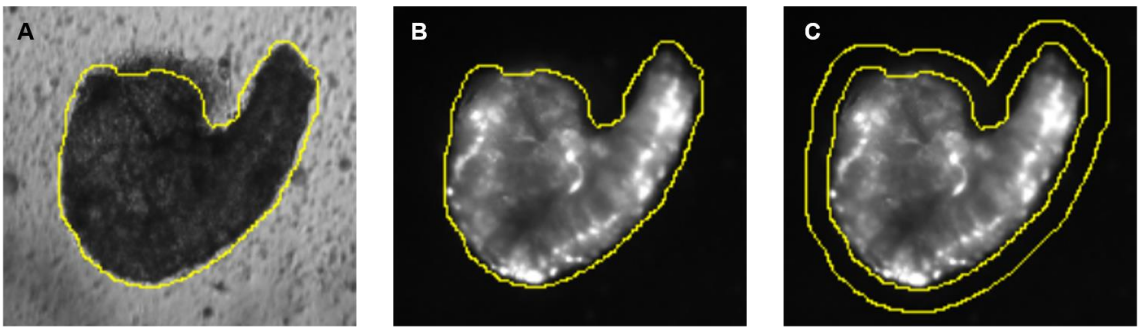

Figure 5.1. Measuring the mean grey value of human retinal tissue *ex vivo*. (**A**) Freehand tracing of the retinal explant transmission light microscopy image using ImageJ. The trace was superimposed onto (**B**) the fluorescence microscopy image and the mean grey value was measured. (**C**) The mean grey value of a 2.54 mm band was subtracted from the total grey value of the retinal explant to account for autofluorescence of the well.

5.3.2 Oral hydroxychloroquine delivery

Seven week-old female C57BL/6J mice were supplied with either 0, 0.058, or 0.116 mg/mL hydroxychloroquine in the drinking water, supplemented with 5% fruit cordial. Water bottles were covered with aluminium foil as hydroxychloroquine is light sensitive and were replaced with fresh water containing hydroxychloroquine every two days. Mice were monitored for two weeks for signs of acute toxicity or dehydration by visual assessments of skin turgor, mucus membranes, eye condition, coat condition, activity, and urine output. Water bottles and animals were weighed each day to calculate the dose of hydroxychloroquine (HCQ) (mg/kg/day) received by each animal as per equation 5.1. Subretinal injections were performed after three weeks of hydroxychloroquine delivery. All animals continued to receive hydroxychloroquine for three weeks post-injection, totalling six weeks on the drug.

$$\text{Mean HCQ dose (mg/kg/day)} = \frac{(\text{Mean vol. of water (mL)}) \times (\text{Conc. of HCQ (mg/mL)})}{\text{Average mass (kg)}} \quad (5.1)$$

5.3.3 Subretinal injections

Mice were subretinally injected as per section 2.5.3. For the oral hydroxychloroquine study, animals were subretinally injected with AAV2.CAG.GFP.WPRE at $5x10^7$ gc/eye in a total volume of 1.5 µL; paired eyes were left uninjected.

To assess the toxicity and autofluorescence of hydroxychloroquine, seven to eight week-old female C57BL/6J mice were subretinally injected with 1.2 µL of 18.75 µM hydroxychloroquine, with sham injections of PBS undertaken in the paired eye.

For assessment of the co-injection of hydroxychloroquine and AAV2.CAG.GFP.WPRE, seven to eight week-old female C57BL/6J mice were injected with $1.2x10^8$ gc/eye in a total volume of 1.2 µL, with injections of a suspension of AAV with either 3.13 or 18.75 µM hydroxychloroquine performed in the contralateral eye. An additional nine mice were injected with 18.75 µM hydroxychloroquine and AAV in one eye and AAV only in the paired eye to supplement the cohort for western blot analysis.

For the co-injection of hydroxychloroquine and AAV8(Y733F).GRK1.GFP, four to five week old female 129S2/SvHsd mice were injected with $1x10^8$ gc/eye in a total volume of 1 µL, with injections of AAV supplemented with 18.75 or 112.5 µM hydroxychloroquine performed in the paired eye. The AAV8(Y733F).GRK1.GFP encoded a *GFP* transgene under control by the photoreceptor-specific G-protein-coupled receptor kinase 1 (GRK1) promoter packaged into a mutant AAV8(Y733F) serotype capsid; the vector was provided as a kind gift from Dr Michelle McClements.

For the co-injection of hydroxychloroquine and the AAV8(Y733F).GRK1.ABCA4.WPRE dual vector, four to five week old male and female *Abca4*$^{-/-}$ mice (129S4/SvJae-*ABCA4*^{tm1Ght}) were subretinally injected with 1x10^{10} gc of both the upstream and downstream vector (total 2x10^{10} gc/eye) in a total volume of 1 µL, with injections of AAV supplemented with 18.75 µM hydroxychloroquine in the paired eye. AAV injections were supplemented with 0.001% of the non-ionic surfactant Pluronic F-68. This dual vector included an upstream vector, with a GRK1 promoter and 1–3,701 bp of the *ABCA4* coding sequence, and a downstream vector, with 3,494–6,822 bp of the coding sequence including a 207 bp overlap region and a WPRE enhancer (Figure 5.2) [284]. The vector was provided as a kind gift from Dr Michelle McClements.

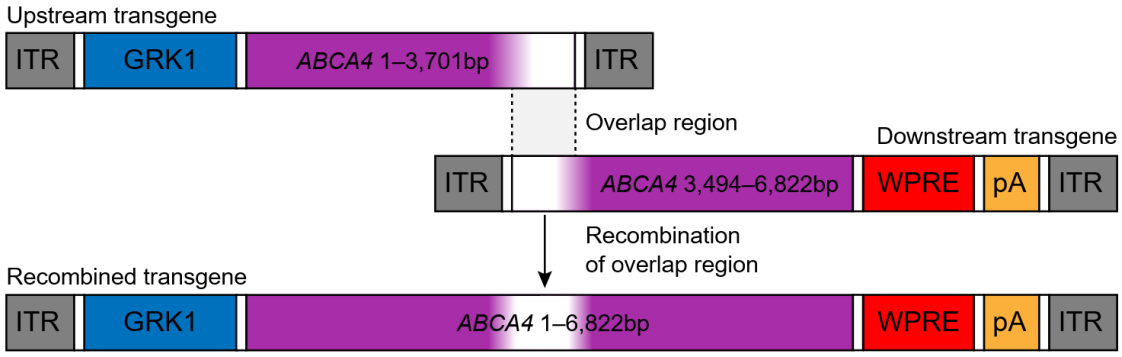

Figure 5.2. Schematic of the ATP binding cassette subfamily A member 4 (ABCA4) dual vector system. The full-length *ABCA4* transgene was split across two vectors (upstream and downstream transgene). The upstream transgene includes 1–3,701 bp of the *ABCA4* coding sequence and the downstream vector includes 3,494–6,822 bp of the coding sequence. Once inside the nucleus, these two vectors recombine at the 207 bp overlap region to produce a full-length recombined transgene. GRK1, G-protein coupled rhodopsin kinase 1 promoter.

5.3.4 Retinal imaging

Retinal fluorescence was measured with cSLO at a standardised detector sensitivity as per section 2.5.4. Retinal fluorescence was determined by measuring the mean grey value (the mean grey value of all the pixels in a region) of BAF images using the ImageJ software. A sampling band centred on the optic disc with an inner radius of 3.65 inches and a width of 2.65 inches was used to measure the mean grey value (Figure 5.3). Retinal thickness was measured with SD-OCT imaging as per section 2.5.4.

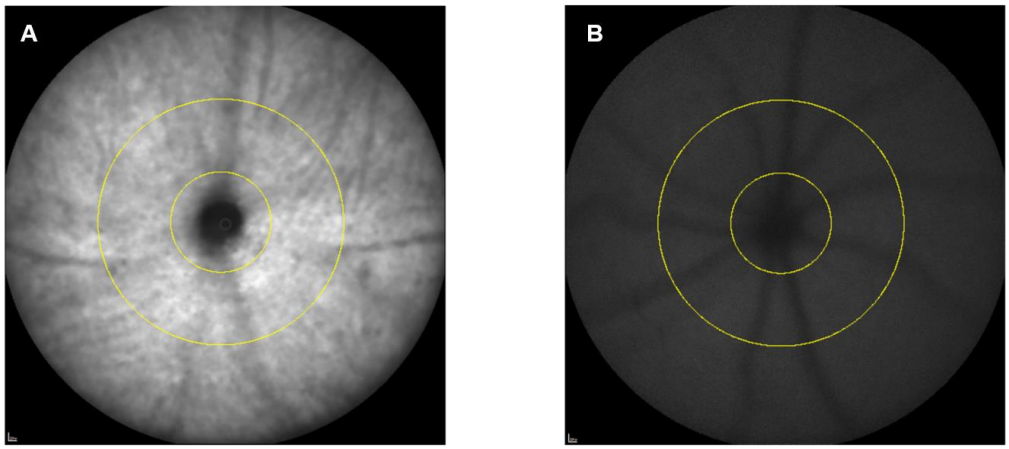

Figure 5.3. Measurement of the mean grey value of blue autofluorescence (BAF) confocal scanning laser ophthalmoscope (cSLO) fundus images. A 2.65 inch-wide sampling band was created around a ring with a radius of 3.65 inches centred on the optic disc using the ImageJ software. Bands were created on (**A**) near-infrared images and superimposed onto (**B**) BAF images. The mean grey value was calculated as the average signal within the sampling band of BAF images.

For the oral hydroxychloroquine study, animals were imaged five and seven weeks post-injection at a cSLO sensitivity of 80. Animals' subretinally injected with

hydroxychloroquine alone were imaged at two, four, and eight weeks post-injection at a cSLO sensitivity of 90. Animals' subretinally injected hydroxychloroquine together with AAV2.CAG.GFP.WPRE were imaged at two, four, and eight weeks post-injection at a cSLO sensitivity of 70. Animals' subretinally injected with hydroxychloroquine with either AAV8(Y733F).GRK1.GFP or AAV8(Y733F).GRK1.ABCA4.WPRE dual vector were imaged at six weeks post-injection.

5.3.5 Western blot analysis

Protein samples were harvested from mouse retinae according to section 2.1.5.

For AAV2.CAG.GFP.WPRE–injected C57BL/6J mice and AAV8(Y733F).GRK1.GFP–injected 129S2/SvHsd mice, 20 μg of protein was subject to western blot analysis as per section 2.1.6. Membranes were stained with primary antibodies to GFP and β-actin, followed by staining with HRP-conjugated secondary antibodies (Table 2.1). AAV8(Y733F).GRK.GFP injected samples were run across three different analyses due to the large number of samples.

For western blot analysis of ABCA4 expression, mouse retinae were lysed in 50 μL of protein lysis buffer (filtered solution of 50 mM HEPES, 100 mM NaCl, 18 mM CHAPS, 1 mM dithiothreitol (DTT), and 3 mM $MgCl_2$ in water) supplemented with PI (prepared with one PI tablet in 9 mL lysis buffer) and 10% glycerol. Protein was extracted as per section 2.1.5 and quantified using the Protein Assay (Bio-Rad), based on the Bradford dye-binding method, according to manufacturer's instructions. 40-50 μg of protein was subject to western blot analysis as per section 2.1.6. Protein samples from a wildtype 129S2/SvHsd and *Abca4*$^{-/-}$ mouse were used as a positive and negative control for ABCA4 protein expression, respectively. A 37 kDa recombinant human ABCA4 protein

(ab114660, Abcam) and a protein sample from HEK293T cells transfected with a CAG.ABCA4 plasmid provided additional positive controls. Following gel transfer, membranes were washed for two minutes in TBS. All subsequent washes in TBS-T were for 10 minutes. Membranes were stained with primary antibodies to ABCA4 and α-tubulin followed by staining with fluorophore-conjugated secondary antibodies (Table 2.1). The ABCA4 western blot assay was run by Dr Michelle McClements.

5.4 Results

5.4.1 Hydroxychloroquine enhances AAV transgene expression in human retinal tissue *ex vivo*

In order to investigate the effect of hydroxychloroquine in retinal tissue, human retinal explants were collected from two patients undergoing routine clinically-indicated retinectomy and were cultured *ex vivo*. The retinal explants were treated with 3.13 μM hydroxychloroquine prior to transduction with $1x10^9$ gc of AAV2.CAG.GFP.WPRE and visualised using fluorescence microscopy on alternate days post-transduction (Figure 5.4A). As the toxicity of hydroxychloroquine in primary tissue was not known, a lower dose was chosen due to limited tissue availability. Quantification of the mean grey value showed increased fluorescence in the hydroxychloroquine-treated explants from day seven onward, when significant GFP fluorescence became detectable, and a mean 1.9-fold increase was detected in the mean grey value at day 11 (Figure 5.4B) (two-way ANOVA, patient 1: p <0.0001, patient 2: p=0.0031; n=3 per patient).

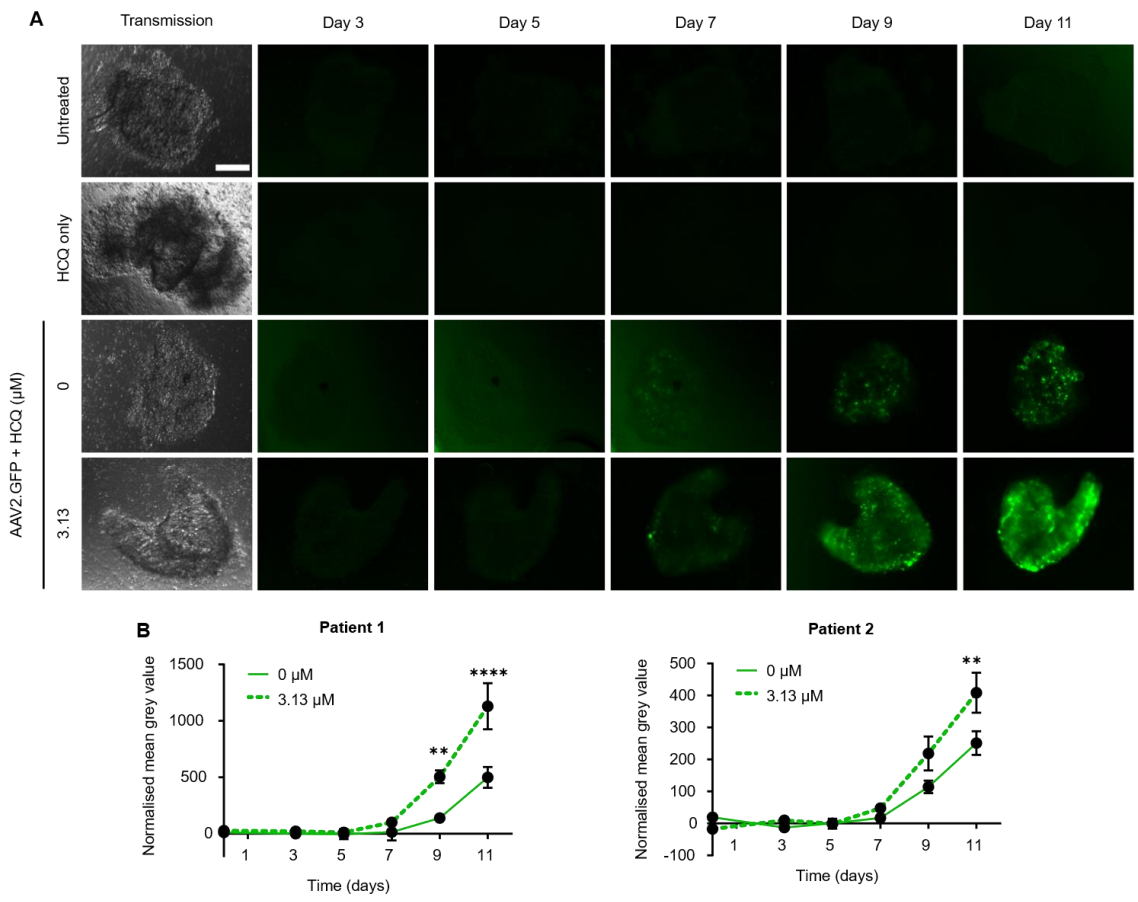

Figure 5.4. Hydroxychloroquine increases AAV transduction in human retinal tissue *ex vivo*. Fresh human retinal explants were treated *ex vivo* with 0 or 3.13 μM hydroxychloroquine one hour prior to transduction with $1x10^9$ gc of AAV2.CAG.GFP.WPRE. (**A**) Representative transmission microscopy images acquired at baseline. Fluorescence images were acquired on alternative days from day 3-11 post-transduction (scale bar: 100 μm). (**B**) Mean grey value of fluorescence images from two individual patients normalised to untransduced controls treated with equivalent concentrations of hydroxychloroquine. Data expressed as mean ±SEM (3 replicates per patient). $^{**}p \leq 0.01$, $^{****}p \leq 0.0001$ (two-way repeated-measures ANOVA with Šidák's multiple comparisons test). Figure published in [175].

5.4.2 Systemic hydroxychloroquine has no effect on AAV2.CAG.GFP.WPRE–mediated gene therapy *in vivo*

Mice were provided with hydroxychloroquine in their drinking water at a total dose of approximately either 0, 20, or 40 mg/kg/day, based on a 16 g mouse drinking 5.5 mL per day. These concentrations were chosen based on a previous study reporting no known toxic effects of orally delivered hydroxychloroquine [289]. No signs of acute toxicity or dehydration were observed during the two week monitoring period. Over this period, the volume of water consumed by each cage and the weight of each mouse was measured; this enabled retrospective calculations of the total dosing of hydroxychloroquine using equation 5.1. Mice were calculated to have received either 0, 31, or 52 mg/kg/day hydroxychloroquine, slightly higher than the intended doses. After three weeks of receiving hydroxychloroquine in their drinking water, mice were subretinally injected with AAV2.CAG.GFP.WPRE at $5x10^7$ gc per eye. Retinal fluorescence was measured at five and seven weeks post-injection using *in vivo* cSLO imaging as a readout for GFP expression. No notable difference in GFP expression was seen in either the low or high dose hydroxychloroquine-treated cohorts compared with the control group (Figure 5.5A). The retinal thickness was monitored using *in vivo* SD-OCT imaging to assess toxicity; no significant difference was found between the low and high dose hydroxychloroquine-treated cohorts (Figure 5.5B).

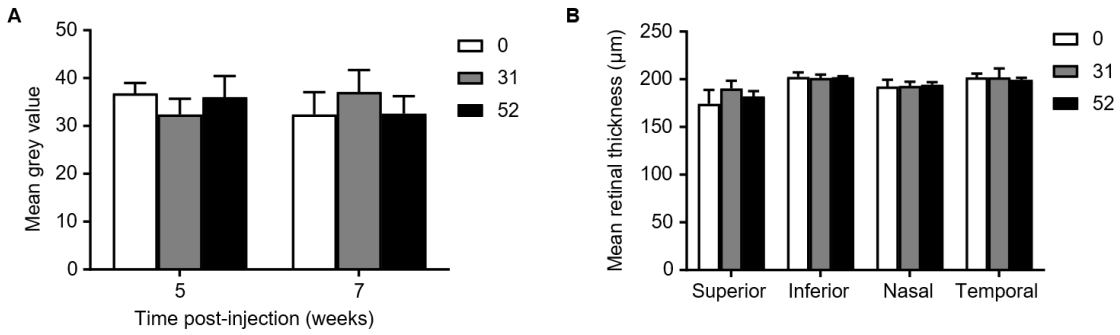

Figure 5.5. Oral delivery of hydroxychloroquine is safe but has no detectable effect of AAV transgene expression. C57BL/6J mice received hydroxychloroquine in the drinking water at 0, 31, or 52 mg/kg/day three weeks prior to subretinal injections of AAV2.CAG.GFP.WPRE at $5x10^7$ gc/eye. (**A**) GFP fluorescence levels were estimated using the mean grey values of cSLO BAF images at five and seven weeks post-injection. (**B**) Mean total retinal thickness measured from SD-OCT images of the superior, inferior, nasal, and temporal regions at eight weeks post-injection. (±SEM; 0 mg/kg/day, n=3; 31 mg/kg/day, n=4; 52 mg/kg/day, n=4).

5.4.3 Safety of subretinal hydroxychloroquine injections *in vivo*

The data collected in Figure 5.5 suggested that systemic delivery of hydroxychloroquine, within the parameters of this experiment, was ineffective at enhancing the efficacy of retinal gene therapy. However, it was unclear if the lack of efficacy was due to the ineffectiveness of hydroxychloroquine or if insufficient concentrations of the drug had reached the retina. To explore alternative routes of administration, C57BL/6J mice were subretinally injected with PBS, with or without 18.75 µM hydroxychloroquine, into paired eyes. *In vivo* SD-OCT imaging demonstrated no detectable change in the lamellar retinal architecture relating to the administration of hydroxychloroquine (Figure 5.6A). Moreover, there was no significant difference in

the mean retinal thickness of eyes injected with hydroxychloroquine compared to paired eyes injected with PBS (Figure 5.6B). By measuring the mean grey value of the fundus using cSLO, it was demonstrated that there was no significant difference in the autofluorescence of eyes injected with PBS compared to those injected with hydroxychloroquine alone, suggesting that hydroxychloroquine is not autofluorescent within the retina (Figure 5.6C). These findings demonstrated subretinal delivery of hydroxychloroquine to be feasible and have no effect on the structural integrity of the retina.

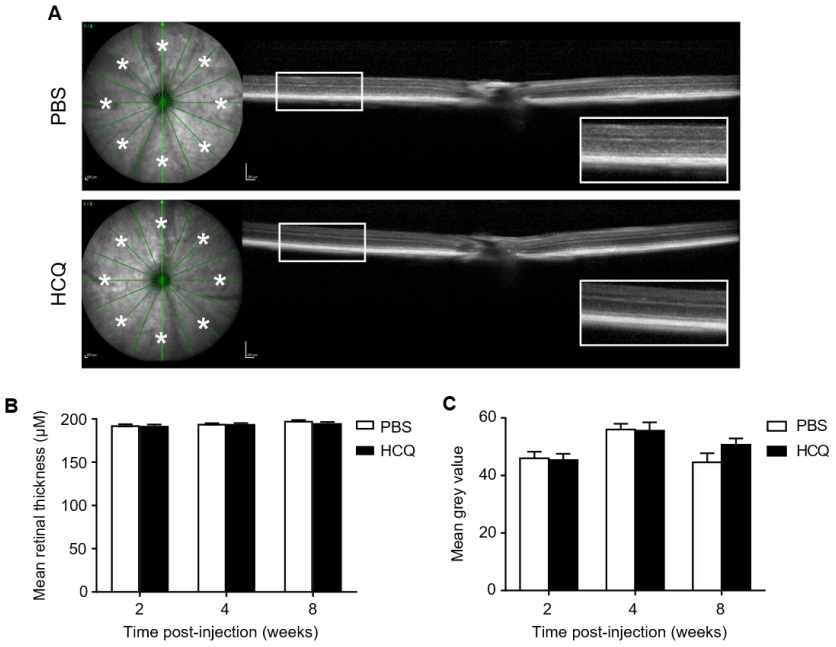

Figure 5.6. Subretinal delivery of hydroxychloroquine has no detectable effect on retinal architecture or thickness. C57BL/6J mice were subretinally injected with 18.75 µM hydroxychloroquine with paired injections of PBS. (**A**) Representative SD-OCT images from fellow eyes that received either PBS or 18.75 µM hydroxychloroquine. Total retinal thickness was measured at indicated points (*). (**B**) Mean total retinal thickness of points (*) at two, four, and eight weeks post-injection (±SEM, n=8). (**C**) Retinal autofluorescence was estimated using the mean grey values of cSLO BAF images of eyes injected with PBS or 18.75 µM hydroxychloroquine at two, four, and eight weeks post-injection (±SEM, n=8).

5.4.4 Subretinal hydroxychloroquine enhances AAV2.CAG.GFP.WPRE–mediated gene therapy *in vivo*

To investigate the effect of subretinal delivery of hydroxychloroquine on AAV-mediated transgene expression, C57BL/6J mice were subretinally injected with $1x10^8$ gc of AAV2.CAG.GFP.WPRE in suspension with either 3.13 or 18.75 µM hydroxychloroquine, with injections of AAV vector only in the fellow eye. GFP

fluorescence was measured using *in vivo* cSLO imaging at two, four, and eight weeks post injection. Retinal fluorescence was found to be increased in eyes that received AAV vector suspension containing 18.75 μM hydroxychloroquine compared with paired eyes that received AAV vector alone (Figure 5.7A). No difference was seen in eyes that received AAV with 3.13 μM hydroxychloroquine (Figure 5.7B). Although a trend in favour of hydroxychloroquine was visible, the differences in retinal fluorescence based on normalised grey value comparisons did not reach statistical significance (two-way repeated measures ANOVA; 3.13 μM: p= 0.4273, n=5; 18.75 μM: p=0.2544, n=4). The statistical power of the comparison was ultimately reduced by the exclusion of four of 13 mice due to unintended intravitreal injections or subretinal bleeds during surgery.

To more specifically compare levels of GFP protein expression between the treatment arms, a larger cohort of mice was co-injected and the retinae were harvested for western blot analysis at eight weeks post-injection. Eyes that received AAV with 18.75 μM hydroxychloroquine showed a mean 4.6-fold increase in GFP protein level compared with paired eyes that received AAV vector alone (Wilcoxon matched-pairs signed rank test, p=0.0034; n=12) (Figure 5.7C and D). If 'animal 1' is removed from the dataset, which falls as an outlier due to its lower level of β-actin, the effect is still significant (Paired t test, p=0.0072; n=11). In addition, co-injection of AAV2.CAG.GFP.WPRE together with 18.75 μM hydroxychloroquine induced no notable differences in total retinal thickness on SD-OCT images (Figure 5.7E).

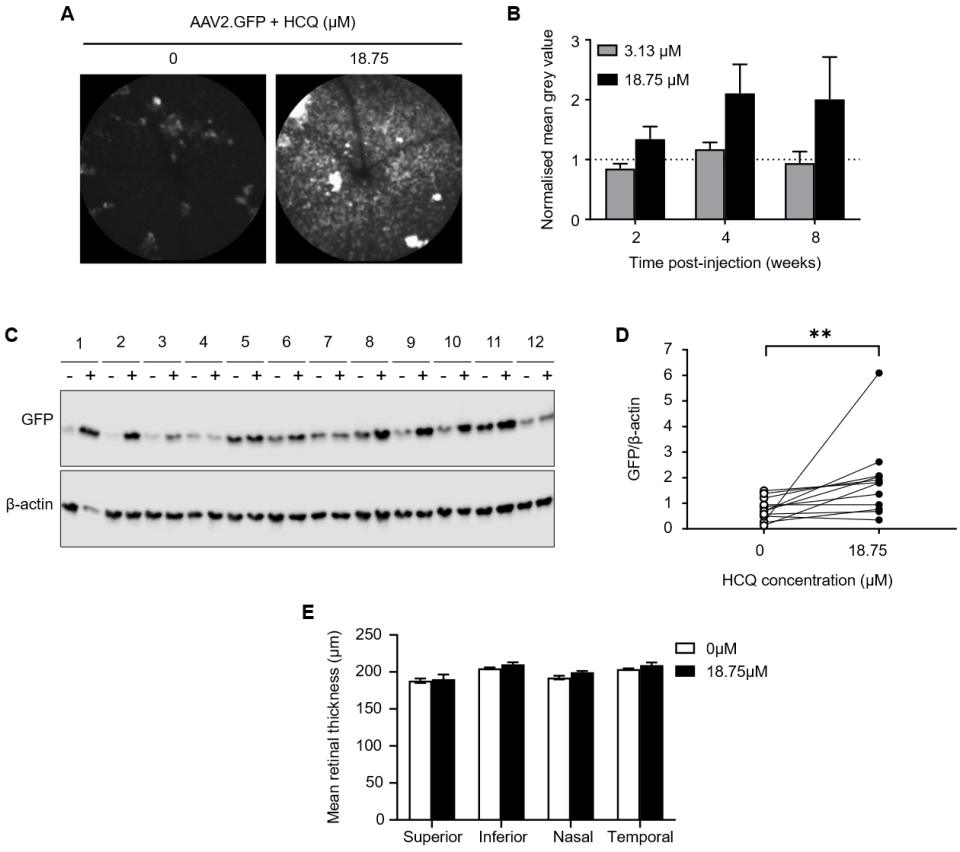

Figure 5.7. Hydroxychloroquine enhances AAV2.CAG.GFP.WPRE transduction of mouse retinae *in vivo*. C57BL/6J mice were subretinally injected with AAV2.CAG.GFP.WPRE vector alone in one eye and co-injected with either 3.13 or 18.75 μM hydroxychloroquine in the fellow eye. (**A**) Representative *in viv*o cSLO BAF images of paired eyes at eight weeks post-injection. (**B**) GFP fluorescence levels were estimated using the mean grey values of cSLO BAF images. Eyes co-injected with hydroxychloroquine were normalised to fellow AAV only-injected eyes at two, four, and eight weeks post-injection (±SEM; 3.13 μM, n=5; 18.75 μM, n=4). (**C**) Western blot of GFP protein levels in paired mouse retinae (animal 1-12) that received either AAV vector alone (-) or vector mixed with 18.75 μM hydroxychloroquine (+) at 8 weeks post-injection. β-actin was used as a loading control. (**D**) Quantification of western blot GFP band density normalised to β-actin in paired eyes (n = 12). $^{**}p \leq 0.01$ (Wilcoxon matched-pairs signed rank test). (**E**) Mean total retinal thickness measured from SD-OCT images of the superior, inferior, nasal, and temporal regions at eight weeks post-injection (±SEM, n=12).

5.4.5 Subretinal hydroxychloroquine enhances AAV8(Y733F).GRK1.GFP–mediated gene therapy *in vivo*

Next, I investigated whether hydroxychloroquine was able to specifically enhance transgene expression within photoreceptors *in vivo* and whether the effect was applicable to different AAV serotypes. 129S2/SvHsd mice were subretinally injected with $1x10^8$ gc of an AAV8(Y733F).GRK1.GFP vector, with injections of AAV combined with 18.75 μM hydroxychloroquine performed in the contralateral eye. The *GFP* transgene was expressed under the control of a photoreceptor-specific promoter (GRK1) with a mutant AAV8 capsid serotype. Retinal GFP protein expression was 5.9-fold higher in eyes injected with AAV containing 18.75 μM hydroxychloroquine compared to AAV only (Wilcoxon matched-pairs signed rank test, p=0.0391; n=9) (Figure 5.8A and B). Co-injection of AAV8(Y733F).GRK1.GFP together with 18.75 μM hydroxychloroquine induced no detectable differences in the total retinal thickness (Figure 5.8C).

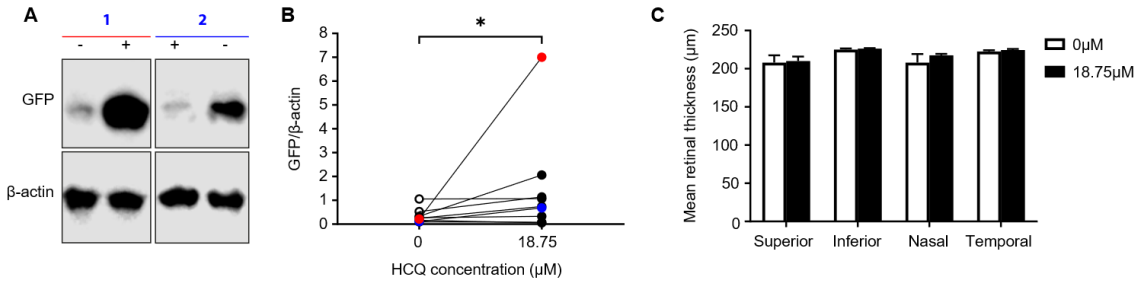

Figure 5.8. Hydroxychloroquine enhances AAV8(Y733F).GRK1.GFP transduction of mouse retinae *in vivo*. 129S2/SvHsd mice were subretinally injected with the AAV8(Y733F).GRK1.GFP vector alone in one eye and co-injected with 18.75 μM hydroxychloroquine in the paired eye. (**A**) Representative western blot of GFP protein levels in the retinae of two mice that received paired injections AAV vector alone (-) and vector mixed with 18.75 μM hydroxychloroquine (+) at six weeks post-injection. Red and blue colours correspond to points on the graph. (**B**) Quantification of GFP band density normalised to β-actin in paired eyes (n=9). *$p \leq 0.05$ (Wilcoxon matched-pairs signed rank test). (**C**) Mean total retinal thickness of the superior, inferior, nasal, and temporal regions at 6 weeks post-injection (±SEM, n=9).

In contrast, 129S2/SvHsd mice subretinally injected with AAV8(Y733F).GRK1.GFP combined with 112.5 μM hydroxychloroquine did not demonstrate any significant changes in GFP transgene expression compared to paired AAV only injected eyes (Figure 5.9A). There were no detectable differences in the total retinal thickness of eyes co-injected with this higher concentration of hydroxychloroquine (Figure 5.9B). Interestingly, mice injected with 18.75 μM hydroxychloroquine generally demonstrated a positive effect on GFP expression, while those injected with 112.5 μM hydroxychloroquine had minimal or negative effect on transgene expression (Figure 5.9C).

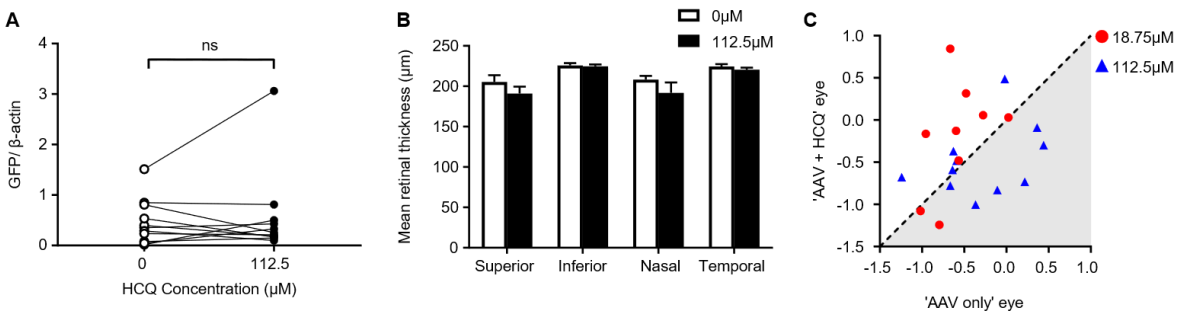

Figure 5.9. 112.5 μM hydroxychloroquine has no effect on AAV8(Y733F).GRK1.GFP transduction of mouse retinae *in vivo*. (**A&B**) 129S2/SvHsd mice were subretinally injected with AAV8(Y733F).GRK1.GFP vector alone in one eye and co-injected with 112.5 μM hydroxychloroquine in the paired eye. (**A**) Western blot analysis quantification of GFP band density normalised to β-actin in paired eyes at six weeks post-injection (n=11). (**B**) Mean total retinal thickness of the superior, inferior, nasal, and temporal regions at six weeks post-injection (±SEM, n=10). (**C**) Normalised GFP protein expression (expressed as $\log_{10}$) of an individual animal's AAV only injected eye (x-axis) plotted against its paired eye injected with AAV mixed with 18.75 or 112.5 μM hydroxychloroquine (y-axis). Data presented from six weeks post-injection. Each point represents an individual animal with points above the line representing a positive effect (in white) and below a negative (in grey).

5.4.6 Subretinal hydroxychloroquine has no effect on *ABCA4* dual vector-mediated gene therapy *in vivo*

To further explore the applicability of hydroxychloroquine to enhance the efficacy retinal gene therapy, the effect of subretinal hydroxychloroquine injections were assessed with a dual *ABCA4* vector system. *Abca4*$^{-/-}$ mice were subretinally injected with $1x10^{10}$ gc per eye of both the upstream and downstream constructs of the AAV8(Y733F).GRK1.ABCA4.WPRE dual vector, with injections of AAV combined with 18.75 μM hydroxychloroquine undertaken in the paired eye. Vectors were injected at

a dose known to produce detectable levels of ABCA4 protein [284]. Expression of the full length ABCA4 protein, suggesting successful recombination of the upstream and downstream *ABCA4* transgene fragments, was detected by western blot six weeks post-injection (Figure 5.10A). A protein band corresponding to full length ABCA4 (250 kDa), α-tubulin (55 kDa), and the ABCA4 peptide fragment (37 kDa) were detected. All other bands were also present in the uninjected *Abca4*$^{-/-}$ and wildtype 129S2/SvHsd mouse retinae, so were deemed to be as a result of non-specific antibody staining. No significant difference in full length ABCA4 protein expression was detectable by western blot between eyes co-injected with 18.75 μM hydroxychloroquine and paired eyes with AAV only (Figure 5.10B). Co-injection of the AAV8(Y733F).GRK1.ABCA4.WPRE dual vector together with 18.75 μM hydroxychloroquine induced no detectable differences in the total retinal thickness (Figure 5.10C).

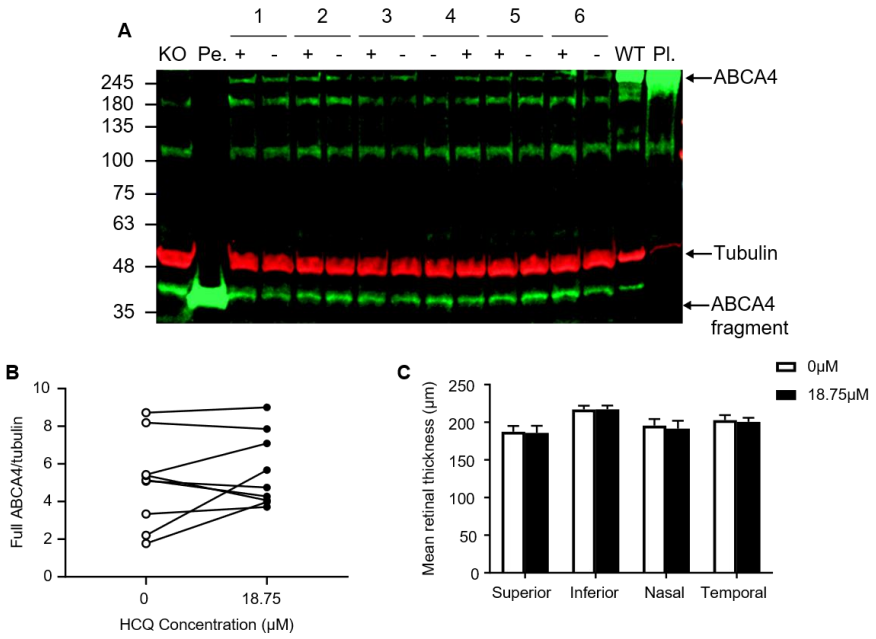

Figure 5.10. Hydroxychloroquine has no effect on ABCA4 transgene expression following subretinal injections with AAV8(Y733F).GRK1.ABCA4.WPRE dual vector *in vivo*. *Abca4*$^{-/-}$ mice were subretinally injected with both the upstream and downstream AAV8(Y733F) ABCA4 dual vector system alone or co-injected with 18.75 μM hydroxychloroquine in the paired eye. (**A**) Representative western blot of ABCA4 and α-tubulin protein levels in the paired retinae of six mice that received either AAV vector alone (-) or vector mixed with 18.75 μM hydroxychloroquine (+) at six weeks post-injection. Bands corresponding to full length ABCA4 (250 kDa), α-tubulin (55 kDa), and the ABCA4 peptide fragment (37 kDa) were detected; all other bands were due to non-specific antibody staining. KO, retinal protein sample from an uninjected *Abca4*$^{-/-}$ mouse (negative control); Pe., 37 kDa fragment of recombinant human ABCA4 protein; WT, retinal protein sample from an uninjected wildtype 129S2/SvHsd mouse (positive control); Pl., protein sample from HEK293T cells transfected with CAG.ABCA4 plasmid (2nd positive control). (**B**) Quantification of ABCA4 band density normalised to α-tubulin in paired eyes (n=9). (**C**) Mean total retinal thickness of the superior, inferior, nasal, and temporal regions at 6 weeks post-injection (±SEM, n=8).

5.5 Discussion

In this chapter I have investigated the use of hydroxychloroquine as an adjunct to AAV retinal gene therapy *ex vivo* and *in vivo*. Initially, I demonstrated hydroxychloroquine treatment to enhance the level of transgene expression in human retinal tissue obtained from patients undergoing clinically indicated retinectomies. Although these tissue fragments will contain multiple retinal cell types, the widespread transduction suggests GFP expression is likely present in photoreceptors; however, this could be confirmed with the use of immunohistochemical staining. Three-dimensional retinal organoids generated from induced pluripotent stem cells of both healthy and retinal degenerate patients, which contain all the major retinal cell types in their biological layers, could help to further investigate the efficacy of hydroxychloroquine in the human retina [290, 291]. I subsequently demonstrated that hydroxychloroquine can be delivered directly in solution with the AAV vector by subretinal injection, to safely enhance the efficacy of retinal gene therapy. Adjunctive hydroxychloroquine treatment increased transgene expression with both an AAV2 and AAV8 capsid serotype, suggesting that the mechanism of action is unlikely to be capsid-dependent. AAV2 vectors have been used in the treatment of RPE-mediated retinal dystrophies, such as LCA and choroideremia [151, 277], while AAV8 capsid serotype vectors have been used in trials treating photoreceptors, such as X-linked retinitis pigmentosa and X-linked retinoschisis [152, 278]. Furthermore, an effect was seen with both a ubiquitous and photoreceptor-specific promoter, suggesting that adjunctive use of hydroxychloroquine is capable of increasing transgene expression levels in photoreceptor cells, which are the primary target for many retinal gene therapies.

Overall, these findings support the potential application of hydroxychloroquine to enhance the efficacy of a range of retinal gene therapies.

Preliminary investigation into systemic orally delivered hydroxychloroquine did not demonstrate any significant effect on AAV transgene expression. However, without quantification of hydroxychloroquine concentrations within the retina, which is technically challenging, it is unclear whether the drug had crossed the blood-retina barrier and reached significant concentrations within the target cells. Given the pharmacokinetics of hydroxychloroquine it may be difficult to achieve appropriate concentrations within the retina. The plasma half-life of hydroxychloroquine is relatively long at 32 days and the drug is highly sequestered in pigmented tissues, such as the uvea, liver, and lung [292], thus a steady state plasma concentration is not achieved until six months of daily dosing in humans [293]. A study found blood hydroxychloroquine concentrations to vary significantly among systemic lupus erythematosus patients taking equivalent doses of the drug [294], thus achieving a consistent and precise concentration of hydroxychloroquine in the retina via oral administration may be challenging. Further work would be needed to optimise the duration and dose of systemically delivered hydroxychloroquine in order to achieve sufficient concentrations within the target tissue. Initial assessment of GFP expression was performed using live cSLO imaging to measure retinal blue autofluorescence, which can be used as a surrogate readout for transgene expression [42]. Following oral delivery of hydroxychloroquine, no trend or significant difference was observed, however, direct subretinal injection of hydroxychloroquine with AAV vectors induced a trend towards increased fluorescence. However, mean grey analysis of cSLO images was unable to distinguish between the diffuse background fluorescence, which

represents GFP expression, and scattered clumps of hyperfluorescence, possibly representing autofluorescent macrophage aggregates associated with inflammation [295]. Western blot analysis provided a more sensitive means of measuring GFP expression and supported the trend observed with cSLO imaging; follow-up quantification of transgene expression was therefore performed using western blot analysis.

Subretinal injection of hydroxychloroquine has the advantage of precise control over the local drug concentration. When comparing the effects of low (18.75 μM) and high (112.5 μM) doses of hydroxychloroquine, 18.75 μM hydroxychloroquine led to significantly increased transgene expression, while 112.5 μM had no effect. One explanation for these differences could be hydroxychloroquine-induced cytotoxicity at higher doses, as seen in Figure 4.5, however, given that there was no difference in the total retinal thickness, it is unlikely that there were dramatic toxic effects in the mouse retina at this concentration. Another potential explanation may be dose-dependent differences in the mechanism of action of hydroxychloroquine. When used at high concentrations (≥100 μM), hydroxychloroquine and chloroquine have been shown to cause a dose-dependent increase in endosomal and lysosomal pH [296, 297]. As many viruses, including AAV, exploit the host endocytic machinery to infect target cells, a rise in endosomal pH by chloroquine or hydroxychloroquine could disrupt *in vitro* viral replication, as observed with Semliki Forest virus [298], HSV-1 [299], and hepatitis A virus [300]. It can also affect production of infectious virions by preventing glycosylation of the human immunodeficiency virus (HIV)-1 glycoprotein gp120 in the usually acidic Golgi complex [301-303]. An *in vitro* study demonstrated a decrease in AAV transduction in a hepatocellular carcinoma cell line (HepG2) when treated with

100 μM chloroquine, a concentration known to raise the pH of these compartments [165]. This led the authors to conclude that chloroquine-mediated impairment of endosomal processing can inhibit AAV transduction. In contrast, many studies have demonstrated low concentrations (≤20 μM) of these drugs to exert an immunomodulatory effect, through the inhibition of PRRs such as TLR9, TLR7, and cGAS, with minimal effect on endosomal pH [250, 251, 253, 258, 297]. *In vitro* hydroxychloroquine and chloroquine can prevent TLR7-mediated responses to RNA viruses such as hepatitis C [262, 263], influenza [264] and vesicular somatic virus [265], as well as TLR9-mediated responses to DNA viruses such as HSV-2 and Epstein-Barr virus [259-261]. Taken together, these findings are consistent with the hypothesis that low concentrations of locally delivered hydroxychloroquine could improve viral transgene expression by inhibiting PRR-mediated anti-viral responses. Subretinal injection, compared to systemic oral delivery, of hydroxychloroquine may therefore allow for control of the mechanism of action and effect on AAV transgene expression.

Long-term systemic hydroxychloroquine treatment has been associated with an increased risk of hydroxychloroquine retinopathy [285]. Despite this, the risk of short-term locally administered hydroxychloroquine is currently unknown. Delivery of a single dose of hydroxychloroquine into the subretinal space was not associated with any retinal structural change, including preservation of the ellipsoid zone within treated areas, which represents organised photoreceptor inner and outer segments up to eight weeks post-injection. Given that hydroxychloroquine was only delivered as a one-off treatment together with the AAV vector, the toxic effects associated with prolonged hydroxychloroquine treatment are unlikely. However, long-term assessment of retinal function using an electroretinogram would be required to fully

investigate the safety of subretinally delivered hydroxychloroquine. Furthermore, while hydroxychloroquine enhanced retinal gene therapy in the healthy retina of wildtype mice without any sign of toxicity, it remains to be seen whether the effects would be the same in the degenerate retina, such as in mouse models of retinitis pigmentosa, which would provide support for future clinical application.

Although success has been observed in the treatment of various inherited retinal dystrophies with a single AAV vector, such as for LCA, choroideremia, and retinitis pigmentosa [150-152, 190, 275, 276], the therapeutic transgene for treatment of some diseases, such as Stargardt disease, are too large to fit into a single AAV capsid. The use of a dual vector system, which relies on homologous recombination of the *ABCA4* therapeutic transgene, has been developed as a novel treatment strategy for Stargardt disease [284]. However, unpublished experimental data collected within the group found the need for significantly higher doses of AAV, at least one order of magnitude higher than single vector treatments, to achieve a therapeutic effect, suggesting that the recombination of the upstream and downstream construct is a limiting step in full-length transgene expression. In light of this limiting step, an AAV dose two orders of magnitude higher than that used with a single vector in this chapter was selected to ensure detectable transgene expression. Although hydroxychloroquine was confirmed to enhance transgene expression of a single AAV8(Y733F) capsid serotype vector with a photoreceptor-specific GRK1 promoter in a 129 strain of mice, co-injection with the AAV8(Y733F).GRK1.ABCA4.WPRE dual vector system did not enhance ABCA4 transgene expression. As the serotype and promoter were equivalent between these two vectors, a reason for the discrepancy could be the recombination step necessary for production of a single transgene. If the mechanism of action of hydroxychloroquine

is dependent on enabling a greater number of viral genomes to reach the nucleus, this beneficial role may be irrelevant at such a high dose. Therefore, additional doses of the dual AAV vector should be tested to further investigate the effect of hydroxychloroquine on this dual vector system.

5.6 Conclusion

The findings presented in this chapter demonstrate that subretinal delivery of hydroxychloroquine in solution with the AAV vector can enhance transgene expression following retinal gene therapy. Adjunctive hydroxychloroquine treatment enhanced both AAV2 and AAV8 capsid serotypes and specifically increased AAV transduction efficacy in photoreceptors. Subretinal delivery of hydroxychloroquine had no effect on the structural integrity of the retina up to eight weeks post-injection, however, full evaluation of potential retinal toxicity will require longer term assessment including the use of functional readouts. Hydroxychloroquine treatment also enhanced AAV transgene expression in human retinal tissue *ex vivo*, thus further demonstrating the potential clinical implications of hydroxychloroquine in retinal gene therapy. No beneficial effect was observed with the use of a dual *ABCA4* vector system, suggesting that hydroxychloroquine treatment may be limited to standard single vector constructs.

6 Determining the mechanism of action of hydroxychloroquine

6.1 Introduction

A major advance in the effort to understand the mechanism of action of hydroxychloroquine and chloroquine was the discovery of their antagonistic effects on PRRs, such as TLR9, TLR7, and cGAS, which can detect molecular signatures of pathogens to elicit rapid intracellular immune responses [51]. Although the interaction between TLR9 and its ligand (CpG sequences) is optimal in acidic endosomal environments [255], TLR9 inhibition can be achieved with significantly lower concentrations of chloroquine than that needed to alter the endosomal pH [251, 253, 297]. Based on these findings, it has been proposed that hydroxychloroquine and chloroquine could bind to CpG-containing nucleic acids and induce conformational changes that prevent them from interacting with and activating TLR9 [251, 256]. Furthermore, the *in silico* study that identified hydroxychloroquine as a possible inhibitor of cGAS, predicted an interaction between hydroxychloroquine and its DNA binding site by computational analysis [250]. It remains unclear whether the inhibitory effect of hydroxychloroquine on cGAS is achieved through hydroxychloroquine binding to cGAS or the DNA substrate. Nonetheless, given the proposed mechanism of action via TLR9, it is possible that hydroxychloroquine and chloroquine might prevent the activation of nucleic acid sensors, TLR9 and cGAS, through a common mechanism such as alteration of the structural configuration of the DNA substrate [252, 304]. Given the potential restrictive role of TLR9 and cGAS on AAV transduction observed in

Chapter 4, it is possible that hydroxychloroquine may enhance transgene expression through inhibition of these anti-viral DNA sensors.

In addition to its direct immunomodulatory effects, hydroxychloroquine is a weak base that can accumulate within acidic intracellular compartments [305]. When used at high concentrations, hydroxychloroquine can lead to a dose-dependent increase in endosomal and lysosomal pH [296, 297]. Although chloroquine can inhibit TLR9 at concentrations lower than that needed to alter endosomal pH, it remains possible that alkalisation of these compartments by hydroxychloroquine treatment can indirectly inhibit TLR9, which requires an acidic environment for optimal interaction with its ligand [255]. During transduction, AAV particles exploit host endocytic machinery to infect target cells. Following cell surface receptor binding, viral particles are internalised via a range of endocytic mechanisms, including clathrin-mediated, caveolin-mediated, clathrin-independent endocytosis, and micropinocytosis [21]. The acidic pH of these endosomal particles has been hypothesised to aid exposure of the hidden phospholipase A2 domain in the N terminus of the capsid protein VP1, a process which is required for endosomal escape [25]. Following cytoplasmic release, AAV particles accumulate in the perinuclear space and enter the nucleus through nuclear pore complexes [21]. Alteration to this pathway will therefore likely induce detectable changes in AAV transduction.

In this chapter I explore potential mechanisms of action for the enhancement of AAV retinal gene therapy by adjunctive hydroxychloroquine treatment. I investigate the role of the PRRs TLR9 and cGAS in hydroxychloroquine-mediated enhancement of AAV transduction and assess its effect on the AAV transduction pathway.

6.2 Aims

The aims of this chapter were as follows:

1. To investigate the role of TLR9 in the hydroxychloroquine-mediated enhancement of AAV transduction.

2. To investigate the role of cGAS in the hydroxychloroquine-mediated enhancement of AAV transduction.

3. To determine the effect of hydroxychloroquine on viral entry and the subcellular localisation of AAV genomes.

6.3 Materials & methods

6.3.1 MEF cell treatment & transduction

For all *in vitro* experiments, MEF cells were seeded 24 hours prior to treatment as per section 2.3.1 and transduced with an AAV2.CAG.GFP.WPRE vector at an MOI of 1,000 as described in section 2.3.5. For TLR9-activating experiments, *Cgas*$^{-/-}$ MEFs were treated with 0, 3.13, or 18.75 μM hydroxychloroquine and either 0 or 754.6 μM CpG-A as per section 2.3.4. For all other experiments, wildtype MEFs were treated with 0 or 18.75 μM hydroxychloroquine as per section 2.3.4.

Prior to harvesting, the growth media was removed from MEFs and replaced with pre-warmed PBS to reduce the background autofluorescence before imaging with the EVOS Cell Imaging System (Thermo Fisher Scientific). Cells were processed for flow cytometry three days post-transduction as described in section 2.6.1 and flow cytometry was performed as per section 2.6.2.

6.3.2 Viral entry assay

Wildtype MEFs were harvested at 0, 10, 30, or 60 minutes post-transduction. Cells were detached using TrypLE Express (Gibco, Thermo Fisher Scientific) and centrifuged at 300 xg for five minutes. The pellet was resuspended in 1 mL of ice-cold PBS and centrifuged at 300 xg for five minutes at 4°C; this wash step was repeated three times to wash away unbound AAV particles. The pellet was flash frozen on dry ice and stored at -80°C. DNA was extracted using the QIAamp DNA Mini kit (QIAGEN) according to manufacturer's instructions and DNA concentrations were determined using the NanoDrop Spectrophotometer (Thermo Fisher Scientific). qPCR was performed with TaqMan probes (all Thermo Fisher Scientific) as per section 2.1.4. *GFP* DNA levels were measured using a gene specific probe (assay ID: Mr03989638_mr) and were normalised to an internal control of genomic glyceraldehyde 3-phosphate dehydrogenase (*Gapdh*) using a copy number assay probe (assay ID: Mm00186822_cn) as a measure of genomic DNA.

6.3.3 Cell fractionation

Cells were fractionated using the Cell Fractionation Kit (Abcam) as per section 2.3.6. DNA was extracted from the cytosolic and nuclear fractions using the QIAamp DNA Mini Kit (QIAGEN). Samples were thawed on ice and made up to 200 µL with sterile PBS. 20 µL of proteinase K (QIAGEN) was added to digest cellular proteins and 4 µL of RNase K (final concentration of 1.8 mg/mL) was added to remove cellular RNAs that may interfere with the downstream qPCR analysis. The remainder of the protocol was followed according to manufacturer's instructions. qPCR analysis was performed using 1 ng of each DNA sample. *GFP* and *Gapdh* DNA levels were assessed using an absolute

quantification method where the amount of DNA was determined by interpolating from a standard curve run in parallel. The final DNA levels were expressed as the number of DNA copies per ng of total DNA.

For protein extraction from the cytosolic and nuclear fractions, one PI tablet was added to 10 mL of Buffer A (Cell Fractionation Kit, Abcam) prior to use. The nuclear fraction pellet was resuspended in RIPA buffer supplemented with PI (one PI tablet to 10 mL RIPA buffer). The samples were homogenised with a hand-held homogeniser and incubated on ice for 30 minutes. The nuclear fraction was centrifuged at 17,000 xg for 20 minutes at 4°C and the supernatant was transferred to a new tube for protein quantification. For the western blot, protein samples were separated according to section 2.1.6. Membranes were stained with primary antibodies to Histone H3, with α-tubulin used as a loading control, followed by incubation with specific fluorophore-conjugated secondary antibodies (Table 2.1).

6.4 Results

6.4.1 Hydroxychloroquine exerts an antagonistic effect on TLR9

Hydroxychloroquine has been suggested to bind to CpG-containing nucleic acids to induce conformational changes that prevent the sequences interacting with and activating TLR9 [251, 256]. All cell samples were treated with 18.75 μM hydroxychloroquine prior treatment with either 0 or 754.6 μM CpG-A. Cells were subsequently transduced with AAV2.CAG.GFP.WPRE at an MOI 1,000 and were harvested for flow cytometric analysis three days post-transduction. CpG-A treatment, in the presence of hydroxychloroquine, induced a 1.9-fold decrease in GFP

fluorescence (paired t-test, p=0.0348; n=7) (Figures 6.1A and B). However, compared to samples treated without hydroxychloroquine (as per Figure 4.2), the inhibitory effect of CpG-A on AAV transduction was significantly reduced in the presence of hydroxychloroquine (Wilcoxon matched-pairs signed rank test, p=0.0156; n=7) (Figure 6.1C). The fold change of CpG-A–treated to untreated samples without hydroxychloroquine treatment was a mean 0.4-fold increase, while in equivalent samples treated with hydroxychloroquine this increase was a mean 0.6-fold, suggesting hydroxychloroquine diminishes the inhibitory effect of CpG-A.

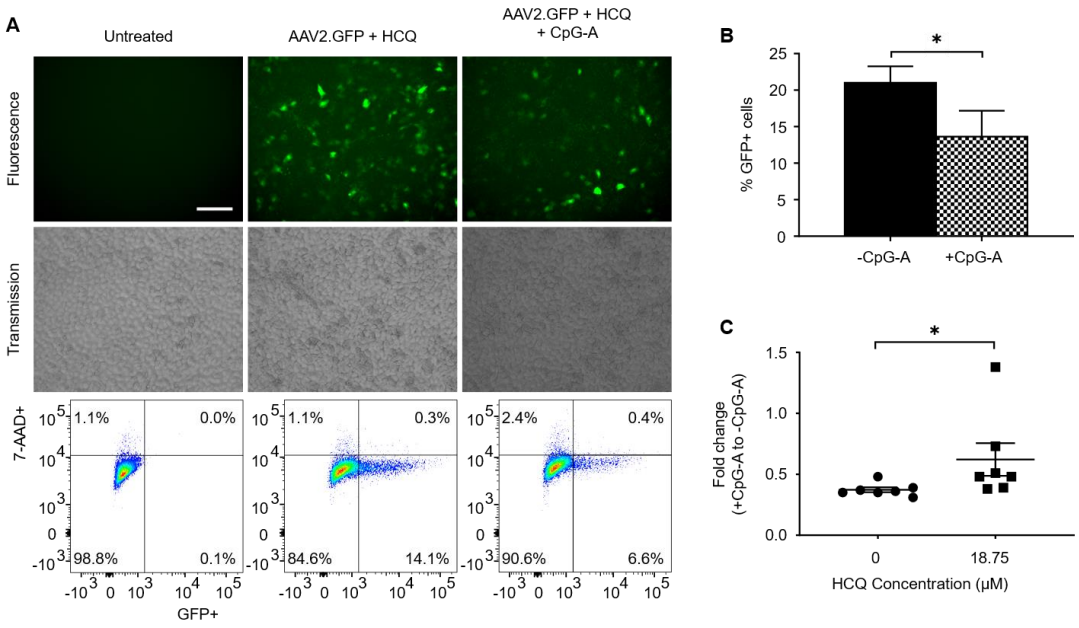

Figure 6.1. The agonistic TLR9 oligodeoxynucleotide CpG-A has a significantly reduced effect in hydroxychloroquine treated cells. (**A&B**) Wildtype MEFs were treated with 18.75 μM hydroxychloroquine one hour prior to transduction with AAV2.CAG.GFP.WPRE at an MOI of 1,000. Cells were also treated with 0 or 754.6 μM CpG-A 30 min prior to transduction. GFP fluorescence and cell viability (7-AAD staining) were assessed three days post-transduction by flow cytometry. (**A**) Representative fluorescence images and corresponding flow cytometry plots (scale bar: 200 μm). (**B**) The mean proportion of GFP⁺ cells (±SEM, n=7). *p ≤0.05 (paired t test). (**C**) The mean fold change of transduced live GFP⁺ cells treated with CpG-A relative to cells with no CpG-A treatment. Cells were either treated with CpG-A alone or with CpG-A and hydroxychloroquine (±SEM, n=7). *p ≤0.05 (Wilcoxon matched-pairs signed rank test).

6.4.2 Absence of cGAS has no effect on hydroxychloroquine efficacy

To test the hypothesis that hydroxychloroquine may improve AAV transduction by inhibiting the anti-viral DNA sensor cGAS, *Cgas*$^{-/-}$ MEFs were treated with

hydroxychloroquine to investigate its effect in the absence of this innate immune factor. *Cgas*$^{-/-}$ MEFs were treated with either 0, 3.13, or 18.75 μM hydroxychloroquine one hour prior to transduction with AAV2.CAG.GFP.WPRE. The addition of hydroxychloroquine increased the mean percentage of GFP^{+} cells from 38% with no hydroxychloroquine, to 65% with 3.13 μM and 74% with 18.75 μM hydroxychloroquine (one-way repeated measures ANOVA, p<0.0001, n=6) (Figure 6.2A–C). There was, however, an increase in 7-AAD staining in hydroxychloroquine treated cells, suggesting that hydroxychloroquine was cytotoxic to the *Cgas*$^{-/-}$ cells (Figure 6.2B). When comparing the effect of hydroxychloroquine in wildtype and *Cgas*$^{-/-}$ MEFs, there was no significant difference in the fold increase of the percentage of live GFP^{+} cells with and without hydroxychloroquine treatment (Figure 6.2D).

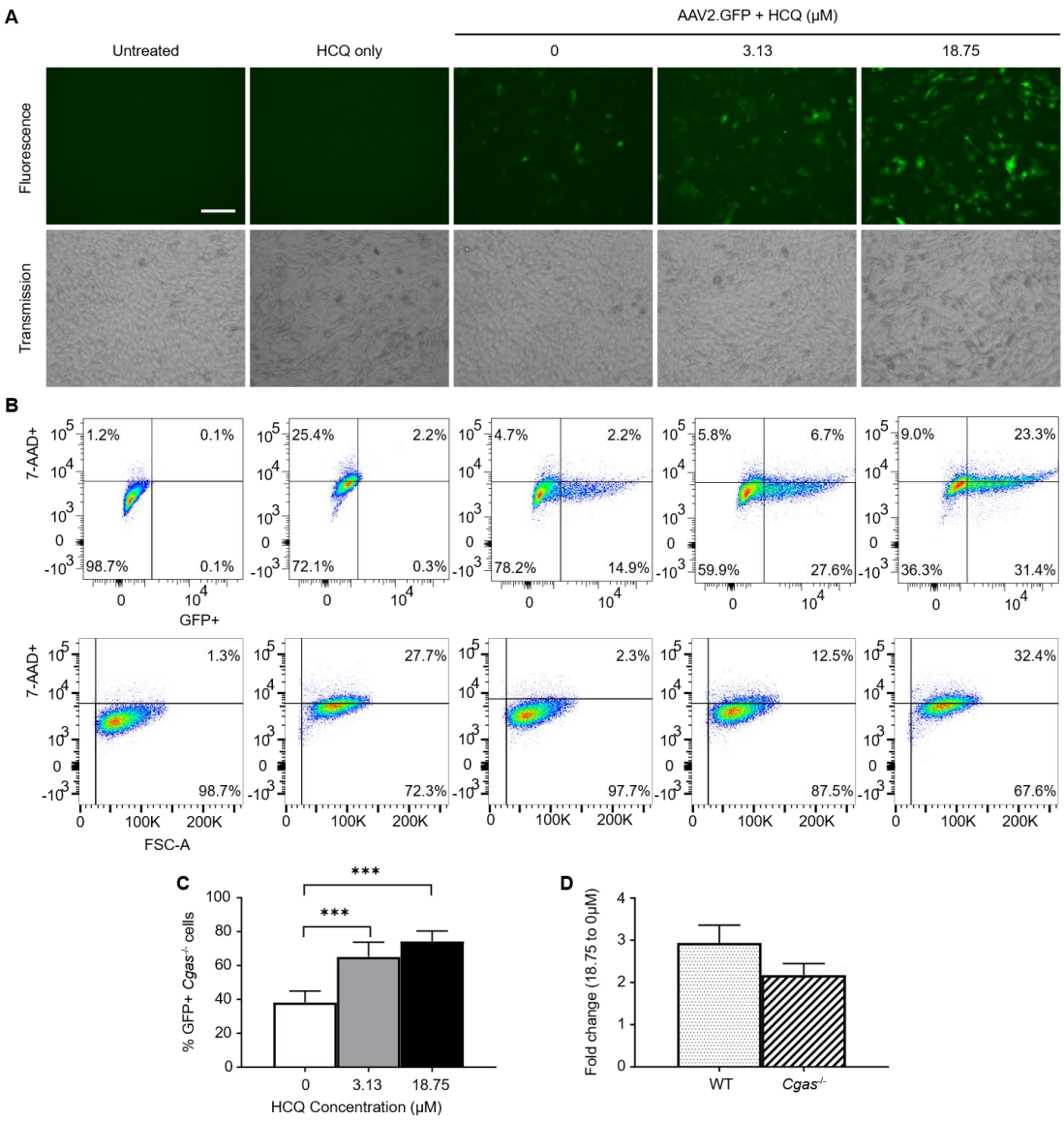

Figure 6.2. Hydroxychloroquine enhances AAV transduction in *Cgas*$^{-/-}$ MEFs. *Cgas*$^{-/-}$ MEFs were treated with 0, 3.13, or 18.75 μM hydroxychloroquine one hour prior to transduction with AAV2.CAG.GFP.WPRE at an MOI of 1,000. (**A**) Representative fluorescence microscopy images of MEFs treated with hydroxychloroquine acquired at three days post-transduction (scale bar: 200 μm). (**B**) Flow cytometry plots of GFP^{+} cells (GFP vs 7-AAD) and cell viability (7-AAD vs FSC-A). (**C**) Mean percentage of live GFP^{+} gated cells measured using flow cytometry (±SEM, n=6). ***p ≤0.001 (one-way repeated-measures ANOVA with Dunnett's multiple

comparison test). (**D**) Fold change of the mean proportion of GFP^+ cells treated with 18.75 μM relative to 0 μM hydroxychloroquine in wildtype and *Cgas*$^{-/-}$ MEFs (± SEM, n=6).

6.4.3 Hydroxychloroquine does not influence AAV entry

To assess the effect of hydroxychloroquine on the number of intracellular viral particles soon after transduction, where a difference could suggest increased viral entry, intracellular AAV genome loads were compared up to one hour post-transduction. Wildtype MEFs were treated with either 0 or 18.75 μM hydroxychloroquine prior to transduction with AAV2.CAG.GFP.WPRE and DNA was extracted from cells for qPCR analysis. *GFP* DNA levels were quantified as a readout for the number of intracellular AAV genomes and quantified to *Gapdh* to determine the mean number of viral genomes per cell. No significant difference in intracellular AAV genome copy numbers was detected by qPCR between hydroxychloroquine treated and untreated cells (Figure 6.3).

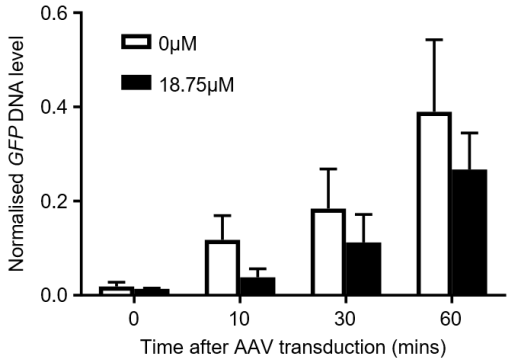

Figure 6.3. Hydroxychloroquine has no effect on the total intracellular AAV genome load. Wildtype MEFs were pre-treated with hydroxychloroquine for one hour prior to transduction with AAV2.CAG.GFP.WPRE at a MOI of 1,000. Cells treated with 0 or 18.75 μM hydroxychloroquine were harvested at 0, 10, 30, and 60 mins post-transduction. DNA was extracted and *GFP* DNA levels were quantified using qPCR. *GFP* DNA was normalised to *Gapdh* genomic DNA copy numbers (±SEM, n=3).

6.4.4 Hydroxychloroquine influences the subcellular localisation of AAV

Cell fractionation was used to determine the subcellular localisation of AAV genomes between the cytosolic and nuclear fractions in wildtype MEFs. Successful isolation of cytosolic and nuclear fractions was confirmed by western blot analysis of proteins unique to each cellular fraction; the cytosolic marker, α-tubulin, and the nuclear marker, histone H3 (Figure 6.4A). Wildtype MEFs were treated with or without 18.75 μM hydroxychloroquine prior to transduction with AAV2.CAG.GFP.WPRE and were harvested 24 hours post-transduction for cellular fractionation. qPCR analysis of genomic *Gapdh* DNA confirmed the successful fractionation of each sample. *Gapdh* DNA was detected in all nuclear fractions and was absent in cytosolic fractions (Figure 6.4B). qPCR analysis of *GFP* DNA, to quantify relative number of AAV genomes

in the nuclear and cytosolic fractions, demonstrated hydroxychloroquine treatment to alter the subcellular distribution of AAV with a trend toward increased nuclear localisation (Figure 6.4C). Although the interaction between the hydroxychloroquine treatment and cellular fraction was statistically significant (two-way ANOVA, p=0.0356; n=3), this did not reach statistical significance upon multiple comparison testing (Figure 6.4C).

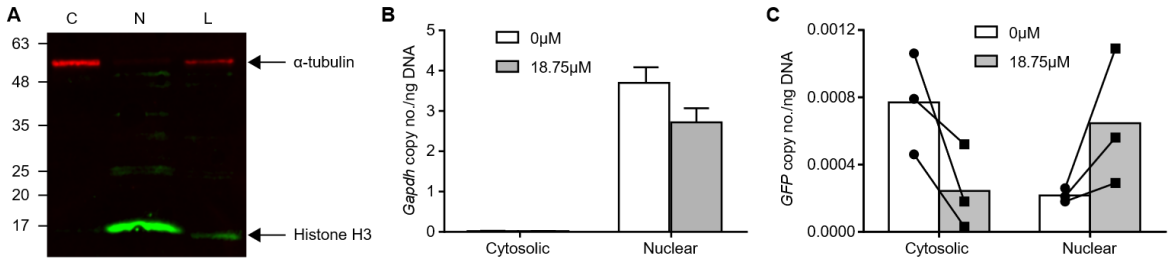

Figure 6.4. Hydroxychloroquine influences the subcellular distribution of AAV viral genomes. Wildtype MEFs were pre-treated with 0 or 18.75 μM hydroxychloroquine for one hour prior to transduction with AAV2.CAG.GFP.WPRE at a MOI of 1,000. Cells were harvested 24 hours post-transduction and separated into cytosolic and nuclear fractions. (**A**) Western blot of α-tubulin and histone H3 protein expression in cytosolic [C] and nuclear [N] fractions, and unfractionated whole cell lysate [L]. (**B**) *Gapdh* genomic DNA levels and (**C**) paired data of 0 or 18.75 μM hydroxychloroquine treated samples plotted onto mean *GFP* DNA copy numbers per ng of DNA (±SEM, n=3).

6.5 Discussion

In this chapter, the immunomodulatory activity of hydroxychloroquine was investigated as a potential mechanism of action for the enhancement of AAV transduction. Several studies have proposed that hydroxychloroquine can inhibit

TLR9 [251, 253, 255, 256, 297]. Hydroxychloroquine partially abrogated the inhibitory effect of CpG-A on AAV transgene expression, suggesting that hydroxychloroquine may be an antagonist of TLR9. If hydroxychloroquine prevents the activation of TLR9 by causing conformational changes in DNA [251, 256], it is possible that this partial response may be a result of the stoichiometric ratio between hydroxychloroquine and CpG-A, such that residual unbound CpG-A was still available to activate TLR9. To further investigate this interaction, the effect of hydroxychloroquine could be assessed in *Tlr9*$^{-/-}$ cell lines. However, despite evidence suggesting hydroxychloroquine can disrupt dsDNA binding and activation of cGAS [250], hydroxychloroquine did not discriminate in its ability to improve AAV transduction between wildtype and *Cgas*$^{-/-}$ MEFs, suggesting that hydroxychloroquine is unlikely to act exclusively through cGAS. Due to the broad range of targets of hydroxychloroquine it is possible that it does not act on one single pathway. Therefore, if hydroxychloroquine was able to also prevent activation of compensatory pathways such as TLR9, which function in the absence of cGAS, then a beneficial effect may still be observed in *Cgas*$^{-/-}$ MEFs. The effect of hydroxychloroquine treatment on *in vitro* and *in vivo* expression of downstream effectors, such as pro-inflammatory cytokines, type I interferons, and the cGAS effector cGAMP, could help confirm the immunomodulatory effect of hydroxychloroquine on AAV-mediated immunity.

Given that hydroxychloroquine has known effects on the endosomal pathway, and that AAV particles rely on endocytosis to travel from the cell membrane to the nucleus [21], I investigated the effect of hydroxychloroquine on the transduction pathway. To assess the effect on AAV cell entry, the number of viral genomes was measured up to one hour post-transduction, given that the half-life for AAV internalisation can be less than 10

minutes [17]. There was no detectable difference in the number of viral genomes following hydroxychloroquine treatment, possibly indicating that hydroxychloroquine does not act by increasing AAV entry in target cells. Although cells were washed several times with buffer prior to qPCR analysis, residual AAV particles may remain bound to the cell surface. The use of vectors with fluorescently-tagged capsid proteins would aid in the tracking of AAV particles during cell surface binding and internalisation [17, 306, 307]. Investigation into the subcellular localisation of AAV revealed that hydroxychloroquine treatment induced a strong trend towards shifting of genomes from the cytosol to the nucleus, suggesting that hydroxychloroquine may influence the ability for AAV particles to reach the nucleus, an essential step in successful transgene expression. This observation may suggest enhanced endosomal escape or nuclear entry, and could account for the increased transgene expression seen following hydroxychloroquine treatment. An *in vitro* study investigating the importance of endosomal pH for the externalisation of the phospholipase A2 domain in the VP1 capsid protein, demonstrated decreased AAV transgene expression in HeLa cells following treatment with bafilomycin A1 and high concentrations of chloroquine (50 μM), which were thought to raise endosomal pH [25]. Although bafilomycin A1 was able to prevent exposure of the VP1 N termini, up to two hours post-transduction, chloroquine enhanced the presentation of this domain. The transient increase in the presentation of the phospholipase A2 domain may enable increased endosomal escape and could encourage a greater number of AAV particles to reach the nucleus, which may explain the increased AAV nuclear localisation. Nonetheless, treatment with 50 μM chloroquine inhibited AAV transduction [25], which contradicts the results observed in this thesis. To further investigate this, detection of AAV genomes with the

recently developed signal amplification by exchange reaction fluorescence *in situ* hybridisation (SABER-FISH) method, may enable increased sensitivity and resolution in the visualisation of the AAV transduction pathway [224]. Ultimately, these findings pose a conflicting view of the role of hydroxychloroquine in viral transduction, challenging the use of this drug to inhibit viral transduction and supporting a complex dose-dependent mechanism of action of hydroxychloroquine [308]. Unfortunately the use of higher hydroxychloroquine doses is limited in MEFs due to cytotoxicity, however the use of other cell lines which can tolerate high doses, such as HepG2 and HeLa cells [25, 165], may help further delineate the dose-dependency of the mechanism of action of hydroxychloroquine in viral infections.

6.6 Conclusion

In this chapter the mechanism for hydroxychloroquine-mediated enhancement of AAV transduction was investigated *in vitro*. Despite the known immunomodulatory effect of hydroxychloroquine, an equally efficacious enhancement of AAV transduction was observed in *Cgas*$^{-/-}$ MEFs, suggesting that hydroxychloroquine does not function primarily through the inhibition of cGAS. However, hydroxychloroquine treatment was able to diminish the inhibitory activity of a TLR9 agonist, which supports hydroxychloroquine as a potential TLR9 antagonist. Although there was no detectable effect on viral entry, hydroxychloroquine enhanced the number of nuclear AAV genomes, which may account for the increased transgene expression observed following hydroxychloroquine treatment.

7 General discussion

The objective of this thesis was to assess immunological responses to AAV retinal gene therapy at both the cellular and intracellular level. One of the major limitations of inflammation in retinal gene therapy clinical trials is the presence of a dose-ceiling beyond which inflammatory immune responses occur. This thesis therefore also assessed the use of an immune inhibitor which can be used to improve the efficacy of retinal gene therapy without increasing vector dose. The immunomodulatory drug hydroxychloroquine presents a means of enhancing AAV transgene expression *in vitro*, *ex vivo*, and *in vivo*, specifically in cell types relevant to retinal gene therapy.

7.1 Cellular immune response to retinal gene therapy

Despite the low immunogenicity of AAV compared to other viral vectors and assumptions of ocular immune privilege, local and systemic immune responses have been observed across numerous retinal gene therapy trials [151, 152, 183]. Inflammatory responses, and associated drops in visual acuity, are typically resolved with corticosteroid treatment, however occasional persistent inflammation occurs suggesting a sustained response to gene therapy [278]. Clinically, local retinal inflammation has been observed with the use of SD-OCT imaging to monitor the appearance of hyper-reflective spots in the retina, indicative of AAV-mediated inflammation [176, 178]. Fluorescein angiography, in which a fluorescent dye is injected into the bloodstream to visualise retinal and choroidal vasculature, has also revealed a transient compromise of the blood-retina barrier following subretinal AAV injections in non-human primates [184]. Furthermore, immunohistochemical staining

in non-human primates and histopathological analysis in dogs has demonstrated the presence of peripheral B and T cells in the retina following subretinal and intravitreal AAV injections, respectively, suggesting leukocyte recruitment and invasion [176, 179]. Together these studies support the presence of a cellular immune response to AAV retinal gene therapy, with leukocyte transmigration across the blood retina barrier.

In Chapter 3, the retinal cellular inflammatory response to AAV subretinal injections in mice was characterised using flow cytometric analysis. In retinae injected with vectors expressing a GFP transgene protein, a significant cellular response was detected 14 days post-injection. The presence of significant numbers of macrophages, NK cells, and CD8 T cells, and the absence of B cells, suggests the initiation of a type 1 cell-mediated effector response coordinated by CD4 T_H1 cells, which functions to provide effective protection against viruses [93]. This is further supported by the expression of the classical type 1 cytokines IFN-γ, TNF-β, and CXCL10, following *in vivo* subretinal AAV injections [175-177]. Our group previously demonstrated the upregulation of key PRRs and type 1 interferon response genes in the retina from day 7 post-subretinal AAV gene therapy [175]. As a significant infiltration of leukocytes was not detected in this thesis until 14 days post-injection, this suggests that expression of these innate immune factors likely originates from resident retinal cells. Together these findings could suggest detection of AAV by a retinal cell, such as microglia, resulting in the production of pro-inflammatory cytokines and the induction of a cellular immune response. However, the function of this coordinated type 1 response is to detect and destroy virus-infected cells, which may have implications in

the therapeutic outcome of gene therapy where the number of successfully transduced cells will be important in the treatment of inherited retinal degenerations.

Following the peak of a T cell response, numbers rapidly decline to leave a pool of memory T cells primed for re-exposure to the viral antigen [96]. Substantial numbers of both CD4 and CD8 T cells were observed in the experiments described in this thesis from 14–28 days post-injection, suggesting the response had not resolved within the time-frame analysed. Investigation at a later time-point, and the use of additional markers, may determine the presence of memory T cells once the response has cleared, which may be an important determinant in the success of AAV re-administration. Despite evidence for the presence of $CD20^+$ B cells in cynomolgus macaques following subretinal injections of AAV8 [176], B cells were not detected in the experiments in this thesis. One possible explanation for these differences may be degree of exposure to AAV antigens in these animal populations. Although low levels of pre-existing antibodies to several AAV serotypes have been detected in wildtype mice obtained from Charles River Laboratories [309], these are likely to be significantly less prevalent than in non-human primates, which, like humans, are natural hosts of wildtype AAV [310]. Despite the detection of possible T and B cell responses to retinal gene therapy, no loss in efficacy has been observed following subsequent AAV subretinal injections of the second eye [189, 311]. This is in contrast to other gene therapies where neutralising antibody responses can be significantly limiting to AAV administration [160, 167, 168] and may indicate that pre-existing adaptive immune responses play a minimal role in the retina. However, many current retinal gene therapy trials adopt a standardised immunosuppression protocol up to 21 days post-treatment which may ameliorate this response [151, 152, 312]. Ultimately there are several differences

between the mouse and human immune system, which may pose a limitation in the use of mice to analyse immunological responses [313]. It thus remains to be seen whether activation of the adaptive immune response will limit the therapeutic effect of retinal gene therapy.

GFP-expressing AAV vectors are commonly utilised in mechanistic *in vitro* and *in vivo* studies, however there has been little investigation of the relative contribution of this fluorophore in retinal inflammation and toxicity. One study demonstrated equivalent immune activation and retinal toxicity between GFP and null expressing vectors [177], while another suggested reduced toxicity with a null expressing vector compared to GFP [185]. However, differences in the design of these null vectors, with the former removing the transgene sequence [177] and the latter enclosing the GFP sequence between two loxP sites [185], may ultimately affect the mechanism of this response. The null vector used in this thesis was designed with a non-functional sequence and the Kozak translation initiation site was removed to prevent protein expression. The toxic reaction to this vector may therefore represent a different mechanism to other null vectors. In Chapter 3, comparison of the retinal immune response to GFP- and REP1-expressing vectors demonstrated a significantly reduced response to REP1. GFP overexpression is associated with oxidative stress and immune activation [228], which may contribute to these inflammatory responses. Furthermore, GFP, originally isolated from the jellyfish *Aequorea Victoria*, is a non-vertebrate protein that will be perceived as a novel antigen to the wildtype retina; this may ultimately increase its immunogenicity compared to expression of the retinal REP1 protein. Nonetheless, gene therapy patients with choroideremia who have a loss-of-function mutation in the *CHM* gene (encoding REP1), may also present an enhanced response due to a possible

lack of tolerance to the REP1 protein. Although further evidence would be needed to conclude that *GFP* is more immunogenic than the therapeutic transgene *REP1*, the experiments presented in this thesis suggest that differences in the immunogenicity of AAV vectors may exist beyond the vector capsid and *cis*-regulatory elements. Investigation into the mechanism of this response may aid the development of less immunogenic vectors and may highlight the need to move away from GFP-expressing vectors in the investigation of AAV-induced immunological responses.

Under normal conditions, the blood-retina barrier, which consists of tight junctions between retinal capillary endothelial and RPE cells, functions to protect the retina from damaging inflammatory responses [314]. However, during retinal inflammation, local expression of pro-inflammatory cytokines can upregulate adhesion molecules and chemokines on the basal RPE membrane [315, 316], which are induced in the retina following AAV subretinal injections [175-177]. These molecules function to promote leukocyte recruitment, adhesion, and infiltration through the blood-retina barrier, ultimately increasing permeability to circulating leukocytes [127, 145, 148, 149]. Although questions remain about the source and mechanism of this response, recruitment of immune cells into the retina suggests infiltration from the peripheral blood, likely across the blood-retina barrier. Reducing the permeability of this barrier may therefore provide an opportunity to block leukocyte infiltration. The monoclonal antibody natalizumab is an antagonist of α4 integrins, which are expressed the surface of leukocytes to mediate their interaction and transmigration across the blood-brain barrier [317], and could be explored as a possible means of restricting infiltration across the blood-retina barrier. Furthermore, subretinal AAV delivery in mice is undertaken with a transcleral injection from the back of eye through the sclera,

choroid, and RPE layers, however, in humans, transretinal subretinal injections are performed from the front of the eye and through the retina [155]. As transcleral injections pass through the choriocapillaris and RPE, there is a chance for increased trauma and breakdown of the blood-retina barrier. Furthermore, suprachoroidal injections (between the choroid and sclera) induce a significant local cellular response [318], so care should be taken to avoid inadvertent suprachoroidal delivery.

The activation and dysregulation of immunity can play a strong role in retinal degenerative diseases which can drive chronic inflammatory responses. During acute inflammation microglia maintain retinal homeostasis by promoting neuroprotection and regeneration, however, during chronic inflammation microglia can contribute to pathogenesis by inducing significant tissue damage [319]. Several features of the immune system play a significant role in driving the pathogenesis of age-related macular degeneration (AMD) [320, 321]. Accumulating evidence suggests that over activity of the complement pathway plays a role in driving AMD pathogenesis and RPE damage [322]. This is the basis of a current AAV retinal gene therapy trial for geographic atrophy (dry AMD) delivering complement factor I (CFI), a negative regulator of the alternative pathway [323]. Furthermore, in response to inflammatory damage, microglia accumulate in the subretinal space, a feature of their activation, which in turn exacerbates retinal degeneration [319]. During neovascular (wet) AMD the breakdown of the blood-retina barrier due to RPE damage can lead to infiltration of choroidal immune cells such as macrophages, dendritic cells, and neutrophils into the retina, which can drive further neovascularisation [320, 324]. Reactivity of microglia, in response to the sequential degeneration of rods and cones, is also a feature of retinitis pigmentosa, and it has been suggested that microglia can drive

pathogenesis by secreting pro-inflammatory factors [319]. The effect of introducing a viral immunogen into an immune-activated environment is currently unclear and it should be considered that patients may be more sensitive to the immunogenic features of AAV. It therefore remains to be seen whether the mechanisms surrounding the immunological events of AAV retinal gene therapy are equivalent in the degenerate retina.

7.2 Activation of intracellular innate immune responses

There are several features of the AAV vector which have the potential to elicit an innate immune response through host cell PRRs. The AAV genome and capsid proteins can elicit a TLR9- and TLR2-mediated intracellular innate response, respectively [157, 169-171], while the double-stranded RNA transgene product has been shown to elicit an immune response through the RNA sensor MDA5 [172]. Furthermore, the PRRs TLR9, RIG-I, and cGAS are locally upregulated following AAV subretinal injections in mice [175]. Activation of these PRRs converge on NF-κB– and IRF–mediated upregulation of pro-inflammatory cytokines and type I interferons, respectively [53, 66, 325]. In turn, these can coordinate the recruitment, infiltration, and activation of immune cells in the retina [127, 148]. It has been hypothesised that the activation of these pathways may be responsible for the retinal inflammation and toxicity observed in some AAV retinal gene therapy studies [176, 177, 184].

In Chapter 4, I expanded on the growing evidence for AAV as a viral antigen by demonstrating AAV transgene expression to be significantly reduced by treatment with a TLR9 agonist. This finding supports a number of studies investigating the role

of TLR9 in AAV-mediated immune responses. Until now, TLR9 has been considered primarily in the context of systemic immunity, in particular its role in CD8 T cell responses against the viral capsid and transgene [169, 170]. However, the impact of TLR9 activation on AAV transduction *in vitro*, as seen in Chapter 4, suggests activation of this pathway can restrict transgene expression independent of the cellular immune response. In this chapter, I also demonstrated a 6.4-fold increase in AAV transgene expression in *Cgas*$^{-/-}$ compared to wildtype MEFs, suggesting that cGAS is a limiting factor in AAV transduction. This is the first evidence of cGAS as a potential restrictive determinant in AAV transduction and suggests that AAV particles may escape from endosomal compartments and expose their genome to the cytosolic cGAS. Typically, the ligand of cGAS is dsDNA [58, 61, 63], however stem structures of ssDNA, such as those seen during the replication cycle of HIV, can induce cGAS-dependent type I interferon responses [62]. This reveals a potential for the secondary hairpin structures of AAV ITRs to induce activation of cGAS. Furthermore, AAV particles are packaged with positive and negative strands, which, when released from the capsid, may anneal to form double-stranded structures [31]. Detection of antibody-bound virions by the cytosolic protein TRIM21, can induce capsid proteasomal degradation and release of viral genomes to activate cGAS [114]. Similarly, TRIM5α is believed to promote disassembly of the capsid and release of the viral genome in retroviruses, with some studies suggesting this to occur via ubiquitin-dependent proteasomal degradation [326, 327]. As AAV has been demonstrated to undergo proteasomal degradation [328, 329], this may suggest that these pathways could induce cytosolic cGAS sensing of the transgenic AAV genome. AAV vectors with a single-polarity genome have been demonstrated to have transduction efficiencies comparable to mixed polarity vectors

following intramuscular and intravenous injections in C57BL/6 mice [32]; this may provide an opportunity to reduce cGAS mediated immunity. Nonetheless, the role of cGAS in AAV detection warrants additional investigation to further uncover the immunogenicity of the AAV genome. There are likely several other, currently unknown, PRRs that may detect AAV vectors to elicit inhibitory effects.

TLR9 and cGAS are expressed in the murine retina and are significantly upregulated following AAV subretinal injections in mice, revealing a potential role of these factors in retinal immunity [175]. As the resident retinal immune cell, microglia are capable of inducing pro-inflammatory cytokine expression through TLR9-mediated responses [132]. Another source of TLR9 are RPE cells [191], which can also mediate cGAS-induced interferon expression to drive inflammasome activation during AMD [192]. Due to the implications of TLR9 and cGAS on the efficacy of AAV transduction, preventing these intracellular innate immune pathways may both directly, by inhibiting restrictive intracellular responses, and indirectly, by minimising retinal inflammation, enhance the therapeutic outcome of gene therapy. In fact, the TLR9-mediated $CD8^+$ T cell response to AAVrh32.33 was significantly diminished upon depletion of CpG sequences (the ligands for TLR9 receptors) in the viral genome [170]. Furthermore, a very recent study, which was published days before submission of this thesis, demonstrated a substantial reduction in AAV immunogenicity and a significant increase in transgene expression when DNA ODNs that antagonise TLR9 activity were directly incorporated into the AAV genome [330]. Incorporation of these sequences significantly reduced Iba1 microglial staining and the number of T cells in the retina following subretinal AAV delivery, thus supporting the role of TLR9 in AAV-induced immunity and validating the findings in this thesis of T cell responses in the retina.

However, between PRR pathways, such as TLR9 and cGAS, there is a significant degree of compensation and redundancy [331], therefore, broadly inhibiting these innate immune pathways may be a practical means of supplementing the therapeutic outcome of retinal gene therapy.

7.3 Improving the efficacy of retinal gene therapy

Results from retinal gene therapy clinical trials and pre-clinical testing in animal models suggest that AAV-mediated inflammation is dose-dependent and often absent at low vector doses [151, 152, 180, 182, 183, 332, 333]. Although the impact of inflammation on the outcome of gene therapy remains unclear, ocular inflammation has been associated with a lack of therapeutic effect and deterioration in visual acuity [152, 179, 183]. However, the efficacy of retinal gene therapy is inversely dependent on viral dose, where low doses can result in minimal improvements in visual acuity, possibly due to insufficient levels of transgene expression [152, 275]. The current aim for gene therapy trials is to find an optimal vector dose that allows for sufficient therapeutic treatment without inducing potential harmful inflammatory responses. In spite of the success of some trials, such as for *RPE65*-associated LCA, which achieved improved visual outcomes with few cases of inflammation [150], others have experienced varying degrees of efficacy, often correlating with inflammatory reactions [183, 334]. A means of improving the efficacy of retinal gene therapy at lower and safer doses may therefore allow for an enhanced therapeutic effect in future applications.

Strategies to enhance AAV transduction have primarily focussed on either modification of the vector itself or the adjunctive use of drugs affecting the

transduction pathway, with many of these strategies targeting retinal inflammation [335]. The use of adjuncts with well-established safety profiles to enhance gene therapy efficacy have the benefit of enabling implementation into current safe gene therapy treatment strategies without the need to modify the vector itself, which adds additional complications in drug development. Currently the only approach widely implemented into AAV retinal gene therapy treatments is a perioperative period of systemic immunosuppression with corticosteroids [150-152]. Although corticosteroids typically provide an effective means of controlling ocular inflammation, at high vector doses cases of intraocular inflammation have persisted, requiring supplementary corticosteroid treatment. This can include oral prednisolone, dexamethasone eye drops, and intravitreal dexamethasone implants (Ozurdex), as demonstrated in the phase 1/2 dose-escalation gene therapy trial for X-linked retinitis pigmentosa [152]. Despite the management of inflammation in the majority of patients, the effect of such reactions on the therapeutic outcome for patients undergoing retinal gene therapy is yet to be established. Given its effect on NF-κB, a downstream effector of TLR9 and cGAS, in Chapter 4 I investigated the effect of dexamethasone on AAV transduction *in vitro.* Treatment with dexamethasone had no effect on AAV transduction and so further testing was not pursued, however, given its ability to suppress inflammation in retinal gene therapy trials, it may have a greater effect if systemically delivered *in vivo*. However, a recent study demonstrated that intraperitoneal injections of the corticosteroid dexamethasone in C57BL/6 mice, given before or at the same time as AAV9 systemic injections, significantly decreased transduction in the majority of tissues due to a predicted inhibition of vascular permeability to AAV vectors [336]. Although changes in vascular permeability may not

be relevant for successful transduction following subretinal injections, given their widespread use in retinal gene therapy, further investigation into the effect of corticosteroids on the therapeutic outcome is warranted.

Other strategies to increase the efficacy of gene therapy with adjunctive treatments that mediate immune reactions have focussed on the avoidance of humoral responses. One study demonstrated the use of the FDA approved drug bortezomib to enhance AAV transduction by inhibiting proteasomal antigen processing and subsequent presentation on MHC I molecules in the human hepatocyte cell line HHL5 [337]. Intravenous co-administration of bortezomib and an AAV2 vector in C57BL/6 mice led to a transient increase in transgene expression (≤6-fold), however this was not extended to use with an AAV8 vector [337]. Alternatively, the endopeptidase imlifidase (IdeS) has been developed as a means of eliminating anti-AAV antibodies [338]. Cynomolgus macaques with pre-existing anti-AAV8 antibodies were intravenously injected with IdeS 24 hours prior to AAV8.FIX injections. This led to decreased titres of AAV8-specific IgG and neutralising antibodies and a significant increase in *FIX* transgene expression. IdeS also enabled re-administration of the novel AAV variant AAV-LK03 in African green monkeys, leading to a significant increase in transgene expression [338]. Although anti-AAV antibodies have been detected in some retinal gene therapy clinical trials following subretinal [183] and intravitreal injections [168, 339], it remains to be seen whether such methods would prove effective in retinal gene therapy given that neutralising antibody responses are generally minimal following subretinal AAV injections [151]. Other approaches have been to inhibit AAV-specific cellular immune responses using the immunosuppressant rapamycin. The co-administration of synthetic nanoparticles containing rapamycin with an AAV8 vector

by intravenous injection in C57BL/6 mice and cynomolgus macaques prevented the induction of B and T cell responses [340]. Despite reducing AAV-specific immune responses, this had no detectable effect on transgene expression.

Given the effect of TLR9 and cGAS on AAV transduction in this thesis, the immunomodulatory drug hydroxychloroquine, a putative inhibitor of these factors, was investigated as a means of enhancing the efficacy of AAV transgene expression. In Chapters 4 and 5, hydroxychloroquine was demonstrated to enhance AAV transgene expression *in vitro* (MEFs and non-human primate primary RPE cells), *ex vivo* (human retinal explants), and *in vivo* (murine retina). Co-injection of hydroxychloroquine into the subretinal space led to increased GFP transgene expression with both an AAV2 (mean 4.6-fold) and AAV8 (5.9-fold) serotype vector, including a ubiquitous and photoreceptor-specific promoter, respectively. This suggests hydroxychloroquine can enhance transduction within multiple retinal cell types and with the two most common vector serotypes in retinal gene therapy. An increased level of transgene expression in eyes co-injected with hydroxychloroquine may have implications in gene therapy trials, for instance a lower and safer viral dose could be utilised to achieve a given treatment effect or increased efficacy could be achieved at current vector doses. The former may have significant implications for treatments that have inflammatory responses at higher doses, while the latter may be important for inefficient gene therapies that need high AAV doses to achieve a treatment effect. The latter hypothesis was investigated in Chapter 5 with the inefficient dual vector system encoding *ABCA4*, however, no effect was observed following co-injection of hydroxychloroquine and the ABCA4 dual vector. It is likely that the dual vector system is limited by the homologous recombination of upstream and downstream vectors necessary to create the full length

ABCA4 transgene. This recombination event may be unaffected by hydroxychloroquine treatment, and thus its application may only be appropriate to single vector constructs. Investigation into the use of hydroxychloroquine with therapeutic transgenes will be key in the application of this adjunct into retinal gene therapy trials.

7.4 Immunomodulatory effect of hydroxychloroquine

The inhibition of key PRRs, such as TLR9 and cGAS, by hydroxychloroquine and chloroquine has been shown to affect downstream pro-inflammatory cytokine and type I interferon responses at concentrations ≤25 μM [250, 251, 258]. *In vitro*, both hydroxychloroquine and chloroquine have been shown to inhibit the production of the pro-inflammatory cytokines TNF-α, IFN-γ, and IL-6 in PBMCs [341], and TNF-α, IL-1β, and IL-6 in human monocytes [342]. In turn these pro-inflammatory cytokines can control cellular immune responses: IFN-γ can prime macrophages for pro-inflammatory responses and render them resistant to suppressive immune factors [343]; IL-6 can control the survival, expansion, and maturation of B cells [344]; and TNFα is key in activating and promoting the long-term survival of macrophages [345]. A type I interferon response also induces an anti-viral state within infected and neighbouring cells, which can limit viral infections across a whole tissue [68].

In addition to the inhibition of PRRs and their downstream signalling pathways, hydroxychloroquine and chloroquine also appear capable of indirectly modulating immune responses though the alkalisation of lysosomes when used at higher concentrations. The processing of extracellular material for antigen presentation is classically undertaken by professional antigen presenting cells, which utilise the

lysosomal pathway to display short peptides on MHC class II molecules for detection by CD4 T cells [99]. By increasing the pH of lysosomes, chloroquine can affect antigen processing, as demonstrated in macrophages (at 100 μM) [346], dendritic cells (at 100 μM) [347], and B cells (at 25–100 μM) [348]. Notably, these effects, which are associated with raised endosomal and lysosomal pH, were primarily observed at high concentrations of chloroquine (100 μM). In addition, chloroquine has been shown to inhibit autophagy, a regulated process for removing damaged intracellular organelles or proteins by enveloping cytoplasmic material, by inhibiting the fusion between autophagosomes and lysosomes [349]. This, in turn, leads to the inhibition of presentation of cytosolic antigens, including autoantigens and viral antigens, on MHC class II molecules via the autophagy-lysosomal pathway [350-352]. Since dysregulation of autophagy contributes to cancer development and chemotherapy resistance, hydroxychloroquine has been evaluated as an autophagy inhibitor in clinical trials for various cancers [353-356]. Very high daily doses of hydroxychloroquine (typically ≤1200 mg/day) have been used in this context in order to effectively block the fusion of lysosomes with autophagosomes, thus supporting the dose-dependent mechanism of action of hydroxychloroquine. Overall, study findings are consistent with hydroxychloroquine and chloroquine having a direct immunosuppressive effect on viral sensing and pro-inflammatory cytokine release at low concentrations, and an indirect immunomodulatory effect via lysosomal antigen processing and presentation at high concentrations.

The data presented in Chapter 6 suggest that hydroxychloroquine may function to enhance AAV transduction by partially preventing the activation of TLR9. Due to the low concentrations of hydroxychloroquine used in these studies (18.75 μM), a

potential mechanism was proposed whereby the diminished inhibitory activity of the TLR9 agonist CpG-A in the presence of hydroxychloroquine was due to an antagonistic role in TLR9 activation, such as inducing conformational changes in nucleic acids to prevent its activation [251, 256]. However, TLR9 activity is ultimately optimal in acidic conditions, so despite assumptions of a minimal effect on endosomal pH at the concentrations of hydroxychloroquine in this thesis, alterations in the pH may indirectly inhibit TLR9 activity [255]. It cannot be ruled out that the diminished inhibitory effect of CpG-A in the presence of hydroxychloroquine may be due to the enhancement of AAV transduction through another, independent mechanism that could mask the inhibitory activity of CpG-A. Furthermore, hydroxychloroquine demonstrated no change in its ability to enhance AAV transduction in the absence of cGAS. This may suggest that either hydroxychloroquine does not function through inhibiting cGAS activation by AAV, or that AAV does not activate cGAS. Further work would therefore be necessary to establish a restrictive role of cGAS in AAV transduction. The immunomodulatory effect of hydroxychloroquine may also have significant implications on the inflammatory response to retinal gene therapy. Unlike adjuncts such as bortezomib and rapamycin, which control humoral and cellular responses respectively, the inhibition of TLR9-mediated responses may prevent induction of upstream intracellular reactions at the point of AAV detection. Thus, given the potential role of hydroxychloroquine and chloroquine in restricting cellular immune responses, it would be of significant interest to assess the effect of subretinal hydroxychloroquine injections on the cellular inflammatory reaction observed in Chapter 3. Nevertheless, further investigation into the restrictive role of

hydroxychloroquine on TLR9 would also be necessary to validate the potential inhibitory effect of this drug on innate immunity.

The effect of hydroxychloroquine on the intracellular localisation of AAV genomes, suggests a possible enhancement in transduction and nuclear entry. As the total number of intracellular genomes was equivalent between hydroxychloroquine treated and untreated cells, it is likely that the effect is on an intracellular processing event such as cell sorting, cytoplasmic escape, or nuclear entry. The current consensus is that acidification of endosomal compartments is necessary for AAV cytoplasmic escape, however, studies investigating this mechanism of action have relied on the use of drugs that inhibit acidification of these compartments, including bafilomycin A_1, ammonium chloride, and chloroquine [17, 165, 357], which are likely to disrupt other cellular processes. Given that the alkalisation of endosomes would be expected to inhibit AAV cytoplasmic escape and, therefore, successful transduction, the mechanism of action of hydroxychloroquine is unlikely to be via the inhibition of endosomal function. Nonetheless, a shift in the localisation of AAV genomes is also potentially consistent with evasion of innate immunity. ISGs upregulated by TLR9-induced type I interferons can affect all stages of a viral infection [68]. For instance, interferon-inducible transmembrane (IFITM) proteins can inhibit endosomal acidification necessary for cytoplasmic escape [358] and the GTP-binding protein myxovirus resistance B (MxB) can block HIV-1 nuclear uptake [359]. Ultimately, investigation into the effect of hydroxychloroquine on AAV intracellular processing and immune responses may help to further dissect the AAV transduction pathway to enable enhancement in transgene expression.

Regardless of its immunomodulatory activity, enhancement of retinal gene therapy efficacy by hydroxychloroquine presents an opportunity to utilise lower doses of AAV to achieve a given treatment effect, which would ultimately help reduce AAV-mediated inflammatory responses. A practical means of both suppressing immune reactions and increasing the therapeutic effect is yet to be implemented into gene therapy trials, however, could potentially address two of the biggest challenges in gene therapy.

7.5 Potential clinical applications of hydroxychloroquine

The adjuvant use of hydroxychloroquine to augment the effects of gene therapy at the time of AAV vector delivery requires some consideration of the route of delivery of hydroxychloroquine, dose administered, and duration of treatment. The use of systemic orally delivered hydroxychloroquine described in Chapter 5 demonstrated no signs of efficacy at the doses and durations tested. However, due to what is known about the pharmacokinetics of hydroxychloroquine, a consistent and predictable tissue concentration of hydroxychloroquine in the retina needed to enhance AAV transduction would be difficult to achieve over a short interval. Comparatively, the delivery of hydroxychloroquine by subretinal injection allows for precise control over the local drug concentration. Furthermore, the use of a single one-off dose minimises the duration for immunomodulation, and prevents systemic immunosuppression which may have further off target effects. Since the dose of hydroxychloroquine administered in the subretinal space in AAV gene therapy potentiates viral action, there is a theoretical risk of viral retinitis. Systemic corticosteroid usage is associated with the activation of viral retinitis in previously immunocompetent patients [360, 361], and intraocular or periocular corticosteroid use has also been associated with

increased risk of acute retinal necrosis secondary to HSV [362, 363]. However, acute retinal necrosis has not been reported in long-term systemic hydroxychloroquine users despite clear evidence for drug accumulation within the RPE. Hydroxychloroquine in the context of subretinal delivery may therefore function as an immunomodulatory rather than immunosuppressive agent. This may suggest that subretinal administration of a single low dose of hydroxychloroquine as an adjuvant to AAV gene therapy is of low risk while offering the potential to reduce the AAV dose required, thus reducing the risk of treatment-induced retinal inflammation and the need for systemic steroids to counter this response. While existing evidence supports the safety of low dose hydroxychloroquine in healthy retinae, it is unclear whether the degenerate RPE and photoreceptors in inherited retinal dystrophies may respond differently to the same concentration of hydroxychloroquine.

7.6 Conclusion

Overall, the results presented in this thesis further elucidate the immunogenicity of recombinant AAV gene therapy vectors. A substantial cellular immune response to AAV-mediated retinal gene therapy was detected *in vivo*, which was significantly influenced by the nature of the vector transgene. Although the source of this response remains uncertain, *in vitro* AAV transduction was limited by anti-viral nucleic acid sensors revealing the potential immunogenicity of transgenic genomes. AAV-mediated host responses will likely reduce the therapeutic efficacy of retinal gene therapy, however the use of increased doses to overcome such limitations is prevented by dose-dependent intraocular inflammation. Hydroxychloroquine presents an opportunity to safely enhance the efficacy of retinal gene therapy when subretinally delivered in

solution with the AAV vector. Together this thesis demonstrates the immunogenicity of AAV vectors in the context of retinal gene therapy and presents a practical means of enhancing therapeutic efficacy to potentially minimise harmful inflammatory responses.

References

1. Wang, D., P.W.L. Tai, and G. Gao, *Adeno-associated virus vector as a platform for gene therapy delivery.* Nat Rev Drug Discov, 2019. **18**(5): p. 358-378.

2. Agbandje-McKenna, M. and J. Kleinschmidt, *AAV capsid structure and cell interactions.* Methods Mol Biol, 2011. **807**: p. 47-92.

3. Sonntag, F., K. Schmidt, and J.A. Kleinschmidt, *A viral assembly factor promotes AAV2 capsid formation in the nucleolus.* Proc Natl Acad Sci U S A, 2010. **107**(22): p. 10220-5.

4. Sonntag, F., et al., *The assembly-activating protein promotes capsid assembly of different adeno-associated virus serotypes.* J Virol, 2011. **85**(23): p. 12686-97.

5. Ogden, P.J., et al., *Comprehensive AAV capsid fitness landscape reveals a viral gene and enables machine-guided design.* Science, 2019. **366**(6469): p. 1139-1143.

6. Wilmott, P., et al., *A User's Guide to the Inverted Terminal Repeats of Adeno-Associated Virus.* Hum Gene Ther Methods, 2019. **30**(6): p. 206-213.

7. Balakrishnan, B. and G.R. Jayandharan, *Basic biology of adeno-associated virus (AAV) vectors used in gene therapy.* Curr Gene Ther, 2014. **14**(2): p. 86-100.

8. Huang, L.Y., S. Halder, and M. Agbandje-McKenna, *Parvovirus glycan interactions.* Curr Opin Virol, 2014. **7**: p. 108-18.

9. Summerford, C. and R.J. Samulski, *Membrane-associated heparan sulfate proteoglycan is a receptor for adeno-associated virus type 2 virions.* J Virol, 1998. **72**(2): p. 1438-45.

10. Summerford, C., J.S. Bartlett, and R.J. Samulski, *AlphaVbeta5 integrin: a co-receptor for adeno-associated virus type 2 infection.* Nat Med, 1999. **5**(1): p. 78-82.

11. Qing, K., et al., *Human fibroblast growth factor receptor 1 is a co-receptor for infection by adeno-associated virus 2.* Nat Med, 1999. **5**(1): p. 71-7.

12. Kashiwakura, Y., et al., *Hepatocyte growth factor receptor is a coreceptor for adeno-associated virus type 2 infection.* J Virol, 2005. **79**(1): p. 609-14.

13. Akache, B., et al., *The 37/67-kilodalton laminin receptor is a receptor for adeno-associated virus serotypes 8, 2, 3, and 9.* J Virol, 2006. **80**(19): p. 9831-6.

14. Pillay, S., et al., *An essential receptor for adeno-associated virus infection.* Nature, 2016. **530**(7588): p. 108-12.

15. Dudek, A.M., et al., *GPR108 Is a Highly Conserved AAV Entry Factor.* Mol Ther, 2020. **28**(2): p. 367-381.

16. Duan, D., et al., *Dynamin is required for recombinant adeno-associated virus type 2 infection.* J Virol, 1999. **73**(12): p. 10371-6.

17. Bartlett, J.S., R. Wilcher, and R.J. Samulski, *Infectious entry pathway of adeno-associated virus and adeno-associated virus vectors.* J Virol, 2000. **74**(6): p. 2777-85.

18. Weinberg, M.S., et al., *Recombinant adeno-associated virus utilizes cell-specific infectious entry mechanisms.* J Virol, 2014. **88**(21): p. 12472-84.

19. Sanlioglu, S., et al., *Endocytosis and nuclear trafficking of adeno-associated virus type 2 are controlled by rac1 and phosphatidylinositol-3 kinase activation.* J Virol, 2000. **74**(19): p. 9184-96.

20. Nonnenmacher, M. and T. Weber, *Adeno-associated virus 2 infection requires endocytosis through the CLIC/GEEC pathway.* Cell Host Microbe, 2011. **10**(6): p. 563-76.

21. Dhungel, B.P., C.G. Bailey, and J.E.J. Rasko, *Journey to the Center of the Cell: Tracing the Path of AAV Transduction.* Trends Mol Med, 2020.

22. Lins-Austin, B., et al., *Adeno-Associated Virus (AAV) Capsid Stability and Liposome Remodeling During Endo/Lysosomal pH Trafficking.* Viruses, 2020. **12**(6).

23. Venkatakrishnan, B., et al., *Structure and dynamics of adeno-associated virus serotype 1 VP1-unique N-terminal domain and its role in capsid trafficking.* J Virol, 2013. **87**(9): p. 4974-84.

24. Huotari, J. and A. Helenius, *Endosome maturation.* EMBO J, 2011. **30**(17): p. 3481-500.

25. Sonntag, F., et al., *Adeno-associated virus type 2 capsids with externalized VP1/VP2 trafficking domains are generated prior to passage through the cytoplasm and are maintained until uncoating occurs in the nucleus.* J Virol, 2006. **80**(22): p. 11040-54.

26. Kronenberg, S., et al., *A conformational change in the adeno-associated virus type 2 capsid leads to the exposure of hidden VP1 N termini.* J Virol, 2005. **79**(9): p. 5296-303.

27. Stahnke, S., et al., *Intrinsic phospholipase A2 activity of adeno-associated virus is involved in endosomal escape of incoming particles.* Virology, 2011. **409**(1): p. 77-83.

28. Nicolson, S.C. and R.J. Samulski, *Recombinant adeno-associated virus utilizes host cell nuclear import machinery to enter the nucleus.* J Virol, 2014. **88**(8): p. 4132-44.

29. Kelich, J.M., et al., *Super-resolution imaging of nuclear import of adeno-associated virus in live cells.* Mol Ther Methods Clin Dev, 2015. **2**: p. 15047.

30. Grieger, J.C., S. Snowdy, and R.J. Samulski, *Separate basic region motifs within the adeno-associated virus capsid proteins are essential for infectivity and assembly.* J Virol, 2006. **80**(11): p. 5199-210.

31. Nakai, H., T.A. Storm, and M.A. Kay, *Recruitment of single-stranded recombinant adeno-associated virus vector genomes and intermolecular recombination are responsible for stable transduction of liver in vivo.* J Virol, 2000. **74**(20): p. 9451-63.

32. Zhou, X., et al., *Adeno-associated virus of a single-polarity DNA genome is capable of transduction in vivo.* Mol Ther, 2008. **16**(3): p. 494-9.

33. Rose, J.A., et al., *Evidence for a single-stranded adenovirus-associated virus genome: formation of a DNA density hybrid on release of viral DNA.* Proc Natl Acad Sci U S A, 1969. **64**(3): p. 863-9.

34. Berns, K.I. and S. Adler, *Separation of two types of adeno-associated virus particles containing complementary polynucleotide chains.* J Virol, 1972. **9**(2): p. 394-6.

35. Kotin, R.M., et al., *Site-specific integration by adeno-associated virus.* Proc Natl Acad Sci U S A, 1990. **87**(6): p. 2211-5.

36. McCarty, D.M., S.M. Young, Jr., and R.J. Samulski, *Integration of adeno-associated virus (AAV) and recombinant AAV vectors.* Annu Rev Genet, 2004. **38**: p. 819-45.

37. Duan, D., et al., *Circular intermediates of recombinant adeno-associated virus have defined structural characteristics responsible for long-term episomal persistence in muscle tissue.* J Virol, 1998. **72**(11): p. 8568-77.

38. Nakai, H., et al., *Extrachromosomal recombinant adeno-associated virus vector genomes are primarily responsible for stable liver transduction in vivo.* J Virol, 2001. **75**(15): p. 6969-76.

39. McCarty, D.M., P.E. Monahan, and R.J. Samulski, *Self-complementary recombinant adeno-associated virus (scAAV) vectors promote efficient transduction independently of DNA synthesis.* Gene Ther, 2001. **8**(16): p. 1248-54.

40. Buck, T.M. and J. Wijnholds, *Recombinant Adeno-Associated Viral Vectors (rAAV)-Vector Elements in Ocular Gene Therapy Clinical Trials and Transgene Expression and Bioactivity Assays.* Int J Mol Sci, 2020. **21**(12).

41. Loeb, J.E., et al., *Enhanced expression of transgenes from adeno-associated virus vectors with the woodchuck hepatitis virus posttranscriptional regulatory element: implications for gene therapy.* Hum Gene Ther, 1999. **10**(14): p. 2295-305.

42. Patrício, M.I., et al., *Inclusion of the Woodchuck Hepatitis Virus Posttranscriptional Regulatory Element Enhances AAV2-Driven Transduction of Mouse and Human Retina.* Mol Ther Nucleic Acids, 2017. **6**: p. 198-208.

43. Peddle, C.F. and R.E. MacLaren, *The Application of CRISPR/Cas9 for the Treatment of Retinal Diseases.* Yale J Biol Med, 2017. **90**(4): p. 533-541.

44. Kumar, H., T. Kawai, and S. Akira, *Pathogen recognition by the innate immune system.* Int Rev Immunol, 2011. **30**(1): p. 16-34.

45. Brubaker, S.W., et al., *Innate immune pattern recognition: a cell biological perspective.* Annu Rev Immunol, 2015. **33**: p. 257-90.

46. Ewald, S.E., et al., *The ectodomain of Toll-like receptor 9 is cleaved to generate a functional receptor.* Nature, 2008. **456**(7222): p. 658-62.

47. Alexopoulou, L., et al., *Recognition of double-stranded RNA and activation of NF-kappaB by Toll-like receptor 3.* Nature, 2001. **413**(6857): p. 732-8.

48. Heil, F., et al., *Species-specific recognition of single-stranded RNA via toll-like receptor 7 and 8.* Science, 2004. **303**(5663): p. 1526-9.

49. Hemmi, H., et al., *A Toll-like receptor recognizes bacterial DNA.* Nature, 2000. **408**(6813): p. 740-5.

50. Bird, A.P., *CpG-rich islands and the function of DNA methylation.* Nature, 1986. **321**(6067): p. 209-13.

51. Pandey, S., T. Kawai, and S. Akira, *Microbial sensing by Toll-like receptors and intracellular nucleic acid sensors.* Cold Spring Harb Perspect Biol, 2014. **7**(1): p. a016246.

52. Lester, S.N. and K. Li, *Toll-like receptors in antiviral innate immunity.* J Mol Biol, 2014. **426**(6): p. 1246-64.

53. Rehwinkel, J. and M.U. Gack, *RIG-I-like receptors: their regulation and roles in RNA sensing.* Nat Rev Immunol, 2020. **20**(9): p. 537-551.

54. Hornung, V., et al., *5′-Triphosphate RNA is the ligand for RIG-I.* Science, 2006. **314**(5801): p. 994-7.

55. Pichlmair, A., et al., *RIG-I-mediated antiviral responses to single-stranded RNA bearing 5′-phosphates.* Science, 2006. **314**(5801): p. 997-1001.

56. Kato, H., et al., *Differential roles of MDA5 and RIG-I helicases in the recognition of RNA viruses.* Nature, 2006. **441**(7089): p. 101-5.

57. Rodriguez, K.R., A.M. Bruns, and C.M. Horvath, *MDA5 and LGP2: accomplices and antagonists of antiviral signal transduction.* J Virol, 2014. **88**(15): p. 8194-200.

58. Sun, L., et al., *Cyclic GMP-AMP synthase is a cytosolic DNA sensor that activates the type I interferon pathway.* Science, 2013. **339**(6121): p. 786-91.

59. Wu, J., et al., *Cyclic GMP-AMP is an endogenous second messenger in innate immune signaling by cytosolic DNA.* Science, 2013. **339**(6121): p. 826-30.

60. Gray, E.E., et al., *The AIM2-like Receptors Are Dispensable for the Interferon Response to Intracellular DNA.* Immunity, 2016. **45**(2): p. 255-66.

61. Li, X., et al., *Cyclic GMP-AMP synthase is activated by double-stranded DNA-induced oligomerization.* Immunity, 2013. **39**(6): p. 1019-31.

62. Herzner, A.M., et al., *Sequence-specific activation of the DNA sensor cGAS by Y-form DNA structures as found in primary HIV-1 cDNA.* Nat Immunol, 2015. **16**(10): p. 1025-33.

63. Gao, P., et al., *Cyclic [G(2',5')pA(3',5')p] is the metazoan second messenger produced by DNA-activated cyclic GMP-AMP synthase.* Cell, 2013. **153**(5): p. 1094-107.

64. Ablasser, A., et al., *cGAS produces a 2'-5'-linked cyclic dinucleotide second messenger that activates STING.* Nature, 2013. **498**(7454): p. 380-4.

65. Ablasser, A., et al., *Cell intrinsic immunity spreads to bystander cells via the intercellular transfer of cGAMP.* Nature, 2013. **503**(7477): p. 530-4.

66. Kawai, T. and S. Akira, *The role of pattern-recognition receptors in innate immunity: update on Toll-like receptors.* Nat Immunol, 2010. **11**(5): p. 373-84.

67. Balka, K.R., et al., *TBK1 and IKKepsilon Act Redundantly to Mediate STING-Induced NF-kappaB Responses in Myeloid Cells.* Cell Rep, 2020. **31**(1): p. 107492.

68. Schneider, W.M., M.D. Chevillotte, and C.M. Rice, *Interferon-stimulated genes: a complex web of host defenses.* Annu Rev Immunol, 2014. **32**: p. 513-45.

69. Sprague, A.H. and R.A. Khalil, *Inflammatory cytokines in vascular dysfunction and vascular disease.* Biochem Pharmacol, 2009. **78**(6): p. 539-52.

70. Turner, M.D., et al., *Cytokines and chemokines: At the crossroads of cell signalling and inflammatory disease.* Biochim Biophys Acta, 2014. **1843**(11): p. 2563-2582.

71. Griffith, J.W., C.L. Sokol, and A.D. Luster, *Chemokines and chemokine receptors: positioning cells for host defense and immunity.* Annu Rev Immunol, 2014. **32**: p. 659-702.

72. Kondo, M., *Lymphoid and myeloid lineage commitment in multipotent hematopoietic progenitors.* Immunol Rev, 2010. **238**(1): p. 37-46.

73. Manz, M.G., et al., *Dendritic cell potentials of early lymphoid and myeloid progenitors.* Blood, 2001. **97**(11): p. 3333-41.

74. Esche, C., C. Stellato, and L.A. Beck, *Chemokines: key players in innate and adaptive immunity.* J Invest Dermatol, 2005. **125**(4): p. 615-28.

75. Naumenko, V., et al., *Neutrophils in viral infection.* Cell Tissue Res, 2018. **371**(3): p. 505-516.

76. Galani, I.E. and E. Andreakos, *Neutrophils in viral infections: Current concepts and caveats.* J Leukoc Biol, 2015. **98**(4): p. 557-64.

77. Hashimoto, Y., et al., *Evidence for phagocytosis of influenza virus-infected, apoptotic cells by neutrophils and macrophages in mice.* J Immunol, 2007. **178**(4): p. 2448-57.

78. Brinkmann, V., et al., *Neutrophil extracellular traps kill bacteria.* Science, 2004. **303**(5663): p. 1532-5.

79. Saitoh, T., et al., *Neutrophil extracellular traps mediate a host defense response to human immunodeficiency virus-1.* Cell Host Microbe, 2012. **12**(1): p. 109-16.

80. Jenne, C.N., et al., *Neutrophils recruited to sites of infection protect from virus challenge by releasing neutrophil extracellular traps.* Cell Host Microbe, 2013. **13**(2): p. 169-80.

81. Taylor, P.R., et al., *Macrophage receptors and immune recognition.* Annu Rev Immunol, 2005. **23**: p. 901-44.

82. Fujimoto, I., et al., *Virus clearance through apoptosis-dependent phagocytosis of influenza A virus-infected cells by macrophages.* J Virol, 2000. **74**(7): p. 3399-403.

83. Roche, P.A. and K. Furuta, *The ins and outs of MHC class II-mediated antigen processing and presentation.* Nat Rev Immunol, 2015. **15**(4): p. 203-16.

84. Jakubzick, C.V., G.J. Randolph, and P.M. Henson, *Monocyte differentiation and antigen-presenting functions.* Nat Rev Immunol, 2017. **17**(6): p. 349-362.

85. Epelman, S., K.J. Lavine, and G.J. Randolph, *Origin and functions of tissue macrophages.* Immunity, 2014. **41**(1): p. 21-35.

86. Szabo, A. and E. Rajnavolgyi, *Collaboration of Toll-like and RIG-I-like receptors in human dendritic cells: tRIGgering antiviral innate immune responses.* Am J Clin Exp Immunol, 2013. **2**(3): p. 195-207.

87. Shortman, K. and Y.J. Liu, *Mouse and human dendritic cell subtypes.* Nat Rev Immunol, 2002. **2**(3): p. 151-61.

88. Merad, M., et al., *The dendritic cell lineage: ontogeny and function of dendritic cells and their subsets in the steady state and the inflamed setting.* Annu Rev Immunol, 2013. **31**: p. 563-604.

89. Swiecki, M. and M. Colonna, *The multifaceted biology of plasmacytoid dendritic cells.* Nat Rev Immunol, 2015. **15**(8): p. 471-85.

90. Brandstadter, J.D. and Y. Yang, *Natural killer cell responses to viral infection.* J Innate Immun, 2011. **3**(3): p. 274-9.

91. Lee, S.H., T. Miyagi, and C.A. Biron, *Keeping NK cells in highly regulated antiviral warfare.* Trends Immunol, 2007. **28**(6): p. 252-9.

92. Walker, J.A., J.L. Barlow, and A.N. McKenzie, *Innate lymphoid cells--how did we miss them?* Nat Rev Immunol, 2013. **13**(2): p. 75-87.

93. Annunziato, F., C. Romagnani, and S. Romagnani, *The 3 major types of innate and adaptive cell-mediated effector immunity.* J Allergy Clin Immunol, 2015. **135**(3): p. 626-35.

94. O'Sullivan, T.E., *Dazed and Confused: NK Cells.* Front Immunol, 2019. **10**: p. 2235.

95. Weizman, O.E., et al., *ILC1 Confer Early Host Protection at Initial Sites of Viral Infection.* Cell, 2017. **171**(4): p. 795-808 e12.

96. Pennock, N.D., et al., *T cell responses: naive to memory and everything in between.* Adv Physiol Educ, 2013. **37**(4): p. 273-83.

97. Gaud, G., R. Lesourne, and P.E. Love, *Regulatory mechanisms in T cell receptor signalling.* Nat Rev Immunol, 2018. **18**(8): p. 485-497.

98. Neefjes, J., et al., *Towards a systems understanding of MHC class I and MHC class II antigen presentation.* Nat Rev Immunol, 2011. **11**(12): p. 823-36.

99. Munz, C., *Autophagy Beyond Intracellular MHC Class II Antigen Presentation.* Trends Immunol, 2016. **37**(11): p. 755-763.

100. Embgenbroich, M. and S. Burgdorf, *Current Concepts of Antigen Cross-Presentation.* Front Immunol, 2018. **9**: p. 1643.

101. Matsuda, J.L., et al., *CD1d-restricted iNKT cells, the 'Swiss-Army knife' of the immune system.* Curr Opin Immunol, 2008. **20**(3): p. 358-68.

102. Gaya, M., et al., *Initiation of Antiviral B Cell Immunity Relies on Innate Signals from Spatially Positioned NKT Cells.* Cell, 2018. **172**(3): p. 517-533 e20.

103. Tupin, E., Y. Kinjo, and M. Kronenberg, *The unique role of natural killer T cells in the response to microorganisms.* Nat Rev Microbiol, 2007. **5**(6): p. 405-17.

104. Bonecchi, R., et al., *Differential expression of chemokine receptors and chemotactic responsiveness of type 1 T helper cells (Th1s) and Th2s.* J Exp Med, 1998. **187**(1): p. 129-34.

105. Carter, L.L. and K.M. Murphy, *Lineage-specific requirement for signal transducer and activator of transcription (Stat)4 in interferon gamma production from CD4(+) versus CD8(+) T cells.* J Exp Med, 1999. **189**(8): p. 1355-60.

106. Crotty, S., *A brief history of T cell help to B cells.* Nat Rev Immunol, 2015. **15**(3): p. 185-9.

107. Doherty, D.G., et al., *Activation and Regulation of B Cell Responses by Invariant Natural Killer T Cells.* Front Immunol, 2018. **9**: p. 1360.

108. Hartmann, G. and A.M. Krieg, *Mechanism and function of a newly identified CpG DNA motif in human primary B cells.* J Immunol, 2000. **164**(2): p. 944-53.

109. Capolunghi, F., et al., *CpG drives human transitional B cells to terminal differentiation and production of natural antibodies.* J Immunol, 2008. **180**(2): p. 800-8.

110. Forthal, D.N., *Functions of Antibodies.* Microbiol Spectr, 2014. **2**(4): p. 1-17.

111. Fletcher, A.J. and L.C. James, *Coordinated Neutralization and Immune Activation by the Cytosolic Antibody Receptor TRIM21.* J Virol, 2016. **90**(10): p. 4856-4859.

112. Mallery, D.L., et al., *Antibodies mediate intracellular immunity through tripartite motif-containing 21 (TRIM21).* Proc Natl Acad Sci U S A, 2010. **107**(46): p. 19985-90.

113. Watkinson, R.E., et al., *Simultaneous neutralization and innate immune detection of a replicating virus by TRIM21.* J Virol, 2013. **87**(13): p. 7309-13.

114. Watkinson, R.E., et al., *TRIM21 Promotes cGAS and RIG-I Sensing of Viral Genomes during Infection by Antibody-Opsonized Virus.* PLoS Pathog, 2015. **11**(10): p. e1005253.

115. Booij, J.C., et al., *The dynamic nature of Bruch's membrane.* Prog Retin Eye Res, 2010. **29**(1): p. 1-18.

116. Masland, R.H., *The neuronal organization of the retina.* Neuron, 2012. **76**(2): p. 266-80.

117. Ortín-Martínez, A., et al., *Number and distribution of mouse retinal cone photoreceptors: differences between an albino (Swiss) and a pigmented (C57/BL6) strain.* PLoS One, 2014. **9**(7): p. e102392.

118. Sung, C.H. and J.Z. Chuang, *The cell biology of vision.* J Cell Biol, 2010. **190**(6): p. 953-63.

119. Baden, T., T. Euler, and P. Berens, *Understanding the retinal basis of vision across species.* Nat Rev Neurosci, 2020. **21**(1): p. 5-20.

120. Reichenbach, A. and A. Bringmann, *New functions of Muller cells.* Glia, 2013. **61**(5): p. 651-78.

121. Watanabe, T. and M.C. Raff, *Retinal astrocytes are immigrants from the optic nerve.* Nature, 1988. **332**(6167): p. 834-7.

122. Rathnasamy, G., et al., *Retinal microglia - A key player in healthy and diseased retina.* Prog Neurobiol, 2019. **173**: p. 18-40.

123. Santos, A.M., et al., *Embryonic and postnatal development of microglial cells in the mouse retina.* J Comp Neurol, 2008. **506**(2): p. 224-39.

124. Nickla, D.L. and J. Wallman, *The multifunctional choroid.* Prog Retin Eye Res, 2010. **29**(2): p. 144-68.

125. Strauss, O., *The retinal pigment epithelium in visual function.* Physiol Rev, 2005. **85**(3): p. 845-81.

126. Taylor, A.W., *Ocular Immune Privilege and Transplantation.* Front Immunol, 2016. **7**: p. 37.

127. Crane, I.J. and J. Liversidge, *Mechanisms of leukocyte migration across the blood-retina barrier.* Semin Immunopathol, 2008. **30**(2): p. 165-77.

128. Copland, D.A., et al., *Monoclonal antibody-mediated CD200 receptor signaling suppresses macrophage activation and tissue damage in experimental autoimmune uveoretinitis.* Am J Pathol, 2007. **171**(2): p. 580-8.

129. Kawanaka, N. and A.W. Taylor, *Localized retinal neuropeptide regulation of macrophage and microglial cell functionality.* J Neuroimmunol, 2011. **232**(1-2): p. 17-25.

130. Saijo, K. and C.K. Glass, *Microglial cell origin and phenotypes in health and disease.* Nat Rev Immunol, 2011. **11**(11): p. 775-87.

131. Zinkernagel, M.S., et al., *Interferon gamma-dependent migration of microglial cells in the retina after systemic cytomegalovirus infection.* Am J Pathol, 2013. **182**(3): p. 875-85.

132. Olson, J.K. and S.D. Miller, *Microglia initiate central nervous system innate and adaptive immune responses through multiple TLRs.* J Immunol, 2004. **173**(6): p. 3916-24.

133. Reinert, L.S., et al., *Sensing of HSV-1 by the cGAS-STING pathway in microglia orchestrates antiviral defence in the CNS.* Nat Commun, 2016. **7**: p. 13348.

134. Kohno, H., et al., *Photoreceptor proteins initiate microglial activation via Toll-like receptor 4 in retinal degeneration mediated by all-trans-retinal.* J Biol Chem, 2013. **288**(21): p. 15326-41.

135. Kochan, T., et al., *Toll-like receptor 2 ligand pretreatment attenuates retinal microglial inflammatory response but enhances phagocytic activity toward Staphylococcus aureus.* Infect Immun, 2012. **80**(6): p. 2076-88.

136. Rojas, B., et al., *Microglia in mouse retina contralateral to experimental glaucoma exhibit multiple signs of activation in all retinal layers.* J Neuroinflammation, 2014. **11**: p. 133.

137. Lapenna, A., M. De Palma, and C.E. Lewis, *Perivascular macrophages in health and disease.* Nat Rev Immunol, 2018. **18**(11): p. 689-702.

138. Dick, A.D., et al., *Flow cytometric identification of a minority population of MHC class II positive cells in the normal rat retina distinct from CD45lowCD11b/c+CD4low parenchymal microglia.* Br J Ophthalmol, 1995. **79**(9): p. 834-40.

139. Cuff, C.A., J.W. Berman, and C.F. Brosnan, *The ordered array of perivascular macrophages is disrupted by IL-1-induced inflammation in the rabbit retina.* Glia, 1996. **17**(4): p. 307-16.

140. Mendes-Jorge, L., et al., *Scavenger function of resident autofluorescent perivascular macrophages and their contribution to the maintenance of the blood-retinal barrier.* Invest Ophthalmol Vis Sci, 2009. **50**(12): p. 5997-6005.

141. de Hoz, R., et al., *Retinal Macroglial Responses in Health and Disease.* Biomed Res Int, 2016. **2016**: p. 2954721.

142. Wyble, C.W., et al., *TNF-alpha and IL-1 upregulate membrane-bound and soluble E-selectin through a common pathway.* J Surg Res, 1997. **73**(2): p. 107-12.

143. Ley, K. and G.S. Kansas, *Selectins in T-cell recruitment to non-lymphoid tissues and sites of inflammation.* Nat Rev Immunol, 2004. **4**(5): p. 325-35.

144. Chen, W., et al., *Anti-inflammatory effect of docosahexaenoic acid on cytokine-induced adhesion molecule expression in human retinal vascular endothelial cells.* Invest Ophthalmol Vis Sci, 2005. **46**(11): p. 4342-7.

145. Bharadwaj, A.S., et al., *Intercellular adhesion molecule 1 mediates migration of Th1 and Th17 cells across human retinal vascular endothelium.* Invest Ophthalmol Vis Sci, 2013. **54**(10): p. 6917-25.

146. Alon, R. and S. Feigelson, *From rolling to arrest on blood vessels: leukocyte tap dancing on endothelial integrin ligands and chemokines at sub-second contacts.* Semin Immunol, 2002. **14**(2): p. 93-104.

147. Lammermann, T. and W. Kastenmuller, *Concepts of GPCR-controlled navigation in the immune system.* Immunol Rev, 2019. **289**(1): p. 205-231.

148. Aveleira, C.A., et al., *TNF-α signals through PKCζ/NF-κB to alter the tight junction complex and increase retinal endothelial cell permeability.* Diabetes, 2010. **59**(11): p. 2872-82.

149. Mesquida, M., et al., *Modelling Macular Edema: The Effect of IL-6 and IL-6R Blockade on Human Blood-Retinal Barrier Integrity In Vitro.* Transl Vis Sci Technol, 2019. **8**(5): p. 32.

150. Russell, S., et al., *Efficacy and safety of voretigene neparvovec (AAV2-hRPE65v2) in patients with RPE65-mediated inherited retinal dystrophy: a randomised, controlled, open-label, phase 3 trial.* Lancet, 2017. **390**(10097): p. 849-860.

151. Xue, K., et al., *Beneficial effects on vision in patients undergoing retinal gene therapy for choroideremia.* Nat Med, 2018. **24**(10): p. 1507-1512.

152. Cehajic-Kapetanovic, J., et al., *Initial results from a first-in-human gene therapy trial on X-linked retinitis pigmentosa caused by mutations in RPGR.* Nat Med, 2020. **26**(3): p. 354-359.

153. Yu-Wai-Man, P., et al., *Bilateral visual improvement with unilateral gene therapy injection for Leber hereditary optic neuropathy.* Sci Transl Med, 2020. **12**(573).

154. Liang, F.Q., et al., *Intraocular delivery of recombinant virus.* Methods Mol Med, 2001. **47**: p. 125-39.

155. Xue, K., et al., *Technique of retinal gene therapy: delivery of viral vector into the subretinal space.* Eye (Lond), 2017. **31**(9): p. 1308-1316.

156. Shirley, J.L., et al., *Immune Responses to Viral Gene Therapy Vectors.* Mol Ther, 2020. **28**(3): p. 709-722.

157. Hosel, M., et al., *Toll-like receptor 2-mediated innate immune response in human nonparenchymal liver cells toward adeno-associated viral vectors.* Hepatology, 2012. **55**(1): p. 287-297.

158. Vandenberghe, L.H., et al., *Heparin binding directs activation of T cells against adeno-associated virus serotype 2 capsid.* Nat Med, 2006. **12**(8): p. 967-71.

159. Mays, L.E., et al., *Adeno-associated virus capsid structure drives CD4-dependent CD8+ T cell response to vector encoded proteins.* J Immunol, 2009. **182**(10): p. 6051-60.

160. Manno, C.S., et al., *Successful transduction of liver in hemophilia by AAV-Factor IX and limitations imposed by the host immune response.* Nat Med, 2006. **12**(3): p. 342-7.

161. Mingozzi, F., et al., *CD8(+) T-cell responses to adeno-associated virus capsid in humans.* Nat Med, 2007. **13**(4): p. 419-22.

162. Hui, D.J., et al., *AAV capsid CD8+ T-cell epitopes are highly conserved across AAV serotypes.* Mol Ther Methods Clin Dev, 2015. **2**: p. 15029.

163. Gao, G., et al., *Adeno-associated virus-mediated gene transfer to nonhuman primate liver can elicit destructive transgene-specific T cell responses.* Hum Gene Ther, 2009. **20**(9): p. 930-42.

164. Nathwani, A.C., et al., *Long-term safety and efficacy following systemic administration of a self-complementary AAV vector encoding human FIX pseudotyped with serotype 5 and 8 capsid proteins.* Mol Ther, 2011. **19**(5): p. 876-85.

165. Li, C., et al., *Adeno-associated virus capsid antigen presentation is dependent on endosomal escape.* J Clin Invest, 2013. **123**(3): p. 1390-401.

166. Boutin, S., et al., *Prevalence of serum IgG and neutralizing factors against adeno-associated virus (AAV) types 1, 2, 5, 6, 8, and 9 in the healthy population: implications for gene therapy using AAV vectors.* Hum Gene Ther, 2010. **21**(6): p. 704-12.

167. Jiang, H., et al., *Effects of transient immunosuppression on adenoassociated, virus-mediated, liver-directed gene transfer in rhesus macaques and implications for human gene therapy.* Blood, 2006. **108**(10): p. 3321-8.

168. Kotterman, M.A., et al., *Antibody neutralization poses a barrier to intravitreal adeno-associated viral vector gene delivery to non-human primates.* Gene Ther, 2015. **22**(2): p. 116-26.

169. Zhu, J., X. Huang, and Y. Yang, *The TLR9-MyD88 pathway is critical for adaptive immune responses to adeno-associated virus gene therapy vectors in mice.* J Clin Invest, 2009. **119**(8): p. 2388-98.

170. Faust, S.M., et al., *CpG-depleted adeno-associated virus vectors evade immune detection.* J Clin Invest, 2013. **123**(7): p. 2994-3001.

171. Martino, A.T., et al., *The genome of self-complementary adeno-associated viral vectors increases Toll-like receptor 9-dependent innate immune responses in the liver.* Blood, 2011. **117**(24): p. 6459-68.

172. Shao, W., et al., *Double-stranded RNA innate immune response activation from long-term adeno-associated virus vector transduction.* JCI Insight, 2018. **3**(12).

173. Boisgerault, F. and F. Mingozzi, *The Skeletal Muscle Environment and Its Role in Immunity and Tolerance to AAV Vector-Mediated Gene Transfer.* Curr Gene Ther, 2015. **15**(4): p. 381-94.

174. Mendell, J.R., et al., *Dystrophin immunity in Duchenne's muscular dystrophy.* N Engl J Med, 2010. **363**(15): p. 1429-37.

175. Chandler, L.C., et al., *Enhancement of Adeno-Associated Virus-Mediated Gene Therapy Using Hydroxychloroquine in Murine and Human Tissues.* Mol Ther Methods Clin Dev, 2019. **14**: p. 77-89.

176. Reichel, F.F., et al., *AAV8 Can Induce Innate and Adaptive Immune Response in the Primate Eye.* Mol Ther, 2017. **25**(12): p. 2648-2660.

177. Xiong, W., et al., *AAV cis-regulatory sequences are correlated with ocular toxicity.* Proc Natl Acad Sci U S A, 2019. **116**(12): p. 5785-5794.

178. Liu, Y.F., et al., *Longitudinal evaluation of immediate inflammatory responses after intravitreal AAV2 injection in rats by optical coherence tomography.* Exp Eye Res, 2020. **193**: p. 107955.

179. Boyd, R.F., et al., *Reduced retinal transduction and enhanced transgene-directed immunogenicity with intravitreal delivery of rAAV following posterior vitrectomy in dogs.* Gene Ther, 2016. **23**(6): p. 548-56.

180. Vandenberghe, L.H., et al., *Dosage thresholds for AAV2 and AAV8 photoreceptor gene therapy in monkey.* Sci Transl Med, 2011. **3**(88): p. 88ra54.

181. Ye, G.J., et al., *Safety and Biodistribution Evaluation in Cynomolgus Macaques of rAAV2tYF-PR1.7-hCNGB3, a Recombinant AAV Vector for Treatment of Achromatopsia.* Hum Gene Ther Clin Dev, 2016. **27**(1): p. 37-48.

182. Ramachandran, P.S., et al., *Evaluation of Dose and Safety of AAV7m8 and AAV8BP2 in the Non-Human Primate Retina.* Hum Gene Ther, 2017. **28**(2): p. 154-167.

183. Bainbridge, J.W., et al., *Long-term effect of gene therapy on Leber's congenital amaurosis.* N Engl J Med, 2015. **372**(20): p. 1887-97.

184. Bucher, K., et al., *Immune responses to retinal gene therapy using adeno-associated viral vectors - Implications for treatment success and safety.* Prog Retin Eye Res, 2020: p. 100915.

185. Khabou, H., et al., *Dosage Thresholds and Influence of Transgene Cassette in Adeno-Associated Virus-Related Toxicity.* Hum Gene Ther, 2018. **29**(11): p. 1235-1241.

186. Seitz, I.P., et al., *Superior Retinal Gene Transfer and Biodistribution Profile of Subretinal Versus Intravitreal Delivery of AAV8 in Nonhuman Primates.* Invest Ophthalmol Vis Sci, 2017. **58**(13): p. 5792-5801.

187. Li, Q., et al., *Intraocular route of AAV2 vector administration defines humoral immune response and therapeutic potential.* Mol Vis, 2008. **14**: p. 1760-9.

188. Reichel, F.F., et al., *Humoral Immune Response After Intravitreal But Not After Subretinal AAV8 in Primates and Patients.* Invest Ophthalmol Vis Sci, 2018. **59**(5): p. 1910-1915.

189. Bennett, J., et al., *Safety and durability of effect of contralateral-eye administration of AAV2 gene therapy in patients with childhood-onset blindness caused by RPE65 mutations: a follow-on phase 1 trial.* Lancet, 2016. **388**(10045): p. 661-72.

190. Edwards, T.L., et al., *Visual Acuity after Retinal Gene Therapy for Choroideremia.* N Engl J Med, 2016. **374**(20): p. 1996-8.

191. Kumar, M.V., et al., *Innate immunity in the retina: Toll-like receptor (TLR) signaling in human retinal pigment epithelial cells.* J Neuroimmunol, 2004. **153**(1-2): p. 7-15.

192. Kerur, N., et al., *cGAS drives noncanonical-inflammasome activation in age-related macular degeneration.* Nat Med, 2018. **24**(1): p. 50-61.

193. Medzhitov, R., *Recognition of microorganisms and activation of the immune response.* Nature, 2007. **449**(7164): p. 819-26.

194. Schoggins, J.W., et al., *Pan-viral specificity of IFN-induced genes reveals new roles for cGAS in innate immunity.* Nature, 2014. **505**(7485): p. 691-5.

195. Charbel Issa, P., et al., *Optimization of in vivo confocal autofluorescence imaging of the ocular fundus in mice and its application to models of human retinal degeneration.* Invest Ophthalmol Vis Sci, 2012. **53**(2): p. 1066-75.

196. Staurenghi, G., et al., *Proposed lexicon for anatomic landmarks in normal posterior segment spectral-domain optical coherence tomography: the IN*OCT consensus.* Ophthalmology, 2014. **121**(8): p. 1572-8.

197. Li, L., N. Eter, and P. Heiduschka, *The microglia in healthy and diseased retina.* Exp Eye Res, 2015. **136**: p. 116-30.

198. Ford, A.L., et al., *Normal adult ramified microglia separated from other central nervous system macrophages by flow cytometric sorting. Phenotypic differences defined and direct ex vivo antigen presentation to myelin basic protein-reactive CD4+ T cells compared.* J Immunol, 1995. **154**(9): p. 4309-21.

199. Gregerson, D.S. and J. Yang, *CD45-positive cells of the retina and their responsiveness to in vivo and in vitro treatment with IFN-gamma or anti-CD40.* Invest Ophthalmol Vis Sci, 2003. **44**(7): p. 3083-93.

200. Li, Q., et al., *Expression of Tmem119/Sall1 and Ccr2/CD69 in FACS-Sorted Microglia- and Monocyte/Macrophage-Enriched Cell Populations After Intracerebral Hemorrhage.* Front Cell Neurosci, 2018. **12**: p. 520.

201. O'Koren, E.G., R. Mathew, and D.R. Saban, *Fate mapping reveals that microglia and recruited monocyte-derived macrophages are definitively distinguishable by phenotype in the retina.* Sci Rep, 2016. **6**: p. 20636.

202. Zhong, L., et al., *Next generation of adeno-associated virus 2 vectors: point mutations in tyrosines lead to high-efficiency transduction at lower doses.* Proc Natl Acad Sci U S A, 2008. **105**(22): p. 7827-32.

203. Petrs-Silva, H., et al., *High-efficiency transduction of the mouse retina by tyrosine-mutant AAV serotype vectors.* Mol Ther, 2009. **17**(3): p. 463-71.

204. Patricio, M.I., et al., *Inclusion of PF68 Surfactant Improves Stability of rAAV Titer when Passed through a Surgical Device Used in Retinal Gene Therapy.* Mol Ther Methods Clin Dev, 2020. **17**: p. 99-106.

205. Flotte, T.R., et al., *Expression of the cystic fibrosis transmembrane conductance regulator from a novel adeno-associated virus promoter.* J Biol Chem, 1993. **268**(5): p. 3781-90.

206. Haberman, R.P., T.J. McCown, and R.J. Samulski, *Novel transcriptional regulatory signals in the adeno-associated virus terminal repeat A/D junction element.* J Virol, 2000. **74**(18): p. 8732-9.

207. Jurga, A.M., M. Paleczna, and K.Z. Kuter, *Overview of General and Discriminating Markers of Differential Microglia Phenotypes.* Front Cell Neurosci, 2020. **14**: p. 198.

208. Liyanage, S.E., et al., *Flow cytometric analysis of inflammatory and resident myeloid populations in mouse ocular inflammatory models.* Exp Eye Res, 2016. **151**: p. 160-70.

209. Krause, T.A., et al., *VEGF-production by CCR2-dependent macrophages contributes to laser-induced choroidal neovascularization.* PLoS One, 2014. **9**(4): p. e94313.

210. Andres, D.A., et al., *cDNA cloning of component A of Rab geranylgeranyl transferase and demonstration of its role as a Rab escort protein.* Cell, 1993. **73**(6): p. 1091-9.

211. Patricio, M.I., et al., *Choroideremia: molecular mechanisms and development of AAV gene therapy.* Expert Opin Biol Ther, 2018. **18**(7): p. 807-820.

212. McMenamin, P.G., D.R. Saban, and S.J. Dando, *Immune cells in the retina and choroid: Two different tissue environments that require different defenses and surveillance.* Prog Retin Eye Res, 2019. **70**: p. 85-98.

213. Forrester, J.V., et al., *Dendritic cell physiology and function in the eye.* Immunol Rev, 2010. **234**(1): p. 282-304.

214. Kim, S., et al., *In vivo developmental stages in murine natural killer cell maturation.* Nat Immunol, 2002. **3**(6): p. 523-8.

215. McFarland, H.I., et al., *CD11b (Mac-1): a marker for CD8+ cytotoxic T cell activation and memory in virus infection.* J Immunol, 1992. **149**(4): p. 1326-33.

216. Christensen, J.E., et al., *CD11b expression as a marker to distinguish between recently activated effector CD8(+) T cells and memory cells.* Int Immunol, 2001. **13**(4): p. 593-600.

217. Shipkova, M. and E. Wieland, *Surface markers of lymphocyte activation and markers of cell proliferation.* Clin Chim Acta, 2012. **413**(17-18): p. 1338-49.

218. Tummala, G., et al., *Characterization of Gene Therapy Associated Uveitis Following Intravitreal Adeno-Associated Virus Injection in Mice.* Invest Ophthalmol Vis Sci, 2021. **62**(2): p. 41.

219. Romero-Suarez, S., et al., *The Central Nervous System Contains ILC1s That Differ From NK Cells in the Response to Inflammation.* Front Immunol, 2019. **10**: p. 2337.

220. Limb, G.A., et al., *Expression of hematopoietic cell markers by retinal pigment epithelial cells.* Curr Eye Res, 1997. **16**(10): p. 985-91.

221. Lane, P.J., F.M. Gaspal, and M.Y. Kim, *Two sides of a cellular coin: CD4(+)CD3- cells regulate memory responses and lymph-node organization.* Nat Rev Immunol, 2005. **5**(8): p. 655-60.

222. Bekiaris, V., et al., *Human CD4+CD3- innate-like T cells provide a source of TNF and lymphotoxin-alphabeta and are elevated in rheumatoid arthritis.* J Immunol, 2013. **191**(9): p. 4611-8.

223. Rosario, A.M., et al., *Microglia-specific targeting by novel capsid-modified AAV6 vectors.* Mol Ther Methods Clin Dev, 2016. **3**: p. 16026.

224. Wang, S.K., et al., *In Situ Detection of Adeno-associated Viral Vector Genomes with SABER-FISH.* Mol Ther Methods Clin Dev, 2020. **19**: p. 376-386.

225. Stieger, K., et al., *Detection of intact rAAV particles up to 6 years after successful gene transfer in the retina of dogs and primates.* Mol Ther, 2009. **17**(3): p. 516-23.

226. Cossarizza, A., et al., *Guidelines for the use of flow cytometry and cell sorting in immunological studies (second edition).* Eur J Immunol, 2019. **49**(10): p. 1457-1973.

227. Bettadapur, A., H.W. Miller, and K.S. Ralston, *Biting Off What Can Be Chewed: Trogocytosis in Health, Infection, and Disease.* Infect Immun, 2020. **88**(7).

228. Ganini, D., et al., *Fluorescent proteins such as eGFP lead to catalytic oxidative stress in cells.* Redox Biol, 2017. **12**: p. 462-468.

229. Jing, G., J.J. Wang, and S.X. Zhang, *ER stress and apoptosis: a new mechanism for retinal cell death.* Exp Diabetes Res, 2012. **2012**: p. 589589.

230. Balakrishnan, B., et al., *Activation of the cellular unfolded protein response by recombinant adeno-associated virus vectors.* PLoS One, 2013. **8**(1): p. e53845.

231. Zhou, T., et al., *Microglia Polarization with M1/M2 Phenotype Changes in rd1 Mouse Model of Retinal Degeneration.* Front Neuroanat, 2017. **11**: p. 77.

232. Greter, M., I. Lelios, and A.L. Croxford, *Microglia Versus Myeloid Cell Nomenclature during Brain Inflammation.* Front Immunol, 2015. **6**: p. 249.

233. Plemel, J.R., et al., *Microglia response following acute demyelination is heterogeneous and limits infiltrating macrophage dispersion.* Sci Adv, 2020. **6**(3): p. eaay6324.

234. Bennett, M.L., et al., *New tools for studying microglia in the mouse and human CNS.* Proc Natl Acad Sci U S A, 2016. **113**(12): p. E1738-46.

235. Hulspas, R., et al., *Flow cytometry and the stability of phycoerythrin-tandem dye conjugates.* Cytometry A, 2009. **75**(11): p. 966-72.

236. *Cytek Full Spectrum Viewer*. 2021 [cited 2021 15/02/2021]; Available from: https://spectrum.cytekbio.com/.

237. Kristensen, M.W., et al., *Behold Cytometrists: One Block is not Enough! Cyanine-Tandems Bind Non-Specifically to Human Monocytes.* Cytometry A, 2020.

238. Elia, J., et al. *True-Stain Monocyte Blocker, an effective blocking buffer to eliminate non-speciofic cyanine-likr dye-mediated monocyte binding*. [cited 2020 16/12/2020]; Available from: https://www.biolegend.com/Files/Images/BioLegend/poster_library/04-0084-00_AAI.pdf.

239. Maecker, H.T. and J. Trotter, *Flow cytometry controls, instrument setup, and the determination of positivity.* Cytometry A, 2006. **69**(9): p. 1037-42.

240. Hulspas, R., et al., *Considerations for the control of background fluorescence in clinical flow cytometry.* Cytometry B Clin Cytom, 2009. **76**(6): p. 355-64.

241. Rabinowitz, J., Y.K. Chan, and R.J. Samulski, *Adeno-associated Virus (AAV) versus Immune Response.* Viruses, 2019. **11**(2).

242. Perng, Y.C. and D.J. Lenschow, *ISG15 in antiviral immunity and beyond.* Nat Rev Microbiol, 2018. **16**(7): p. 423-439.

243. Nguyen, K.B., et al., *Coordinated and distinct roles for IFN-alpha beta, IL-12, and IL-15 regulation of NK cell responses to viral infection.* J Immunol, 2002. **169**(8): p. 4279-87.

244. Zhang, X., et al., *Potent and selective stimulation of memory-phenotype CD8+ T cells in vivo by IL-15.* Immunity, 1998. **8**(5): p. 591-9.

245. Schrezenmeier, E. and T. Dorner, *Mechanisms of action of hydroxychloroquine and chloroquine: implications for rheumatology.* Nat Rev Rheumatol, 2020. **16**(3): p. 155-166.

246. Means, T.K., et al., *Human lupus autoantibody-DNA complexes activate DCs through cooperation of CD32 and TLR9.* J Clin Invest, 2005. **115**(2): p. 407-17.

247. Barrat, F.J., et al., *Nucleic acids of mammalian origin can act as endogenous ligands for Toll-like receptors and may promote systemic lupus erythematosus.* J Exp Med, 2005. **202**(8): p. 1131-9.

248. Kato, Y., et al., *Apoptosis-derived membrane vesicles drive the cGAS-STING pathway and enhance type I IFN production in systemic lupus erythematosus.* Ann Rheum Dis, 2018. **77**(10): p. 1507-1515.

249. An, J., et al., *Expression of Cyclic GMP-AMP Synthase in Patients With Systemic Lupus Erythematosus.* Arthritis Rheumatol, 2017. **69**(4): p. 800-807.

250. An, J., et al., *Cutting edge: Antimalarial drugs inhibit IFN-beta production through blockade of cyclic GMP-AMP synthase-DNA interaction.* J Immunol, 2015. **194**(9): p. 4089-93.

251. Kuznik, A., et al., *Mechanism of endosomal TLR inhibition by antimalarial drugs and imidazoquinolines.* J Immunol, 2011. **186**(8): p. 4794-804.

252. An, J., et al., *Antimalarial Drugs as Immune Modulators: New Mechanisms for Old Drugs.* Annu Rev Med, 2017. **68**: p. 317-330.

253. Macfarlane, D.E. and L. Manzel, *Antagonism of immunostimulatory CpG-oligodeoxynucleotides by quinacrine, chloroquine, and structurally related compounds.* J Immunol, 1998. **160**(3): p. 1122-31.

254. Hacker, H., et al., *CpG-DNA-specific activation of antigen-presenting cells requires stress kinase activity and is preceded by non-specific endocytosis and endosomal maturation.* EMBO J, 1998. **17**(21): p. 6230-40.

255. Rutz, M., et al., *Toll-like receptor 9 binds single-stranded CpG-DNA in a sequence- and pH-dependent manner.* Eur J Immunol, 2004. **34**(9): p. 2541-50.

256. Lamphier, M., et al., *Novel small molecule inhibitors of TLR7 and TLR9: mechanism of action and efficacy in vivo.* Mol Pharmacol, 2014. **85**(3): p. 429-40.

257. de Bouteiller, O., et al., *Recognition of double-stranded RNA by human toll-like receptor 3 and downstream receptor signaling requires multimerization and an acidic pH.* J Biol Chem, 2005. **280**(46): p. 38133-45.

258. Vollmer, J., et al., *Immune stimulation mediated by autoantigen binding sites within small nuclear RNAs involves Toll-like receptors 7 and 8.* J Exp Med, 2005. **202**(11): p. 1575-85.

259. Lund, J., et al., *Toll-like receptor 9-mediated recognition of Herpes simplex virus-2 by plasmacytoid dendritic cells.* J Exp Med, 2003. **198**(3): p. 513-20.

260. Fiola, S., et al., *TLR9 contributes to the recognition of EBV by primary monocytes and plasmacytoid dendritic cells.* J Immunol, 2010. **185**(6): p. 3620-31.

261. Quan, T.E., et al., *Epstein-Barr virus promotes interferon-alpha production by plasmacytoid dendritic cells.* Arthritis Rheum, 2010. **62**(6): p. 1693-701.

262. Lee, J., et al., *TNF-alpha Induced by Hepatitis C Virus via TLR7 and TLR8 in Hepatocytes Supports Interferon Signaling via an Autocrine Mechanism.* PLoS Pathog, 2015. **11**(5): p. e1004937.

263. Zhang, Y., et al., *HCV RNA Activates APCs via TLR7/TLR8 While Virus Selectively Stimulates Macrophages Without Inducing Antiviral Responses.* Sci Rep, 2016. **6**: p. 29447.

264. Diebold, S.S., et al., *Innate antiviral responses by means of TLR7-mediated recognition of single-stranded RNA.* Science, 2004. **303**(5663): p. 1529-31.

265. Lund, J.M., et al., *Recognition of single-stranded RNA viruses by Toll-like receptor 7.* Proc Natl Acad Sci U S A, 2004. **101**(15): p. 5598-603.

266. Rhen, T. and J.A. Cidlowski, *Antiinflammatory action of glucocorticoids--new mechanisms for old drugs.* N Engl J Med, 2005. **353**(16): p. 1711-23.

267. Ogawa, S., et al., *Molecular determinants of crosstalk between nuclear receptors and toll-like receptors.* Cell, 2005. **122**(5): p. 707-21.

268. Glass, C.K. and K. Saijo, *Nuclear receptor transrepression pathways that regulate inflammation in macrophages and T cells.* Nat Rev Immunol, 2010. **10**(5): p. 365-76.

269. Hudson, W.H., et al., *Cryptic glucocorticoid receptor-binding sites pervade genomic NF-kappaB response elements.* Nat Commun, 2018. **9**(1): p. 1337.

270. Rynes, R.I., *Ophthalmologic safety of long-term hydroxychloroquine sulfate treatment.* Am J Med, 1983. **75**(1A): p. 35-9.

271. Tsai, Y.C., et al., *Linear correlation between average fluorescence intensity of green fluorescent protein and the multiplicity of infection of recombinant adenovirus.* J Biomed Sci, 2015. **22**: p. 31.

272. Gill, J.E., et al., *7-Amino-actinomycin D as a cytochemical probe. I. Spectral properties.* J Histochem Cytochem, 1975. **23**(11): p. 793-9.

273. Cheng, R., et al., *Influence of Fixation and Permeabilization on the Mass Density of Single Cells: A Surface Plasmon Resonance Imaging Study.* Front Chem, 2019. **7**: p. 588.

274. Tamiya, S., L. Liu, and H.J. Kaplan, *Epithelial-mesenchymal transition and proliferation of retinal pigment epithelial cells initiated upon loss of cell-cell contact.* Invest Ophthalmol Vis Sci, 2010. **51**(5): p. 2755-63.

275. MacLaren, R.E., et al., *Retinal gene therapy in patients with choroideremia: initial findings from a phase 1/2 clinical trial.* Lancet, 2014. **383**(9923): p. 1129-37.

276. Bainbridge, J.W., et al., *Effect of gene therapy on visual function in Leber's congenital amaurosis.* N Engl J Med, 2008. **358**(21): p. 2231-9.

277. Pierce, E.A. and J. Bennett, *The Status of RPE65 Gene Therapy Trials: Safety and Efficacy.* Cold Spring Harb Perspect Med, 2015. **5**(9): p. a017285.

278. Cukras, C., et al., *Retinal AAV8-RS1 Gene Therapy for X-Linked Retinoschisis: Initial Findings from a Phase I/IIa Trial by Intravitreal Delivery.* Mol Ther, 2018. **26**(9): p. 2282-2294.

279. Cideciyan, A.V., et al., *Human retinal gene therapy for Leber congenital amaurosis shows advancing retinal degeneration despite enduring visual improvement.* Proc Natl Acad Sci U S A, 2013. **110**(6): p. E517-25.

280. Jacobson, S.G., et al., *Improvement and decline in vision with gene therapy in childhood blindness.* N Engl J Med, 2015. **372**(20): p. 1920-6.

281. Mingozzi, F. and K.A. High, *Immune responses to AAV in clinical trials.* Curr Gene Ther, 2011. **11**(4): p. 321-30.

282. Shirley, J.L. and R.W. Herzog, *AAV Immunogenicity: New Answers Create New Questions.* Mol Ther, 2018. **26**(11): p. 2538-2539.

283. Tanna, P., et al., *Stargardt disease: clinical features, molecular genetics, animal models and therapeutic options.* Br J Ophthalmol, 2017. **101**(1): p. 25-30.

284. McClements, M.E., et al., *An AAV Dual Vector Strategy Ameliorates the Stargardt Phenotype in Adult Abca4(-/-) Mice.* Hum Gene Ther, 2019. **30**(5): p. 590-600.

285. Melles, R.B. and M.F. Marmor, *The risk of toxic retinopathy in patients on long-term hydroxychloroquine therapy.* JAMA Ophthalmol, 2014. **132**(12): p. 1453-60.

286. Wainer, I.W., et al., *Distribution of the enantiomers of hydroxychloroquine and its metabolites in ocular tissues of the rabbit after oral administration of racemic-hydroxychloroquine.* Chirality, 1994. **6**(4): p. 347-54.

287. Schroeder, R.L. and J.P. Gerber, *Chloroquine and hydroxychloroquine binding to melanin: Some possible consequences for pathologies.* Toxicol Rep, 2014. **1**: p. 963-968.

288. Yusuf, I.H., et al., *Hydroxychloroquine retinopathy.* Eye (Lond), 2017. **31**(6): p. 828-845.

289. Shimomatsu, T., et al., *The effect of hydroxychloroquine on lupus erythematosus-like skin lesions in MRL/lpr mice.* Mod Rheumatol, 2016. **26**(5): p. 744-8.

290. Zhong, X., et al., *Generation of three-dimensional retinal tissue with functional photoreceptors from human iPSCs.* Nat Commun, 2014. **5**: p. 4047.

291. Gao, M.L., et al., *Patient-Specific Retinal Organoids Recapitulate Disease Features of Late-Onset Retinitis Pigmentosa.* Front Cell Dev Biol, 2020. **8**: p. 128.

292. Browning, D.J., *Pharmacology of Chloroquine and Hydroxychloroquine.* Hydroxychloroquine and Chloroquine Retinopathy, 2014: p. 35-63.

293. Tett, S.E., et al., *Bioavailability of hydroxychloroquine tablets in healthy volunteers.* Br J Clin Pharmacol, 1989. **27**(6): p. 771-9.

294. Jallouli, M., et al., *Determinants of hydroxychloroquine blood concentration variations in systemic lupus erythematosus.* Arthritis Rheumatol, 2015. **67**(8): p. 2176-84.

295. Luhmann, U.F., et al., *The drusenlike phenotype in aging Ccl2-knockout mice is caused by an accelerated accumulation of swollen autofluorescent subretinal macrophages.* Invest Ophthalmol Vis Sci, 2009. **50**(12): p. 5934-43.

296. Ohkuma, S. and B. Poole, *Fluorescence probe measurement of the intralysosomal pH in living cells and the perturbation of pH by various agents.* Proc Natl Acad Sci U S A, 1978. **75**(7): p. 3327-31.

297. Manzel, L., et al., *Antagonism of immunostimulatory CpG-oligodeoxynucleotides by 4-aminoquinolines and other weak bases: mechanistic studies.* J Pharmacol Exp Ther, 1999. **291**(3): p. 1337-47.

298. Helenius, A., M. Marsh, and J. White, *Inhibition of Semliki forest virus penetration by lysosomotropic weak bases.* J Gen Virol, 1982. **58 Pt 1**: p. 47-61.

299. Harley, C.A., A. Dasgupta, and D.W. Wilson, *Characterization of herpes simplex virus-containing organelles by subcellular fractionation: role for organelle acidification in assembly of infectious particles.* J Virol, 2001. **75**(3): p. 1236-51.

300. Bishop, N.E., *Examination of potential inhibitors of hepatitis A virus uncoating.* Intervirology, 1998. **41**(6): p. 261-71.

301. Tsai, W.P., et al., *Inhibition of human immunodeficiency virus infectivity by chloroquine.* AIDS Res Hum Retroviruses, 1990. **6**(4): p. 481-9.

302. Sperber, K., et al., *Inhibition of human immunodeficiency virus type 1 replication by hydroxychloroquine in T cells and monocytes.* AIDS Res Hum Retroviruses, 1993. **9**(1): p. 91-8.

303. Chiang, G., et al., *Inhibition of HIV-1 replication by hydroxychloroquine: mechanism of action and comparison with zidovudine.* Clin Ther, 1996. **18**(6): p. 1080-92.

304. Bose, D., et al., *An RNA-Based Fluorescent Biosensor for High-Throughput Analysis of the cGAS-cGAMP-STING Pathway.* Cell Chem Biol, 2016. **23**(12): p. 1539-1549.

305. Fox, R.I., *Mechanism of action of hydroxychloroquine as an antirheumatic drug.* Semin Arthritis Rheum, 1993. **23**(2 Suppl 1): p. 82-91.

306. Seisenberger, G., et al., *Real-time single-molecule imaging of the infection pathway of an adeno-associated virus.* Science, 2001. **294**(5548): p. 1929-32.

307. Lux, K., et al., *Green fluorescent protein-tagged adeno-associated virus particles allow the study of cytosolic and nuclear trafficking.* J Virol, 2005. **79**(18): p. 11776-87.

308. Chandler, L.C., et al., *Immunomodulatory Effects of Hydroxychloroquine and Chloroquine in Viral Infections and Their Potential Application in Retinal Gene Therapy.* Int J Mol Sci, 2020. **21**(14).

309. Rapti, K., et al., *Neutralizing antibodies against AAV serotypes 1, 2, 6, and 9 in sera of commonly used animal models.* Mol Ther, 2012. **20**(1): p. 73-83.

310. Wang, L., et al., *The pleiotropic effects of natural AAV infections on liver-directed gene transfer in macaques.* Mol Ther, 2010. **18**(1): p. 126-34.

311. Amado, D., et al., *Safety and efficacy of subretinal readministration of a viral vector in large animals to treat congenital blindness.* Sci Transl Med, 2010. **2**(21): p. 21ra16.

312. Maguire, A.M., et al., *Safety and efficacy of gene transfer for Leber's congenital amaurosis.* N Engl J Med, 2008. **358**(21): p. 2240-8.

313. Mestas, J. and C.C. Hughes, *Of mice and not men: differences between mouse and human immunology.* J Immunol, 2004. **172**(5): p. 2731-8.

314. Cunha-Vaz, J., R. Bernardes, and C. Lobo, *Blood-retinal barrier.* Eur J Ophthalmol, 2011. **21 Suppl 6**: p. S3-9.

315. Crane, I.J., et al., *Control of chemokine production at the blood-retina barrier.* Immunology, 2000. **101**(3): p. 426-433.

316. Da Cunha, A.P., et al., *The Hierarchy of Proinflammatory Cytokines in Ocular Inflammation.* Curr Eye Res, 2018. **43**(4): p. 553-565.

317. Linker, R.A., B.C. Kieseier, and R. Gold, *Identification and development of new therapeutics for multiple sclerosis.* Trends Pharmacol Sci, 2008. **29**(11): p. 558-65.

318. Yiu, G., et al., *Suprachoroidal and Subretinal Injections of AAV Using Transscleral Microneedles for Retinal Gene Delivery in Nonhuman Primates.* Mol Ther Methods Clin Dev, 2020. **16**: p. 179-191.

319. Rashid, K., I. Akhtar-Schaefer, and T. Langmann, *Microglia in Retinal Degeneration.* Front Immunol, 2019. **10**: p. 1975.

320. Ambati, J., J.P. Atkinson, and B.D. Gelfand, *Immunology of age-related macular degeneration.* Nat Rev Immunol, 2013. **13**(6): p. 438-51.

321. Nussenblatt, R.B., et al., *Immune responses in age-related macular degeneration and a possible long-term therapeutic strategy for prevention.* Am J Ophthalmol, 2014. **158**(1): p. 5-11 e2.

322. Khandhadia, S., et al., *Age-related macular degeneration and the complement system.* Immunobiology, 2012. **217**(2): p. 127-46.

323. Ellis, S., et al., *GT005, a gene therapy for the treatment of dry age-related macular degeneration (AMD).* Investigative Ophthalmology & Visual Science, 2020. **61**(7): p. 2295-2295.

324. Tsutsumi, C., et al., *The critical role of ocular-infiltrating macrophages in the development of choroidal neovascularization.* J Leukoc Biol, 2003. **74**(1): p. 25-32.

325. Chen, Q., L. Sun, and Z.J. Chen, *Regulation and function of the cGAS-STING pathway of cytosolic DNA sensing.* Nat Immunol, 2016. **17**(10): p. 1142-9.

326. Ganser-Pornillos, B.K. and O. Pornillos, *Restriction of HIV-1 and other retroviruses by TRIM5.* Nat Rev Microbiol, 2019. **17**(9): p. 546-556.

327. Wu, X., et al., *Proteasome inhibitors uncouple rhesus TRIM5alpha restriction of HIV-1 reverse transcription and infection.* Proc Natl Acad Sci U S A, 2006. **103**(19): p. 7465-70.

328. Yan, Z., et al., *Ubiquitination of both adeno-associated virus type 2 and 5 capsid proteins affects the transduction efficiency of recombinant vectors.* J Virol, 2002. **76**(5): p. 2043-53.

329. Mitchell, A.M. and R.J. Samulski, *Mechanistic insights into the enhancement of adeno-associated virus transduction by proteasome inhibitors.* J Virol, 2013. **87**(23): p. 13035-41.

330. Chan, Y.K., et al., *Engineering adeno-associated viral vectors to evade innate immune and inflammatory responses.* Sci Transl Med, 2021. **13**(580).

331. Nish, S. and R. Medzhitov, *Host defense pathways: role of redundancy and compensation in infectious disease phenotypes.* Immunity, 2011. **34**(5): p. 629-36.

332. Beltran, W.A., et al., *rAAV2/5 gene-targeting to rods:dose-dependent efficiency and complications associated with different promoters.* Gene Ther, 2010. **17**(9): p. 1162-74.

333. Dufour, V.L., et al., *Toxicity and Efficacy Evaluation of an Adeno-Associated Virus Vector Expressing Codon-Optimized RPGR Delivered by Subretinal Injection in a Canine Model of X-linked Retinitis Pigmentosa.* Hum Gene Ther, 2020. **31**(3-4): p. 253-267.

334. Dimopoulos, I.S., et al., *Two-Year Results After AAV2-Mediated Gene Therapy for Choroideremia: The Alberta Experience.* Am J Ophthalmol, 2018. **193**: p. 130-142.

335. Li, C. and R.J. Samulski, *Engineering adeno-associated virus vectors for gene therapy.* Nat Rev Genet, 2020. **21**(4): p. 255-272.

336. Chai, Z., et al., *Optimization of Dexamethasone Administration for Maintaining Global Transduction Efficacy of Adeno-Associated Virus Serotype 9.* Hum Gene Ther, 2019. **30**(7): p. 829-840.

337. Finn, J.D., et al., *Proteasome inhibitors decrease AAV2 capsid derived peptide epitope presentation on MHC class I following transduction.* Mol Ther, 2010. **18**(1): p. 135-42.

338. Leborgne, C., et al., *IgG-cleaving endopeptidase enables in vivo gene therapy in the presence of anti-AAV neutralizing antibodies.* Nat Med, 2020.

339. Heier, J.S., et al., *Intravitreous injection of AAV2-sFLT01 in patients with advanced neovascular age-related macular degeneration: a phase 1, open-label trial.* Lancet, 2017. **390**(10089): p. 50-61.

340. Meliani, A., et al., *Antigen-selective modulation of AAV immunogenicity with tolerogenic rapamycin nanoparticles enables successful vector re-administration.* Nat Commun, 2018. **9**(1): p. 4098.

341. van den Borne, B.E., et al., *Chloroquine and hydroxychloroquine equally affect tumor necrosis factor-alpha, interleukin 6, and interferon-gamma production by peripheral blood mononuclear cells.* J Rheumatol, 1997. **24**(1): p. 55-60.

342. Jang, C.H., et al., *Chloroquine inhibits production of TNF-alpha, IL-1beta and IL-6 from lipopolysaccharide-stimulated human monocytes/macrophages by different modes.* Rheumatology (Oxford), 2006. **45**(6): p. 703-10.

343. Ivashkiv, L.B., *IFNgamma: signalling, epigenetics and roles in immunity, metabolism, disease and cancer immunotherapy.* Nat Rev Immunol, 2018. **18**(9): p. 545-558.

344. Hunter, C.A. and S.A. Jones, *IL-6 as a keystone cytokine in health and disease.* Nat Immunol, 2015. **16**(5): p. 448-57.

345. Parameswaran, N. and S. Patial, *Tumor necrosis factor-alpha signaling in macrophages.* Crit Rev Eukaryot Gene Expr, 2010. **20**(2): p. 87-103.

346. Ziegler, H.K. and E.R. Unanue, *Decrease in macrophage antigen catabolism caused by ammonia and chloroquine is associated with inhibition of antigen presentation to T cells.* Proc Natl Acad Sci U S A, 1982. **79**(1): p. 175-8.

347. Chain, B.M., P.M. Kay, and M. Feldmann, *The cellular pathway of antigen presentation: biochemical and functional analysis of antigen processing in dendritic cells and macrophages.* Immunology, 1986. **58**(2): p. 271-6.

348. Robson, N.C., A.M. Donachie, and A.M. Mowat, *Simultaneous presentation and cross-presentation of immune-stimulating complex-associated cognate antigen by antigen-specific B cells.* Eur J Immunol, 2008. **38**(5): p. 1238-46.

349. Mauthe, M., et al., *Chloroquine inhibits autophagic flux by decreasing autophagosome-lysosome fusion.* Autophagy, 2018. **14**(8): p. 1435-1455.

350. Nimmerjahn, F., et al., *Major histocompatibility complex class II-restricted presentation of a cytosolic antigen by autophagy.* Eur J Immunol, 2003. **33**(5): p. 1250-9.

351. Dengjel, J., et al., *Autophagy promotes MHC class II presentation of peptides from intracellular source proteins.* Proc Natl Acad Sci U S A, 2005. **102**(22): p. 7922-7.

352. Paludan, C., et al., *Endogenous MHC class II processing of a viral nuclear antigen after autophagy.* Science, 2005. **307**(5709): p. 593-6.

353. Rosenfeld, M.R., et al., *A phase I/II trial of hydroxychloroquine in conjunction with radiation therapy and concurrent and adjuvant temozolomide in patients with newly diagnosed glioblastoma multiforme.* Autophagy, 2014. **10**(8): p. 1359-68.

354. Rangwala, R., et al., *Phase I trial of hydroxychloroquine with dose-intense temozolomide in patients with advanced solid tumors and melanoma.* Autophagy, 2014. **10**(8): p. 1369-79.

355. Karasic, T.B., et al., *Effect of Gemcitabine and nab-Paclitaxel With or Without Hydroxychloroquine on Patients With Advanced Pancreatic Cancer: A Phase 2 Randomized Clinical Trial.* JAMA Oncol, 2019. **5**(7): p. 993-998.

356. Haas, N.B., et al., *Autophagy Inhibition to Augment mTOR Inhibition: a Phase I/II Trial of Everolimus and Hydroxychloroquine in Patients with Previously Treated Renal Cell Carcinoma.* Clin Cancer Res, 2019. **25**(7): p. 2080-2087.

357. Douar, A.M., et al., *Intracellular trafficking of adeno-associated virus vectors: routing to the late endosomal compartment and proteasome degradation.* J Virol, 2001. **75**(4): p. 1824-33.

358. Wee, Y.S., et al., *Interferon-inducible transmembrane proteins of the innate immune response act as membrane organizers by influencing clathrin and v-ATPase localization and function.* Innate Immun, 2012. **18**(6): p. 834-45.

359. Haller, O., et al., *Mx GTPases: dynamin-like antiviral machines of innate immunity.* Trends Microbiol, 2015. **23**(3): p. 154-63.

360. Satoh, N., et al., *Recurrent varicella-zoster virus retinitis in a patient treated with systemic corticosteroids.* Ocul Immunol Inflamm, 1998. **6**(3): p. 185-8.

361. Benz, M.S., J.S. Glaser, and J.L. Davis, *Progressive outer retinal necrosis in immunocompetent patients treated initially for optic neuropathy with systemic corticosteroids.* Am J Ophthalmol, 2003. **135**(4): p. 551-3.

362. Han, J.M., et al., *Presumed necrotizing viral retinitis after intravitreal triamcinolone injection: case report.* Korean J Ophthalmol, 2011. **25**(6): p. 451-4.

363. Takakura, A., et al., *Viral retinitis following intraocular or periocular corticosteroid administration: a case series and comprehensive review of the literature.* Ocul Immunol Inflamm, 2014. **22**(3): p. 175-82.

Appendices

The following published conference abstracts and manuscripts are based on the work I undertook for this thesis and are appended below:

1. Hydroxychloroquine enhances the efficacy of retinal gene therapy. Presented at: *ARVO annual meeting 2018*.

2. Photoreceptor-specific AAV gene replacement enhanced by the adjunctive use of hydroxychloroquine *in vivo. ARVO annual meeting 2019.*

3. Cell-Mediated Inflammatory Response to AAV Gene Therapy in the Retina. *ASGCT annual meeting 2020*.

4. Enhancement of Adeno-Associated Virus-Mediated Gene Therapy Using Hydroxychloroquine in Murine and Human Tissues. Published in: *Molecular Therapy – Methods & Clinical Development* (2019).

5. Immunomodulatory Effects of Hydroxychloroquine and Chloroquine in Viral Infections and Their Potential Application in Retinal Gene Therapy. Published in: *International Journal of Molecular Sciences* (2020).

Hydroxychloroquine enhances the efficacy of retinal gene therapy. Laurel C. Chandler, Alun R. Barnard, Maria I. Patrício, Robert E. MacLaren, Kanmin Xue. *ARVO annual meeting 2018.*

Purpose: Gene therapies for inherited retinal dystrophies using adeno-associated viral (AAV) vectors have shown early signs of efficacy in clinical trials. We have previously reported the activation of intracellular immune responses to AAV in the retina, and postulated that these may limit viral transduction and therefore therapeutic effects. Here we demonstrate that the use of a putative inhibitor of innate immunity, hydroxychloroquine (HCQ), during gene therapy could significantly enhance the efficacy of transgene expression in vitro and in vivo.

Methods: Mouse embryonic fibroblasts (MEFs), primary non-human primate (NHP) retinal pigment epithelial (RPE) cells, and human retinal explants were treated with HCQ prior to transduction with an AAV2 vector expressing green fluorescent protein (GFP) as a reporter for successful transduction. On day 3 GFP expression was quantified by flow cytometry in the MEFs and by reverse transcription qPCR in the NHP RPE cells, and on day 11 by mean fluorescence grey value in the retinal explants. To test the safety and efficacy of HCQ in vivo, subretinal injections of AAV2.GFP with or without the addition of HCQ were performed in matched eyes of 7-week old C57BL/6J mice. Confocal scanning laser ophthalmoscopy with retinal autofluorescence (AF) imaging was performed at 2, 4 and 8 weeks post-injection, retinal thickness was measured using optical coherence tomography.

Results: Compared with vector alone, the use of HCQ increased AAV transduction in vitro/ex vivo. GFP expression was increased by 3.4-fold in MEFs (one-way ANOVA:

n=4, p=0.0013), 3-fold in NHP RPE cells (n=3, p=0.0253), and 2-fold in human retinal explants (n=6, p=0.0213). In vivo, mean retinal AF, which represents GFP expression, demonstrated a 2-fold increase in eyes that received gene therapy with HCQ at 4 and 8 weeks, relative to paired eyes injected with AAV vector only (two-way ANOVA: n=5, p=0.0057). No difference in retinal thickness (one-way ANOVA: n=5, p=0.4306) or architecture were seen between eyes injected with and without HCQ, indicating absence of toxicity.

Conclusions: HCQ significantly enhances AAV transduction across species. Subretinal injection of a single pulse of HCQ together with the gene therapy vector appears to be safe and leads to sustained increase in transgene expression. While the precise mechanism of action remains unclear, adjunctive use of HCQ can potentially enhance the therapeutic effects of gene therapy.

Photoreceptor-specific AAV gene replacement enhanced by the adjunctive use of hydroxychloroquine *in vivo.* Laurel C. Chandler, Michelle E. McClements, Alun R. Barnard, Maria I. Patrício, Robert E. MacLaren, Kanmin Xue. *ARVO annual meeting 2019.*

Purpose: One of the major challenges of gene therapy for retinal diseases using adeno-associated viral (AAV) vectors is how to achieve sufficient levels of gene replacement within photoreceptors at a safe vector dose. Methods to improve efficacy of AAV transduction, without increasing vector dose, could be key in achieving a greater treatment effect. We previously reported that adjunctive use of hydroxychloroquine (HCQ) could improve AAV transduction with a ubiquitous reporter construct. Here, we further investigate whether HCQ can specifically enhance transgene expression in photoreceptor cells in vivo and whether the effect is applicable to different AAV serotypes.

Methods: Subretinal injection of $1x10^8$ genome copies (gc) of an AAV serotype 8 (Y733F) vector expressing GFP under the human photoreceptor-specific rhodopsin kinase promoter (GRK1) were performed in SVEV mice with or without the addition of 3.13 or 18.75 μM HCQ in paired eyes. Six weeks post-injection, retinal thickness was measured by in vivo optical coherence tomography (OCT) and retinal GFP protein expression assessed by western blot; analysis was performed blind. For comparison, C57BL/6J mice were subretinally injected with $1x10^8$ gc of an AAV serotype 2 vector expressing GFP under the ubiquitous CAG promoter with or without 18.75 μM HCQ in paired eyes. Eight weeks post-injection retinal GFP protein expression was measured.

Results: Compared with AAV vector alone, a 6.6 and 4.6-fold increase in retinal GFP protein expression was seen in mice injected with 18.75 μM HCQ together with AAV8(Y733F).GRK1.GFP (Wilcoxon matched-pairs signed rank test: p=0.0391; n=9) or AAV2.CAG.GFP (p=0.0034; n=12), respectively. No significant increase in GFP protein expression was found in eyes treated with 3.13 μM adjunctive HCQ compared with vector alone. OCT showed no difference in retinal thickness or laminar structure in eyes injected with AAV and 3.13 or 18.75 μM HCQ.

Conclusions: Adjunctive use of HCQ significantly increased retinal transgene expression in vivo following retinal gene therapy using either AAV8 or AAV2 vectors containing photoreceptor-specific or ubiquitous promoters. This potentially provides a means of achieving clinically efficacious levels of transgene expression in photoreceptors without a need to increase viral dose. Further work is needed to assess the mechanism of action of HCQ and its effects in the degenerate retina.

Cell-Mediated Inflammatory Response to AAV Gene Therapy in the Retina. Laurel C. Chandler, Helen Ferry, Imran H. Yusuf, Michelle E. McClements, Robert E. MacLaren, Kanmin Xue. *ASGCT annual meeting 2020.*

Introduction: Adeno-associated viral (AAV) vector-mediated gene therapies have demonstrated efficacy in the treatment of a range of inherited retinal diseases, including Leber congenital amaurosis, choroideremia and X-linked retinitis pigmentosa. Despite promising results, clinical trials have revealed intraocular inflammatory reactions to AAV as an important determinant of visual outcome. Resident microglia play a central role in the immune surveillance of the retina and can be activated by a wide range of stimuli. Here, we investigate the effects of AAV gene therapy on the retinal microglia and immune cell population.

Methods: Subretinal injections of $1x10^9$ genome copies of an AAV serotype 8 (Y733F) vector expressing GFP (AAV8. GFP) were performed in three-week old C57BL/6J mice with sham injections of PBS undertaken in the contralateral eyes. Retinae were harvested at baseline and 3, 7 and 14 days post-injection (n=5 per time point) and enzymatically dissociated into single cell suspensions. Cells were stained with antibodies to CD45 (a pan-leukocyte marker) and CD11b (a marker for microglia and macrophages) prior to flow cytometric analysis.

Results: Following subretinal injection of AAV8. GFP, a mean 3.2 ± 0.4% of retinal cells were GFP^+ on day 3, rising to 42 ± 15.7% by day 7 and 66.6 ± 24% by day 14, indicating successful AAV transduction. In 3 out of 5 AAV-treated retinae, all with the highest transduction efficiencies by day 14, signs of mild vitreous inflammation were detectable by optical coherence tomography as pre-retinal opacities. The retinal $CD45^+$

cell population at baseline was predominantly $CD45^{lo}CD11b^{+}$ (indicative of resident microglia) with a small proportion of $CD45^{hi}CD11b^{+}$ cells (likely macrophages). No significant increase in the $CD45^{+}$ cell population was seen at days 3 and 7 post-injection. However, at day 14, sharp rises in the number of $CD45^{+}$ cells were observed in the AAV-treated retinae with a mean 8.7-fold increase relative to PBS-injected eyes, positively correlating with the level of AAV transduction (Spearman's rho = 1.0). These $CD45^{+}$ cells were now predominantly a mixture of $CD45^{hi}CD11b^{+}$ macrophage-like cells and $CD45^{hi}CD11b^{-}$ cells, which are indicative of infiltrating lymphocytes (Figure 1). Moreover, a mean 8.3% of the $CD45^{+}$ cells, which were almost exclusively $CD11b^{+}$, were also GFP^{+}, suggestive of AAV8-transduced resident microglia. The higher level of CD45 expression among this GFP^{+} population raises the possibility of microglial activation. In contrast, these responses were not seen in the PBS-injected eyes.

Conclusion: Subretinal gene therapy with AAV8.GFP in mice leads to a cell-mediated retinal inflammatory response, despite the use of a dose of vector previously shown to be safe. The inflammatory responses are suggestive of both activation of resident microglia and infiltration of lymphocytes independent of surgical trauma.

Molecular Therapy
Methods & Clinical Development
Original Article

Enhancement of Adeno-Associated Virus-Mediated Gene Therapy Using Hydroxychloroquine in Murine and Human Tissues

Laurel C. Chandler,[1,2] Alun R. Barnard,[1,2] Sarah L. Caddy,[3] Maria I. Patrício,[1,2] Michelle E. McClements,[1] Howell Fu,[1] Cristina Rada,[3] Robert E. MacLaren,[1,2] and Kanmin Xue[1,2]

[1]Nuffield Laboratory of Ophthalmology, Nuffield Department of Clinical Neurosciences, University of Oxford, John Radcliffe Hospital, Oxford OX3 9DU, UK; [2]Oxford Eye Hospital, Oxford University Hospitals NHS Foundation Trust, NIHR Biomedical Research Centre, Oxford OX3 9DU, UK; [3]Medical Research Council Laboratory of Molecular Biology, Cambridge CB2 0QH, UK

The therapeutic effects of gene therapy using adeno-associated virus (AAV) vectors are dependent on the efficacy of viral transduction. Currently, we have reached the safe limits of AAV vector dose, beyond which damaging inflammatory responses are seen. To improve the efficacy of AAV transduction, we treated mouse embryonic fibroblasts, primate retinal pigment epithelial cells, and human retinal explants with hydroxychloroquine (HCQ) 1 h prior to transduction with an AAV2 vector encoding GFP driven by a ubiquitous CAG promoter. This led to a consistent increase in GFP expression, up to 3-fold, compared with vector alone. Comparing subretinal injections of AAV2.CAG.GFP vector alone versus co-injection with 18.75 μM HCQ in paired eyes in mice, mean GFP expression was 4.6-fold higher in retinae co-treated with HCQ without retinal toxicity. A comparative 5.9-fold effect was seen with an AAV8(Y733F).GRK1.GFP vector containing the photoreceptor-specific rhodopsin kinase promoter. While the mechanism of action remains to be fully elucidated, our data suggest that a single pulse of adjunctive HCQ could safely improve AAV transduction *in vivo*, thus providing a novel strategy for enhancing the clinical effects of gene therapy.

INTRODUCTION

Gene therapies based on adeno-associated virus (AAV) vector-mediated gene transfer are at advanced stages of clinical development to treat a broad range of monogenic disorders, including inherited retinal dystrophies,[1–4] hemophilia B,[5] hemophilia A,[6] muscular dystrophies,[7] and inherited neurodegenerations.[8] The approval of voretigene neparvovec by the US Food and Drug Administration (FDA) for the treatment of Leber congenital amaurosis caused by mutations in *RPE65* has paved the way for similar AAV-based gene therapies in the near future.[9] Recombinant AAV vectors are considered ideal vehicles for transgene delivery compared with lentiviral or adenoviral vectors due to their low immunogenicity; broad tissue tropism; and the ability of the delivered therapeutic transgenes to persist as episomes, which carry low mutagenic potential while allowing sustained transgene expression.

The clinical efficacy of AAV-mediated gene therapy is strongly dependent on the proportion of target cells transduced, particularly when trying to halt disease progression in post-mitotic tissues such as the retinal pigment epithelium (RPE), photoreceptors, neurones, and myocytes. While transduction can be increased to some extent by vector dosage, host inflammatory and immune responses to AAV become limiting factors at high doses, and they may compromise the persistence of transgene expression and therapeutic effects.[10–13] Consequently, despite promising results seen with retinal gene therapy, cases of intraocular inflammation have been encountered.[14–16] Therefore, one of the major challenges of gene therapy for retinal diseases is how to achieve sufficient levels of gene replacement at a safe vector dose.

After initially detecting specific upregulation of a panel of intracellular innate immune factors following AAV retinal gene therapy in mice, we investigated hydroxychloroquine (HCQ), a putative inhibitor of anti-viral pattern recognition receptors Toll-like receptor 9 (TLR9) and cyclic guanosine monophosphate (GMP)-AMP synthase (cGAS),[17–19] as a means of improving the efficacy of AAV gene therapy. Here we demonstrate the enhancement of AAV transduction *in vitro*, *ex vivo*, and *in vivo* using HCQ in both murine and human tissues and specifically within RPE and photoreceptor cells. We investigated the effect of HCQ across two commonly used serotypes of AAV, and we assessed its safety and efficacy when co-administered subretinally with AAV *in vivo*. Together, these findings suggest that the adjunctive use of HCQ during AAV gene therapy may provide a safe means of improving AAV transduction within the retina *in vivo*.

Received 9 October 2018; accepted 20 May 2019;
https://doi.org/10.1016/j.omtm.2019.05.012.

Correspondence: Kanmin Xue, Nuffield Laboratory of Ophthalmology, Nuffield Department of Clinical Neurosciences, University of Oxford, Level 6 West Wing, John Radcliffe Hospital, Headley Way, Oxford OX3 9DU, UK.
E-mail: kanmin.xue@eye.ox.ac.uk

Table 1. Summary of the Anti-viral Functions of Key Intracellular Innate Immune Mediators

Gene	Alias	Summary of Function	Reference
Tlr9		detects unmethylated CpG DNA within the cytosol to activate downstream anti-viral responses	24
Rig-I	*Ddx58*	detects cytosolic viral RNA, including sequences that have been transcribed by RNA polymerase III from AT-rich dsDNA	37
Cgas	*Mb21d1*	detects cytosolic dsDNA and synthesizes the secondary signaling molecule cGAMP	38,39
Sting	*Tmem173*	activated by cGAMP, stimulates TBK1 to phosphorylate IRF3, which can induce type I interferon response	40,41
Trim21		detects and neutralizes antibody-bound virions after endosomal escape	42,43
Ifn-γ		type II interferon that controls innate and adaptive anti-viral immune responses	44
Tnf-α		proinflammatory cytokine that can induce the breakdown of the blood-retina barrier	25–27
Cxcl10		chemokine secreted in response to IFN-γ and activates leukocytes to regulate immune responses	45
Isg15		an ubiquitin-like molecule stimulated by type I interferon in response to viral infection; covalent and non-covalent binding can disrupt viral replication	46
Apobec3		deaminates cytidine to uridine in viral DNA, causing hypermutations that inhibit viral replication	47
Apobec2		lacks identifiable cytidine deaminase activity and no known anti-viral activity	48
Aid	*Aicda*	cytidine deaminase involved in immunoglobulin gene hypermutation and class switching	49

Tlr9, Toll-like receptor 9; *Ddx58*, DExD/H-Box Helicase 58; *Rig-I*, retinoic acid-inducible gene 1; *Mb21d1*, mab-21 domain containing 1; Cgas, cyclic GMP-AMP synthase; dsDNA, double-stranded DNA; cGAMP, cyclic GMP-AMP; *Tmem173*, transmembrane protein 173; *Sting*, stimulator of interferon genes; TBK1, TANK-binding kinase 1; IRF3, interferon regulatory factor 3; *Trim21*, tripartite motif containing 21; *Tnf-α*, tumor necrosis factor-α; *Ifn-γ*, interferon-γ; *Cxcl10*, C-X-C motif chemokine ligand 10; *Isg15*, interferon-stimulated gene 15; *Apobec3*, apolipoprotein B mRNA-editing enzyme, catalytic polypeptide 3; *Aicda*, activation-induced cytidine deaminase (*Aid*).

RESULTS

AAV Retinal Gene Therapy Activates Intracellular Innate Immune Responses *In Vivo*

To assess the activation of innate immune responses to AAV following retinal gene therapy, we first performed subretinal injections of an AAV serotype 2 vector encoding GFP driven by a ubiquitous CAG promoter (AAV2.CAG.GFP) and sham injections of diluent in paired eyes of 4-week-old female C57BL/6J mice. The purity of the AAV vector was confirmed during the production process (Figure S1).

Expression of a panel of key anti-viral sensors and effectors (Table 1) was assessed using qRT-PCR of retinal samples collected on days 3, 7, and 15 post-injection. Significant upregulation of the intracellular viral sensors *Tlr9*, *Rig-I* (also known as *Ddx58*), *Cgas* (*Mb21d1*), *Sting* (*Tmem173*), and *Trim21* (Figure 1A) and anti-viral effectors *Ifn-γ*, *Tnf-α*, *Cxcl10*, *Isg1*, and *Apobec3* (Figure 1B) was detected in eyes treated with AAV compared to those sham injected with PBS. Although there was no effect on gene expression soon after gene therapy (3 days post-injection), after 7 days all the viral sensors and effectors were significantly upregulated compared to sham controls, with *Ifn-γ*, *Tnf-α*, and *Cxcl10* exhibiting >10-fold increases in gene expression. By day 15, the expression levels of all these genes dropped relative to day 7, with *Rig-I*, *Mb21d1*, *Ifn-γ*, *Cxcl10*, and *Isg15* no longer demonstrating a significant difference from the sham eye. In contrast, no change in the expressions of *Apobec2* and *Aid* (also known as *Aicda*), both members of the same family of cytidine deaminases as *Apobec3*, was seen over the 15-day course, suggesting that AAV induced selective activation of innate immune responses (Figure 1C). GFP transgene expression was significantly above baseline from day 7 onward (one-way ANOVA, $p = 0.0003$; $n = 5–7$) (Figure S2).

The Antimalarial Drugs HCQ and Chloroquine Can Increase AAV Transduction in Mouse Embryonic Fibroblasts

Since the activation of proinflammatory cytokines could create an anti-viral environment within the target tissue, thus restricting AAV transgene expression and persistence, we postulated that the suppression of intracellular immunity might enhance the efficacy of AAV transduction. We identified HCQ as a putative inhibitor of two key sentinels in the initiation of intracellular anti-DNA viral response: cGAS, which detects the presence of cytosolic double-stranded DNA (dsDNA),[17] such as inverted terminal repeats (ITRs) that form secondary structures in single-stranded AAV genomes; and TLR9, which detects unmethylated CpG sequences,[18,20] also present in AAV ITRs.

In an initial dose-escalation trial, wild-type mouse embryonic fibroblasts (MEFs) were treated with increasing concentrations of HCQ up to 50 μM for 1 h prior to transduction with AAV2.GFP, followed by flow cytometry analysis of GFP fluorescence on day 3. HCQ treatment increased the number of GFP-positive cells up to 18.75 μM; however, concentrations greater than 18.75 μM appeared to be cytotoxic, as evidenced by an increase in 7-aminoactinomycin D (7-AAD) staining, which coincided with a decrease in GFP positivity (Figure 2A). Subsequent in-depth testing of HCQ was limited to 3.13- and 18.75-μM concentrations. The mean proportion of GFP-positive cells increased in a dose-dependent manner from 6% with no HCQ to 9% with 3.13 μM HCQ and 19% with 18.75 μM HCQ (one-way ANOVA, $p = 0.0026$; $n = 6$), without adverse effects on cell survival (Figures 2B and 2C).

To see if the enhancement of AAV transduction by HCQ might be a drug class effect, we also tested the structurally similar 4-aminoquinoline antimalarial compound chloroquine (CQ). Pre-incubation of MEFs with CQ for 1 h prior to transduction with AAV2.GFP also improved transduction from 2.5% with no CQ to 6.4% with 12 μM CQ (Figure S3). Since HCQ is known to be less retinal toxic than CQ in patients on long-term therapy for lupus and rheumatoid

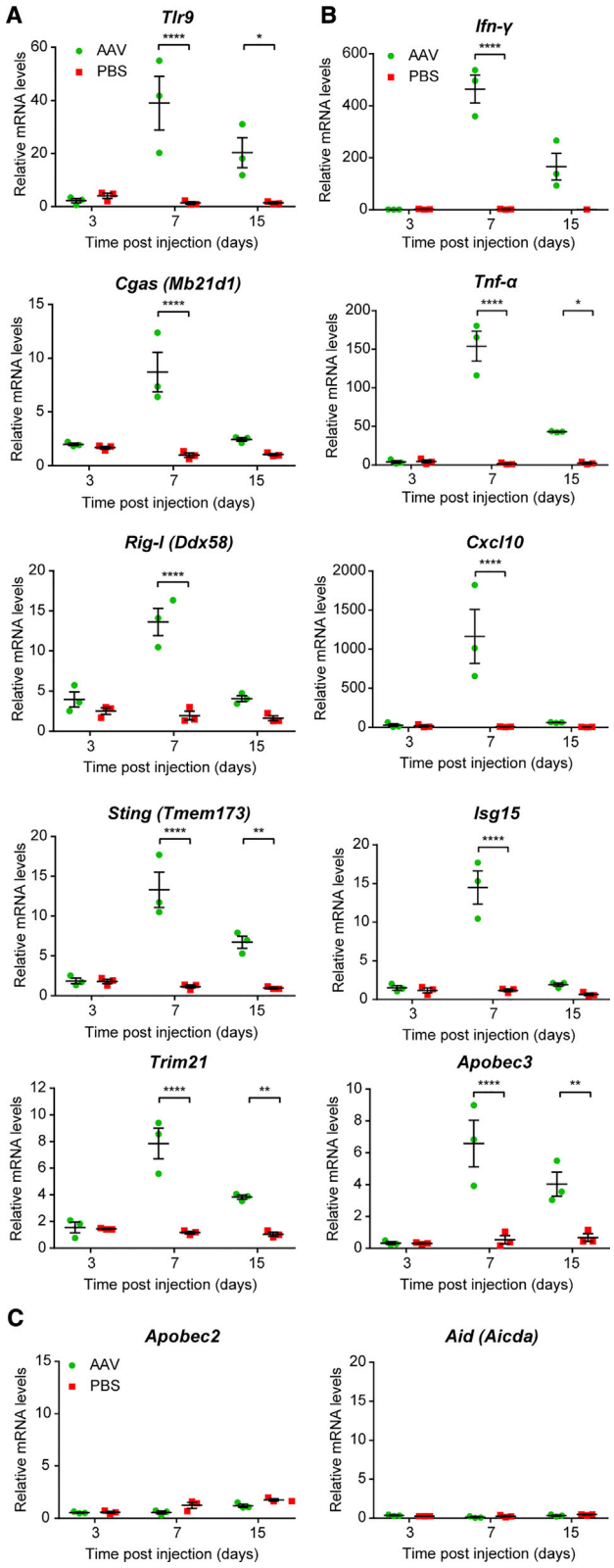

Figure 1. Intracellular Innate Immune Responses Are Activated by AAV Gene Therapy

AAV2.GFP vector (1×10^9 gc) was subretinally injected into wild-type C57BL/6 mice, with sham injections of PBS undertaken in the contralateral eye. RNA was extracted from the mouse retina on days 3, 7, and 15 post-injection (n = 3/time point). The expressions of a range of cytosolic anti-viral (A) sensor and (B) effector genes and (C) two genes from the APOBEC family were quantified using qRT-PCR. Relative expression was calculated as a mean fold change (±SEM) relative to the mean of both eyes from uninjected baseline controls (n = 2). *$p \leq 0.05$, **$p \leq 0.01$, ****$p \leq 0.0001$ (two-way ANOVA with Šídák's multiple comparison test).

arthritis,[21] we chose 3.13 and 18.75 μM HCQ as the minimum and maximum effective concentrations of HCQ to move forward for testing in other *in vitro*, *ex vivo*, and *in vivo* systems.

HCQ Increases AAV Transduction in Non-human Primate RPE Cells and Human Retina *Ex Vivo*

To assess the applicability of HCQ augmentation of AAV transduction in retinal gene therapy, primary RPE cells were isolated from non-human primate (NHP; rhesus macaque) eyes and immediately placed into culture. The RPE cells were treated with 0, 3.13, or 18.75 μM HCQ for 1 h prior to transduction with AAV2.GFP. At 3 days post-transduction, GFP expression was visualized by fluorescence microscopy and quantified by qRT-PCR and western blot. A visible increase in GFP fluorescence could be seen in RPE cells treated with HCQ compared with AAV vector alone (Figure 3A), which correlated to an up to 3-fold increase in GFP mRNA expression in cells treated with 18.75 μM HCQ (one-way ANOVA, p = 0.0253; n = 3 eyes) (Figure 3B). A similar magnitude of increase in GFP protein expression associated with HCQ was also detected by western blot; however, this did not reach statistical significance due to limited NHP tissue availability (n = 2) (Figures 3C and 3D).

Since inherited retinal degenerations can affect both RPE and photoreceptor cells, we next tested whether the effect of HCQ on AAV transduction also applied to photoreceptors. To this end, human retinal explants were collected from patients undergoing routine clinically indicated retinectomy as part of retinal detachment repair. The retinal explants were treated with either 0 or 3.13 μM HCQ for 1 h prior to transduction with AAV2.GFP. GFP fluorescence was visualized using fluorescence microscopy on days 3, 5, 7, 9, and 11 post-transduction (Figure 3E), and it was quantified using mean gray values of the explants imaged under standardized conditions.[22] The data from retinal tissue harvested from two (of two) patients independently showed consistent trends of increased fluorescence in the explants treated with HCQ from day 7 onward when significant GFP fluorescence became detectable. A statistically significant difference was observed with the treatment effect of HCQ over time (two-way ANOVA, patient 1 p = 0.0002; patient 2 p = 0.0092; n = 3), with a mean 2-fold increase in mean gray value at day 11 for the two patients (Figure 3F).

Co-administration of HCQ with AAV Vector Improves Retinal Gene Therapy *In Vivo* without Detectable Toxicity

To assess the translational potential of HCQ to retinal gene therapy, we tested the effect of co-administration of HCQ with AAV vector

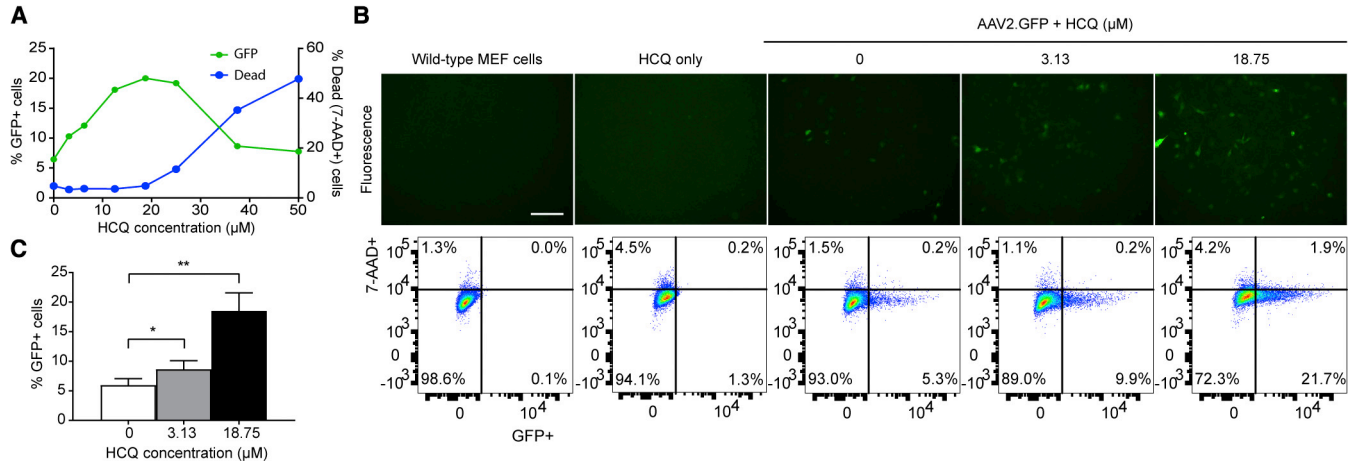

Figure 2. Hydroxychloroquine (HCQ) Increases AAV Transduction in Mouse Embryonic Fibroblasts (MEFs)

Wild-type MEFs were pre-treated with HCQ for 1 h prior to transduction with AAV2.GFP at an MOI of 1,000. (A) Representative dose-response curve of HCQ concentration versus either GFP-positive or dead (7-AAD-positive) cells, represented as a percentage of the total number of cells. (B) Representative fluorescence microscopy images of MEFs treated with 0, 3.13, or 18.75 μM HCQ acquired at 3 days post-transduction (scale bar: 200 μm), shown alongside flow cytometry analyses gated for GFP fluorescence and the cell viability marker 7-AAD. (C) Proportion of GFP-positive (GFP+) cells expressed as a percentage of the total number of live (7-AAD-negative) cells at day 3. Data are presented as mean ± SEM (n = 6). *$p \leq 0.05$, **$p \leq 0.01$ (one-way repeated-measures ANOVA with Dunnett's multiple comparison test).

in vivo. The 7-week-old female C57BL/6J mice were subretinally injected with 1×10^8 genome copies (gc) of AAV2.GFP containing either 3.13 or 18.75 μM HCQ in one eye and AAV vector only in the fellow eye. The fluorescence of the mouse retina was measured at regular intervals up to 8 weeks using *in vivo* confocal scanning laser ophthalmoscopy (cSLO) at standardized detector sensitivity. Cross-sectional structure of the retina was also monitored using *in vivo* spectral domain optical coherence tomography (OCT) to look for signs of retinal toxicity.

Retinal fluorescence was found to be increased in eyes that received AAV vector suspension containing 18.75 μM HCQ compared with paired eyes that received AAV vector alone (Figure 4A). No difference was seen in eyes that received AAV with 3.13 μM HCQ (Figure 4B). Although a clear trend in favor of HCQ was visible, the differences in mean retinal fluorescence based on normalized gray value comparisons did not reach statistical significance. This is likely because the method did not distinguish between the diffuse background fluorescence (which represents GFP expression) and scattered clumps of hyperfluorescence (representing autofluorescent macrophage aggregates associated with inflammation). In addition, the statistical power of the comparison was reduced by the exclusion of 4 of 13 mice (final n = 5 for 3.13 μM and n = 4 for 18.75 μM) due to unintended intravitreal injections or subretinal bleed during surgery.

To more specifically compare levels of GFP protein expression between the treatment arms, the mouse retinae were harvested for western blot analysis at the final time point (8 weeks). Eyes that received AAV with 18.75 μM HCQ showed a mean 4.6-fold increase in GFP protein level compared with paired eyes that received AAV vector alone (Wilcoxon matched-pairs signed rank test, p = 0.0034; n = 12) (Figure 4C). In terms of the safety of HCQ administration into the subretinal space, *in vivo* OCT imaging demonstrated no detectable change in lamellar retinal architecture relating to the administration of HCQ (Figure 4D). Moreover, there was no significant difference in the mean retinal thickness of eyes injected with HCQ compared to paired eyes sham injected with PBS (Figure 4E). By measuring the mean gray value of the fundus using cSLO, we demonstrated that there was no significant difference in the autofluorescence of eyes injected with PBS compared to those injected with HCQ alone, suggesting that HCQ is not autofluorescent (Figure 4F).

Next, we investigated whether HCQ was able to specifically enhance transgene expression within photoreceptors *in vivo* and whether the effect was applicable to different AAV serotypes. 4- to 5-week-old 129S2/SvHsd mice were subretinally injected with 1×10^8 gc of an AAV8(Y733F) serotype vector expressing GFP under the photoreceptor-specific promoter G protein-coupled receptor kinase 1 (GRK1) (AAV8(Y773F).GRK1.GFP), with injections of AAV combined with 18.75 μM HCQ performed in the contralateral eye. Retinal GFP protein expression was found to be 5.9-fold higher in eyes injected with AAV containing 18.75 μM HCQ compared to AAV only (Wilcoxon matched-pairs signed rank test, p = 0.0391; n = 9) (Figure 4G).

Mechanism of Action of HCQ

While HCQ is routinely used in the treatment of autoimmune diseases, its exact mechanism of action remains unclear. Several studies support the main mode of action of HCQ as via inhibition of the innate immune factors TLR9[18,20] and cGAS.[17]

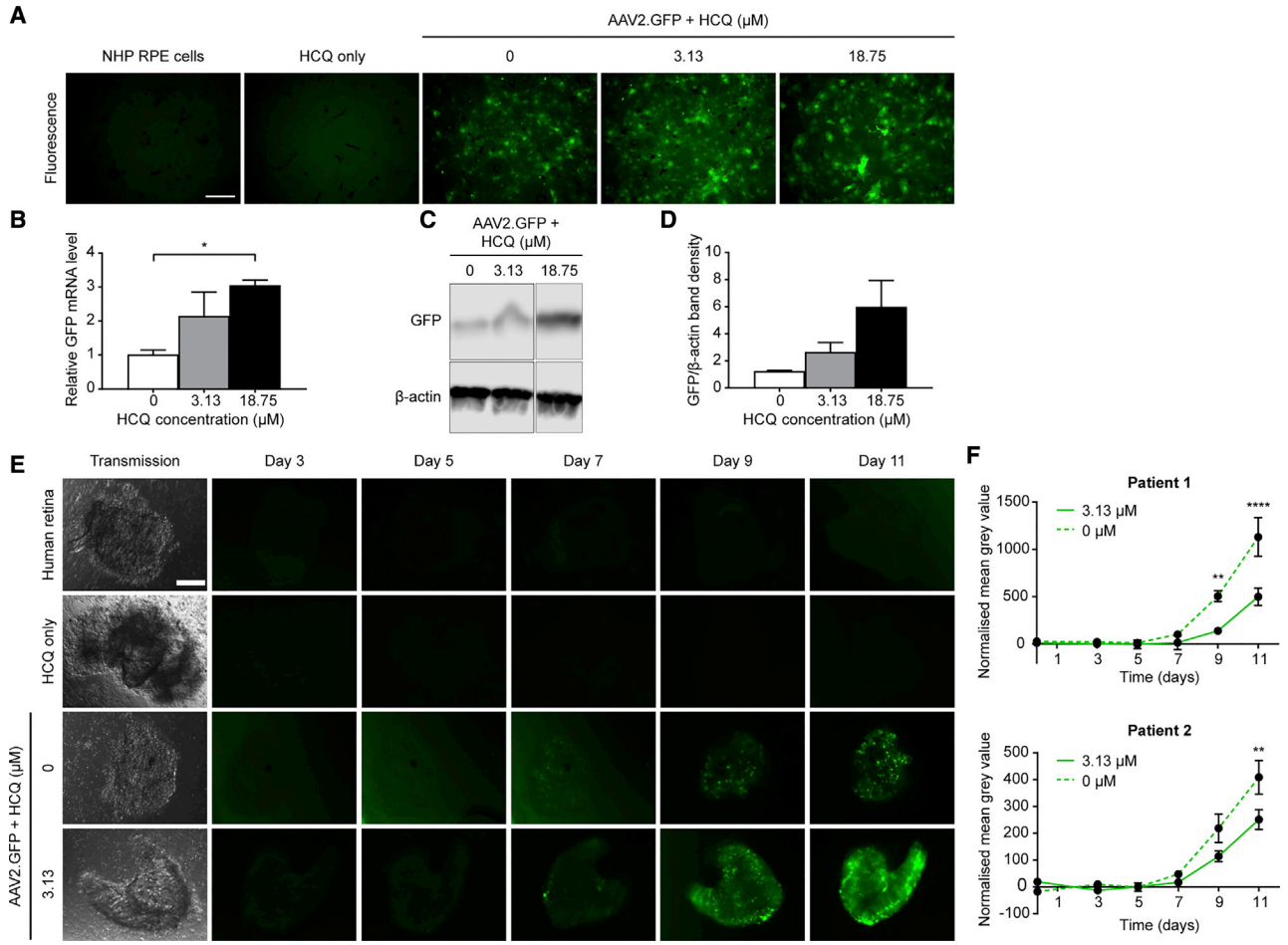

Figure 3. HCQ Increases AAV Transduction in Non-human Primate (NHP) Retinal Pigment Epithelium (RPE) Cells and Human Retina

(A–D) Primary macaque RPE cells were treated with 0, 3.13, or 18.75 μM HCQ for 1 h prior to transduction with 2×10^9 gc AAV2.GFP. (A) Representative fluorescence microscopy images acquired on day 3 post-transduction (scale bar, 200 μm). (B) Levels of *GFP* mRNA in AAV- and HCQ-treated RPE cells were quantified using qRT-PCR on day 3 post-transduction, and they are expressed as mean fold change relative to cells treated with AAV only (±SEM, n = 3). *$p \leq 0.05$ (one-way ANOVA with Dunnett's multiple comparison test). (C) Representative western blot of GFP protein expression with β-actin used as a loading control. (D) Quantification of GFP band density normalized to β-actin. Data are presented as mean ± SEM (n = 2). (E and F) Fresh patient-derived retinal explants were treated *ex vivo* with 0 or 3.13 μM HCQ for 1 h prior to transduction with 1×10^9 gc AAV2.GFP (UK research ethics approval 10/H0505/8). (E) Representative transmission microscopy image at baseline and fluorescence images acquired on alternate days up to day 11 post-transduction (scale bar, 100 μm). (F) GFP expression was estimated by calculating the mean gray value of fluorescence images from two separate patients. These were normalized to untransduced controls treated with equivalent concentrations of HCQ. Data are expressed as mean ± SEM (3 replicates/patient). **$p \leq 0.01$, ****$p \leq 0.0001$ (two-way repeated-measures ANOVA with Šídák's multiple comparisons test).

We first tested the effect of HCQ on AAV transduction in *Cgas*$^{-/-}$ MEFs with the hypothesis that, if HCQ acted via the inhibition of cGAS, its effect would be diminished in the absence of cGAS. While we found that *Cgas*$^{-/-}$ MEFs transduced with up to 6.4-fold greater efficacy than wild-type MEFs at the same MOI (t test, p = 0.0008; n = 6) (Figure 5A), the addition of HCQ was still able to increase the mean rate of AAV transduction from 38% with no HCQ to 65% with 3.13 μM HCQ and 74% with 18.75 μM HCQ (one-way ANOVA, $p < 0.0001$; n = 6) (Figures 5B and 5C). Consequently, there was no significant difference in the effects of 18.75 μM HCQ on wild-type versus *Cgas*$^{-/-}$ MEFs (Figure 5D). This indicates that HCQ is unlikely to act exclusively via the inhibition of cGAS.

Next we explored the role of TLR9 in AAV transduction with the use of the agonistic TLR9 oligodeoxynucleotide CpG-A,[23] which contains unmethlyated CpG sequences known to stimulate TLR9 activity.[24] Cells were treated with CpG-A for 30 min prior to AAV2.GFP transduction with or without HCQ, and GFP fluorescence was quantified using flow cytometry 3 days post-transduction. CpG-A treatment significantly reduced the mean number of GFP-fluorescing cells by 2.7-fold relative to untreated cells (Figures 6A and 6B) (paired t test, p = 0.0001; n = 7) and by 1.9-fold in HCQ-treated cells (Figures 6C and 6D) (p = 0.0348; n = 7). Therefore, the inhibitory effect of CpG-A on AAV transduction was significantly reduced by the presence of HCQ

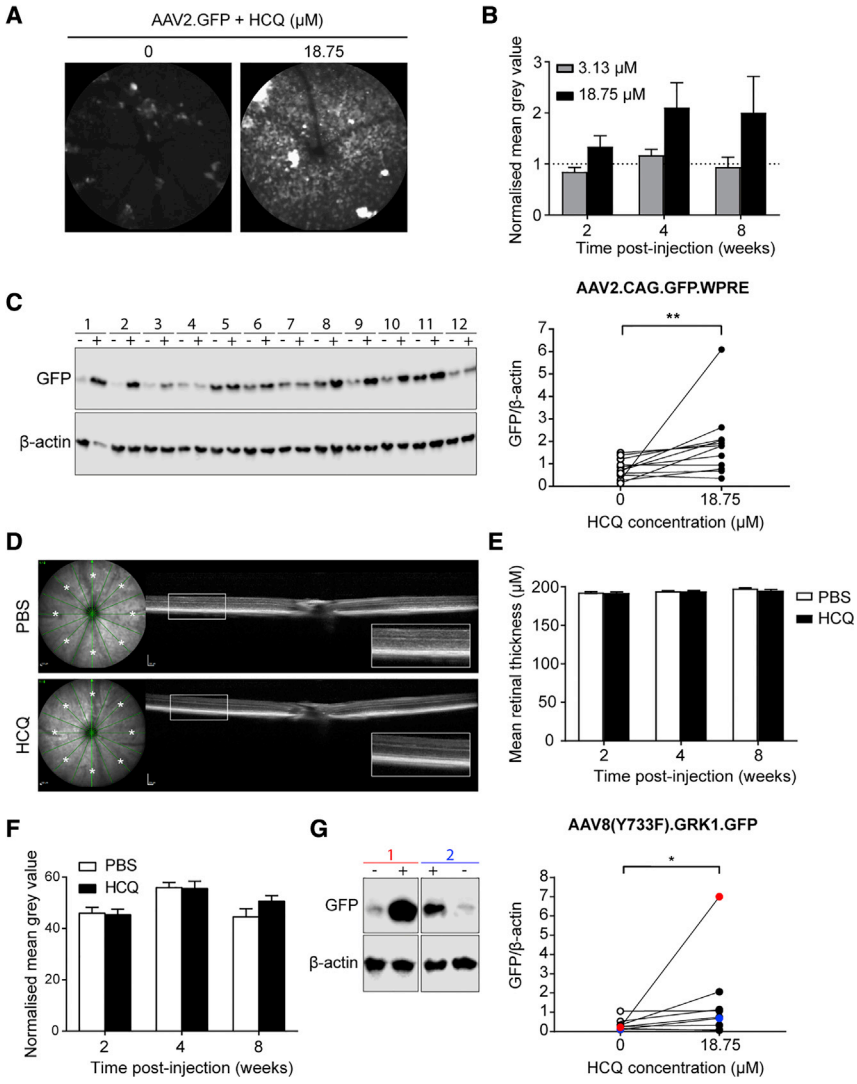

Figure 4. HCQ Enhances AAV Transduction of Mouse Retina *In Vivo* and Has No Detectable Effect on Retinal Architecture or Thickness

(A–F) C57BL/6J mice were subretinally injected with AAV2.GFP vector alone in one eye and co-injected with either 3.13 or 18.75 μM HCQ in the fellow eye. (A) Representative *in vivo* confocal scanning laser ophthalmoscopy autofluorescence images of paired eyes at 8 weeks post-injection. (B) GFP fluorescence levels were estimated using the mean gray values of autofluorescence images. Eyes co-injected with HCQ were normalized to fellow AAV only-injected eyes at 2, 4, and 8 weeks post-transduction (±SEM; 3.13 μM, n = 5; 18.75 μM, n = 4). (C) Western blot of GFP protein levels in paired mouse retinae that received either AAV vector alone (–) or vector mixed with HCQ (18.75 μM) (+) at 8 weeks post-injection. β-actin was used as a loading control. Quantification of western blot GFP band density normalized to β-actin in paired eyes is shown (n = 12). (D) Representative spectral domain optical coherence tomography images from fellow eyes that received either PBS or 18.75 μM HCQ, showing normal retina lamellar architecture. Total retinal thickness was measured at points marked with an asterisk. (E) Mean total retinal thickness of points (*) at 2, 4, and 8 weeks post-injection (±SEM, n = 8). (F) Mean gray value of eyes injected with 18.75 μM HCQ alone normalized to paired PBS-injected eyes at 2, 4, and 8 weeks post-injection (±SEM, n = 8). (G) 129S2/SvHsd mice were subretinally injected with AAV8(Y733F).GRK1.GFP vector alone in one eye and co-injected with 18.75 μM HCQ in the paired eye. Representative western blot of GFP protein levels in paired retinae of two mice, with red and blue colors corresponding to points on the graph, is shown. Quantification of GFP band density normalized to β-actin in paired eyes is also shown (n = 9). *p ≤ 0.05, **p ≤ 0.01 (Wilcoxon matched-pairs signed rank test).

(Figure 6E) (Wilcoxon matched-pairs signed rank test, p = 0.0156; n = 7).

To assess the effect of HCQ on viral entry, we compared the intracellular AAV genome loads up to 1 h post-transduction between HCQ-treated and untreated wild-type MEFs. No significant difference in overall intracellular AAV genome copy numbers was detected by qPCR between HCQ-treated and untreated cells (Figure S4). Further analysis of subcellular localization of AAV genomes was conducted by cell fractionation followed by qPCR in HCQ-treated versus untreated wild-type MEFs 24 h post-transduction. The presence of HCQ was found to alter the subcellular distribution of AAV with a trend toward increased nuclear localization (two-way ANOVA, p = 0.0356; n = 3) (Figure S5B). However, the effect did not reach statistical significance upon multiple comparison testing due to the high level of variation in the qPCR assay. Successful separation of cytosolic versus nuclear fractions was confirmed using the cytosolic marker α-tubulin and nuclear marker histone H3 (Figure S5A). Genomic glyceraldehyde 3-phosphate dehydrogenase (GAPDH) DNA was used as a marker for nuclear DNA (Figure S5C).

DISCUSSION

Despite AAV vectors being considered to have low immunogenicity, particularly when administered into the subretinal space, our data suggest that AAV transduction is associated with the activation of intracellular innate immunity as well as downstream proinflammatory cytokines independent of surgical trauma. The induction of *Tnf-α*, *IFN-γ*, and type I interferon responses could lead to the breakdown of the blood-retina barrier and recruitment of adaptive immunity.[25–27] This occurrence would ultimately cause localized tissue inflammation and reduced therapeutic efficacy, and it may underlie

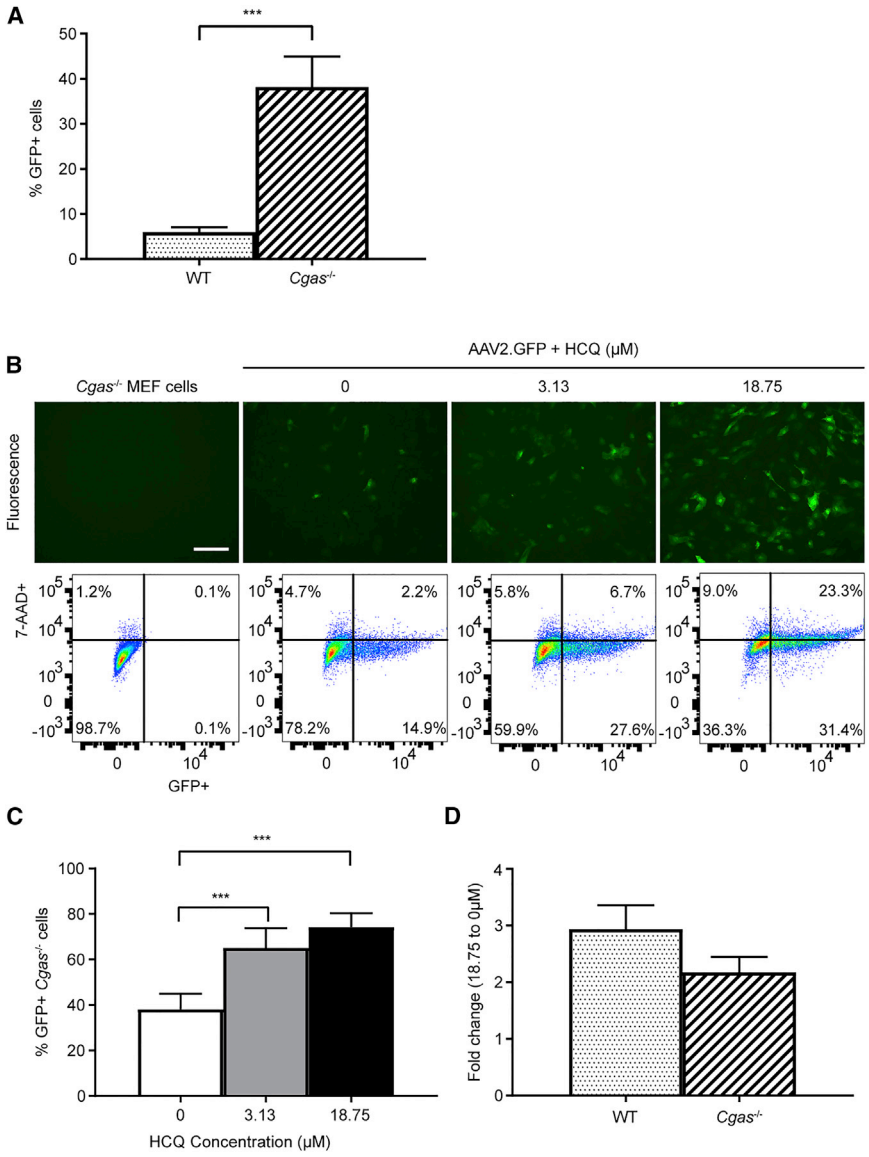

Figure 5. *Cgas*$^{-/-}$ MEFs Transduce Significantly Better Than Wild-Type Cells, and HCQ Further Enhances AAV Transduction in *Cgas*$^{-/-}$ MEFs

MEFs were transduced with AAV2.GFP at an MOI of 1,000. GFP fluorescence and cell viability (7-AAD staining) were assessed on day 3 post-transduction by flow cytometry. The mean proportion of GFP-positive (GFP+) cells was expressed as a percentage of the total number of live (7-AAD-negative) cells. (A) Mean proportion of GFP+ cells in wild-type and *Cgas*$^{-/-}$ MEFs after transduction with the same MOI (±SEM, n = 6). ***$p \leq 0.001$ (paired t test). (B) Representative fluorescence images and flow cytometry plots of *Cgas*$^{-/-}$ MEFs treated with 0, 3.13, or 18.75 μM HCQ 1 h prior to transduction (scale bar: 200 μm). (C) Mean proportion of GFP+ *Cgas*$^{-/-}$ cells measured using flow cytometry (±SEM, n = 6). ***$p \leq 0.001$ (one-way repeated-measures ANOVA with Dunnett's multiple comparison). (D) Fold change of mean proportion of GFP+ cells treated with 18.75 μM relative to 0 μM HCQ in wild-type and *Cgas*$^{-/-}$ MEFs. Data are presented as mean ± SEM (n = 6).

the cases of intraocular inflammation encountered in retinal gene therapy trials.[14–16]

The upregulation of innate immune mediators detected on day 7 post-subretinal gene therapy *in vivo* does not rule out the presence of background levels of pre-existing surveillance innate sensors. Active AAV particles may be present within the subretinal space for a prolonged period (e.g., days) during which repeated waves of viral entry into the host cells may occur. The signaling molecule generated by activated cGAS, cyclic GMP-AMP (cGAMP) has been shown to traverse intercellular junctions and cause field effects, which could account for the delayed peaking of innate immune responses.[28] In addition, significant GFP mRNA expression was not seen *in vivo* until 7 days post-injection, which corresponds to the induction of the innate immune genes and may also suggest a delay in the uptake of AAV from the subretinal space. Retinal microglia are resident macrophages that play an important role in immune defense in the eye, and they are capable of detecting viruses and secreting inflammatory cytokines to amplify an inflammatory response.[29] As these cells are capable of mounting an antiviral response through the activation of cGAS[30] and TLR9,[31] we cannot rule out the possibilities that resident microglia may have been responsible for the upregulation of the innate immune factors and that the delay could represent the activation of resident microglia or recruitment of lymphocytes.

HCQ is an approved antimalarial drug with a well-established safety profile. It is a putative inhibitor of innate immunity, consistent with known efficacy in the treatments of autoimmune diseases such as systemic lupus erythematosus and rheumatoid arthritis.[19,32] A recent *in silico* analysis suggested that HCQ can disrupt dsDNA binding and the activation of cGAS.[17] However, we found that HCQ did not discriminate in its ability to improve AAV transduction between wild-type and *Cgas*$^{-/-}$ MEFs, which suggests that HCQ is unlikely to act exclusively through cGAS. Also, although *Cgas*$^{-/-}$ MEFs transduce with 6.4-fold greater efficiency than wild-type MEFs, this does not necessarily imply that cGAS is the sole limiting factor for AAV transduction, given that the absence of cGAS is likely to affect the expression of other intracellular innate immune genes.

Additional studies have proposed that HCQ may act through the inhibition of TLR9. One group suggested that HCQ may bind to DNA

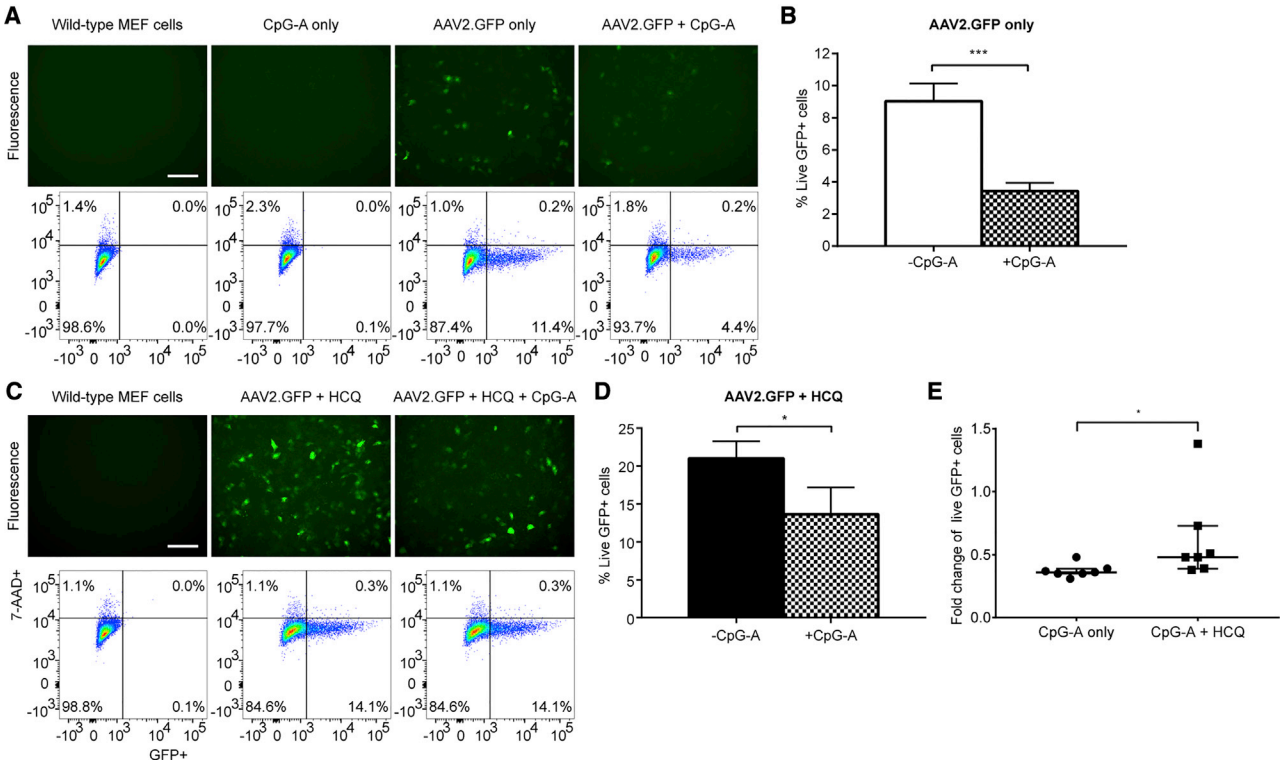

Figure 6. The Agonistic TLR9 Oligodeoxynucleotide CpG-A Decreases AAV Transduction in Wild-Type MEFs and Has a Significantly Reduced Effect in HCQ-Treated Cells

Wild-type MEFs were treated with or without CpG-A (754.6 μM) 30 min prior to transduction with AAV2.GFP at an MOI of 1,000. GFP fluorescence and cell viability (7-AAD staining) were assessed on day 3 post-transduction by flow cytometry. (A) Representative fluorescence images and flow cytometry plots (scale bar, 200 μm). (B) The mean proportion of GFP-positive (GFP+) cells expressed as a percentage of the total number of live (7-AAD-negative) cells (±SEM, n = 7). ***$p \leq 0.001$ (paired t test). (C and D) Wild-type MEFs were treated with 18.75 μM HCQ 1 h prior to transduction with AAV2.GFP, followed by treatment with or without CpG-A 30 min prior to transduction. (C) Representative fluorescence images and flow cytometry plots (scale bar, 200 μm). (D) The mean proportion of GFP+ cells (±SEM, n = 7). *$p \leq 0.05$ (paired t test). (E) The fold change of transduced live GFP+ cells treated with CpG-A relative to cells with no CpG-A treatment. Cells were either treated with CpG-A alone or with CpG-A and HCQ (median ± interquartile range, n = 7). *$p \leq 0.05$ (Wilcoxon matched-pairs signed rank test).

and cause conformational changes that prevent the activation of TLR9,[18] while others have suggested that the effect of HCQ on endosomal pH can indirectly inhibit TLR9, which is localized within endosomes and activated by an acidic environment.[20] We found that treatment of wild-type MEFs with a TLR9-activating oligonucleotide (CpG-A) caused a 2.7-fold reduction in transgene expression, suggesting that the stimulation of TLR9-mediated innate immunity can lead to reduced AAV transduction. HCQ significantly, but incompletely, abrogated the inhibitory effect of CpG-A on AAV transduction, suggesting that HCQ may be an antagonist of TLR9. If HCQ prevents the activation of TLR9 by causing conformational changes in DNA,[18] it is possible that the partial response seen may be a result of the stoichiometric ratio between HCQ and CpG-A, such that some unbound CpG-A was able to adversely affect AAV transduction.

However, the possibility of HCQ acting via alternative targets cannot be ruled out. Our viral entry assay did not show any notable difference in AAV viral loads soon after transduction, possibly indicating that HCQ does not act by decreasing degradation or by increasing AAV binding or entry into the target cells. Investigation into the subcellular localization of AAV revealed a strong trend toward shifting from the cytosol to the nucleus upon HCQ treatment. This observation is potentially consistent with evasion of intracellular innate immunity, and it could account for the increased transgene expression seen following HCQ treatment. Further work is required to clarify the molecular mechanism of action of HCQ, and it seems likely that the proposed interactions of HCQ are not mutually exclusive, as the drug may have multimodal effects.

It should be noted that a previous study using a much higher concentration of CQ (at 100 μM, compared with up to 12 μM in this study) showed a reduction in AAV2 transduction in a human hepatocellular carcinoma cell line.[33] The difference may be the result of the CQ concentrations used, e.g., greater lysosomal acidification at the much higher drug concentration may inhibit lysosomal escape of AAV particles. However, since CQ is known to be associated with a far greater chance of retinal toxicity than HCQ at therapeutic concentrations,

significant differences in their mechanisms of action and effects on AAV transduction may exist but are outside the scope of this translational study.

Our data demonstrate that HCQ is able to increase GFP transgene expression following AAV transduction *in vitro*, *ex vivo*, and *in vivo* across a range of species. The data also suggest that HCQ can improve AAV transduction of both RPE and photoreceptors, two key cell targets for retinal gene therapy. Subretinal injection of HCQ together with an AAV vector led to increased transgene expression, which was sustained up to 8 weeks. This effect was seen with both an AAV2 and AAV8(Y733F) vector, suggesting HCQ has an effect across multiple serotypes of AAV commonly used in retinal gene therapy. Furthermore, we have demonstrated HCQ to work with vectors containing both ubiquitous and photoreceptor-specific promoters, suggesting that adjunctive use of HCQ is capable of increasing transgene expression levels in photoreceptor cells, which are the primary target for many retinal degenerations.

While long-term high-dose systemic HCQ therapy is known to carry a cumulative risk of retinopathies,[34] the risk of retinal toxicity associated with locally administered HCQ was previously unknown. Our *in vivo* data indicate that the delivery of a single pulse of HCQ into the subretinal space was not associated with any retinal structural change, including preservation of the ellipsoid zone on the OCT within treated areas, which represents organized photoreceptor inner and outer segments up to 8 weeks post-injection. One of the limitations of the study is that, while HCQ enhanced retinal gene therapy in the healthy retina of wild-type mice without any sign of toxicity, it remains to be seen whether the effects would be the same in the degenerate retina of mouse models of retinitis pigmentosa, which would provide support for future clinical application.

The proportion of retinal cells that successfully acquire and maintain transgene expression determines the clinical efficacy of gene therapy in neurodegenerative diseases. For X-linked and autosomal recessive retinitis pigmentosa, which account for approximately 40% of patients with identified mutations, achieving over 50% photoreceptor transduction may be seen as a threshold for halting disease progression, since female carriers of X-linked mutations are usually minimally affected (e.g., choroideremia, X-linked retinitis pigmentosa associated with mutations in *RPGR* or *RP2*). Therefore, a 2-fold increase in transgene expression with the adjunctive use of HCQ has the potential to push the therapeutic effect beyond the threshold required to halt disease progression. Alternatively, co-administration of HCQ with the AAV vector could enable a lower vector dose to be used to achieve a given therapeutic effect, thus reducing the risk of inflammation and improving safety for the patient. The approach is broadly applicable and has the potential to augment the effects of existing gene therapies under investigation, without the need to modify the clinical grade vector, an important practical consideration given the prohibitive costs of developing gene therapies for orphan diseases.

MATERIALS AND METHODS

Vector Design

The vector pAAV2.CAG.GFP.WPRE.pA contained a GFP transgene under control of the ubiquitous CAG promoter with a Woodchuck hepatitis virus post-transcriptional regulatory element (WPRE) enhancer. The vector pAAV8(Y733F).GRK1.GFP.pA contained the reporter GFP under control of a photoreceptor-specific promoter GRK1. Both vectors were single-stranded AAVs.

AAV Production

HEK293T cells were grown in HYPERFlasks (Scientific Laboratory Supplies) and transfected with a total of 500 μg endotoxin-free plasmid using polyethylenimine (Sigma-Aldrich). The plasmid pCAG.GFP.WPRE.pA was co-transfected with pDG (PlasmidFactory) to package into recombinant AAV serotype 2, and pGRK1.GFP.pA was co-transfected with pRepCap and pHelper (pDeltaAdF6) for packaging into AAV serotype 8 Y733F. Then 3 days post-transfection, the cells were harvested, lysed, and treated with nuclease. The AAV population was isolated from the cell lysates by ultracentrifugation with an iodixanol gradient and purified using Amicon Ultra-15 100K filter units (Merck Millipore). The final preparations were washed and collected in sterile PBS. The purity of the AAV preparations were determined by SDS-PAGE analysis, followed by staining with EZBlue (Sigma-Aldrich) (Figure S1), and the titers were determined by qPCR. Lot 1 of AAV2.CAG.GFP.WPRE was used for Figure 1, lot 3 was used for Figure S5, and lot 2 was used for all other experiments.

Mice

Wild-type C57BL/6J mice (Charles River Laboratories) were maintained by the Biomedical Science Division, University of Oxford, UK. Mice were housed in a 12 h light-dark cycle, with food and water available *ad libitum*. All procedures were performed under general anesthesia. All animal procedures were undertaken in accordance with the Association for Research in Vision and Ophthalmology guidelines for the humane use of laboratory animals in ophthalmic research, and they were approved by local and national ethical and legal authorities.

Subretinal AAV Vector-Mediated Gene Therapy

For assessment of the activation of innate immune factors, 4-week-old female C57BL/6J mice were subretinally injected with 1.5 μL (1×10^9 gc) of the vector pAAV2.CAG.GFP.WPRE.pA (AAV2.GFP)[35] in the left eye and sham injected with PBS in the right eye (n = 3/time point). For GFP expression analysis, mice were injected with 1×10^8 gc (n = 7/time point). Two mice (four for GFP expression analysis) were left uninjected to determine baseline gene expression. Retinas were harvested at baseline and on days 3, 7, and 15 post-injection.

For assessment of the effect of HCQ *in vivo*, 7- to 8-week-old female C57BL/6J mice were subretinally injected with 1.2 μL (1.2×10^8 gc) AAV2.GFP, with injections of a suspension of AAV2.GFP with either 3.13 μM (n = 7) or 18.75 μM (n = 6) HCQ performed in the contralateral eye. An additional nine mice were injected with 18.75 μM

HCQ and AAV in one eye and AAV only in the paired eye to supplement the cohort for western blot analysis (n = 13). To assess the toxicity and autofluorescence of HCQ, 7- to 8-week-old female C57BL/6J mice were subretinally injected with 1.2 μL 18.75 μM HCQ, with sham injections of PBS undertaken in the paired eye (n = 12).

The 4- to 5-week-old 129S2/SvHsd mice were subretinally injected with 1 μL (1×10^8 gc) AAV8(Y733F).GRK1.GFP, with injections of AAV8(Y733F).GRK1.GFP with 18.75 μM HCQ performed in the paired eye (n = 9).

Cell and Tissue Cultures

MEF cells were cultured in DMEM supplemented with L-glutamine (2 mM), penicillin (100 U/mL), streptomycin (100 μg/mL), and 10% fetal bovine serum. Cells were maintained at 37°C in a humidified 5% CO_2 environment. Wild-type and *Cgas*$^{-/-}$ MEFs were transduced with AAV2.GFP at an MOI of 1,000. When appropriate, cells were incubated in media with HCQ or CQ for 1 h prior to transduction. The cells were cultured in HCQ- or CQ-containing media for 3 days post-transduction, at which point fluorescence and transmission images were acquired and cells were harvested for flow cytometry. TLR9 was activated in wild-type MEFs by pre-treatment with 754.6 μM CpG-A (5′-GGGGGACGATCGTCGGGGGG-3′) for 30 min prior to transduction with AAV2.GFP. CpG-A was phosphorothioated at each base (Integrated DNA Technologies). For assessing viral entry, cell pellets were washed four times with PBS and harvested for DNA extraction 0, 10, 30, and 60 min post-transduction. For assessing subcellular localization, cell pellets were washed four times with PBS, and the cytosolic and nuclear fractions were isolated using the Cell Fractionation Kit (ab109719, Abcam), according to the manufacturer's instructions.

Primary NHP RPE cells were derived from rhesus macaque (*M. mullata*) eyes collected post-mortem from animals euthanized for other purposes, provided by the MRC Centre for Macaques (Porton Down, UK). After enucleation, the cornea and lens were removed under direct visualization with a surgical microscope. Radial incisions were made toward the posterior pole to flatten the eyecup. The retina was removed by blunt dissection, and the remaining eyecup was placed in media and stored on ice until the RPE cells were removed. RPE cells were detached using 2.5% trypsin, and they were cultured in advanced DMEM supplemented with L-glutamine (2 mM), penicillin (100 U/mL), streptomycin (100 μg/mL), and 10% fetal bovine serum. Cells were maintained at 37°C in a humidified 5% CO_2 environment. The RPE cells were incubated in media with 0, 3.13, or 18.75 μM HCQ for 1 h prior to transduction with AAV2.GFP at 2×10^9 gc/well of a 12-well plate (n = 3). The cells were cultured in HCQ-containing media for 3 days post-transduction, at which point fluorescence and transmission images were acquired and the cells were harvested for RNA and protein extraction using buffer RLT (QIAGEN).

Fresh human retinal explants were collected from two patients with informed consent during routine retinal detachment surgery where a retinectomy was clinically indicated, with approval by the UK National Research Ethics Committee (10/H0505/8). Small retinal fragments approximately 500 μm in diameter were obtained using a 23G cutter of a surgical vitrectomy system (Constellation Vision System, Alcon). Within 1 h of tissue collection, individual retinal fragments were transferred using a Pasteur pipette into organotypic culture inserts (Falcon, Corning) within 24-well plates. The retinal explants were cultured in 500 μL Neurobasal-A medium supplemented with L-glutamine (0.8 mM), penicillin (100 U/mL), streptomycin (100 μg/mL), 2% B-27 Supplement, and 1% N-2 Supplement (Thermo Fisher Scientific). Samples were maintained at 34°C in a humidified 5% CO_2 environment. After 24 h, the fragments were transferred to culture media containing either 0 or 3.13 μM HCQ for 1 h prior to transduction with AA2.GFP at 1×10^9 gc/well (n = 3/patient).

Fluorescence and transmission microscopy images were obtained on alternate days up to day 11 under standardized conditions. The culture media were replaced on alternate days with fresh media containing the same concentration of HCQ. To measure the mean gray value of an explant, as a surrogate for GFP fluorescence, the area of unfolded retina was traced on the transmission image and overlaid onto the fluorescence image in ImageJ (NIH, USA).[22,36] To account for background autofluorescence of the well, the mean gray value of a 2.54-mm band around the retinal tissue was subtracted from the mean gray value of the tissue. Normalized gray value was then calculated by subtracting the mean gray value of untransduced retinal tissue (treated with the same HCQ concentration) to account for any background autofluorescence of the tissue and drug.

Flow Cytometry

Dissociated cells were fixed in 4% methanol-free paraformaldehyde in PBS for 15 min at room temperature. The fixative was replaced with 1% BSA in PBS and samples were stored on ice until assessment. Cells were incubated with the cell viability dye 7-AAD for 5 min in the dark immediately prior to flow cytometry analysis using a BD LSRFortessa. Fluorescent light was measured using a blue laser at the band-pass filter 695 nm/40 mW and 530 nm/30 mW to detect the fluorochromes of 7-AAD and GFP, respectively. Cells expressing GFP were gated for using untransduced controls, and dead (7-AAD-positive) cells were excluded using a dead cell population control prepared by heating the samples to 60°C for 20 min.

qRT-PCR

Total RNA was extracted from mouse retinae and NHP RPE cells using the RNeasy mini kit (QIAGEN). An additional DNA digestion step was included for the extraction from NHP RPE cells using the RNase-free DNase kit (QIAGEN). Buffer RLT lysates were kept from the NHP RPE cells for protein extraction according to the manufacturer's instructions. cDNA was synthesized with an oligonucleotide deoxythymine (dT) primer using the Superscript III Kit (Invitrogen). qPCR of the mouse retinal cDNA samples was undertaken using iTaq Universal SYBR Green Mastermix (Bio-Rad) for *Apobec3*, *Apobec2*, and *Aicda*. qPCR of the other innate immune

genes (*Tlr9*, *Mb21d1*, *Ddx58*, *Sting*, *Trim21*, *Ifn-γ*, *Tnfα*, *Cxcl10*, and *Isg15*) was undertaken using TaqMan probes (Thermo Fisher Scientific) and TaqMan Fast Universal PCR Master Mix (Applied Biosciences). qPCR of *GFP* expression in mouse retinae and NHP RPE cells was performed using specific TaqMan probes and Fast Universal PCR Master Mix. Gene expression of all genes was normalized to *β-actin* and analyzed according to the $2^{(-\Delta\Delta Ct)}$ method.

DNA was extracted using the QIAamp DNA Mini Kit (QIAGEN) from wild-type MEFs; an additional RNase digest was performed on the cell fractionation samples. qPCR was performed using *GFP* and *Gapdh* genomic DNA copy number TaqMan probes and Fast Universal PCR Master Mix.

In Vivo Retinal Imaging

cSLO imaging was performed on anesthetized C57BL/6J mice at 2, 4, and 8 weeks post-subretinal gene therapy using a 55° lens (Spectralis HRA, Heidelberg Engineering, Heidelberg, Germany), with a real-time average process of 25 frames and a standardized signal detector sensitivity of 70. Fundus autofluorescence imaging was measured within a ring section with a radius between 350 and 860 pixels from the optic disc, using the ImageJ software (NIH).[36] Animals were also subject to wide-field OCT (Spectralis HRA, Heidelberg Engineering) 2, 4, and 8 weeks post-injection. Mice were scanned using a 55° lens, and 8 radial sections were taken with a real-time average process of 25 frames. The total retinal thickness was manually measured 3,700 nm from the optic disc at alternate radial sections using a calliper. Mice with unintended intravitreal injections, significant subretinal bleeding, or opacities were excluded from analysis. For the AAV-injected mice, the number included for final SLO and OCT analysis was n = 5 for those injected with 3.13 μM HCQ and n = 4 for mice injected with 18.75 μM HCQ, and for western blot analysis the number included was n = 12. For mice injected with HCQ only in the toxicity study, the final cohort size was n = 8.

Western Blot Analysis

Mouse retinae were lysed in radioimmunoprecipitation (RIPA) buffer supplemented with protease inhibitors (PIs) and homogenized using a hand-held homogenizer. NHP RPE protein lysates extracted from buffer RLT (QIAGEN) were resuspended in 1% SDS. For confirmation of the isolation of cytosolic versus nuclear fractions, PI was added to Buffer A (ab109719, Abcam) before cell fractionation. Cytosolic proteins were lysed in Buffer A and nuclear proteins were lysed in RIPA buffer supplemented with PI.

Protein concentration was measured using a bicinchoninic assay (Thermo Fisher Scientific). Protein samples were separated using SDS-PAGE on a 10% or 4%–20% (for Figure S5A) Criterion TGX Precast gel (Bio-Rad), and they were transferred to a polyvinylidene difluoride membrane using the TransBlot Turbo system (Bio-Rad). Membranes were blocked in 3% BSA in PBS + 0.1% Tween-20 prior to incubation for 1 h with anti-GFP (ab32146, Abcam) or anti-β-actin (AM4302, Thermo Fisher Scientific) monoclonal primary antibodies. Cell fractionation membranes were blocked in 5% donkey serum in Tris-buffered saline + 0.1% Tween-20 prior to incubation with anti-histone H3 (ab7291, Abcam) and anti-α-tubulin (ab1791, Abcam) antibodies. After washing in buffer, GFP- and β-actin-probed membranes were incubated with a corresponding horseradish peroxidase-conjugated secondary antibody for 30 min (Abcam) and developed using Clarity ECL (Bio-Rad). Histone H3- and α-tubulin-probed membranes were incubated with corresponding IRDye secondary antibodies (LI-COR Biosciences). Membranes were detected using the Odyssey Imaging System (LI-COR Biosciences). Protein band densities were quantified using the ImageStudio Lite software (LI-COR Biosciences).

Statistical Analysis

All statistical analysis was performed on GraphPad Prism 7.00. Datasets that were normally distributed were analyzed using a parametric test (t test or ANOVA). Data were assessed for equal variance using the Brown-Forsythe test. Data that were skewed or had an unequal variance were analyzed using a non-parametric test (Wilcoxon signed rank test). Multiple comparison corrections were performed using a Dunnett or Šídák's test for a one- or two-way ANOVA, respectively. Paired data were handled accordingly. All statistical tests were performed using an alpha level of 0.05 and using two-tailed testing. The n and p values are indicated in the figure legends where appropriate. Data are presented as mean ± SEM.

SUPPLEMENTAL INFORMATION

Supplemental Information can be found online at https://doi.org/10.1016/j.omtm.2019.05.012.

AUTHOR CONTRIBUTIONS

Conceptualization, L.C.C., A.R.B., C.R., R.E.M., and K.X.; Methodology, L.C.C., A.R.B., S.L.C., M.I.P., M.E.M., H.F., and C.R.; Formal Analysis, L.C.C., S.L.C., and H.F.; Investigation, L.C.C., A.R.B., S.L.C., M.I.P., M.E.M., and H.F.; Resources, C.R.; Writing – Original Draft, L.C.C.; Writing – Review & Editing, L.C.C., A.R.B., M.I.P., M.E.M., R.E.M., and K.X.; Supervision, R.E.M. and K.X.; Funding Acquisition, K.X.

CONFLICTS OF INTEREST

K.X., L.C.C., R.E.M., A.R.B., and M.I.P. have filed a patent on behalf of the University of Oxford relating to the use of hydroxychloroquine as an adjunct for gene therapy (PCT/EP2019/053193). R.E.M. is a scientific co-founder of Nightstar Therapeutics Inc., a gene therapy company established by the University of Oxford and originally funded by the Wellcome Trust through Syncona Partners Ltd.

ACKNOWLEDGMENTS

The project was funded by the Oxford University Medical Sciences Division Medical Research Fund (MRF/MT2014/2114) (K.X.), the Oxford University Clinical Academic Graduate School (K.X.), the Academy of Medical Sciences (SGL016\1034) (K.X.), Fight for Sight UK (5039/5040) (R.E.M. and K.X.), and the National Institute for Health Research (K.X.). K.X. and L.C.C. are indebted to Dr. Leo James at the MRC Laboratory of Molecular Biology for kind gifts of

wild-type and *Cgas*$^{-/-}$ MEF cell lines, discussion, and support during the production of this work.

REFERENCES

1. MacLaren, R.E., Groppe, M., Barnard, A.R., Cottriall, C.L., Tolmachova, T., Seymour, L., Clark, K.R., During, M.J., Cremers, F.P., Black, G.C., et al. (2014). Retinal gene therapy in patients with choroideremia: initial findings from a phase 1/2 clinical trial. Lancet *383*, 1129–1137.
2. Bainbridge, J.W., Smith, A.J., Barker, S.S., Robbie, S., Henderson, R., Balaggan, K., Viswanathan, A., Holder, G.E., Stockman, A., Tyler, N., et al. (2008). Effect of gene therapy on visual function in Leber's congenital amaurosis. N. Engl. J. Med. *358*, 2231–2239.
3. Pierce, E.A., and Bennett, J. (2015). The Status of RPE65 Gene Therapy Trials: Safety and Efficacy. Cold Spring Harb. Perspect. Med. *5*, a017285.
4. Edwards, T.L., Jolly, J.K., Groppe, M., Barnard, A.R., Cottriall, C.L., Tolmachova, T., Black, G.C., Webster, A.R., Lotery, A.J., Holder, G.E., et al. (2016). Visual Acuity after Retinal Gene Therapy for Choroideremia. N. Engl. J. Med. *374*, 1996–1998.
5. George, L.A., Sullivan, S.K., Giermasz, A., Rasko, J.E.J., Samelson-Jones, B.J., Ducore, J., Cuker, A., Sullivan, L.M., Majumdar, S., Teitel, J., et al. (2017). Hemophilia B Gene Therapy with a High-Specific-Activity Factor IX Variant. N. Engl. J. Med. *377*, 2215–2227.
6. Rangarajan, S., Walsh, L., Lester, W., Perry, D., Madan, B., Laffan, M., Yu, H., Vettermann, C., Pierce, G.F., Wong, W.Y., and Pasi, K.J. (2017). AAV5-Factor VIII Gene Transfer in Severe Hemophilia A. N. Engl. J. Med. *377*, 2519–2530.
7. Le Guiner, C., Servais, L., Montus, M., Larcher, T., Fraysse, B., Moullec, S., Allais, M., François, V., Dutilleul, M., Malerba, A., et al. (2017). Long-term microdystrophin gene therapy is effective in a canine model of Duchenne muscular dystrophy. Nat. Commun. *8*, 16105.
8. Simonato, M., Bennett, J., Boulis, N.M., Castro, M.G., Fink, D.J., Goins, W.F., Gray, S.J., Lowenstein, P.R., Vandenberghe, L.H., Wilson, T.J., et al. (2013). Progress in gene therapy for neurological disorders. Nat. Rev. Neurol. *9*, 277–291.
9. Russell, S., Bennett, J., Wellman, J.A., Chung, D.C., Yu, Z.F., Tillman, A., Wittes, J., Pappas, J., Elci, O., McCague, S., et al. (2017). Efficacy and safety of voretigene neparvovec (AAV2-hRPE65v2) in patients with RPE65-mediated inherited retinal dystrophy: a randomised, controlled, open-label, phase 3 trial. Lancet *390*, 849–860.
10. Reichel, F.F., Dauletbekov, D.L., Klein, R., Peters, T., Ochakovski, G.A., Seitz, I.P., Wilhelm, B., Ueffing, M., Biel, M., Wissinger, B., et al.; RD-CURE Consortium (2017). AAV8 Can Induce Innate and Adaptive Immune Response in the Primate Eye. Mol. Ther. *25*, 2648–2660.
11. Mingozzi, F., and High, K.A. (2011). Immune responses to AAV in clinical trials. Curr. Gene Ther. *11*, 321–330.
12. Rabinowitz, J., Chan, Y.K., and Samulski, R.J. (2019). Adeno-associated Virus (AAV) versus Immune Response. Viruses *11*, E102.
13. Shirley, J.L., and Herzog, R.W. (2018). AAV Immunogenicity: New Answers Create New Questions. Mol. Ther. *26*, 2538–2539.
14. Bainbridge, J.W., Mehat, M.S., Sundaram, V., Robbie, S.J., Barker, S.E., Ripamonti, C., Georgiadis, A., Mowat, F.M., Beattie, S.G., Gardner, P.J., et al. (2015). Long-term effect of gene therapy on Leber's congenital amaurosis. N. Engl. J. Med. *372*, 1887–1897.
15. Guy, J., Feuer, W.J., Davis, J.L., Porciatti, V., Gonzalez, P.J., Koilkonda, R.D., Yuan, H., Hauswirth, W.W., and Lam, B.L. (2017). Gene Therapy for Leber Hereditary Optic Neuropathy: Low- and Medium-Dose Visual Results. Ophthalmology *124*, 1621–1634.
16. Xue, K., Jolly, J.K., Barnard, A.R., Rudenko, A., Salvetti, A.P., Patrício, M.I., Edwards, T.L., Groppe, M., Orlans, H.O., Tolmachova, T., et al. (2018). Beneficial effects on vision in patients undergoing retinal gene therapy for choroideremia. Nat. Med. *24*, 1507–1512.
17. An, J., Woodward, J.J., Sasaki, T., Minie, M., and Elkon, K.B. (2015). Cutting edge: Antimalarial drugs inhibit IFN-β production through blockade of cyclic GMP-AMP synthase-DNA interaction. J. Immunol. *194*, 4089–4093.
18. Kuznik, A., Bencina, M., Svajger, U., Jeras, M., Rozman, B., and Jerala, R. (2011). Mechanism of endosomal TLR inhibition by antimalarial drugs and imidazoquinolines. J. Immunol. *186*, 4794–4804.
19. An, J., Minie, M., Sasaki, T., Woodward, J.J., and Elkon, K.B. (2017). Antimalarial Drugs as Immune Modulators: New Mechanisms for Old Drugs. Annu. Rev. Med. *68*, 317–330.
20. Rutz, M., Metzger, J., Gellert, T., Luppa, P., Lipford, G.B., Wagner, H., and Bauer, S. (2004). Toll-like receptor 9 binds single-stranded CpG-DNA in a sequence- and pH-dependent manner. Eur. J. Immunol. *34*, 2541–2550.
21. Marmor, M.F., Kellner, U., Lai, T.Y., Melles, R.B., and Mieler, W.F.; American Academy of Ophthalmology (2016). Recommendations on Screening for Chloroquine and Hydroxychloroquine Retinopathy (2016 Revision). Ophthalmology *123*, 1386–1394.
22. Orlans, H.O., Edwards, T.L., De Silva, S.R., Patrício, M.I., and MacLaren, R.E. (2018). Human Retinal Explant Culture for Ex Vivo Validation of AAV Gene Therapy. Methods Mol. Biol. *1715*, 289–303.
23. Zhu, J., Huang, X., and Yang, Y. (2009). The TLR9-MyD88 pathway is critical for adaptive immune responses to adeno-associated virus gene therapy vectors in mice. J. Clin. Invest. *119*, 2388–2398.
24. Kawai, T., and Akira, S. (2010). The role of pattern-recognition receptors in innate immunity: update on Toll-like receptors. Nat. Immunol. *11*, 373–384.
25. Aveleira, C.A., Lin, C.M., Abcouwer, S.F., Ambrósio, A.F., and Antonetti, D.A. (2010). TNF-α signals through PKCζ/NF-κB to alter the tight junction complex and increase retinal endothelial cell permeability. Diabetes *59*, 2872–2882.
26. Claudio, L., Martiney, J.A., and Brosnan, C.F. (1994). Ultrastructural studies of the blood-retina barrier after exposure to interleukin-1 beta or tumor necrosis factor-alpha. Lab. Invest. *70*, 850–861.
27. Bamforth, S.D., Lightman, S., and Greenwood, J. (1996). The effect of TNF-alpha and IL-6 on the permeability of the rat blood-retinal barrier in vivo. Acta Neuropathol. *91*, 624–632.
28. Ablasser, A., Schmid-Burgk, J.L., Hemmerling, I., Horvath, G.L., Schmidt, T., Latz, E., and Hornung, V. (2013). Cell intrinsic immunity spreads to bystander cells via the intercellular transfer of cGAMP. Nature *503*, 530–534.
29. Li, L., Eter, N., and Heiduschka, P. (2015). The microglia in healthy and diseased retina. Exp. Eye Res. *136*, 116–130.
30. Reinert, L.S., Lopušná, K., Winther, H., Sun, C., Thomsen, M.K., Nandakumar, R., Mogensen, T.H., Meyer, M., Vægter, C., Nyengaard, J.R., et al. (2016). Sensing of HSV-1 by the cGAS-STING pathway in microglia orchestrates antiviral defence in the CNS. Nat. Commun. *7*, 13348.
31. Olson, J.K., and Miller, S.D. (2004). Microglia initiate central nervous system innate and adaptive immune responses through multiple TLRs. J. Immunol. *173*, 3916–3924.
32. Wallace, D.J., Gudsoorkar, V.S., Weisman, M.H., and Venuturupalli, S.R. (2012). New insights into mechanisms of therapeutic effects of antimalarial agents in SLE. Nat. Rev. Rheumatol. *8*, 522–533.
33. Li, C., He, Y., Nicolson, S., Hirsch, M., Weinberg, M.S., Zhang, P., Kafri, T., and Samulski, R.J. (2013). Adeno-associated virus capsid antigen presentation is dependent on endosomal escape. J. Clin. Invest. *123*, 1390–1401.
34. Melles, R.B., and Marmor, M.F. (2014). The risk of toxic retinopathy in patients on long-term hydroxychloroquine therapy. JAMA Ophthalmol. *132*, 1453–1460.
35. Patrício, M.I., Barnard, A.R., Orlans, H.O., McClements, M.E., and MacLaren, R.E. (2017). Inclusion of the Woodchuck Hepatitis Virus Posttranscriptional Regulatory Element Enhances AAV2-Driven Transduction of Mouse and Human Retina. Mol. Ther. Nucleic Acids *6*, 198–208.
36. Schneider, C.A., Rasband, W.S., and Eliceiri, K.W. (2012). NIH Image to ImageJ: 25 years of image analysis. Nat. Methods *9*, 671–675.
37. Ablasser, A., Bauernfeind, F., Hartmann, G., Latz, E., Fitzgerald, K.A., and Hornung, V. (2009). RIG-I-dependent sensing of poly(dA:dT) through the induction of an RNA polymerase III-transcribed RNA intermediate. Nat. Immunol. *10*, 1065–1072.
38. Sun, L., Wu, J., Du, F., Chen, X., and Chen, Z.J. (2013). Cyclic GMP-AMP synthase is a cytosolic DNA sensor that activates the type I interferon pathway. Science *339*, 786–791.

39. Wu, J., Sun, L., Chen, X., Du, F., Shi, H., Chen, C., and Chen, Z.J. (2013). Cyclic GMP-AMP is an endogenous second messenger in innate immune signaling by cytosolic DNA. Science *339*, 826–830.

40. Ishikawa, H., Ma, Z., and Barber, G.N. (2009). STING regulates intracellular DNA-mediated, type I interferon-dependent innate immunity. Nature *461*, 788–792.

41. Burdette, D.L., Monroe, K.M., Sotelo-Troha, K., Iwig, J.S., Eckert, B., Hyodo, M., Hayakawa, Y., and Vance, R.E. (2011). STING is a direct innate immune sensor of cyclic di-GMP. Nature *478*, 515–518.

42. Mallery, D.L., McEwan, W.A., Bidgood, S.R., Towers, G.J., Johnson, C.M., and James, L.C. (2010). Antibodies mediate intracellular immunity through tripartite motif-containing 21 (TRIM21). Proc. Natl. Acad. Sci. USA *107*, 19985–19990.

43. Watkinson, R.E., Tam, J.C., Vaysburd, M.J., and James, L.C. (2013). Simultaneous neutralization and innate immune detection of a replicating virus by TRIM21. J. Virol. *87*, 7309–7313.

44. Lazear, H.M., Nice, T.J., and Diamond, M.S. (2015). Interferon-λ: Immune Functions at Barrier Surfaces and Beyond. Immunity *43*, 15–28.

45. Lee, E.Y., Lee, Z.H., and Song, Y.W. (2009). CXCL10 and autoimmune diseases. Autoimmun. Rev. *8*, 379–383.

46. Perng, Y.C., and Lenschow, D.J. (2018). ISG15 in antiviral immunity and beyond. Nat. Rev. Microbiol. *16*, 423–439.

47. Harris, R.S., and Dudley, J.P. (2015). APOBECs and virus restriction. Virology *479-480*, 131–145.

48. Knisbacher, B.A., Gerber, D., and Levanon, E.Y. (2016). DNA Editing by APOBECs: A Genomic Preserver and Transformer. Trends Genet. *32*, 16–28.

49. Neuberger, M.S., and Rada, C. (2007). Somatic hypermutation: activation-induced deaminase for C/G followed by polymerase eta for A/T. J. Exp. Med. *204*, 7–10.

OMTM, Volume *14*

Supplemental Information

Enhancement of Adeno-Associated Virus-Mediated Gene Therapy Using Hydroxychloroquine in Murine and Human Tissues

Laurel C. Chandler, Alun R. Barnard, Sarah L. Caddy, Maria I. Patrício, Michelle E. McClements, Howell Fu, Cristina Rada, Robert E. MacLaren, and Kanmin Xue

Supplemental figures

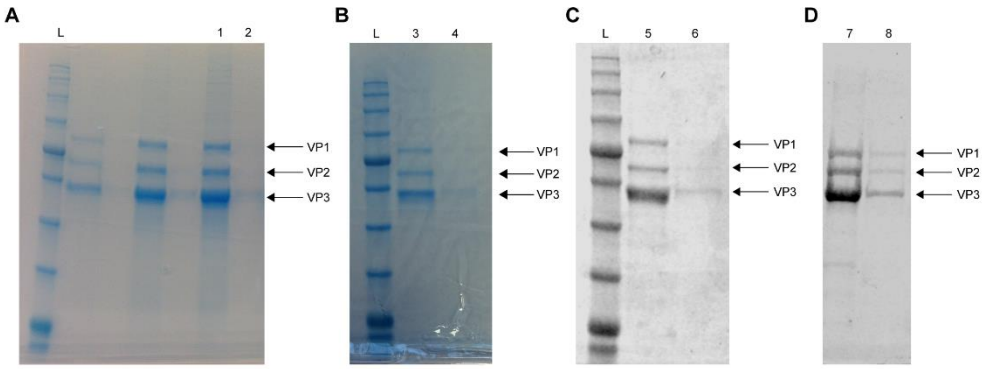

Fig S1. EZBlue stained SDS-PAGE of AAV vectors to assess purity. Image of the purified preparation of AAV2.GFP (**A**) lot #1, (**B**) lot #2 and (**C**) lot #3. (**D**) Purified preparation of AAV8(Y733F).GRK1.GFP, image taken on Odyssey Imaging System (LI-COR Biosciences). The presence of AAV virion protein 1 (VP1), VP2 and VP3 are indicated. Lanes 1, 3 & 5: AAV2.GFP concentrated sample; lanes 2, 4 & 6: AAV2.GFP wash; lane 7: concentrated AAV8(Y733F).GRK1.GFP; lane 8: AAV8(Y733F).GRK1.GFP wash; L: protein ladder.

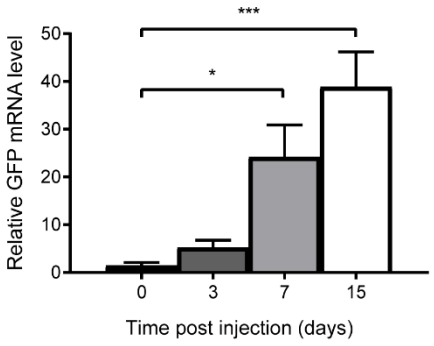

Fig S2. GFP expression following AAV2.GFP subretinal injection *in vivo*. Wild-type C57BL/6 mice were subretinally injected with AAV2.GFP ($1.2x10^8$ gc). RNA was extracted from the mouse retina at baseline (n=5) and on day 3 (n=6), 7 (n=6) and 15 (n=7) post-injection. GFP expression was quantified using RT-qPCR. Relative expression was calculated as a mean fold change (±SEM) relative to the mean of uninjected baseline controls. *$p \leq 0.05$ and ***$p \leq 0.001$ (one-way ANOVA with Dunn's multiple comparison test).

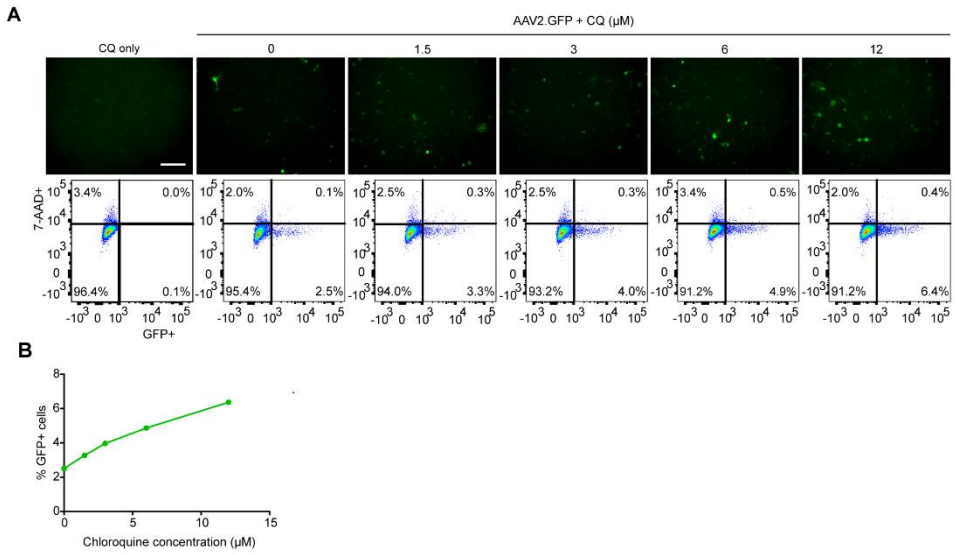

Fig S3. Chloroquine (CQ) increases AAV transduction in MEFs. Wild-type MEFs were pre-treated with 0, 1.5, 3, 6 or 12 μM of CQ for 1h prior to transduction with AAV2.GFP at a MOI of 1000. (**A**) Representative fluorescence microscopy images acquired at day 3 post-transduction (scale bar: 200 μm) shown alongside flow cytometry analyses gated for GFP fluorescence and the cell viability marker, 7-AAD. (**B**) Proportion of GFP positive (GFP+) cells expressed as a percentage of the total number of live (7-AAD negative) cells at day 3 (n=1).

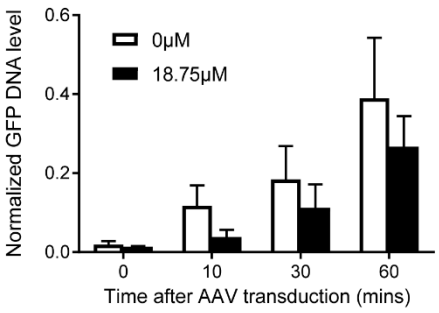

Fig S4. Effect of HCQ on intracellular AAV genome load post-transduction. Wild-type MEFs were pre-treated with HCQ for 1h prior to transduction with AAV2.GFP at a MOI of 1000. Cells treated with 0 or 18.75 μM HCQ were harvested at 0, 10, 30 and 60 mins post-transduction. DNA was extracted and *GFP* DNA copy numbers were quantified using qPCR. *GFP* DNA was normalized to *Gapdh* genomic DNA levels (±SEM, n=3).

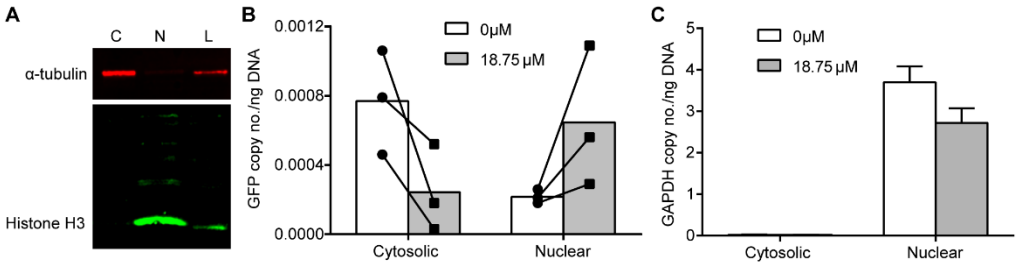

Fig S5. HCQ influences the subcellular distribution of AAV viral genomes. Wild-type MEFs were pre-treated with 0 or 18.75 μM HCQ for 1h prior to transduction with AAV2.GFP at a MOI of 1000. Cells were harvested 24h post-transduction and DNA was extracted. (**A**) Western blot of α-tubulin and histone H3 protein expression in cytosolic [C] and nuclear [N] fractions, and unfractionated whole cell lysate [L]. (**B**) Paired data of 0 or 18.75 μM HCQ treated samples plotted onto mean *GFP* DNA copy numbers per ng of DNA quantified using qPCR (n=3). (**C**) *Gapdh* genomic DNA levels (±SEM, n=3).

International Journal of
Molecular Sciences

MDPI

Review

Immunomodulatory Effects of Hydroxychloroquine and Chloroquine in Viral Infections and Their Potential Application in Retinal Gene Therapy

Laurel C. Chandler [1,2,*], Imran H. Yusuf [1,2], Michelle E. McClements [1], Alun R. Barnard [1,2], Robert E. MacLaren [1,2] and Kanmin Xue [1,2,*]

1 Nuffield Laboratory of Ophthalmology, Nuffield Department of Clinical Neurosciences & NIHR Oxford Biomedical Research Centre, University of Oxford, Oxford OX3 9DU, UK
2 Oxford Eye Hospital, Oxford University Hospitals NHS Foundation Trust, Oxford OX3 9DU, UK
* Correspondence: laurel.chandler@merton.ox.ac.uk (L.C.C.); kanmin.xue@eye.ox.ac.uk (K.X.)

Received: 6 June 2020; Accepted: 9 July 2020; Published: 14 July 2020

Abstract: Effective treatment of retinal diseases with adeno-associated virus (AAV)-mediated gene therapy is highly dependent on the proportion of successfully transduced cells. However, due to inflammatory reactions at high vector doses, adjunctive treatment may be necessary to enhance the therapeutic outcome. Hydroxychloroquine and chloroquine are anti-malarial drugs that have been successfully used in the treatment of autoimmune diseases. Evidence suggests that at high concentrations, hydroxychloroquine and chloroquine can impact viral infection and replication by increasing endosomal and lysosomal pH. This effect has led to investigations into the potential benefits of these drugs in the treatment of viral infections, including human immunodeficiency virus and severe acute respiratory syndrome coronavirus-2. However, at lower concentrations, hydroxychloroquine and chloroquine appear to exert immunomodulatory effects by inhibiting nucleic acid sensors, including toll-like receptor 9 and cyclic GMP-AMP synthase. This dose-dependent effect on their mechanism of action supports observations of increased viral infections associated with lower drug doses. In this review, we explore the immunomodulatory activity of hydroxychloroquine and chloroquine, their impact on viral infections, and their potential to improve the efficacy and safety of retinal gene therapy by reducing AAV-induced immune responses. The safety and practicalities of delivering hydroxychloroquine into the retina will also be discussed.

Keywords: hydroxychloroquine; chloroquine; adeno-associated virus; AAV; gene therapy; innate immunity; TLR9; cGAS; SARS-CoV-2

1. Introduction

The 4-aminoquinoline anti-malarial drugs, hydroxychloroquine and chloroquine, have been frequently used in the treatment of autoimmune diseases such as systemic lupus erythematosus and rheumatoid arthritis. Their utility in dampening these autoimmune diseases provides insights into their immunomodulatory activities [1]. Hydroxychloroquine and chloroquine are weak bases that accumulate within acidic intracellular compartments, such as lysosomes [2]. When used at high concentrations, hydroxychloroquine and chloroquine appear to lead to a dose-dependent increase in endosomal and lysosomal pH [3,4]. In contrast, low concentrations of hydroxychloroquine and chloroquine may exert a separate immunomodulatory effect on intracellular innate immune responses to viral infections, with minimal interference in lysosomal activity [5,6].

Adeno-associated viruses (AAV) are the most commonly used viral vectors for gene therapy due to their broad tissue tropism, relatively low immunogenicity, and lack of pathogenicity.

AAV are non-replicating, non-enveloped parvoviruses with a single-stranded DNA (ssDNA) genome. A recombinant AAV transgene typically contains a therapeutic gene expression cassette driven by a ubiquitous or tissue-specific promoter with a generic polyadenylation signal. The cassette is flanked by viral inverted terminal repeats (ITRs), which aid persistence through the formation of concatemeric episomes within the host cell nucleus [7]. The episomes can sustain long-term transgene expression while minimising the potential for mutagenesis. Nonetheless, AAV-specific immune responses have been observed, which may induce potentially harmful inflammatory reactions and compromise the outcome of gene therapy [8].

AAV-mediated gene therapies have been successfully applied to a number of monogenic retinal dystrophies, including *RPE65*-associated Leber congenital amaurosis which has received Food and Drug Administration (FDA) approval, and choroideremia and *RPGR*-associated X-linked retinitis pigmentosa which are in advanced clinical trials [9–14]. Despite promising results in clinical trials, dose-dependent immunogenicity of AAV has been observed following retinal gene therapy, requiring high-dose immunosuppression in some cases [14–17]. There is thus interest in adjuvant therapies, either local or systemic, to reduce inflammatory responses and improve the long-term durability of gene therapies.

In this review, we discuss the immunomodulatory effects of hydroxychloroquine and chloroquine and how these might be relevant in the treatment of viral infections. We will then discuss how hydroxychloroquine might be used to control immune responses to AAV and enhance the efficacy of gene therapy.

2. Immunomodulatory Mechanisms of Hydroxychloroquine and Chloroquine

Hydroxychloroquine and chloroquine have been used for many decades in the treatment of a wide range of infections, including malaria (prozozoal), Q fever (bacterial), and human immunodeficiency virus (HIV) (viral), and autoimmune diseases such as systemic lupus erythematosus and rheumatoid arthritis [18]. Despite the proposal of numerous putative modes of action involving interactions with a range of molecular targets and signalling pathways, the immunomodulatory effects of hydroxychloroquine and chloroquine remain uncertain.

2.1. Effects on Intracellular Innate Immune Responses

A major advance in the effort to understand the mechanism of action of hydroxychloroquine and chloroquine was the discovery of their antagonistic effects on members of the toll-like receptor (TLR) family, a group of pattern recognition receptors (PRRs) that can detect molecular signatures of pathogens, such as bacteria and viruses, in order to elicit rapid intracellular immune responses [19]. Within this family, TLR3, TLR7, TLR8, and TLR9 are nucleic acid sensors that are exclusively found within endosomes so to minimise exposure to self-DNA or –RNA [20]. TLR3 detects double-stranded RNA (dsRNA) [21], TLR7 and TLR8 recognise single-stranded RNA (ssRNA) [22], and TLR9 is activated by DNA containing unmethylated CpGs which are abundant in microbial but rare in vertebrate genomes (i.e., 60–90% of mammalian CpGs are methylated) [23,24]. These nucleic acid ligands are also common features of viral genomes, thus TLRs play an important role in the detection of viruses within cells as part of the innate immune defence against viral infections. Initial in vitro studies demonstrated that chloroquine could suppress the stimulatory activity of CpG-oligodeoxynucleotides (ODNs) at concentrations ≤10 μM, thereby inhibiting cytokine release [5,25]. Subsequent studies demonstrated the dose-dependent inhibition of CpG-ODN binding to TLR9 by ≤2.5 μM chloroquine in human embryonic kidney 293 (HEK293) cells [26] (Figure 1). Although this interaction was optimal in acidic endosomal environments at pH 5.5–6.5 [26], TLR9 inhibition can be achieved with significantly lower concentrations of chloroquine than that needed to alter the pH of endosomal compartments (≤20 μM) [4–6]. Based on these findings, it was proposed that hydroxychloroquine and chloroquine could bind to CpG-containing nucleic acids and induce conformational changes that prevent them from interacting with and activating TLR9 [6,27]. Furthermore, chloroquine inhibited ssRNA-mediated

TLR8 activation and poly(I:C) (synthetic analogue of dsRNA)-mediated TLR3 activation in HEK293 cells in a dose-dependent manner (≤20 μM) [6]. In human monocyte-derived dendritic cells and peripheral blood mononuclear cells (PBMCs), chloroquine inhibited poly(I:C)-induced TLR3 responses at concentrations ≤10 μM [28]. Chloroquine has also been shown to inhibit TLR7-mediated responses to small nuclear ssRNA in human PBMCs at a concentration ≤10 μM, resulting in the downregulation of IFN-α expression [29] (Figure 1).

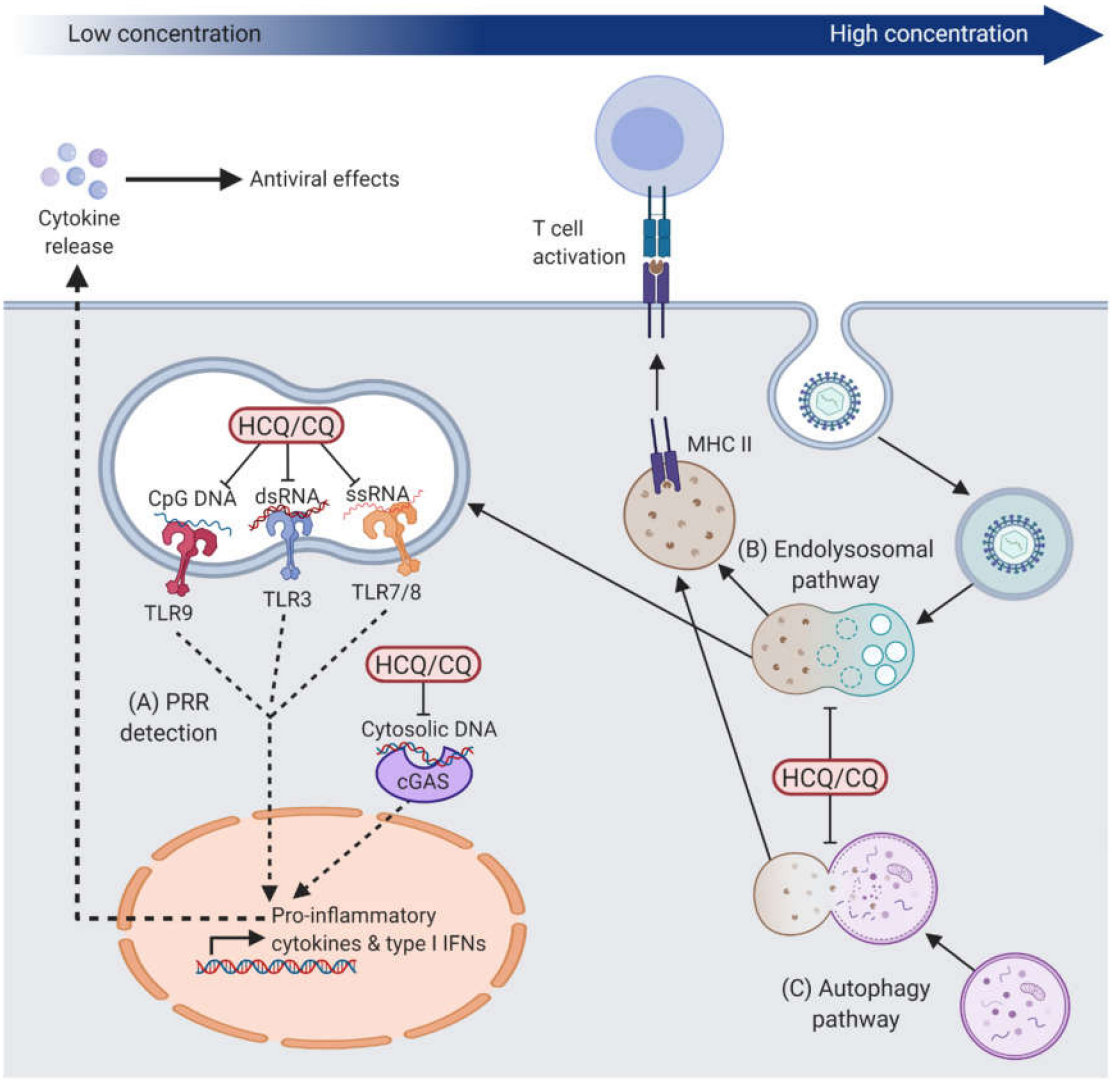

Figure 1. Immunomodulatory mechanisms of hydroxychloroquine (HCQ) and chloroquine (CQ). (**A**) At lower concentrations, which we define as ≤20 μM, HCQ and CQ can inhibit the activation of nucleic acid sensors, Toll-like receptors (TLR) in endosomes and cyclic GMP-AMP synthase (cGAS) in the cytoplasm. This leads to the inhibition of pattern recognition receptor (PRR)-induced activation of downstream pro-inflammatory cytokine and type I interferon (IFN) gene expression. At high concentrations (≥100 μM), HCQ and CQ can increase lysosomal pH, which leads to disruption of presentation of (**B**) extracellular antigens processed through the endolysosomal pathway and (**C**) intracellular antigens processed through the autophagosome-lysosome fusion pathway by antigen presenting cells. dsRNA, double-stranded RNA; ssRNA; single-stranded RNA; MHC II, major histocompatibility complex class II.

In addition to the inhibition of TLRs, hydroxychloroquine has been shown to have an inhibitory effect on the PRR cyclic GMP-AMP synthase (cGAS). cGAS is activated by cytosolic DNA, which is

indicative of viral infection, to initiate a signalling cascade leading to a type I interferon response [30,31]. An in silico screen of drug libraries to find cGAS antagonists identified several antimalarial drugs as putative inhibitors and further computational analysis predicted an interaction between hydroxychloroquine and the DNA binding site of cGAS [32]. Following dsDNA transfection of the human monocytic cell line (THP1), hydroxychloroquine treatment decreased expression of interferon (IFN)-β, a downstream cytokine of cGAS activation, in a dose-dependent manner with a half-maximal inhibitory concentration (IC50) of 25 μM [32] (Figure 1). It remains unclear whether the inhibitory effect of hydroxychloroquine on cGAS is achieved through hydroxychloroquine binding to cGAS or the DNA. Nonetheless, given the proposed mechanism of action via TLR9, it seems possible that hydroxychloroquine and chloroquine might prevent the activation of nucleic acid sensors cGAS and TLR9 through a common mechanism such as alteration of the structural configuration of the DNA substrate [33,34].

These findings have gone some way to explain the efficacy of hydroxychloroquine and chloroquine in the treatment of systemic lupus erythematosus and rheumatoid arthritis. A hallmark of both autoimmune diseases is the accumulation of DNA- or RNA-containing complexes due to a build-up of apoptotic bodies, which have been implicated in the activation of TLR9 or TLR7, respectively [35,36]. Recent studies in patient-derived PBMCs have suggested that cGAS may also be important in the detection of DNA in systemic lupus erythematosus [37,38]. Indeed, redundancy and overlap between the substrates of different nucleic acid sensors seem likely and evolutionarily advantageous. In preventing the activation of these PRRs, hydroxychloroquine or chloroquine may be able to dampen an overactive innate immune response to self-nucleic acids in systemic lupus erythematosus and rheumatoid arthritis. The same mechanism would also enable hydroxychloroquine and chloroquine to reduce the immune response to foreign nucleic acid antigens, such as those derived from viral infections.

2.2. *Effects on Cellular Immune Responses*

The inhibition of key PRRs, such as TLR9 and cGAS, by hydroxychloroquine and chloroquine has been shown to affect downstream pro-inflammatory cytokine and type I interferon responses (Figure 2) [6,29,32]. In vitro, both hydroxychloroquine and chloroquine have been shown to inhibit the production of the pro-inflammatory cytokines tumour necrosis factor-α (TNF-α), IFN-γ and interleukin (IL)-6 in PBMCs [39], and TNF-α, IL-1β, and IL-6 in human monocytes [40]. IFN-γ can prime macrophages for pro-inflammatory responses and render them resistant to suppressive immune factors [41]; IL-6 can control the survival, expansion, and maturation of B cells [42]; and TNFα is key in activating and promoting the long-term survival of macrophages [43]. Chloroquine has also been demonstrated to inhibit c-Jun N-terminal kinase (JNK)-mediated activation of the transcription factor activator protein 1 (AP-1) in $CD4^+$ T cells [44]. The resulting reduction in helper T cell activation, proliferation, and cytokine release would be expected to reduce the level of immune response. A type I interferon response also induces an anti-viral state within the infected and neighbouring cells by upregulating a large number of interferon-stimulated genes (ISGs) via the Janus kinase-signal transducer and activator of transcription (JAK-STAT) pathway [45]. Examples include tripartite motif-containing 5α (TRIM5α) that can bind to viral capsid proteins to promote viral disassembly and restrict infection [45]; ISG15 which is a ubiquitin-like protein that can covalently bind to viral proteins to disrupt replication [46]; and IL-15 that helps to eliminate infected cells by inducing the proliferation and maintenance of natural killer cells and $CD8^+$ T cells [47,48].

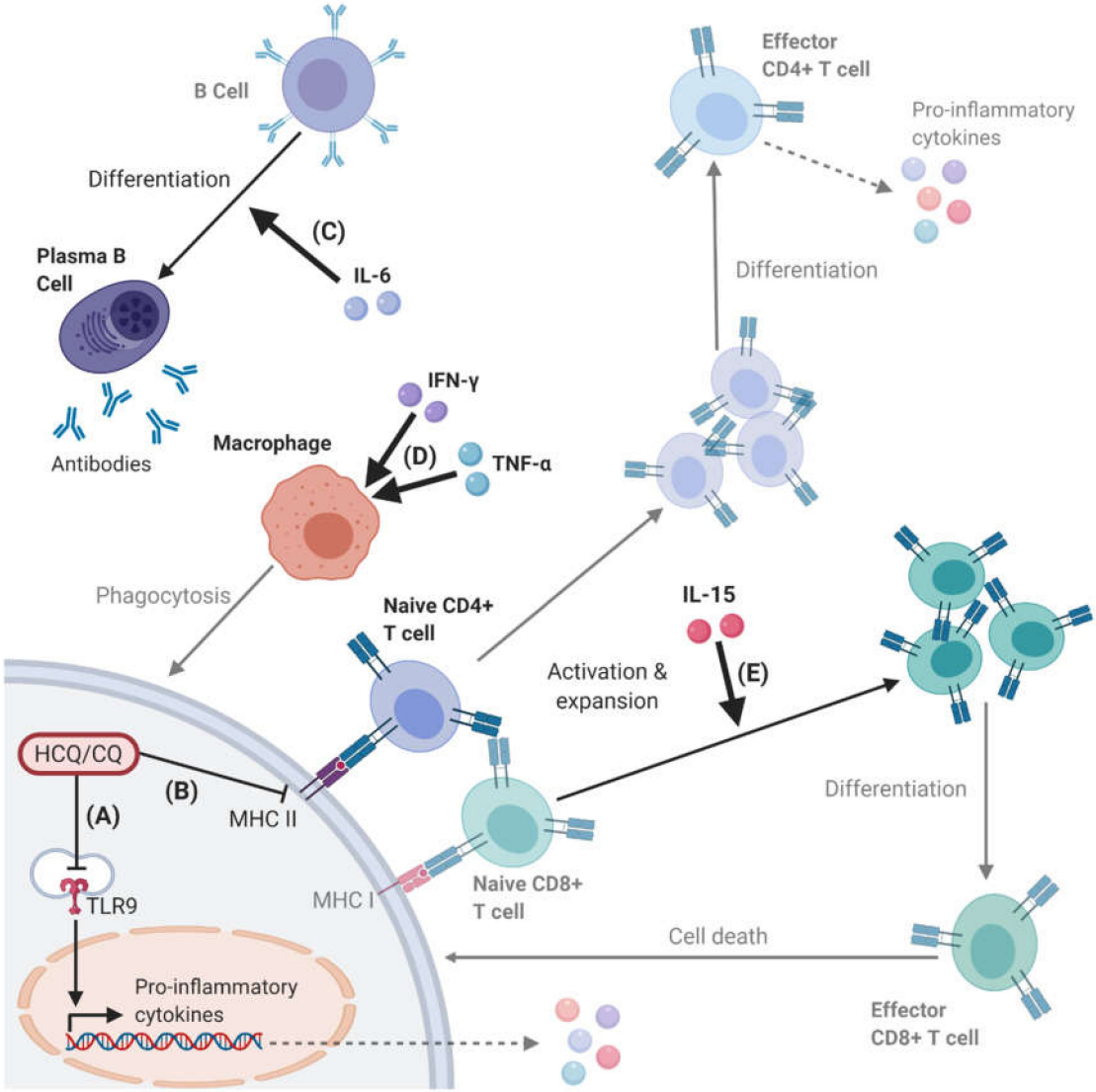

Figure 2. Effects of pro-inflammatory cytokines on cell-mediated immune responses. An example of cell-mediated immune responses downstream of the immunomodulatory effects of HCQ and CQ. HCQ and CQ can reduce pro-inflammatory cytokine expression by inhibition of (**A**) PRRs (e.g., TLR9) at low concentrations or (**B**) MHC II-mediated antigen presentation at high concentrations (see Figure 1). MHC II can activate $CD4^+$ T cells, which are another major source of pro-inflammatory cytokines. Key pro-inflammatory cytokines include (**C**) interleukin (IL)-6 that can stimulate the maturation and expansion of B cells into antibody-producing plasma cells, (**D**) IFN-γ and tumour necrosis factor-α (TNF-α) that can activate macrophages, and (**E**) IL-15 that can stimulate the activation and expansion of $CD8^+$ T cells. Lower opacity text and images represent the indirect effects, while those in bold highlight the direct effects of HCQ, CQ, and pro-inflammatory cytokines.

In addition to the inhibition of PRRs and their downstream signalling cascades, hydroxychloroquine and chloroquine also appear capable of indirectly modulating immune responses though the alkalisation of lysosomes when used at higher concentrations. The processing of extracellular material for antigen presentation is classically undertaken by professional antigen-presenting cells, which utilise the lysosomal pathway to display short peptides on major histocompatibility complex (MHC) class II molecules for detection by $CD4^+$ T cells [49]. By increasing the pH of lysosomes, chloroquine can affect antigen processing, as demonstrated in macrophages (at 100 μM) [50], dendritic cells (at 100 μM) [51] and B cells (at 25–100 μM) [52]. Notably, these effects, which are

associated with raised endosomal and lysosomal pH, were primarily observed at high concentrations of chloroquine (100 μM). In addition, chloroquine has been shown to inhibit autophagy, a regulated process for removing damaged intracellular organelles or proteins by enveloping cytoplasmic material, by inhibiting the fusion between autophagosomes and lysosomes [53]. This, in turn, leads to the inhibition of presentation of cytosolic antigens, including autoantigens and viral antigens, on MHC class II molecules via the autophagy-lysosomal pathway [54–56] (Figure 1). Since dysregulation of autophagy contributes to cancer development and chemotherapy resistance, hydroxychloroquine has been evaluated as an autophagy inhibitor in clinical trials for various cancers [57–60]. Very high daily doses of hydroxychloroquine (typically ≤1200 mg/day) have been used in this context in order to effectively block the fusion of lysosomes with autophagosomes, thus supporting a dose-dependent mechanism of action of hydroxychloroquine. Overall, study findings are consistent with hydroxychloroquine and chloroquine having a direct immunosuppressive effect on viral sensing and pro-inflammatory cytokine release at low concentrations, and an indirect immunomodulatory effect via lysosomal antigen processing and presentation at high concentrations (Figure 1).

3. Effects of Hydroxychloroquine and Chloroquine on Viral Infections

Historically, hydroxychloroquine and chloroquine have been utilised as tools to assess the effect of endosomal and lysosomal processes on viral entry, as many viruses exploit the host endocytic machinery to infect target cells. Following cell surface receptor binding, viral particles are internalised via a range of endocytic mechanisms, including clathrin-mediated, caveolin-mediated, and non-clathrin non-caveolin endocytosis. Endosomes undergo gradual acidification from an early to late stage, which acts as a trigger for viral uncoating and genome release so that endosomal escape is precisely timed to prevent overexposure of viral contents to the acidic environment [61]. The inhibition of replication of Semliki Forest virus [62], Chikungunya virus [63], and hepatitis A virus [64] by chloroquine in vitro has been suggested to occur as a result of impaired endosomal acidification and viral entry due to the concentration of this drug in intracellular compartments. In addition, the acidification of vesicular compartments along the secretory pathway is important in the post-translational modification of viral envelope proteins during the production of new infectious virions. For example, in vitro studies demonstrated that hydroxychloroquine and chloroquine could inhibit the production of infectious HIV-1 virions by preventing glycosylation of the viral glycoprotein gp120, which normally occurs within the acidic Golgi complex [65–67]. In addition, chloroquine treatment resulted in the accumulation of non-infectious herpes simplex virus (HSV)-1 virions in the trans-Golgi network in vitro [68]. Taken together, these observations support the potential anti-viral effects of hydroxychloroquine and chloroquine in vitro when used at sufficient concentrations to alter endosomal pH, but in vivo efficacy remains unclear.

3.1. Immunomodulatory Effects on Viral Infections

The combination of the alkalisation of the endolysosomal pathway and the immunomodulatory effects of hydroxychloroquine and chloroquine have led to speculations surrounding their potential benefits in the treatment of viral infections. Although both innate and adaptive immune responses are vital to recovery from viral infections, over activation of immune responses may lead to harmful tissue damage and disease progression. Such counterproductive immune responses have been observed in chronic HIV [69], severe acute respiratory syndrome coronavirus (SARS-CoV) [70], and SARS-CoV-2 infections [71], leading to investigation of hydroxychloroquine and chloroquine as potential immunomodulatory therapies. Systemic T cell activation in chronic HIV infection is thought to be associated with disease progression. A randomised controlled trial showed that chloroquine therapy could reduce the proportion of $CD38^+$ $HLA\text{-}DR^+$ CD8 T cells, thus supporting its usage in certain groups of HIV patients [72]. The effect may be explained by chloroquine-mediated suppression of TLR7 activation by HIV RNA in primary monocytes and plasmacytoid dendritic cells (pDCs) [73–75]. Similarly, in vitro chloroquine has been shown to prevent TLR7-mediated responses to

other RNA viruses such as hepatitis C [76,77], influenza [78] and vesicular somatic virus [79], as well as TLR9-mediated responses to DNA viruses such as HSV-2 and Epstein–Barr virus [80–82]. There appears to be a general correlation between the concentration of chloroquine or hydroxychloroquine used and the effects seen in vitro (Table 1). High doses of these drugs, which we define as ≥100 μM, tend to inhibit viral replication, while low doses (≤20 μM) tend to inhibit innate immune pathways without detectable effect on viral replication. This correlation is consistent with the hypothesis that high concentrations of hydroxychloroquine or chloroquine could inhibit viral entry or assembly by increasing the pH of intracellular vesicular compartments, while low concentrations could reduce pro-inflammatory cytokine release by preventing the activation of nucleic acid sensors. Nonetheless, a degree of overlap could be expected between these two types of effects, which may be variable between different cell lines. Of note, Vero cells derived from the kidney epithelium of the African green monkey, which are commonly used to propagate viruses in vitro, harbour a 9 Mb deletion leading to loss of the type I interferon gene cluster [83,84]. Therefore, Vero cells would not be an appropriate model for assessing the immunomodulatory effects of these drugs during viral infection. Further work is needed to assess the effects of hydroxychloroquine and chloroquine on viral infection in biologically relevant cell types and in vivo.

Table 1. Effects of hydroxychloroquine and chloroquine on selected viruses in vitro.

Effect	Drug	Concentration (μM)	Virus	Viral Genome	Cells	Reference
Inhibition of viral replication [1]	CQ	75	Yellow fever virus	ssRNA	P388D1	[85]
		100	Semliki Forest virus	ssRNA	BHK-21	[62]
		10–100	Hepatitis A virus	ssRNA	BS-C-1	[64]
		150	HSV-1	dsDNA	HuH7	[68]
		250–4000	Varicella zoster virus	dsDNA	Mononuclear cells	[86]
	HCQ	1–1000	HIV-1	ssRNA	T cell and macrophage hybridoma cell line	[67]
Inhibition of virus-mediated immune response [1]	CQ	10 and 100	Hepatitis C virus	ssRNA	Huh7 and macrophages	[76,77]
		10	HSV-2	dsDNA	pDCs	[80]
		1–100	Vesicular stomatitis virus	ssRNA	pDCs	[79]
		10	Influenza A virus	ssRNA	pDCs	[78]
		5 and 100	HIV-1	ssRNA	pDCs and PBMCs	[73,74]
	HCQ	10 and 20	Epstein Barr virus	dsDNA	pDCs and monocytes	[81,82]

[1] In vitro studies conducted in Vero cells were excluded because of the inability for these cells to produce type I interferon responses, making them unsuitable for assessing the immunomodulatory effects of HCQ and CQ. HSV, herpes simplex virus; pDC, plasmacytoid dendritic cell; HIV, human immunodeficiency virus.

In contrast to their inhibitory effects on viral replication in vitro, hydroxychloroquine and chloroquine may have different effects in vivo due to the lower systemic concentrations achieved and their inhibitory effects on anti-viral responses, such as those mediated through TLRs. In a randomised, double-blind, controlled trial of 400 mg/day of hydroxychloroquine versus placebo in patients with asymptomatic HIV infection and not on anti-retroviral therapy, hydroxychloroquine was found to be associated with an increased HIV viral RNA load as well as a faster decline in $CD4^+$ cell counts, leading to the need to initiate anti-retroviral therapy [87]. Another double-blind controlled trial of HIV-1 infected patients randomised to either 250 mg/day of chloroquine or placebo, demonstrated a significant increase in HIV viral RNA in patients not taking anti-retroviral therapy and a decrease in ISG expression [88]. While in vitro experiments in Vero cells showed chloroquine could inhibit the replication of Semliki Forest virus and the closely related Chikungunya virus, these effects were not seen in animal studies where chloroquine was associated with higher viral loads [89,90]. In addition, when used to treat Chikungunya viral infection in a clinical trial, chloroquine led to clinical deterioration without significant effect on viral load, which was attributed to a delaying effect on adaptive immunity [90,91].

3.2. Treatment of SARS-CoV-2 Infections

The anti-viral applications of hydroxychloroquine and chloroquine have gained renewed interest in the wake of the 2020 SARS-CoV-2 pandemic. In vitro studies of SARS-CoV, responsible for the

2003 epidemic, demonstrated that chloroquine had an inhibitory effect on viral replication in Vero cells [92–94]. However, intraperitoneal and intranasal injections of chloroquine ultimately induced no effect in vivo in BALB/c mice [95]. Nevertheless, with the emergence of the SARS-CoV-2 global pandemic, several in vitro studies have demonstrated hydroxychloroquine and chloroquine inhibit viral replication of this new strain of coronavirus in Vero cells [96–98]. However, the potential benefits of these drugs in the treatment of SARS-CoV-2 infected patients are highly disputed. Preliminary clinical trials in China claimed that chloroquine treatment might inhibit exacerbation of pneumonia, improve radiographic appearances, enhance virus-negative conversion, and reduce the overall length of the illness [99]. However, the results of these trials are yet to be formally peer-reviewed. A subsequent French trial with 20 SARS-CoV-2 patients suggested that hydroxychloroquine treatment (at 600 mg daily) significantly reduced viral load [100]. However, methodological concerns, such as a lack of randomisation and unexplained exclusion of patients in the hydroxychloroquine-treated arm (three of which were transferred to intensive care and another died), have since led to the discounting of the study's findings [101]. In a subsequent larger double-blind clinical trial, 81 SARS-CoV-2 infected patients randomised to either low (450 mg twice daily on the first day and once daily for four days) or high dose (600 mg twice daily for 10 days) chloroquine were compared, with both groups also receiving the antibiotic azithromycin. Increased lethality from cardiac effects associated with a prolongation of the corrected QT interval was observed on electrocardiography in the high dose group [102]. As the trial had to be stopped due to safety concerns, the study became underpowered to detect a treatment benefit of chloroquine [102]. An open-label clinical trial was undertaken in China on 150 SARS-CoV-2 infected patients with mild to moderate symptoms. Patients were either randomised to the normal standard of care or treated with hydroxychloroquine at 1200 mg daily for three days followed by a maintenance dose of 800 mg daily for another 2–3 weeks depending on severity [103]. There was no detectable difference in virus-negative conversion, although there was a greater report of adverse effects in the hydroxychloroquine treated patients [103]. There is currently no evidence to show any significant benefit of hydroxychloroquine or chloroquine in SARS-CoV-2 infection and high doses of the drugs may be associated with adverse effects. One explanation for the discrepancy between in vitro and in vivo findings may be due to the use of Vero cells for all in vitro experiments performed with SARS-CoV and SARS-CoV-2, which do not produce type I interferons [92–94,96–98].

In summary, despite various attempts to utilise hydroxychloroquine and chloroquine to control viral infections, they have not demonstrated clinical efficacy in treating any acute viral infections to date, either as a primary or adjunctive therapy. On the contrary, the immunomodulatory effects of hydroxychloroquine and chloroquine at in vivo biological concentrations may be exploited to enhance viral transduction during gene therapy.

4. Application of Hydroxychloroquine to Viral Vector-Mediated Retinal Gene Therapy

4.1. Immune Responses to AAV-Mediated Retinal Gene Therapy

AAV vectors have been widely utilised in gene therapy to treat a range of retinal genetic diseases due to their broad tissue tropisms, low pathogenicity, and relative low immunogenicity compared to other major viral vectors, such as lentiviruses and adenoviruses. Despite assumptions of immune privilege in the eye and low immunogenicity of AAV, inflammatory responses have been observed following subretinal injections of AAV. For instance, AAV2- and AAV8-injected cynomolgus macaques demonstrated a dose-dependent increase in capsid-specific neutralising antibodies and a systemic T cell response to the GFP transgene in two of the 14 animals that received high vector doses (1×10^{11} vector genomes (vg)/eye) [104]. Subretinal injection of cynomolgus macaques with an AAV2tYF vector (with three capsid tyrosine to phenylalanine mutations) expressing the gene *CNGB3* led to inflammatory responses in the anterior and posterior segments at both 1.2×10^{11} and 1.2×10^{12} vg/eye, with one animal developing severe endophthalmitis; all animals had an increase in neutralising antibodies to the AAV2tYF capsid [105]. Cynomolgous macaques injected

with the AAV7m8 demonstrated high expression of glial fibrillary acidic protein (GFAP) (a marker for glial activation) at the highest vector dose (1×10^{12} vg/eye) [106]. Severe retinal inflammation was detected with signs of lymphocytic retinal infiltrates, perivascular inflammation, loss of RPE, and chronic choroidal inflammation [106]. The presence of a dose-dependent inflammatory response to AAV2-mediated retinal gene therapy was first observed in humans in a phase 1/2 clinical trial treating *RPE65*-associated Leber congenital amaurosis where five of the eight high dose patients (1×10^{12} vg/eye) had signs of intraocular inflammation, such as anterior uveitis, mild vitritis, and optic disc swelling [15]. In a phase 1/2 clinical trial of AAV2-mediated gene therapy for choroideremia, one of 14 high dose patients (1×10^{11} vg/eye) developed intraocular inflammation in the form of vitritis, retinitis, and choroiditis, which was associated with reduced visual function [17]. Similarly, in a phase 1/2 trial of AAV8-mediated gene therapy for *RPGR*-associated X-linked retinitis pigmentosa, seven out of nine high dose patients ($0.6–4 \times 10^{11}$ vg/eye) developed steroid-responsive subretinal inflammation associated with transient changes in retinal sensitivity [14]. Typically, inflammatory responses have been controlled in retinal gene therapy trials using a course of systemic immunosuppression (e.g., oral corticosteroid). However, persistent immune responses against the AAV transgene may diminish the long-term durability of the treatment. Currently, it is uncertain whether intraocular inflammation following AAV-mediated retinal gene therapy is directed at the viral capsid, therapeutic cassette, or the transgene product itself. Characterising the exact nature of the immune responses to AAV and devising methods for overcoming these counterproductive responses have become of great interest as gene therapies go from proof-of-concept to clinical application.

Intramuscular injection of recombinant AAV in wildtype mice elicited TLR9-mediated activation of pDCs and a type I interferon response independent of AAV serotype, suggesting that the TLR9-Myd88 pathway was critical for the activation of a $CD8^+$ T cell response against the AAV capsid and transgene [107]. The immunogenic serotype AAVrh32.33 has also been shown to elicit a TLR9-mediated $CD8^+$ T cell response in vivo, which was significantly diminished upon depletion of CpG sequences (the ligands for TLR9 receptors) in the viral genome [108]. The activation of adaptive immunity against AAV could lead to the production of transgene-specific antibodies, reduced transgene expression, and diminished durability of gene therapy. For instance, in a gene therapy trial for haemophilia B, an AAV serotype 2 vector containing the human Factor IX transgene delivered via hepatic artery infusion, led to a transient therapeutic level of transgene expression lasting 8 weeks due to destruction of transduced hepatocytes by an AAV capsid-specific $CD8^+$ T cell response [109]. While AAVs containing self-complementary genomes can provide higher levels of transgene expression in vitro, they are associated with greater pro-inflammatory innate immune responses in vivo as the double-stranded AAV genome can activate TLR9 more strongly than ssDNA in standard AAV vectors [110]. Furthermore, we found that mouse embryonic fibroblasts lacking cGAS, which is capable of sensing secondary structures of ssDNA such as the AAV ITRs, showed significant increases AAV transgene expression compared with wildtype cells, suggesting that nucleic acid-sensing innate immune responses may be a key limiting factor for AAV transduction [111]. Together, these studies reveal the ability for AAV, similar to other viruses, to activate PRRs and elicit both intracellular and cellular immune responses that can determine the efficacy of gene therapy.

Key anti-viral sensors, including TLR9 and cGAS, and effectors, including IFN-γ, TNF-α, and IL-1β are upregulated in the retina following AAV gene therapy in vivo, in wildtype mice and non-human primates [111–113]. Release of pro-inflammatory cytokines within the retina can lead to increased permeability of the blood-retina barrier and enable infiltration of circulating leukocytes into the normally "immune-privileged" retinal environment [114–116]. This is supported by positive retinal immunohistochemical staining for MHC class I and II (suggestive of active antigen presentation) and CD8 (indicative of infiltrating cytotoxic T cells) following subretinal injection of AAV8 in non-human primates [112]. One possible source of retinal inflammation following AAV gene therapy may be related to the activation of retinal microglia, which are resident macrophage-like cells capable of detecting viral infections and orchestrating local immune responses through the activation of TLR9 [117] and

cGAS [118], and recruitment of infiltrating leukocytes [119]. This would be consistent with increased immunohistochemical staining for ionized calcium-binding adaptor molecule 1 (IBA1) (a microglia activation marker) in the retina following subretinal injection of AAV in mice [112,113].

4.2. Improving the Efficacy of Retinal Gene Therapy

Since hydroxychloroquine and chloroquine are inhibitors of the anti-viral PRRs TLR9 and cGAS, they may provide a means of improving AAV transduction by modulating anti-viral responses during gene therapy. We tested this hypothesis by examining the effect of hydroxychloroquine on AAV2 transduction in vitro at a range of concentrations and found a significant increase in transgene expression at around 19 μM of hydroxychloroquine [111]. Similar enhancing effects on AAV transduction were observed in primary non-human primate retinal pigment epithelium (RPE) cells and human retina explants [111]. Co-administration of AAV vector and 19 μM hydroxychloroquine via subretinal injection in mice led to improved transgene expression compared with vector alone using both an AAV2 vector with a ubiquitous CAG promoter (4.6-fold improvement) and an AAV8(Y733F) vector with a photoreceptor-specific promoter (GRK1) (5.9-fold improvement) [111]. However, additional in vivo studies with therapeutic vectors and different AAV doses would be beneficial to further investigate the efficacy of hydroxychloroquine in retinal gene therapy.

The suppression of anti-viral pathways by hydroxychloroquine or chloroquine may ultimately prevent expression of downstream pro-inflammatory cytokines and recruitment of infiltrating leukocytes to the retina following AAV gene therapy. In addition, the cytokine IL-6, which has been shown to be inhibited by hydroxychloroquine and chloroquine, can induce B cell maturation and antibody production [42]. This may be of particular concern in patients seronegative for anti-AAV antibodies where AAV gene therapy to the first eye may lead to B cell maturation and the production of anti-AAV antibodies that could diminish the efficacy of repeat treatment to the second eye at a later date. Although AAV2 capsid-specific antibodies and T cell responses have been seen in animal models following readministration via the subretinal route [120], no such reaction was seen in a trial with 11 patients [121]. Nonetheless, transduction of the second eye did not seem to be significantly affected in either cases [120,121]. On the other hand, intravitreal administration of AAV appears to induce a significantly greater level of anti-AAV antibody response [122] and is more prone to antibody-mediated reduction of AAV transduction over repeated treatments [123]. This may be because of increased vector shedding in intravitreal AAV delivery [124], while the blood-retina barrier may limit exposure to circulating antibodies and immune cells during subretinal injections. Therefore, adjunctive therapy with hydroxychloroquine might be beneficial in intravitreally delivered retinal gene therapies by reducing the level of AAV neutralising antibody production to facilitate second eye treatment. Alternatively, the endopeptidase imlifidase (IdeS) has been developed as a means of eliminating anti-AAV antibodies [125]. Cynomologus macaques with pre-existing anti-AAV8 antibodies were intravenously injected with IdeS 24 h prior to AAV8-hFIX injections. This led to decreased titres of AAV8-specific IgG and neutralising antibodies and a significant increase in hFIX transgene expression. IdeS also enabled readministration of the novel AAV variant AAV-LK03 in African green monkeys, leading to a significant increase in transgene expression [125]. It remains to be seen whether such methods would prove effective in retinal gene therapy given that neutralising antibody responses are minimal following subretinal AAV injections [17]. Nonetheless, anti-AAV antibodies have been detected in some retinal gene therapy clinical trials following subretinal [15] and intravitreal injections [126,127], thus further work is necessary to determine the effect of retinal gene therapy on neutralising antibody responses.

Corticosteroids provide an additional means of controlling AAV-mediated inflammation and have been widely used in retinal gene therapy trials to control inflammatory responses [11,14,17]. Corticosteroid activity exists at the apex of an extensive signalling pathway that blocks several downstream inflammatory responses. For instance, by inducing expression of the anti-inflammatory molecule mitogen-activated protein kinase (MAPK) phosphatase 1; preventing transcriptional activity

of nuclear factor kappa-light-chain-enhancer of activated B cells (NF-κB) that regulates downstream transcription of a vast range of cytokines; and blocking c-Jun–mediated transcription of innate immune factors [128]. However, despite this significant anti-inflammatory activity, little is known about the effect of corticosteroids on the efficacy of retinal gene therapy. In vivo studies to investigate the level of retinal transduction with and without corticosteroid treatment would thus be of significant interest. Further work is therefore needed to analyse the mechanism of the AAV-mediated immune responses and how these may be modified using adjunctive treatments during gene therapy.

5. Safety and Delivery of Hydroxychloroquine in Retinal Gene Therapy

5.1. Hydroxychloroquine Retinopathy

Although the first cases of retinopathy associated with chloroquine therapy were described in the late 1950s [129], retinal toxicity was considered infrequent until the turn of the century as only patients with symptoms of hydroxychloroquine retinopathy were detected [130]. The recognition of an increased risk of retinopathy in chloroquine users, as compared to hydroxychloroquine users, led to the reduction in the use of chloroquine across its treatment indications [131]. However, modern retinal imaging techniques, such as optical coherence tomography (OCT) and fundus autofluorescence, over the past 20 years have enabled the detection of pre-symptomatic disease [132]. Using such techniques, a major case-control study identified the prevalence of hydroxychloroquine retinopathy at 7.5% of patients taking the drug for more than 5 years, increasing to 20–50% after 20 years of therapy [133]. The risk factors for retinopathy included daily dose, duration of therapy, renal impairment, and concurrent tamoxifen therapy [133]. A daily dose of >5 mg/kg/day over a prolonged period was considered to confer a greater risk of hydroxychloroquine retinopathy [133], and safe dosing guidelines for chronic use of hydroxychloroquine were defined by this threshold [134]. Due to the risk of hydroxychloroquine retinopathy following chronic use, screening programmes were recommended in several countries to reduce the risk of permanent visual loss in this group [135,136]. It is important to note that clinically, hydroxychloroquine and chloroquine are not bioequivalent, and different daily doses are needed to achieve similar therapeutic effects. The safe limits of daily dosing with regards to retinopathy also differ, with 5 mg/kg/day for hydroxychloroquine and 2.3 mg/kg/day for chloroquine [136].

5.2. Routes of Administration

The adjuvant use of hydroxychloroquine to augment the effects of gene therapy at the time of AAV vector delivery requires some consideration of the route of delivery of hydroxychloroquine, the dose administered and the duration of therapy. The safe limits of orally administered hydroxychloroquine have been defined over the past 60 years. Although there is no identified safe dose which confers no risk, retinopathy is unlikely in the first 5 years of therapy unless concomitant risk factors are present [133]. Very high doses of hydroxychloroquine (1000 mg/day) used in clinical trials in oncology, where hydroxychloroquine is used as an inhibitor of autophagy, have resulted in retinopathy in two out of seven patients at 15 and 25 months, respectively [137,138]. Although the mechanism of retinal toxicity of systemically administered hydroxychloroquine is unknown, the dosing characteristics which produce retinopathy have been well described. In the context of retinal gene therapy, it is unlikely that short courses of orally administered hydroxychloroquine in the peri-operative period will have any detectable effects on retinal structure or function, even at a high daily dose of 1000 mg/day.

Although the systemic adjunctive use of hydroxychloroquine in retinal gene therapy has not yet been tested, this approach may be problematic given what is known about the pharmacokinetics of the drug. Hydroxychloroquine has a relatively long plasma half-life of 32 days, and elimination half-life in blood is approximately 50 days. The drug is highly sequestered in tissues, and therefore a steady-state plasma concentration is only achieved after 6 months of daily dosing [139]. Moreover, a study evaluating serum hydroxychloroquine levels in different individuals identified significant variability between subjects [140]. Thus, a consistent and predictable tissue concentration of hydroxychloroquine

within the retina to enhance AAV retinal gene therapy would be difficult to achieve over a short interval. Furthermore, given that the effects of hydroxychloroquine on the intracellular innate immune response appear highly dose-dependent, this variability in tissue drug concentrations may have a significant influence on retinal photoreceptor or RPE transduction. A greater variability in clinical outcome measures might, therefore, be expected when compared to locally delivered hydroxychloroquine. Rabbit models have demonstrated the sequestration of systemically administered hydroxychloroquine within the pigmented tissues of the eye, such as the RPE, choroid, and ciliary body, where it is bound to melanin [141]. It is unclear how the immunomodulatory effects of hydroxychloroquine may influence the relative efficiency of transduction of AAV-delivered transgenes to the RPE or photoreceptors given this RPE-predominant tissue distribution from systemically administered hydroxychloroquine. Although the effects of systemically administered hydroxychloroquine have not been evaluated in any AAV gene therapy studies, it is likely that hydroxychloroquine would need to be administered in the weeks prior to AAV delivery to allow hydroxychloroquine to reach appropriate tissue concentrations within the eye. Both the efficacy of systemic hydroxychloroquine in the context of retinal gene therapy and tissue concentrations of hydroxychloroquine within the retina and RPE require further evaluation.

The delivery of hydroxychloroquine by subretinal injection allows for precise control over the local drug concentration. In 2013, an in vitro study used chloroquine at 100 μM as a tool for alkalising endosomes, a concentration known to raise the pH of these compartments, and demonstrated a decrease in AAV transduction in a hepatocellular carcinoma cell line (HepG2) [142]. In contrast, we showed that 19 μM hydroxychloroquine enhanced AAV-mediated transgene expression in vivo by around 5-fold [111]. The lower concentration of hydroxychloroquine used would primarily be expected to have an immunomodulatory effect and minimal influence on endosomal pH. When comparing the effects of low (19 μM) versus high (113 μM) dose of hydroxychloroquine co-administered subretinally with AAV in vivo, we found that 19 μM hydroxychloroquine led to significantly increased transgene expression, while 113 μM hydroxychloroquine had no effect or in some cases a negative effect on AAV transduction (Figure 3A). Moreover, no retinal structural change was detected by OCT with this single low dose of hydroxychloroquine (Figure 3B) [111]. Given that hydroxychloroquine was only delivered as a one-off treatment together with the AAV vector, the toxic effects associated with prolonged hydroxychloroquine treatment are unlikely. However, long-term assessment of retinal function using an electroretinogram would be required to fully investigate the safety of subretinally delivering hydroxychloroquine. Taken together, these findings are consistent with the hypothesis that a low concentration of locally delivered hydroxychloroquine could improve viral transgene expression by inhibiting PRR-mediated anti-viral responses, while high concentrations of hydroxychloroquine may impair viral entry by altering endosomal pH.

5.3. Potential Clinical Applications

Current AAV retinal gene therapy trials and therapeutic protocols, in the case of voretigene neparvovec for *RPE65*-associated Leber congenital amaurosis, generally include a perioperative period of systemic immunosuppression with prednisolone to reduce the risk of retinal inflammation [11,14,17]. Nevertheless, at high vector doses cases of intraocular inflammation have been observed requiring supplementary corticosteroid treatment. This can include oral prednisolone, dexamethasone eye drops, and intravitreal dexamethasone implants (Ozurdex), as demonstrated in the phase 1/2 dose-escalation gene therapy trial for X-linked retinitis pigmentosa [14]. Corticosteroids provide an effective means of controlling ocular inflammation; however, systemic corticosteroid usage may be associated with a range of potential adverse effects, including activation of viral retinitis in previously immunocompetent patients [143,144]. Intraocular or periocular corticosteroid use may also be associated with an increased risk of acute retinal necrosis secondary to HSV [145,146]. Since the dose of hydroxychloroquine administered in the sub-retinal space in AAV gene therapy potentiates viral action, there is a theoretical risk of viral retinitis. However, acute retinal necrosis has not been reported in long-term systemic hydroxychloroquine users despite clear evidence for drug accumulation

within the RPE. Hydroxychloroquine in the context of subretinal delivery may, therefore, function as an immunomodulatory rather than immunosuppressive agent. This may suggest that subretinal administration of a single low dose of hydroxychloroquine as an adjuvant to AAV gene therapy is of low risk while offering the potential to reduce the AAV dose required, thus reducing the risk of treatment-induced retinal inflammation and the need for systemic steroids to counter this response. However, while existing evidence supports the safety of low dose hydroxychloroquine in healthy retinae, it is unclear whether the degenerate RPE and photoreceptors in inherited retinal dystrophies may respond differently to the same concentration of hydroxychloroquine.

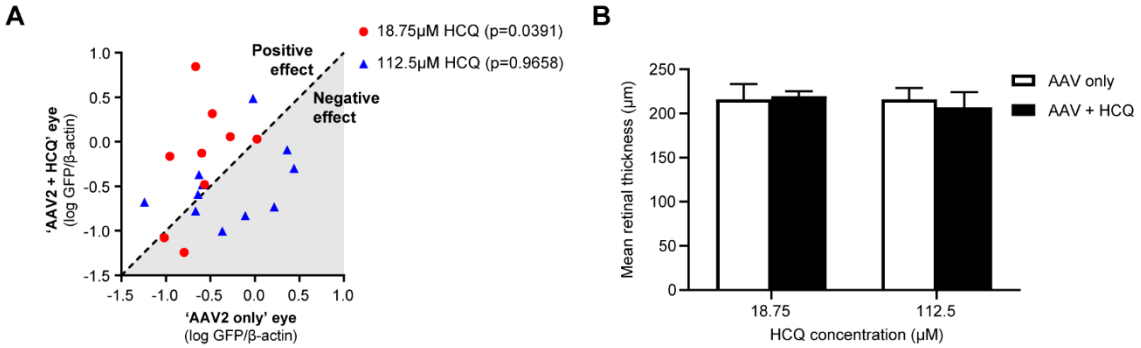

Figure 3. Dose effect of HCQ on improving the efficacy of adeno-associated viral (AAV)-mediated retinal gene therapy in vivo. C57BL/6J mice were subretinally injected with 1×10^8 vector genomes of AAV8(Y733F) GRK1.GFP with and without either 18.75 μM (n = 10) or 112.5 μM (n = 11) HCQ. (**A**) The protein quantification of GFP expression normalised to β-actin (expressed as $\log_{10}$) 6 weeks post-injection of AAV only injected eyes (x-axis) plotted against AAV with HCQ injected eyes (y-axis). Each point represents an individual animal. Points above the line represent a positive effect and below a negative. The p-value for analysis between paired eyes is given in the legend using a Wilcoxon matched-pairs signed rank test. (**B**) Mean total retinal thickness measured by in vivo spectral domain optical coherence tomography imaging (± SEM).

6. Conclusions

An important feature of the mechanism of action of HCQ and CQ is their ability to accumulate in intracellular compartments. However, the activity of these drugs within acidic vesicles may largely rely on their concentration. High doses of HCQ and CQ can alkalise endosomes and lysosomes to impair their function, while low doses appear to have minimal effects on pH but can prevent activation of intracellular PRRs to modulate downstream innate immune responses. This dual activity may explain the contradictory effects of HCQ and CQ seen in viral infections, with low concentrations providing potential to minimise anti-viral responses. AAV gene therapy is a promising treatment for inherited retinal disease; however, clinical efficacy is limited by the proportion of target cells that successfully express the therapeutic transgene. Adjunctive use of HCQ provides a means of inhibiting restrictive anti-viral intracellular immune responses to improve transgene expression and enhance the therapeutic effect to reach the transduction threshold needed to prevent disease progression. Given the risk of deleterious tissue inflammation with high doses of AAV, HCQ may also enable the use of lower and safer vector doses to achieve a given treatment effect. When applied to viral infections in general, it remains to be seen whether an optimal dosage of HCQ may be found to reduce unwanted tissue inflammation due to anti-viral immune responses in order to reduce overall disease severity or duration.

Author Contributions: Conceptualisation, L.C.C. and K.X.; formal analysis, L.C.C.; investigation, L.C.C., M.E.M. and A.R.B.; writing—original draft preparation, L.C.C. and I.H.Y.; writing—review and editing, L.C.C., I.H.Y., M.E.M., A.R.B., R.E.M. and K.X.; supervision, R.E.M. and K.X.; funding acquisition, I.H.Y., R.E.M. and K.X. All authors have read and agreed to the published version of the manuscript.

Funding: This research was funded by support from Fight for Sight UK (L.C.C. and K.X.), the Medical Research Council (MRC) (I.H.Y), National Institute for Health Research (NIHR) Oxford Biomedical Research Centre (M.E.M. and R.E.M.), the Wellcome Trust (K.X.), and the Academy of Medical Sciences (K.X.).

Conflicts of Interest: L.C.C., A.R.B., R.E.M. and K.X. hold a patent on behalf of the University of Oxford relating to the use of hydroxychloroquine as an adjunct for gene therapy. The funders had no role in the design of the study; in the collection, analyses, or interpretation of data; in the writing of the manuscript, or in the decision to publish the results.

Abbreviations

AAV	Adeno-associated virus
HCQ	Hydroxychloroquine
CQ	Chloroquine
ssDNA	Single-stranded DNA
ITR	Inverted terminal repeat
HIV	Human immunodeficiency virus
TLR	Toll-like receptor
PRR	Pattern recognition receptor
dsRNA	Double-stranded RNA
ssRNA	Single-stranded RNA
ODN	Oligodeoxynucleotide
PBMC	Peripheral blood mononuclear cell
cGAS	Cyclic GMP-AMP synthase
IFN	Interferon
TNF	Tumour necrosis factor
IL	Interleukin
ISG	Interferon-stimulated gene
MHC	Major histocompatibility complex
HSV	Herpes simplex virus
SARS-CoV	Severe acute respiratory syndrome coronavirus
pDC	Plasmacytoid dendritic cell
vg	Vector genomes
OCT	Optical coherence tomography

References

1. Schrezenmeier, E.; Dorner, T. Mechanisms of action of hydroxychloroquine and chloroquine: Implications for rheumatology. *Nat. Rev. Rheumatol.* **2020**, *16*, 155–166. [CrossRef] [PubMed]
2. Fox, R.I. Mechanism of action of hydroxychloroquine as an antirheumatic drug. *Semin. Arthritis Rheum.* **1993**, *23*, 82–91. [CrossRef]
3. Ohkuma, S.; Poole, B. Fluorescence probe measurement of the intralysosomal pH in living cells and the perturbation of pH by various agents. *Proc. Natl. Acad. Sci. USA* **1978**, *75*, 3327–3331. [CrossRef] [PubMed]
4. Manzel, L.; Strekowski, L.; Ismail, F.M.; Smith, J.C.; Macfarlane, D.E. Antagonism of immunostimulatory CpG-oligodeoxynucleotides by 4-aminoquinolines and other weak bases: Mechanistic studies. *J. Pharmacol. Exp. Ther.* **1999**, *291*, 1337–1347. [PubMed]
5. Macfarlane, D.E.; Manzel, L. Antagonism of immunostimulatory CpG-oligodeoxynucleotides by quinacrine, chloroquine, and structurally related compounds. *J. Immunol.* **1998**, *160*, 1122–1131.
6. Kuznik, A.; Bencina, M.; Svajger, U.; Jeras, M.; Rozman, B.; Jerala, R. Mechanism of endosomal TLR inhibition by antimalarial drugs and imidazoquinolines. *J. Immunol.* **2011**, *186*, 4794–4804. [CrossRef]
7. Duan, D.; Sharma, P.; Yang, J.; Yue, Y.; Dudus, L.; Zhang, Y.; Fisher, K.J.; Engelhardt, J.F. Circular intermediates of recombinant adeno-associated virus have defined structural characteristics responsible for long-term episomal persistence in muscle tissue. *J. Virol.* **1998**, *72*, 8568–8577. [CrossRef]
8. Rabinowitz, J.; Chan, Y.K.; Samulski, R.J. Adeno-associated Virus (AAV) versus Immune Response. *Viruses* **2019**, *11*, 102. [CrossRef]

9. Bainbridge, J.W.; Smith, A.J.; Barker, S.S.; Robbie, S.; Henderson, R.; Balaggan, K.; Viswanathan, A.; Holder, G.E.; Stockman, A.; Tyler, N.; et al. Effect of gene therapy on visual function in Leber's congenital amaurosis. *N. Engl. J. Med.* **2008**, *358*, 2231–2239. [CrossRef]
10. Pierce, E.A.; Bennett, J. The Status of RPE65 Gene Therapy Trials: Safety and Efficacy. *Cold Spring Harb. Perspect Med.* **2015**, *5*, a017285. [CrossRef]
11. Russell, S.; Bennett, J.; Wellman, J.A.; Chung, D.C.; Yu, Z.F.; Tillman, A.; Wittes, J.; Pappas, J.; Elci, O.; McCague, S.; et al. Efficacy and safety of voretigene neparvovec (AAV2-hRPE65v2) in patients with RPE65-mediated inherited retinal dystrophy: A randomised, controlled, open-label, phase 3 trial. *Lancet* **2017**, *390*, 849–860. [CrossRef]
12. MacLaren, R.E.; Groppe, M.; Barnard, A.R.; Cottriall, C.L.; Tolmachova, T.; Seymour, L.; Clark, K.R.; During, M.J.; Cremers, F.P.; Black, G.C.; et al. Retinal gene therapy in patients with choroideremia: Initial findings from a phase 1/2 clinical trial. *Lancet* **2014**, *383*, 1129–1137. [CrossRef]
13. Edwards, T.L.; Jolly, J.K.; Groppe, M.; Barnard, A.R.; Cottriall, C.L.; Tolmachova, T.; Black, G.C.; Webster, A.R.; Lotery, A.J.; Holder, G.E.; et al. Visual Acuity after Retinal Gene Therapy for Choroideremia. *N. Engl. J. Med.* **2016**, *374*, 1996–1998. [CrossRef] [PubMed]
14. Cehajic-Kapetanovic, J.; Xue, K.; Martinez-Fernandez de la Camara, C.; Nanda, A.; Davies, A.; Wood, L.J.; Salvetti, A.P.; Fischer, M.D.; Aylward, J.W.; Barnard, A.R.; et al. Initial results from a first-in-human gene therapy trial on X-linked retinitis pigmentosa caused by mutations in RPGR. *Nat. Med.* **2020**, *26*, 354–359. [CrossRef]
15. Bainbridge, J.W.; Mehat, M.S.; Sundaram, V.; Robbie, S.J.; Barker, S.E.; Ripamonti, C.; Georgiadis, A.; Mowat, F.M.; Beattie, S.G.; Gardner, P.J.; et al. Long-term effect of gene therapy on Leber's congenital amaurosis. *N. Engl. J. Med.* **2015**, *372*, 1887–1897. [CrossRef]
16. Guy, J.; Feuer, W.J.; Davis, J.L.; Porciatti, V.; Gonzalez, P.J.; Koilkonda, R.D.; Yuan, H.; Hauswirth, W.W.; Lam, B.L. Gene Therapy for Leber Hereditary Optic Neuropathy: Low- and Medium-Dose Visual Results. *Ophthalmology* **2017**, *124*, 1621–1634. [CrossRef]
17. Xue, K.; Jolly, J.K.; Barnard, A.R.; Rudenko, A.; Salvetti, A.P.; Patrício, M.I.; Edwards, T.L.; Groppe, M.; Orlans, H.O.; Tolmachova, T.; et al. Beneficial effects on vision in patients undergoing retinal gene therapy for choroideremia. *Nat. Med.* **2018**, *24*, 1507–1512. [CrossRef]
18. Ben-Zvi, I.; Kivity, S.; Langevitz, P.; Shoenfeld, Y. Hydroxychloroquine: From malaria to autoimmunity. *Clin. Rev. Allergy Immunol.* **2012**, *42*, 145–153. [CrossRef]
19. Pandey, S.; Kawai, T.; Akira, S. Microbial sensing by Toll-like receptors and intracellular nucleic acid sensors. *Cold Spring Harb. Perspect. Biol.* **2014**, *7*, a016246. [CrossRef]
20. Ewald, S.E.; Lee, B.L.; Lau, L.; Wickliffe, K.E.; Shi, G.P.; Chapman, H.A.; Barton, G.M. The ectodomain of Toll-like receptor 9 is cleaved to generate a functional receptor. *Nature* **2008**, *456*, 658–662. [CrossRef]
21. Alexopoulou, L.; Holt, A.C.; Medzhitov, R.; Flavell, R.A. Recognition of double-stranded RNA and activation of NF-kappaB by Toll-like receptor 3. *Nature* **2001**, *413*, 732–738. [CrossRef]
22. Heil, F.; Hemmi, H.; Hochrein, H.; Ampenberger, F.; Kirschning, C.; Akira, S.; Lipford, G.; Wagner, H.; Bauer, S. Species-specific recognition of single-stranded RNA via toll-like receptor 7 and 8. *Science* **2004**, *303*, 1526–1529. [CrossRef] [PubMed]
23. Hemmi, H.; Takeuchi, O.; Kawai, T.; Kaisho, T.; Sato, S.; Sanjo, H.; Matsumoto, M.; Hoshino, K.; Wagner, H.; Takeda, K.; et al. A Toll-like receptor recognizes bacterial DNA. *Nature* **2000**, *408*, 740–745. [CrossRef] [PubMed]
24. Bird, A.P. CpG-rich islands and the function of DNA methylation. *Nature* **1986**, *321*, 209–213. [CrossRef] [PubMed]
25. Hacker, H.; Mischak, H.; Miethke, T.; Liptay, S.; Schmid, R.; Sparwasser, T.; Heeg, K.; Lipford, G.B.; Wagner, H. CpG-DNA-specific activation of antigen-presenting cells requires stress kinase activity and is preceded by non-specific endocytosis and endosomal maturation. *EMBO J.* **1998**, *17*, 6230–6240. [CrossRef]
26. Rutz, M.; Metzger, J.; Gellert, T.; Luppa, P.; Lipford, G.B.; Wagner, H.; Bauer, S. Toll-like receptor 9 binds single-stranded CpG-DNA in a sequence- and pH-dependent manner. *Eur. J. Immunol.* **2004**, *34*, 2541–2550. [CrossRef] [PubMed]
27. Lamphier, M.; Zheng, W.; Latz, E.; Spyvee, M.; Hansen, H.; Rose, J.; Genest, M.; Yang, H.; Shaffer, C.; Zhao, Y.; et al. Novel small molecule inhibitors of TLR7 and TLR9: Mechanism of action and efficacy in vivo. *Mol. Pharmacol.* **2014**, *85*, 429–440. [CrossRef]

28. de Bouteiller, O.; Merck, E.; Hasan, U.A.; Hubac, S.; Benguigui, B.; Trinchieri, G.; Bates, E.E.; Caux, C. Recognition of double-stranded RNA by human toll-like receptor 3 and downstream receptor signaling requires multimerization and an acidic pH. *J. Biol. Chem.* **2005**, *280*, 38133–38145. [CrossRef]
29. Vollmer, J.; Tluk, S.; Schmitz, C.; Hamm, S.; Jurk, M.; Forsbach, A.; Akira, S.; Kelly, K.M.; Reeves, W.H.; Bauer, S.; et al. Immune stimulation mediated by autoantigen binding sites within small nuclear RNAs involves Toll-like receptors 7 and 8. *J. Exp. Med.* **2005**, *202*, 1575–1585. [CrossRef]
30. Sun, L.; Wu, J.; Du, F.; Chen, X.; Chen, Z.J. Cyclic GMP-AMP synthase is a cytosolic DNA sensor that activates the type I interferon pathway. *Science* **2013**, *339*, 786–791. [CrossRef]
31. Wu, J.; Sun, L.; Chen, X.; Du, F.; Shi, H.; Chen, C.; Chen, Z.J. Cyclic GMP-AMP is an endogenous second messenger in innate immune signaling by cytosolic DNA. *Science* **2013**, *339*, 826–830. [CrossRef] [PubMed]
32. An, J.; Woodward, J.J.; Sasaki, T.; Minie, M.; Elkon, K.B. Cutting edge: Antimalarial drugs inhibit IFN-beta production through blockade of cyclic GMP-AMP synthase-DNA interaction. *J. Immunol.* **2015**, *194*, 4089–4093. [CrossRef] [PubMed]
33. An, J.; Minie, M.; Sasaki, T.; Woodward, J.J.; Elkon, K.B. Antimalarial Drugs as Immune Modulators: New Mechanisms for Old Drugs. *Annu. Rev. Med.* **2017**, *68*, 317–330. [CrossRef] [PubMed]
34. Bose, D.; Su, Y.; Marcus, A.; Raulet, D.H.; Hammond, M.C. An RNA-Based Fluorescent Biosensor for High-Throughput Analysis of the cGAS-cGAMP-STING Pathway. *Cell Chem. Biol.* **2016**, *23*, 1539–1549. [CrossRef] [PubMed]
35. Means, T.K.; Latz, E.; Hayashi, F.; Murali, M.R.; Golenbock, D.T.; Luster, A.D. Human lupus autoantibody-DNA complexes activate DCs through cooperation of CD32 and TLR9. *J. Clin. Investig.* **2005**, *115*, 407–417. [CrossRef]
36. Barrat, F.J.; Meeker, T.; Gregorio, J.; Chan, J.H.; Uematsu, S.; Akira, S.; Chang, B.; Duramad, O.; Coffman, R.L. Nucleic acids of mammalian origin can act as endogenous ligands for Toll-like receptors and may promote systemic lupus erythematosus. *J. Exp. Med.* **2005**, *202*, 1131–1139. [CrossRef]
37. Kato, Y.; Park, J.; Takamatsu, H.; Konaka, H.; Aoki, W.; Aburaya, S.; Ueda, M.; Nishide, M.; Koyama, S.; Hayama, Y.; et al. Apoptosis-derived membrane vesicles drive the cGAS-STING pathway and enhance type I IFN production in systemic lupus erythematosus. *Ann. Rheum. Dis.* **2018**, *77*, 1507–1515. [CrossRef]
38. An, J.; Durcan, L.; Karr, R.M.; Briggs, T.A.; Rice, G.I.; Teal, T.H.; Woodward, J.J.; Elkon, K.B. Expression of Cyclic GMP-AMP Synthase in Patients with Systemic Lupus Erythematosus. *Arthritis Rheumatol.* **2017**, *69*, 800–807. [CrossRef]
39. van den Borne, B.E.; Dijkmans, B.A.; de Rooij, H.H.; le Cessie, S.; Verweij, C.L. Chloroquine and hydroxychloroquine equally affect tumor necrosis factor-alpha, interleukin 6, and interferon-gamma production by peripheral blood mononuclear cells. *J. Rheumatol.* **1997**, *24*, 55–60.
40. Jang, C.H.; Choi, J.H.; Byun, M.S.; Jue, D.M. Chloroquine inhibits production of TNF-alpha, IL-1beta and IL-6 from lipopolysaccharide-stimulated human monocytes/macrophages by different modes. *Rheumatology (Oxford)* **2006**, *45*, 703–710. [CrossRef]
41. Ivashkiv, L.B. IFNgamma: Signalling, epigenetics and roles in immunity, metabolism, disease and cancer immunotherapy. *Nat. Rev. Immunol.* **2018**, *18*, 545–558. [CrossRef] [PubMed]
42. Hunter, C.A.; Jones, S.A. IL-6 as a keystone cytokine in health and disease. *Nat. Immunol.* **2015**, *16*, 448–457. [CrossRef] [PubMed]
43. Parameswaran, N.; Patial, S. Tumor necrosis factor-alpha signaling in macrophages. *Crit. Rev. Eukaryot Gene Expr.* **2010**, *20*, 87–103. [CrossRef] [PubMed]
44. Schmidt, R.L.; Jutz, S.; Goldhahn, K.; Witzeneder, N.; Gerner, M.C.; Trapin, D.; Greiner, G.; Hoermann, G.; Steiner, G.; Pickl, W.F.; et al. Chloroquine inhibits human CD4(+) T-cell activation by AP-1 signaling modulation. *Sci. Rep.* **2017**, *7*, 42191. [CrossRef]
45. Schneider, W.M.; Chevillotte, M.D.; Rice, C.M. Interferon-stimulated genes: A complex web of host defenses. *Annu Rev. Immunol.* **2014**, *32*, 513–545. [CrossRef]
46. Perng, Y.C.; Lenschow, D.J. ISG15 in antiviral immunity and beyond. *Nat. Rev. Microbiol.* **2018**, *16*, 423–439. [CrossRef]
47. Nguyen, K.B.; Salazar-Mather, T.P.; Dalod, M.Y.; Van Deusen, J.B.; Wei, X.Q.; Liew, F.Y.; Caligiuri, M.A.; Durbin, J.E.; Biron, C.A. Coordinated and distinct roles for IFN-alpha beta, IL-12, and IL-15 regulation of NK cell responses to viral infection. *J. Immunol.* **2002**, *169*, 4279–4287. [CrossRef]

48. Zhang, X.; Sun, S.; Hwang, I.; Tough, D.F.; Sprent, J. Potent and selective stimulation of memory-phenotype CD8+ T cells in vivo by IL-15. *Immunity* **1998**, *8*, 591–599. [CrossRef]
49. Munz, C. Autophagy Beyond Intracellular MHC Class II Antigen Presentation. *Trends Immunol.* **2016**, *37*, 755–763. [CrossRef]
50. Ziegler, H.K.; Unanue, E.R. Decrease in macrophage antigen catabolism caused by ammonia and chloroquine is associated with inhibition of antigen presentation to T cells. *Proc. Natl. Acad. Sci. USA* **1982**, *79*, 175–178. [CrossRef]
51. Chain, B.M.; Kay, P.M.; Feldmann, M. The cellular pathway of antigen presentation: Biochemical and functional analysis of antigen processing in dendritic cells and macrophages. *Immunology* **1986**, *58*, 271–276.
52. Robson, N.C.; Donachie, A.M.; Mowat, A.M. Simultaneous presentation and cross-presentation of immune-stimulating complex-associated cognate antigen by antigen-specific B cells. *Eur. J. Immunol.* **2008**, *38*, 1238–1246. [CrossRef]
53. Mauthe, M.; Orhon, I.; Rocchi, C.; Zhou, X.; Luhr, M.; Hijlkema, K.J.; Coppes, R.P.; Engedal, N.; Mari, M.; Reggiori, F. Chloroquine inhibits autophagic flux by decreasing autophagosome-lysosome fusion. *Autophagy* **2018**, *14*, 1435–1455. [CrossRef] [PubMed]
54. Nimmerjahn, F.; Milosevic, S.; Behrends, U.; Jaffee, E.M.; Pardoll, D.M.; Bornkamm, G.W.; Mautner, J. Major histocompatibility complex class II-restricted presentation of a cytosolic antigen by autophagy. *Eur. J. Immunol.* **2003**, *33*, 1250–1259. [CrossRef] [PubMed]
55. Dengjel, J.; Schoor, O.; Fischer, R.; Reich, M.; Kraus, M.; Muller, M.; Kreymborg, K.; Altenberend, F.; Brandenburg, J.; Kalbacher, H.; et al. Autophagy promotes MHC class II presentation of peptides from intracellular source proteins. *Proc. Natl. Acad. Sci. USA* **2005**, *102*, 7922–7927. [CrossRef] [PubMed]
56. Paludan, C.; Schmid, D.; Landthaler, M.; Vockerodt, M.; Kube, D.; Tuschl, T.; Munz, C. Endogenous MHC class II processing of a viral nuclear antigen after autophagy. *Science* **2005**, *307*, 593–596. [CrossRef]
57. Rosenfeld, M.R.; Ye, X.; Supko, J.G.; Desideri, S.; Grossman, S.A.; Brem, S.; Mikkelson, T.; Wang, D.; Chang, Y.C.; Hu, J.; et al. A phase I/II trial of hydroxychloroquine in conjunction with radiation therapy and concurrent and adjuvant temozolomide in patients with newly diagnosed glioblastoma multiforme. *Autophagy* **2014**, *10*, 1359–1368. [CrossRef]
58. Rangwala, R.; Leone, R.; Chang, Y.C.; Fecher, L.A.; Schuchter, L.M.; Kramer, A.; Tan, K.S.; Heitjan, D.F.; Rodgers, G.; Gallagher, M.; et al. Phase I trial of hydroxychloroquine with dose-intense temozolomide in patients with advanced solid tumors and melanoma. *Autophagy* **2014**, *10*, 1369–1379. [CrossRef]
59. Karasic, T.B.; O'Hara, M.H.; Loaiza-Bonilla, A.; Reiss, K.A.; Teitelbaum, U.R.; Borazanci, E.; De Jesus-Acosta, A.; Redlinger, C.; Burrell, J.A.; Laheru, D.A.; et al. Effect of Gemcitabine and nab-Paclitaxel With or Without Hydroxychloroquine on Patients With Advanced Pancreatic Cancer: A Phase 2 Randomized Clinical Trial. *JAMA Oncol.* **2019**, *5*, 993–998. [CrossRef]
60. Haas, N.B.; Appleman, L.J.; Stein, M.; Redlinger, M.; Wilks, M.; Xu, X.; Onorati, A.; Kalavacharla, A.; Kim, T.; Zhen, C.J.; et al. Autophagy Inhibition to Augment mTOR Inhibition: A Phase I/II Trial of Everolimus and Hydroxychloroquine in Patients with Previously Treated Renal Cell Carcinoma. *Clin. Cancer Res.* **2019**, *25*, 2080–2087. [CrossRef]
61. Vazquez-Calvo, A.; Saiz, J.C.; McCullough, K.C.; Sobrino, F.; Martin-Acebes, M.A. Acid-dependent viral entry. *Virus Res.* **2012**, *167*, 125–137. [CrossRef] [PubMed]
62. Helenius, A.; Marsh, M.; White, J. Inhibition of Semliki forest virus penetration by lysosomotropic weak bases. *J. Gen. Virol.* **1982**, *58 Pt 1*, 47–61. [CrossRef]
63. Khan, M.; Santhosh, S.R.; Tiwari, M.; Lakshmana Rao, P.V.; Parida, M. Assessment of in vitro prophylactic and therapeutic efficacy of chloroquine against Chikungunya virus in vero cells. *J. Med. Virol.* **2010**, *82*, 817–824. [CrossRef] [PubMed]
64. Bishop, N.E. Examination of potential inhibitors of hepatitis A virus uncoating. *Intervirology* **1998**, *41*, 261–271. [CrossRef]
65. Tsai, W.P.; Nara, P.L.; Kung, H.F.; Oroszlan, S. Inhibition of human immunodeficiency virus infectivity by chloroquine. *AIDS Res. Hum. Retrovir.* **1990**, *6*, 481–489. [CrossRef]
66. Sperber, K.; Kalb, T.H.; Stecher, V.J.; Banerjee, R.; Mayer, L. Inhibition of human immunodeficiency virus type 1 replication by hydroxychloroquine in T cells and monocytes. *AIDS Res. Hum. Retrovir.* **1993**, *9*, 91–98. [CrossRef] [PubMed]

67. Chiang, G.; Sassaroli, M.; Louie, M.; Chen, H.; Stecher, V.J.; Sperber, K. Inhibition of HIV-1 replication by hydroxychloroquine: Mechanism of action and comparison with zidovudine. *Clin. Ther.* **1996**, *18*, 1080–1092. [CrossRef]
68. Harley, C.A.; Dasgupta, A.; Wilson, D.W. Characterization of herpes simplex virus-containing organelles by subcellular fractionation: Role for organelle acidification in assembly of infectious particles. *J. Virol.* **2001**, *75*, 1236–1251. [CrossRef]
69. Brenchley, J.M.; Price, D.A.; Schacker, T.W.; Asher, T.E.; Silvestri, G.; Rao, S.; Kazzaz, Z.; Bornstein, E.; Lambotte, O.; Altmann, D.; et al. Microbial translocation is a cause of systemic immune activation in chronic HIV infection. *Nat. Med.* **2006**, *12*, 1365–1371. [CrossRef]
70. Peiris, J.S.; Chu, C.M.; Cheng, V.C.; Chan, K.S.; Hung, I.F.; Poon, L.L.; Law, K.I.; Tang, B.S.; Hon, T.Y.; Chan, C.S.; et al. Clinical progression and viral load in a community outbreak of coronavirus-associated SARS pneumonia: A prospective study. *Lancet* **2003**, *361*, 1767–1772. [CrossRef]
71. Tay, M.Z.; Poh, C.M.; Renia, L.; MacAry, P.A.; Ng, L.F.P. The trinity of COVID-19: Immunity, inflammation and intervention. *Nat. Rev. Immunol.* **2020**. [CrossRef] [PubMed]
72. Murray, S.M.; Down, C.M.; Boulware, D.R.; Stauffer, W.M.; Cavert, W.P.; Schacker, T.W.; Brenchley, J.M.; Douek, D.C. Reduction of immune activation with chloroquine therapy during chronic HIV infection. *J. Virol.* **2010**, *84*, 12082–12086. [CrossRef] [PubMed]
73. Beignon, A.S.; McKenna, K.; Skoberne, M.; Manches, O.; DaSilva, I.; Kavanagh, D.G.; Larsson, M.; Gorelick, R.J.; Lifson, J.D.; Bhardwaj, N. Endocytosis of HIV-1 activates plasmacytoid dendritic cells via Toll-like receptor-viral RNA interactions. *J. Clin. Investig.* **2005**, *115*, 3265–3275. [CrossRef]
74. Martinson, J.A.; Montoya, C.J.; Usuga, X.; Ronquillo, R.; Landay, A.L.; Desai, S.N. Chloroquine modulates HIV-1-induced plasmacytoid dendritic cell alpha interferon: Implication for T-cell activation. *Antimicrob. Agents Chemother.* **2010**, *54*, 871–881. [CrossRef]
75. Han, X.; Li, X.; Yue, S.C.; Anandaiah, A.; Hashem, F.; Reinach, P.S.; Koziel, H.; Tachado, S.D. Epigenetic regulation of tumor necrosis factor alpha (TNFalpha) release in human macrophages by HIV-1 single-stranded RNA (ssRNA) is dependent on TLR8 signaling. *J. Biol. Chem.* **2012**, *287*, 13778–13786. [CrossRef]
76. Lee, J.; Tian, Y.; Chan, S.T.; Kim, J.Y.; Cho, C.; Ou, J.H. TNF-alpha Induced by Hepatitis C Virus via TLR7 and TLR8 in Hepatocytes Supports Interferon Signaling via an Autocrine Mechanism. *PLoS Pathog.* **2015**, *11*, e1004937. [CrossRef] [PubMed]
77. Zhang, Y.; El-Far, M.; Dupuy, F.P.; Abdel-Hakeem, M.S.; He, Z.; Procopio, F.A.; Shi, Y.; Haddad, E.K.; Ancuta, P.; Sekaly, R.P.; et al. HCV RNA Activates APCs via TLR7/TLR8 While Virus Selectively Stimulates Macrophages Without Inducing Antiviral Responses. *Sci. Rep.* **2016**, *6*, 29447. [CrossRef] [PubMed]
78. Diebold, S.S.; Kaisho, T.; Hemmi, H.; Akira, S.; Reis e Sousa, C. Innate antiviral responses by means of TLR7-mediated recognition of single-stranded RNA. *Science* **2004**, *303*, 1529–1531. [CrossRef]
79. Lund, J.M.; Alexopoulou, L.; Sato, A.; Karow, M.; Adams, N.C.; Gale, N.W.; Iwasaki, A.; Flavell, R.A. Recognition of single-stranded RNA viruses by Toll-like receptor 7. *Proc. Natl. Acad. Sci. USA* **2004**, *101*, 5598–5603. [CrossRef]
80. Lund, J.; Sato, A.; Akira, S.; Medzhitov, R.; Iwasaki, A. Toll-like receptor 9-mediated recognition of Herpes simplex virus-2 by plasmacytoid dendritic cells. *J. Exp. Med.* **2003**, *198*, 513–520. [CrossRef] [PubMed]
81. Quan, T.E.; Roman, R.M.; Rudenga, B.J.; Holers, V.M.; Craft, J.E. Epstein-Barr virus promotes interferon-alpha production by plasmacytoid dendritic cells. *Arthritis Rheum.* **2010**, *62*, 1693–1701. [CrossRef] [PubMed]
82. Fiola, S.; Gosselin, D.; Takada, K.; Gosselin, J. TLR9 contributes to the recognition of EBV by primary monocytes and plasmacytoid dendritic cells. *J. Immunol.* **2010**, *185*, 3620–3631. [CrossRef] [PubMed]
83. Desmyter, J.; Melnick, J.L.; Rawls, W.E. Defectiveness of interferon production and of rubella virus interference in a line of African green monkey kidney cells (Vero). *J. Virol.* **1968**, *2*, 955–961. [CrossRef]
84. Osada, N.; Kohara, A.; Yamaji, T.; Hirayama, N.; Kasai, F.; Sekizuka, T.; Kuroda, M.; Hanada, K. The genome landscape of the african green monkey kidney-derived vero cell line. *DNA Res.* **2014**, *21*, 673–683. [CrossRef] [PubMed]
85. Brandriss, M.W.; Schlesinger, J.J. Antibody-mediated infection of P388D1 cells with 17D yellow fever virus: Effects of chloroquine and cytochalasin B. *J. Gen. Virol.* **1984**, *65*, 791–794. [CrossRef] [PubMed]
86. Pontesilli, O.; Carotenuto, P.; Levin, M.J.; Suez, D.; Hayward, A.R. Processing and presentation of cell-associated varicella-zoster virus antigens by human monocytes. *Clin. Exp. Immunol.* **1987**, *70*, 127–135. [PubMed]

87. Paton, N.I.; Goodall, R.L.; Dunn, D.T.; Franzen, S.; Collaco-Moraes, Y.; Gazzard, B.G.; Williams, I.G.; Fisher, M.J.; Winston, A.; Fox, J.; et al. Effects of hydroxychloroquine on immune activation and disease progression among HIV-infected patients not receiving antiretroviral therapy: A randomized controlled trial. *JAMA* **2012**, *308*, 353–361. [CrossRef]
88. Jacobson, J.M.; Bosinger, S.E.; Kang, M.; Belaunzaran-Zamudio, P.; Matining, R.M.; Wilson, C.C.; Flexner, C.; Clagett, B.; Plants, J.; Read, S.; et al. The Effect of Chloroquine on Immune Activation and Interferon Signatures Associated with HIV-1. *AIDS Res. Hum. Retrovir.* **2016**, *32*, 636–647. [CrossRef]
89. Maheshwari, R.K.; Srikantan, V.; Bhartiya, D. Chloroquine enhances replication of Semliki Forest virus and encephalomyocarditis virus in mice. *J. Virol.* **1991**, *65*, 992–995. [CrossRef]
90. Roques, P.; Thiberville, S.D.; Dupuis-Maguiraga, L.; Lum, F.M.; Labadie, K.; Martinon, F.; Gras, G.; Lebon, P.; Ng, L.F.P.; de Lamballerie, X.; et al. Paradoxical Effect of Chloroquine Treatment in Enhancing Chikungunya Virus Infection. *Viruses* **2018**, *10*, 268. [CrossRef]
91. De Lamballerie, X.; Boisson, V.; Reynier, J.C.; Enault, S.; Charrel, R.N.; Flahault, A.; Roques, P.; Le Grand, R. On chikungunya acute infection and chloroquine treatment. *Vector Borne Zoonotic Dis.* **2008**, *8*, 837–839. [CrossRef] [PubMed]
92. Keyaerts, E.; Vijgen, L.; Maes, P.; Neyts, J.; Van Ranst, M. In vitro inhibition of severe acute respiratory syndrome coronavirus by chloroquine. *Biochem. Biophys. Res. Commun.* **2004**, *323*, 264–268. [CrossRef] [PubMed]
93. Vincent, M.J.; Bergeron, E.; Benjannet, S.; Erickson, B.R.; Rollin, P.E.; Ksiazek, T.G.; Seidah, N.G.; Nichol, S.T. Chloroquine is a potent inhibitor of SARS coronavirus infection and spread. *Virol. J.* **2005**, *2*, 69. [CrossRef] [PubMed]
94. Biot, C.; Daher, W.; Chavain, N.; Fandeur, T.; Khalife, J.; Dive, D.; De Clercq, E. Design and synthesis of hydroxyferroquine derivatives with antimalarial and antiviral activities. *J. Med. Chem.* **2006**, *49*, 2845–2849. [CrossRef] [PubMed]
95. Barnard, D.L.; Day, C.W.; Bailey, K.; Heiner, M.; Montgomery, R.; Lauridsen, L.; Chan, P.K.; Sidwell, R.W. Evaluation of immunomodulators, interferons and known in vitro SARS-coV inhibitors for inhibition of SARS-coV replication in BALB/c mice. *Antivir. Chem. Chemother.* **2006**, *17*, 275–284. [CrossRef]
96. Wang, M.; Cao, R.; Zhang, L.; Yang, X.; Liu, J.; Xu, M.; Shi, Z.; Hu, Z.; Zhong, W.; Xiao, G. Remdesivir and chloroquine effectively inhibit the recently emerged novel coronavirus (2019-nCoV) in vitro. *Cell Res.* **2020**, *30*, 269–271. [CrossRef]
97. Yao, X.; Ye, F.; Zhang, M.; Cui, C.; Huang, B.; Niu, P.; Liu, X.; Zhao, L.; Dong, E.; Song, C.; et al. In Vitro Antiviral Activity and Projection of Optimized Dosing Design of Hydroxychloroquine for the Treatment of Severe Acute Respiratory Syndrome Coronavirus 2 (SARS-CoV-2). *Clin. Infect. Dis.* **2020**, *10*. [CrossRef]
98. Liu, J.; Cao, R.; Xu, M.; Wang, X.; Zhang, H.; Hu, H.; Li, Y.; Hu, Z.; Zhong, W.; Wang, M. Hydroxychloroquine, a less toxic derivative of chloroquine, is effective in inhibiting SARS-CoV-2 infection in vitro. *Cell Discov.* **2020**, *6*, 16. [CrossRef]
99. Gao, J.; Tian, Z.; Yang, X. Breakthrough: Chloroquine phosphate has shown apparent efficacy in treatment of COVID-19 associated pneumonia in clinical studies. *Biosci. Trends* **2020**, *14*, 72–73. [CrossRef]
100. Gautret, P.; Lagier, J.C.; Parola, P.; Hoang, V.T.; Meddeb, L.; Mailhe, M.; Doudier, B.; Courjon, J.; Giordanengo, V.; Vieira, V.E.; et al. Hydroxychloroquine and azithromycin as a treatment of COVID-19: Results of an open-label non-randomized clinical trial. *Int. J. Antimicrob. Agents* **2020**. [CrossRef]
101. Voss, A. Statement on IJAA Paper. Available online: https://www.isac.world/news-and-publications/official-isac-statement (accessed on 30 April 2020).
102. Borba, M.G.S.; Val, F.F.A.; Sampaio, V.S.; Alexandre, M.A.A.; Melo, G.C.; Brito, M.; Mourao, M.P.G.; Brito-Sousa, J.D.; Baia-da-Silva, D.; Guerra, M.V.F.; et al. Effect of High vs Low Doses of Chloroquine Diphosphate as Adjunctive Therapy for Patients Hospitalized With Severe Acute Respiratory Syndrome Coronavirus 2 (SARS-CoV-2) Infection: A Randomized Clinical Trial. *JAMA Netw. Open* **2020**, *3*, e208857. [CrossRef] [PubMed]
103. Tang, W.; Cao, Z.; Han, M.; Wang, Z.; Chen, J.; Sun, W.; Wu, Y.; Xiao, W.; Liu, S.; Chen, E.; et al. Hydroxychloroquine in patients with mainly mild to moderate coronavirus disease 2019: Open label, randomised controlled trial. *BMJ* **2020**, *369*, m1849. [CrossRef] [PubMed]

104. Vandenberghe, L.H.; Bell, P.; Maguire, A.M.; Cearley, C.N.; Xiao, R.; Calcedo, R.; Wang, L.; Castle, M.J.; Maguire, A.C.; Grant, R.; et al. Dosage thresholds for AAV2 and AAV8 photoreceptor gene therapy in monkey. *Sci. Transl. Med.* **2011**, *3*, 88ra54. [CrossRef] [PubMed]
105. Ye, G.J.; Budzynski, E.; Sonnentag, P.; Nork, T.M.; Miller, P.E.; Sharma, A.K.; Ver Hoeve, J.N.; Smith, L.M.; Arndt, T.; Calcedo, R.; et al. Safety and Biodistribution Evaluation in Cynomolgus Macaques of rAAV2tYF-PR1.7-hCNGB3, a Recombinant AAV Vector for Treatment of Achromatopsia. *Hum. Gene Ther. Clin. Dev.* **2016**, *27*, 37–48. [CrossRef]
106. Ramachandran, P.S.; Lee, V.; Wei, Z.; Song, J.Y.; Casal, G.; Cronin, T.; Willett, K.; Huckfeldt, R.; Morgan, J.I.; Aleman, T.S.; et al. Evaluation of Dose and Safety of AAV7m8 and AAV8BP2 in the Non-Human Primate Retina. *Hum. Gene Ther.* **2017**, *28*, 154–167. [CrossRef]
107. Zhu, J.; Huang, X.; Yang, Y. The TLR9-MyD88 pathway is critical for adaptive immune responses to adeno-associated virus gene therapy vectors in mice. *J. Clin. Investig.* **2009**, *119*, 2388–2398. [CrossRef] [PubMed]
108. Faust, S.M.; Bell, P.; Cutler, B.J.; Ashley, S.N.; Zhu, Y.; Rabinowitz, J.E.; Wilson, J.M. CpG-depleted adeno-associated virus vectors evade immune detection. *J. Clin. Investig.* **2013**, *123*, 2994–3001. [CrossRef]
109. Manno, C.S.; Pierce, G.F.; Arruda, V.R.; Glader, B.; Ragni, M.; Rasko, J.J.; Ozelo, M.C.; Hoots, K.; Blatt, P.; Konkle, B.; et al. Successful transduction of liver in hemophilia by AAV-Factor IX and limitations imposed by the host immune response. *Nat. Med.* **2006**, *12*, 342–347. [CrossRef]
110. Martino, A.T.; Suzuki, M.; Markusic, D.M.; Zolotukhin, I.; Ryals, R.C.; Moghimi, B.; Ertl, H.C.; Muruve, D.A.; Lee, B.; Herzog, R.W. The genome of self-complementary adeno-associated viral vectors increases Toll-like receptor 9-dependent innate immune responses in the liver. *Blood* **2011**, *117*, 6459–6468. [CrossRef]
111. Chandler, L.C.; Barnard, A.R.; Caddy, S.L.; Patricio, M.I.; McClements, M.E.; Fu, H.; Rada, C.; MacLaren, R.E.; Xue, K. Enhancement of Adeno-Associated Virus-Mediated Gene Therapy Using Hydroxychloroquine in Murine and Human Tissues. *Mol. Ther. Methods Clin. Dev.* **2019**, *14*, 77–89. [CrossRef]
112. Reichel, F.F.; Dauletbekov, D.L.; Klein, R.; Peters, T.; Ochakovski, G.A.; Seitz, I.P.; Wilhelm, B.; Ueffing, M.; Biel, M.; Wissinger, B.; et al. AAV8 Can Induce Innate and Adaptive Immune Response in the Primate Eye. *Mol. Ther.* **2017**, *25*, 2648–2660. [CrossRef] [PubMed]
113. Xiong, W.; Wu, D.M.; Xue, Y.; Wang, S.K.; Chung, M.J.; Ji, X.; Rana, P.; Zhao, S.R.; Mai, S.; Cepko, C.L. AAV cis-regulatory sequences are correlated with ocular toxicity. *Proc. Natl. Acad. Sci. USA* **2019**, *116*, 5785–5794. [CrossRef] [PubMed]
114. Claudio, L.; Martiney, J.A.; Brosnan, C.F. Ultrastructural studies of the blood-retina barrier after exposure to interleukin-1 beta or tumor necrosis factor-alpha. *Lab. Investig.* **1994**, *70*, 850–861. [PubMed]
115. Bamforth, S.D.; Lightman, S.; Greenwood, J. The effect of TNF-alpha and IL-6 on the permeability of the rat blood-retinal barrier in vivo. *Acta Neuropathol.* **1996**, *91*, 624–632. [CrossRef]
116. Aveleira, C.A.; Lin, C.M.; Abcouwer, S.F.; Ambrósio, A.F.; Antonetti, D.A. TNF-α signals through PKCζ/NF-κB to alter the tight junction complex and increase retinal endothelial cell permeability. *Diabetes* **2010**, *59*, 2872–2882. [CrossRef]
117. Olson, J.K.; Miller, S.D. Microglia initiate central nervous system innate and adaptive immune responses through multiple TLRs. *J. Immunol.* **2004**, *173*, 3916–3924. [CrossRef]
118. Reinert, L.S.; Lopušná, K.; Winther, H.; Sun, C.; Thomsen, M.K.; Nandakumar, R.; Mogensen, T.H.; Meyer, M.; Vægter, C.; Nyengaard, J.R.; et al. Sensing of HSV-1 by the cGAS-STING pathway in microglia orchestrates antiviral defence in the CNS. *Nat. Commun.* **2016**, *7*, 13348. [CrossRef]
119. Li, L.; Eter, N.; Heiduschka, P. The microglia in healthy and diseased retina. *Exp. Eye Res.* **2015**, *136*, 116–130. [CrossRef]
120. Amado, D.; Mingozzi, F.; Hui, D.; Bennicelli, J.L.; Wei, Z.; Chen, Y.; Bote, E.; Grant, R.L.; Golden, J.A.; Narfstrom, K.; et al. Safety and efficacy of subretinal readministration of a viral vector in large animals to treat congenital blindness. *Sci. Transl. Med.* **2010**, *2*, 21ra16. [CrossRef]
121. Bennett, J.; Wellman, J.; Marshall, K.A.; McCague, S.; Ashtari, M.; DiStefano-Pappas, J.; Elci, O.U.; Chung, D.C.; Sun, J.; Wright, J.F.; et al. Safety and durability of effect of contralateral-eye administration of AAV2 gene therapy in patients with childhood-onset blindness caused by RPE65 mutations: A follow-on phase 1 trial. *Lancet* **2016**, *388*, 661–672. [CrossRef]

122. Reichel, F.F.; Peters, T.; Wilhelm, B.; Biel, M.; Ueffing, M.; Wissinger, B.; Bartz-Schmidt, K.U.; Klein, R.; Michalakis, S.; Fischer, M.D.; et al. Humoral Immune Response After Intravitreal But Not After Subretinal AAV8 in Primates and Patients. *Investig. Ophthalmol. Vis. Sci.* **2018**, *59*, 1910–1915. [CrossRef] [PubMed]
123. Li, Q.; Miller, R.; Han, P.Y.; Pang, J.; Dinculescu, A.; Chiodo, V.; Hauswirth, W.W. Intraocular route of AAV2 vector administration defines humoral immune response and therapeutic potential. *Mol. Vis.* **2008**, *14*, 1760–1769.
124. Seitz, I.P.; Michalakis, S.; Wilhelm, B.; Reichel, F.F.; Ochakovski, G.A.; Zrenner, E.; Ueffing, M.; Biel, M.; Wissinger, B.; Bartz-Schmidt, K.U.; et al. Superior Retinal Gene Transfer and Biodistribution Profile of Subretinal Versus Intravitreal Delivery of AAV8 in Nonhuman Primates. *Invest. Ophthalmol. Vis. Sci.* **2017**, *58*, 5792–5801. [CrossRef] [PubMed]
125. Leborgne, C.; Barbon, E.; Alexander, J.M.; Hanby, H.; Delignat, S.; Cohen, D.M.; Collaud, F.; Muraleetharan, S.; Lupo, D.; Silverberg, J.; et al. IgG-cleaving endopeptidase enables in vivo gene therapy in the presence of anti-AAV neutralizing antibodies. *Nat. Med.* **2020**, *7*. [CrossRef]
126. Heier, J.S.; Kherani, S.; Desai, S.; Dugel, P.; Kaushal, S.; Cheng, S.H.; Delacono, C.; Purvis, A.; Richards, S.; Le-Halpere, A.; et al. Intravitreous injection of AAV2-sFLT01 in patients with advanced neovascular age-related macular degeneration: A phase 1, open-label trial. *Lancet* **2017**, *390*, 50–61. [CrossRef]
127. Kotterman, M.A.; Yin, L.; Strazzeri, J.M.; Flannery, J.G.; Merigan, W.H.; Schaffer, D.V. Antibody neutralization poses a barrier to intravitreal adeno-associated viral vector gene delivery to non-human primates. *Gene Ther.* **2015**, *22*, 116–126. [CrossRef]
128. Rhen, T.; Cidlowski, J.A. Antiinflammatory action of glucocorticoids–new mechanisms for old drugs. *N. Engl. J. Med.* **2005**, *353*, 1711–1723. [CrossRef] [PubMed]
129. Hobbs, H.E.; Sorsby, A.; Freedman, A. Retinopathy following chloroquine therapy. *Lancet* **1959**, *2*, 478–480. [CrossRef]
130. Mavrikakis, I.; Sfikakis, P.P.; Mavrikakis, E.; Rougas, K.; Nikolaou, A.; Kostopoulos, C.; Mavrikakis, M. The incidence of irreversible retinal toxicity in patients treated with hydroxychloroquine: A reappraisal. *Ophthalmology* **2003**, *110*, 1321–1326. [CrossRef]
131. Rynes, R.I. Ophthalmologic safety of long-term hydroxychloroquine sulfate treatment. *Am. J. Med.* **1983**, *75*, 35–39. [CrossRef]
132. Yusuf, I.H.; Sharma, S.; Luqmani, R.; Downes, S.M. Hydroxychloroquine retinopathy. *Eye* **2017**, *31*, 828–845. [CrossRef]
133. Melles, R.B.; Marmor, M.F. The risk of toxic retinopathy in patients on long-term hydroxychloroquine therapy. *JAMA Ophthalmol.* **2014**, *132*, 1453–1460. [CrossRef] [PubMed]
134. Fanouriakis, A.; Kostopoulou, M.; Alunno, A.; Aringer, M.; Bajema, I.; Boletis, J.N.; Cervera, R.; Doria, A.; Gordon, C.; Govoni, M.; et al. 2019 update of the EULAR recommendations for the management of systemic lupus erythematosus. *Ann. Rheum. Dis.* **2019**, *78*, 736–745. [CrossRef] [PubMed]
135. Yusuf, I.H.; Foot, B.; Galloway, J.; Ardern-Jones, M.R.; Watson, S.L.; Yelf, C.; Burdon, M.A.; Bishop, P.N.; Lotery, A.J. The Royal College of Ophthalmologists recommendations on screening for hydroxychloroquine and chloroquine users in the United Kingdom: Executive summary. *Eye* **2018**, *32*, 1168–1173. [CrossRef]
136. Marmor, M.F.; Kellner, U.; Lai, T.Y.; Melles, R.B.; Mieler, W.F. Recommendations on Screening for Chloroquine and Hydroxychloroquine Retinopathy (2016 Revision). *Ophthalmology* **2016**, *123*, 1386–1394. [CrossRef] [PubMed]
137. Leung, L.S.; Neal, J.W.; Wakelee, H.A.; Sequist, L.V.; Marmor, M.F. Rapid Onset of Retinal Toxicity from High-Dose Hydroxychloroquine Given for Cancer Therapy. *Am. J. Ophthalmol.* **2015**, *160*, 799–805. [CrossRef]
138. Marmor, M.F. COVID-19 and Chloroquine/Hydroxychloroquine: Is there Ophthalmological Concern? *Am. J. Ophthalmol.* **2020**, *213*, A3–A4. [CrossRef]
139. Tett, S.E.; Cutler, D.J.; Day, R.O.; Brown, K.F. Bioavailability of hydroxychloroquine tablets in healthy volunteers. *Br. J. Clin. Pharmacol.* **1989**, *27*, 771–779. [CrossRef]
140. Jallouli, M.; Galicier, L.; Zahr, N.; Aumaitre, O.; Frances, C.; Le Guern, V.; Liote, F.; Smail, A.; Limal, N.; Perard, L.; et al. Determinants of hydroxychloroquine blood concentration variations in systemic lupus erythematosus. *Arthritis Rheumatol.* **2015**, *67*, 2176–2184. [CrossRef]
141. Wainer, I.W.; Chen, J.C.; Parenteau, H.; Abdullah, S.; Ducharme, J.; Fieger, H.; Iredale, J. Distribution of the enantiomers of hydroxychloroquine and its metabolites in ocular tissues of the rabbit after oral administration of racemic-hydroxychloroquine. *Chirality* **1994**, *6*, 347–354. [CrossRef]

142. Li, C.; He, Y.; Nicolson, S.; Hirsch, M.; Weinberg, M.S.; Zhang, P.; Kafri, T.; Samulski, R.J. Adeno-associated virus capsid antigen presentation is dependent on endosomal escape. *J. Clin. Investig.* **2013**, *123*, 1390–1401. [CrossRef] [PubMed]
143. Satoh, N.; Abe, T.; Nakajima, A.; Sakuragi, S. Recurrent varicella-zoster virus retinitis in a patient treated with systemic corticosteroids. *Ocul. Immunol. Inflamm.* **1998**, *6*, 185–188. [CrossRef]
144. Benz, M.S.; Glaser, J.S.; Davis, J.L. Progressive outer retinal necrosis in immunocompetent patients treated initially for optic neuropathy with systemic corticosteroids. *Am. J. Ophthalmol.* **2003**, *135*, 551–553. [CrossRef]
145. Han, J.M.; Ahn, J.; Park, K.H.; Woo, S.J. Presumed necrotizing viral retinitis after intravitreal triamcinolone injection: Case report. *Korean J. Ophthalmol.: KJO* **2011**, *25*, 451–454. [CrossRef] [PubMed]
146. Takakura, A.; Tessler, H.H.; Goldstein, D.A.; Guex-Crosier, Y.; Chan, C.C.; Brown, D.M.; Thorne, J.E.; Wang, R.; Cunningham, E.T., Jr. Viral retinitis following intraocular or periocular corticosteroid administration: A case series and comprehensive review of the literature. *Ocul. Immunol. Inflamm.* **2014**, *22*, 175–182. [CrossRef] [PubMed]